THESIS

ENSEMBLE-BASED ANALYSIS OF EXTREME PRECIPITATION EVENTS FROM 2007-2011

Submitted by

Samantha Lynch

Department of Atmospheric Science

In partial fulfillment of the requirements

For the Degree of Master of Science

Colorado State University

Fort Collins, Colorado

Fall 2012

Master's Committee:

Advisor: Russ Schumacher

Richard Johnson
Jeffrey Niemann

ABSTRACT

ENSEMBLE-BASED ANALYSIS OF EXTREME PRECIPITATION

EVENTS FROM 2007-2011

From 2007 to 2011, 22 widespread, multiday rain events occurred across the United States. This study makes use of the European Centre for Medium-Range Weather Forecasts (ECMWF), the National Centers of Environmental Prediction (NCEP), and the United Kingdom Office of Meteorology (UKMET) ensemble prediction systems (EPS) in order to assess their forecast skill of these 22 widespread, precipitation events. Overall, the ECMWF had a skillful forecast for almost every event, with an exception of the 25-30 June 2007 event, the mesoscale convective vortex (MCV) over the southern plains of the United States. Additionally, the ECMWF EPS generally outperformed both the NCEP and UKMET EPS. To better evaluate the ECMWF, two widespread, multiday precipitation events were selected for closer examination: 29 April-4 May 2010 and 23-28 April 2011.

The 29 April-4 May 2010 case study used ECMWF ensemble forecasts to explore the processes responsible for the development and maintenance of a multiday precipitation event that occurred in early May 2010, due to two successive quasi-stationary mesoscale convective systems. Locations in central Tennessee accumulated more than 483 millimeters (19 inches) of rain and the city of Nashville experienced a historic flash flood. Differences between ensemble members that correctly predicted heavy precipitation and those that did not were determined in order to determine the processes that were favorable or detrimental to the system's development. Statistical analysis was used to determine how synoptic-scale flows were correlated to area-averaged precipitation. For this particular case, the distribution of precipitation was found to be

closely related to the strength of an upper-level trough in the central United States and an associated surface cyclone, with a weaker trough and cyclone being associated with more precipitation in the area of interest.

The 23-28 April 2011 case study also used ECMWF ensemble forecasts to explore the processes responsible for the development and maintenance of a multiday precipitation event. This event was associated with persistent heavy rainfall, flooding more than six states lining the Mississippi River. In this case, the largest difference in the ensemble members' forecasts was the strength of the upper-level trough and associated occluded low, as well as the speed at which this system moved off to the east. These relatively small differences in the height field ultimately resulted in different forecasts of precipitation over the Mississippi Valley. This sensitivity to small-scale differences in the initial conditions highlights the importance of using ensembles for predicting the development of precipitation systems over both land and ocean.

Comparison between the 29 April-4 May 2010 and 23-28 April 2011 widespread precipitation events provide information regarding which of the two case studies was better predicted in relation to both location and amount of precipitation. Heavy rainfall totals, exceeding the 100 and 150 mm threshold, were better anticipated for the 29 April-4 May 2010 event, while location of the precipitation was better predicted for the 23-28 April 2011 widespread rain event.

ACKNOWLEDGEMENTS

This research was support by National Science Foundation grants AGS-0954908 and AGS-1157425.

Ensemble data were provided by The Observing System Research and Predictability Experiment (THORPEX) Interactive Grand Global Ensemble (TIGGE). Precipitation data were provided by the Climate Prediction Center (CPC). Upper-air data for the individual case studies, as well as, radar reflectivity data were obtained from the National Center of Atmospheric Research (NCAR). Observed 12-hr precipitation were acquired from the National Mosaic and Multi-sensor QPE (NMQ). Composite anomalies were obtained from the Earth System Research Laboratory (ESRL) of NOAA. Archived surface analyses were obtained from the Hydrometeorological Prediction Center (HPC), while storm reports were obtained from the Storm Prediction Center (SPC). Skew-T-logp soundings and hodographs were provided by the University of Wyoming, Department of Atmospheric Science. Finally, the number of flood-related fatalities and the amount of flood damage for each widespread, precipitation event were obtained from the Storm Events Database of the National Climatic Data Center (NCDC).

I would like to thank the members of my graduate committee, Dr. Richard Johnson and Dr. Jeffrey Niemann, for reviewing my work and providing appreciated suggestions. I would especially like to thank my advisor, Dr. Russ Schumacher, for all of his continuous support and encouragement in the process of completing this research and manuscript, as well as for the weekly meetings to discuss my progress and offer valuable recommendations.

Thanks to all the members of the Schumacher research group – Charles Yost, Vanessa Vincente, John Peters, and Kelly Keene – for continual motivation in this project. Finally, I would like to thank my family and friends for supporting me in this and all my life ventures.

TABLE OF CONTENTS

LIST OF TABLES

LIST OF FIGURES

CHAPTER 1

INTRODUCTION

Widespread, heavy precipitation, capable of producing flooding, is often responsible for crop damage, property damage, injuries and even fatalities across the United States. Chappell (1986) noted that heavy precipitation is often a result of quasi-stationary convective systems. Quasi-stationary convective systems occur when convective cells repeatedly form over the same location, having the potential for exceptionally high point rainfall totals. For heavy rainfall to occur, there also has to be sufficient moisture in the atmosphere. One mechanism that can provide this moisture is an “atmospheric river.” An “atmospheric river” pulls tropical water vapor straight into the midlatitudes, often time leading to an extreme precipitation event (Ralph et al. 2011). Although all the necessary ingredients for heavy rainfall may be present, forecasting for an event of such magnitude can prove to be difficult, especially when multiple threats are present. One compelling problem found in operational meteorology is forecasting for multifaceted weather systems. Forecasters can have an overriding concern for hail, high winds, and tornadoes, seeming to overlook any imminent flood threat.

Ensemble prediction systems can be used to better forecast for these widespread, heavy precipitation events by providing more understanding into the dynamics of weather systems capable of producing heavy rainfall amounts and subsequent flooding. One benefit of using an ensemble prediction system is that they are readily available. Ensemble prediction systems also allow for the opportunity of studying multiple cases with very little computation. Considering the countless impacts that heavy rainfall and flooding have on society, there is a need to further research and understand the processes that lead to extreme precipitation events.

In the chapters to follow, a comparison will be made between the ECMWF, NCEP, and UKMET EPS in order to assess model performance of 22 widespread rain events from 2007-2011. This will provide insight into which model has consistently output a more skillful forecast for widespread rain events, allowing forecasters to put more confidence into a single ensemble prediction system for events of similar spatial scale. Then, two individual case studies will be investigated using the ECMWF EPS in order to determine the key factors that were favorable for, or detrimental to, the development of widespread, multiple day rainfall. The results could then be used to provide a better forecast for future events of similar spatial scale. Finally, a comparison is made between the two individual case studies to offer information regarding which of the two case studies was better predicted in relation to both location and amount of precipitation.

CHAPTER 2

BACKGROUND AND MOTIVATION

2.1 Flash flooding

Flash flooding has become the convective storm related event annually producing the most fatalities in the United States (Doswell et al. 1996). The major challenge associated with flash flooding is the quantitative character of the forecast: the task is not just to forecast the occurrence of an event, which is difficult enough by itself, but to anticipate the magnitude of the event (Doswell et al. 1996). The magnitude of precipitation is what turns an otherwise ordinary, short-term rainfall event into an extraordinary, life-threatening situation, likely to have a profound impact over a large area. Doswell (1994) and Doswell et al. (1996) determined that in order for large precipitation accumulations to occur, high rainfall rates must be sustained over an extended period of time. That is, at any point on the earth, the total precipitation produced, P, is simply:

$$P = \bar{R}D \tag{2.1}$$

where $\bar{R}$ is the average rainfall rate and D is the duration of the rainfall (Eqn. 2.1). Instantaneous rainfall rate, R, depends on q the mixing ratio of rising air, w the ascent rate, and E the precipitation efficiency:

$$R = Ewq \tag{2.2}$$

while duration of an event is associated with its speed of movement and the size of the system causing the event along the direction of system movement (Eqn. 2.2). Chappell (1986) found that the most important flash floods are produced by quasi-stationary convective systems, wherein

many convective cells reach maturity and produce their heaviest rainfall over the same area for an extended period of time. Predicting an event of such magnitude remains a difficult task for forecasters, in part because they often occur on very small scales and can result from a wide variety of storm types including landfalling hurricanes, tropical storms, synoptic cyclones, etc. Flash flood forecasting posing a challenge because not only is an accurate meteorological prediction required, a hydrological prediction is required as well. As stated by Doswell et al. (1996), "this challenge is acerbated by the interaction of the meteorology with hydrology."

Although the hydrological aspects of flash flooding are beyond the scope of this study, it is still entirely relevant to the flash flood problem. The reminder of this study will investigate the meteorological aspects of weather systems that often produce flooding, which, using the terminology of Schumacher and Davis (2010), will be called "widespread rain events." The widespread rain events considered here will be selected and evaluated using meteorological observations (i.e., rain gauge data), following the criteria of Schumacher and Davis (2010), without regard for the magnitude of flooding. Ensemble forecasts are used in order to analyze the synoptic- and mesoscale factors that led to the development of the widespread, multiday rain events from the year 2007 to 2011.

2.2 Standardized anomalies

Many studies have used standardized anomalies as a tool to help explain and predict heavy rainfall events (Hart and Grumm 2001, Kahana et al. 2002, Lyon 2003, Bond and Vecchi 2003, Graham and Grumm 2010, Romatschke and Houze 2011a, Houze et al. 2011, Romatschke and Houze 2011b, Grumm 2011b, Lau and Kim 2012, Galarneau et al. 2012). For the 29 April-4 May 2010 widespread rain event, Moore et al. (2012) found integrated water vapor (IWV) anomalies of 1.5-2.5 standard deviations above the mean extended from the Yucatan Peninsula

into the central Mississippi Valley at 1200 UTC 1 May 2010, as well as a large region of IWV anomalies ranging from 2.5 to well above 4 standard deviations above the mean, which coincided with the tropical IWV reservoir near Central America. These two conveyor belts of moisture from both the eastern tropical Pacific and the Caribbean Sea will be discussed in detail later in the study. For the 23-28 April 2011 widespread rain event, Doswell et al. (2012) found an anomalously deep trough across the north-central United States and much of western Canada, anomalously strong upper-level ridging along the east coast and over the Atlantic, as well as, highly anomalous moisture further supporting the potential for widespread severe thunderstorms.

2.3 Ensemble-based methodology

Another approach often used is the ensemble-based approach of predicting weather systems. Ensembles of numerical weather prediction models, comprised of many individual deterministic forecasts, are now commonly used in weather forecasting. Additionally, researchers are beginning to use ensemble forecasts to gain more understanding of the dynamics of weather systems. Ensemble forecasting follows the work of Epstein (1969), Gleeson (1970), Fleming (1971a, b), and Leith (1974), who all made contributions to stochastic dynamic prediction, laying the theoretical and numerical foundations of a probabilistic approach to weather forecasting. In the past, the use of an ensemble was most commonly applied to extended range forecasts (6-10 days) (Tracton and Kalnay 1993, Toth and Kalnay 1993, Mureau et al. 1993, Molteni et al. 1996), however, studies also suggest that ensemble methods can benefit short-range forecasts (1-2 days) (Mullen and Baumhefner 1991 and 1994, Brooks and Doswell 1993, Brooks et al. 1995, Du et al. 1997, Hamill et al. 2000). Many studies have evaluated the performance of ensemble methods for precipitation forecasts (Hamill and Colucci 1997 and 1998, Du et al. 1997, Petroliagis et al. 1997, Eckel and Walters 1998, Buizza et al. 1999, Mullen

and Buizza 2001, Venugopal et al. 2005). Hakim and Torn (2008) executed ensemble synoptic analysis of an extratropical cyclone, finding the relationships between different synoptic features and computing statistical operators. Shortly after, using short-term ensemble forecasts, Torn (2010) examined the dynamical mechanisms that led to downstream ridging during extratropical transition. Hawblitzel et al. (2007) used similar techniques to examine the dynamics and predictability of a mesoscale convective vortex (MCV). Sippel and Zhang (2008) and Sippel and Zhang (2010) used short-range ensemble forecasts to study the dynamics and predictability of a nondeveloping tropical disturbance in the Gulf of Mexico and Hurricane Humberto, which made landfall along the Texas coast in 2007.

Froude et al. (2007) used both the ECMWF ensemble prediction system and the NCEP ensemble prediction system to evaluate the predictions of extratropical cyclone storm tracks in both the northern and southern hemisphere. Buizza et al. (1999) and Mullen and Buizza (2001) assessed the performance of the ECMWF EPS on predicting accumulated rainfall, proposing precipitation is more predictable during the winter than the summer due to enhanced synoptic forcing and less prevalent convection. Buizza et al. (1999) and Mullen and Buizza (2001) also found that the accuracy in precipitation forecasts decreases as the rainfall threshold increases. As one would expect, Petroliagis et al. (1995) advised that probability forecasts of low-level temperature and wind are more reliable than those of precipitation. Majumdar and Finocchio (2010) evaluated the ability of ECMWF and UKMET to predict the probability that a tropical cyclone would fall within a certain area for the 2008 Atlantic and western North Pacific seasons. Additionally, Grumm (2008) compared forecasts from NCEP GFS, ECMWF, CMC, and UKMET for the east coast winter storm of 14 January 2008. Schumacher (2011) used the ECMWF to study the predictability of a long-lived continental vortex that impacted the southern

plains on 25-30 June 2007. Chapter 4 of this study is essentially an extension of the work done by Schumacher and Davis (2010), who used the ECMWF to identify the skill and uncertainty of nine widespread, multiple day precipitation events in the years 2007 and 2008. The Observing System Research and Predictability Experiment (THORPEX) Interactive Grand Global Ensemble (TIGGE, Bougeault et al. 2010) was used by Schumacher and Davis (2010) to investigate the atmospheric processes associated with these events. TIGGE will also be used for this study; the details of TIGGE will be described later in the study.

2.4 Synoptic type flash flood event

Maddox et al. (1979) has identified three primary types of synoptic and mesoscale patterns as often producing excessive rain. Both the meso-high and frontal types are primarily mesoscale phenomena, while synoptic forcing drives the synoptic type events. This study will focus on synoptic type events because the widespread precipitation events on 29 April-4 May 2010 and 23-28 April 2011 were synoptic type events (event details are described later in the study). Typically, the occurrence of synoptic type events peaks in October, with a second peak during the spring and early summer (Fig. 2.1). During the spring, synoptic type events are most commonly observed in the Mississippi Valley and the Midwest of the United States (Fig. 2.2). A strong 500-hPa trough is seen slowly pushing to the east/northeast, and it is usually located to the west of the location that experiences severe weather and flooding (Fig. 2.3a). The frontal boundary begins to slow or stall as it becomes parallel to the upper-level flow. The associated frontal boundaries are usually oriented southwest to northeast. Dew point temperatures at the location prone to severe weather and flooding are typically 70°F or higher (Fig. 2.3c). Winds at the 850- hPa level are typically strong, with strong vertical wind shear present through the cloud

depth (Fig. 2.3b, Maddox et al. 1979). All of these features are common for synoptic type flash flood events.

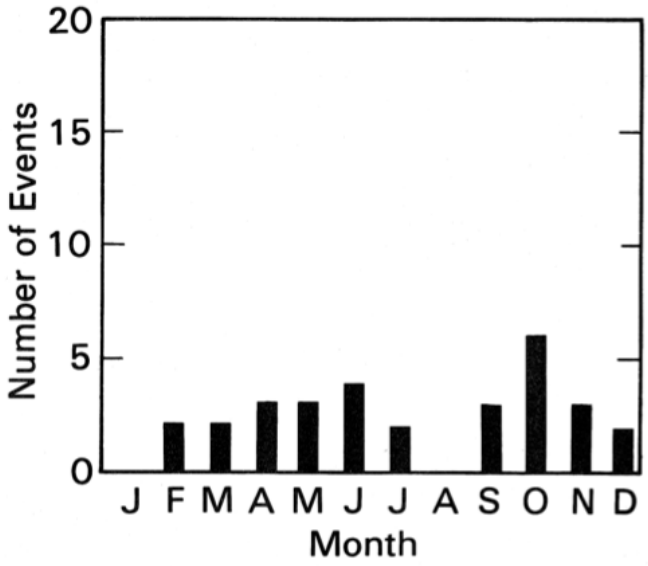

Figure 2.1: Monthly distribution of synoptic type flash flood events. From Maddox et al. (1979).

Figure 2.2: Locations of 151 flash floods shown by season (Winter = Dec., Jan., Feb.; Spring = Mar., Apr., May; etc.). Synoptic events are denoted by the shaded areas; mesohigh events by squares; and frontal events by open circles. All events west of the heavy line were designated western events (indicated by the solid circles). The five stars and shaded areas in the west were explained in Section 6 of Maddox et al. (1979).

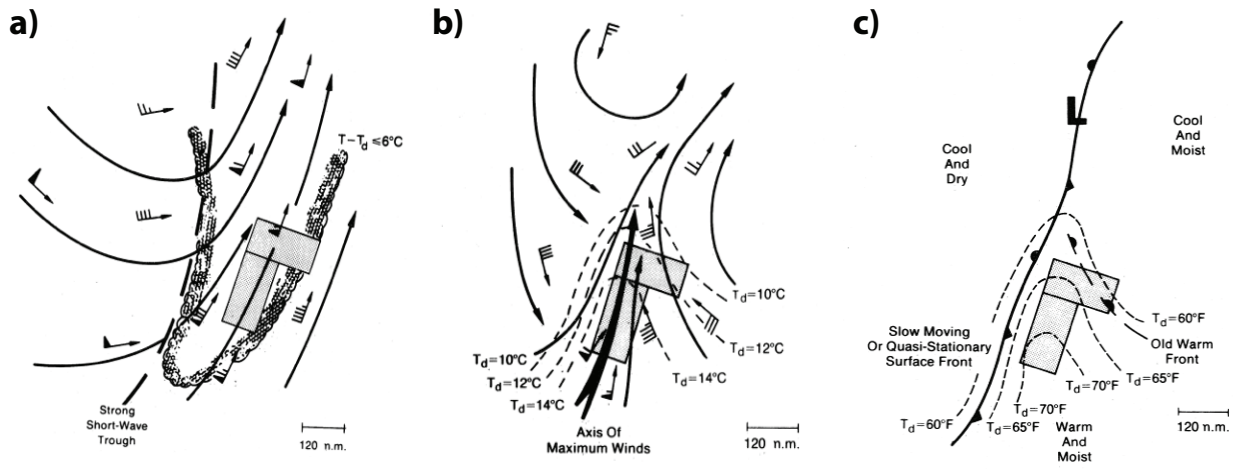

Figure 2.3: (a) 500-hPa flow pattern, (b) 850-hPa flow pattern, and (c) surface pattern for a synoptic type flash flood event. From Maddox et al. (1979).

2.5 Quasi-stationary mesoscale convective systems

The widespread precipitation events on 29 April-4 May 2010 and 23-28 April 2011 were a result of mesoscale convective systems. The 29 April-4 May 2010 precipitation event was due to two quasi-stationary mesoscale convective systems passing through Nashville, TN on the 1 and 2 May 2010 (Moore et al. 2012). Fritsch et al. (1986) found that mesoscale convective weather systems account for approximately 30% - 70% of the warm-season (April – September) precipitation over much of the region between the Rocky Mountains and the Mississippi River. Almost always, linear warm sector MCSs occur near linear surface boundaries, most often near warm or stationary fronts, with the presence of a low-level jet increasing the activity (Parker and Johnson 2000). Tuttle and Davis (2006) have shown that corridors of warm season precipitation over the central United States are associated with the northern terminus region of the nocturnal low-level jet. Furthermore, the intensity of the rainfall is positively correlated with the strength of the low-level jet through enhanced convergence and lifting, moisture transport, and

frontogenesis. A number of studies have then linked MCSs with many warm-season flash flood events (Bosart and Sanders 1981, Maddox and Grice 1986, Junker et al. 1999, Glass 2000, Moore et al. 2003, Schumacher and Johnson 2005 and 2006). Schumacher and Johnson (2009) found that extreme rain producing mesoscale convective systems (MCSs) typically form in a thermodynamic environment characterized by high relative humidity at low levels, moderate convective available potential energy (CAPE), and very little convective inhibition (CIN, Fig. 2.4). The presence of a southerly low-level jet transporting water vapor poleward combined with the above characteristics is favorable for deep moist convection. Deep moist convection fixed over the same area for an extended period of time can result in extreme localized rainfall and devastating flooding, a situation that often occurs in connection with quasi-stationary or backbuilding MCSs (Bluestein and Jain 1985, Chappell 1986, Doswell 1994, Doswell et al.

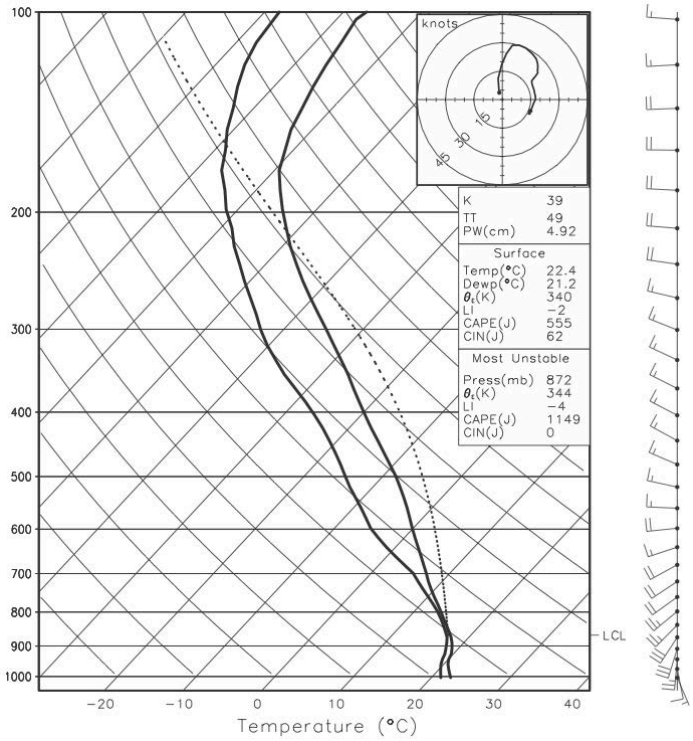

Figure 2.4: Composite skew-T-log*p* diagram for the extreme rainfall environment. The parcel path for the parcel with the highest θ_e in the lowest 3 km is shown by the dotted line. From Schumacher and Johnson (2009).

1996, Schumacher and Johnson 2005). Quasi-stationary or backbuilding MCSs occur when convective cells repeatedly form over the same location, having the potential for exceptionally high point rainfall totals. The decaying convective cells move downstream, relative to cell motion, while new convective cells begin to form upstream (Fig. 2.5, Schumacher and Johnson 2005). Shi and Scofield (1987) and Juying and Scofield (1989) observed mesoscale convective systems in satellite imagery, finding that the majority of the flash floods in the study were produced by backward propagating MCSs. These systems appear to be moving very slowly or remain stationary producing excessive rain because the propagation vector is opposite or nearly opposite to the mean cell motion vector as described by Corfidi (1996 and 2003) and Chappell (1986).

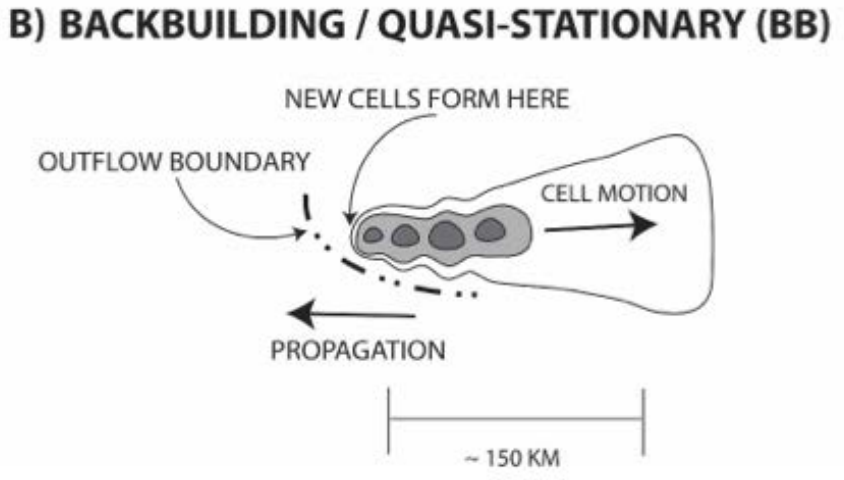

Figure 2.5: Schematic diagram of the radar-observed features of the (b) BB patterns of extreme-rain-producing MCSs. Contours (and shading) represent approximate radar reflectivity values of 20, 40, and 50 dBZ. The dash–dot line represents an outflow boundary; such boundaries were observed in many of the BB MCS cases. The length scale at the bottom is approximate and can vary substantially, especially for BB systems, depending on the number of mature convective cells present at a given time. From Schumacher and Johnson (2005).

2.6 Atmospheric rivers

For the event that took place 29 April-4 May 2010, there was a concentrated plume of tropical moisture from the Caribbean Sea being advected poleward into the Mississippi Valley, providing anomalous moisture to the region of interest. This narrow corridor of anomalously high tropical water vapor has been termed "atmospheric river" (Fig. 2.6, Newell et al. 1992, Zhu and Newell 1998, Ralph et al. 2004). These features pull tropical water vapor straight into the

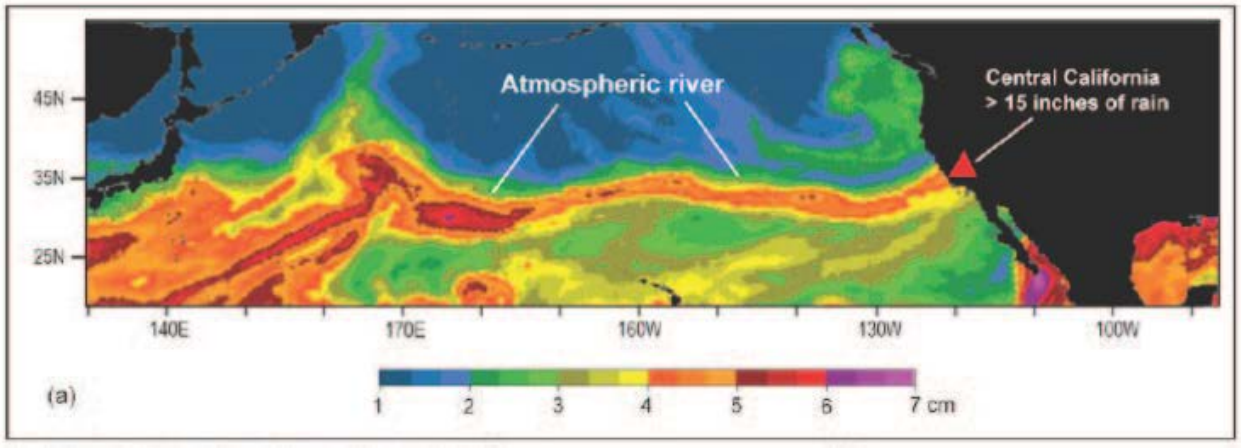

Figure 2.6: Analysis of an atmospheric river (AR) that hit California on 13–14 October 2009. (a) A Special Sensor Microwave Imager (SSM/I) satellite image from 13–14 October showing the AR hitting the California coast; color bar shows, in centimeters, the amount of water vapor present throughout the air column at any given point if all the water vapor were condensed into one layer of liquid (vertically integrated water vapor). From Ralph and Dettinger (2011).

midlatitudes, often time leading to an extreme precipitation event (Ralph et al. 2011). A variety of studies have linked water vapor transport from the western Gulf of Mexico and the western Caribbean Sea to extreme rainfall events in the Midwest (Benton and Estoque 1954, Bell and Janowiak 1995, Trenberth and Guillemot 1996, Higgins et al. 1997, Dirmeyer and Kinter 2009, Bodner et al. 2011, Moore et al. 2012). Dirmeyer and Kinter (2009) dubbed this the "Maya Express," which is dependent upon the strength and location of the North Atlantic subtropical ridge, a belt of high pressure also known as the "Bermuda High" (Dirmeyer and Kinter 2010).

The North Atlantic subtropical ridge produces the easterly trade winds, carrying moisture from the tropical north Atlantic into the Caribbean Sea. This moisture is then transported poleward into the central United States by the Great Plains low-level jet, commonly observed during the summer. A stronger than normal anticyclonic circulation around the subtropical ridge appears to strengthen the "Maya Express," as does the subtropical ridge being displaced west (Wang et al. 2007, 2008). The aforementioned Great Plains low-level jet plays a crucial role in the onset of heavy precipitation in the central United States, allowing for the transport of tropical moisture into the Midwest (Djurić and Damiani 1980, Uccellini 1980, Mo et al. 1995, Whiteman et al. 1997). Higgins et al. (2011) examined five heavy rain events that occurred in 2010, including the historic flood of Nashville, Tennessee. All five of the cases studied were associated with moisture plumes that extended from deep in the Caribbean into the United States. Additionally, these five heavy precipitation events exhibited the characteristics of "Maya Express" flood events (Dirmeyer and Kinter 2009), which link tropical moisture from the Caribbean and Gulf of Mexico to mid-latitude flooding over North America. More recently, Moore et al. (2012) emphasized the role of an "atmospheric river" in the 29 April-4 May 2010 precipitation event, providing support for the development and persistence of the two quasi-stationary mesoscale convective systems that produced prolonged heavy rainfall and substantial flash flooding in the Mississippi Valley.

A more common phenomena, the "Pineapple Express," was coined for its ability to draw warm, moist air from the Hawaiian tropics, transporting it to the west coast of the United States (Fig. 2.6, Dettinger 2004, Dettinger et al. 2011). When atmospheric rivers impinge upon the west coast of North America, orographic precipitation processes can occur producing heavy rainfall and flooding along the mountainous terrain (Ralph and Dettinger 2011, Smith et al. 2010, Junker

et al. 2009, Leung and Qian 2009, Neiman et al. 2008a, 2008b, and 2011, Ralph et al. 2004, 2005, and 2006).

Stohl et al. (2008) documented the formation of an atmospheric river due to two former hurricanes, Nate and Maria, undergoing extratropical transition. This generated an atmospheric river transporting water vapor from the tropical western North Atlantic and ending in the Norwegian southwest coast, producing strong orographic enhancement of the precipitation. Additionally, Halverson and Rabenhorst (2010) suggested a rich conveyor belt of tropical moisture, originating as far away as the equator, contributed to the 5-6 February 2010 heavy snowfall, bringing an impressive swath of 25-30 inches of snow to the Baltimore-Philadelphia region.

2.7 Severe weather outbreaks and widespread flash flooding

The 23-28 April 2011 precipitation event was due to a series of mesoscale convective systems impacting the Mississippi Valley. Heavy precipitation was not the only threat for this particular event; tornadoes tore through the Mississippi Valley for the entire 5-day period, culminating in a violent and destructive tornado outbreak on 27 April 2011. Several studies have found thunderstorm complexes that produce both severe weather outbreaks and widespread flash flooding (Maddox and Grice 1986, Corfidi et al. 1990, Schwartz et al. 1990, Rogash and Smith 2000, Smith et al. 2001, Rogash and Racy 2002). Doswell (1994) found that supercells, themselves, can be prolific precipitation producers due to their ability to process enormous amounts of moist air through their powerful, persistent updrafts, and their relatively slow movement and long lifetime. This type of supercell was termed the high-precipitation supercell (HP), characterized by a mesocyclone thoroughly wrapped in precipitation (Moller and Doswell 1988, Doswell et al. 1990, Moller et al. 1990).

2.8 Forecasting concerns

One compelling problem found in operational meteorology is forecasting for multifaceted weather systems. For the Minneapolis flash flood on 23-24 July 1987, Schwartz et al. (1990) suggested that forecasters had an overriding concern for hail, high winds, and tornadoes, seeming to overlook the imminent flash-flood threat. Similarly, Rogash and Smith (2000) propose thunderstorm outbreaks that produce both violent tornadoes and flash flooding within a limited time and area represent an exceptional challenge to operational meteorologists.

CHAPTER 3

DATA AND METHODS

3.1 Precipitation dataset

The primary precipitation dataset used in this study is the U.S. Daily Precipitation Analysis (Chen et al. 2008), obtained from the National Oceanographic and Atmospheric Administration/Climate Prediction Center (NOAA/CPC) (information online at http://www.cpc.ncep.noaa.gov/products/precip/realtime/GIS/retro.shtml). This dataset consists of roughly 16,000 rain gauge observations, gridded to a 0.25° latitude by 0.25° longitude grid. Because this dataset has relatively coarse resolution, it does not accurately represent local precipitation maxima. However, this dataset is sufficient for analyzing the widespread, multiday precipitation events that will be discussed below.

3.2 Selection of cases

To select the precipitation events for this study, the gridded precipitation data were assessed to find widespread, multiday heavy rainfall. The 5-day periods in which 100 mm of precipitation fell over more than 350 grid points (approximately 800,000 km^2) were identified; hereafter referred to as widespread rain events. The 350 grid points were not required to be adjacent. Five days was chosen as the accumulation period to differentiate localized, short-term rainfall events from those that persist for multiple days, likely to have a profound impact over a large area. During the years 2007 to 2011, 22 cases met these criteria. Details about the location of impact, forcing mechanism, as well as the number of fatalities and cost of damage for each of the 22 cases are provided in Table 3.1. Additionally, the five-day accumulated precipitation for the 22 widespread rain events is shown in Figs. 3.1a-v to provide an idea of the total rainfall

amount and spatial distribution for each event. Schumacher and Davis (2010) found that from 1948 to 2006, these widespread heavy rain events were most common in the cool season near the Gulf of Mexico coast and were rare in the warm season (Fig. 3.2). The characteristics of the widespread precipitation events from 2007 to 2011 are consistent with their findings.

Table 3.1: Listing of the 22 widespread 5-day rain events between 2007 and 2011, selected as described in the text. Each event has an areal coverage of 100 mm of precipitation greater than 350 precipitation grid points (approximately 800,000 km^2). Each event is considered to have started at 1200 UTC on the first date given and ended at 1200 UTC on the second date given. The events have been classified as either cool season (CS), warm season (WS), or tropical cyclone (TC). The number of flood-related fatalities and the amount of flood damage for each event are shown, based on data from the Storm Events database. Asterisks are shown for three of the landfalling tropical cyclones that had damage from both flooding and from other causes.

Dates	Location	Type	Process	No. of fatalities	Damage ($M)
25-30 Jun 2007	Southern Plains	WS	Midlevel vortex	3	160
18-23 Aug 2007	Upper Midwest	WS	Stationary front	15	625
22-27 Oct 2007	Southeast	CS	Cutoff synoptic cyclone	0	0
15-20 Mar 2008	Mississippi Valley	CS	Synoptic-scale front	10	240
4-9 Jun 2008	Upper Midwest	WS	Stationary front	11	2000
22-27 Aug 2008	Southeast	TC	Tropical Storm Fay	3	40
1-6 Sep 2008	South	TC	Hurricane Gustav	*	*
10-15 Sep 2008	South, Midwest	TC	Hurricane Ike, frontal system	*	*
8-13 Dec 2008	Southeast	CS	Synoptic cyclone	0	1.4
24-29 Mar 2009	Southeast	CS	Synoptic cyclone	2	3.1
1-6 May 2009	Mississippi Valley	CS	Slow-moving front	2	30
5-10 Oct 2009	Mississippi Valley	CS	Synoptic cyclone	0	1.9
11-16 Oct 2009	South	CS	Stationary front	0	30
26-31 Oct 2009	South	CS	Two synoptic cyclones	6	30
9-14 Nov 2009	East Coast	TC	Extratropical transition of Hurricane Ida	0	0.3
18-23 Jan 2010	West Coast	CS	Synoptic cyclone, orographic	2	35
29 Apr-4 May 2010	Midwest	CS	Synoptic cyclone	31	2290
26 Sep-1 Oct 2010	East Coast	TC	Tropical Storm Nicole	12	165
17-22 Dec 2010	West Coast	CS	"Atmospheric river", orographic	2	190
23-28 Apr 2011	Mississippi Valley	CS	Synoptic cyclone	14	125
25-30 Aug 2011	East Coast	TC	Hurricane Irene	*	*
3-8 Sep 2011	South	TC	Tropical Storm Lee, frontal system	23	1555

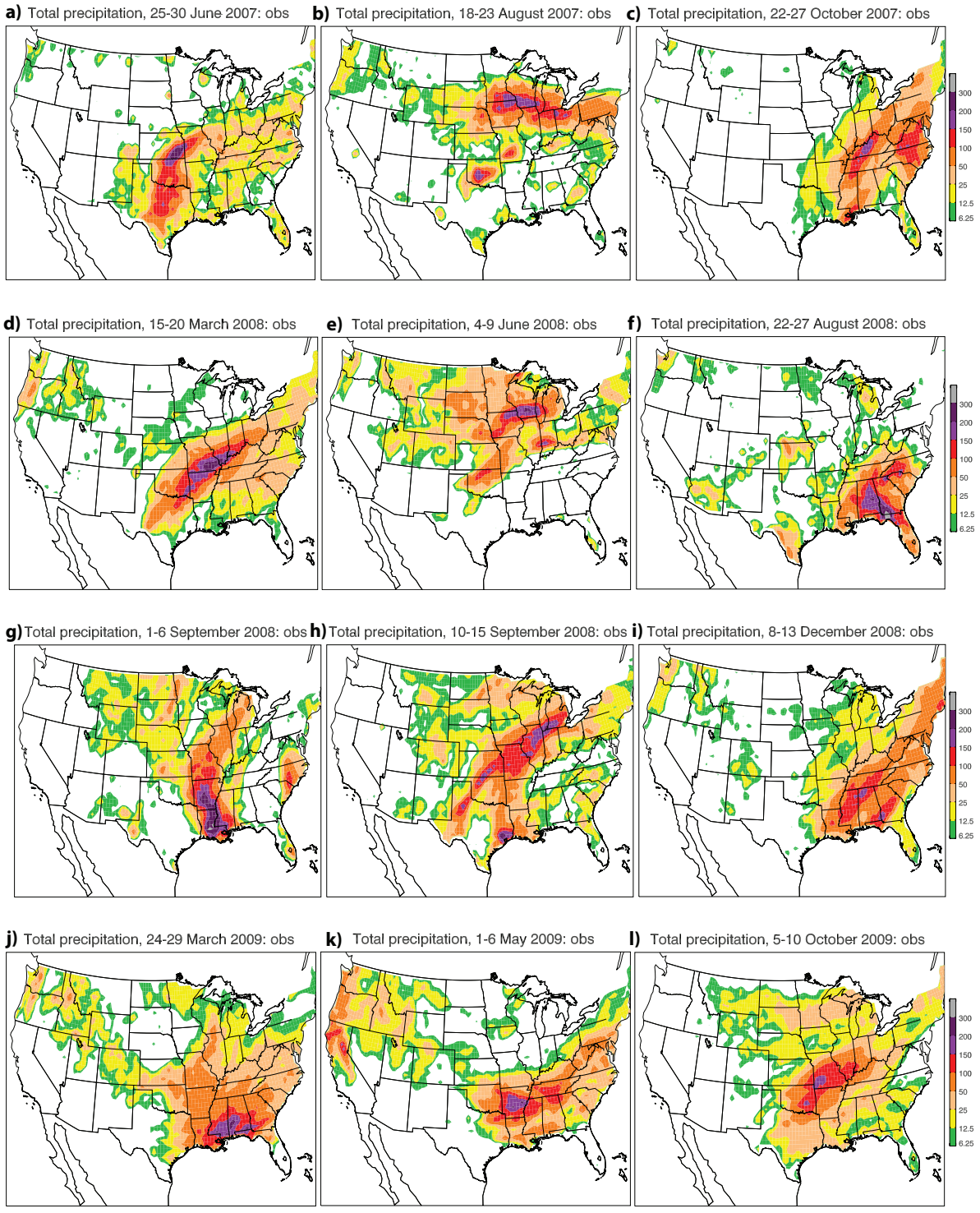
a) Total precipitation, 25-30 June 2007: obs
b) Total precipitation, 18-23 August 2007: obs
c) Total precipitation, 22-27 October 2007: obs
d) Total precipitation, 15-20 March 2008: obs
e) Total precipitation, 4-9 June 2008: obs
f) Total precipitation, 22-27 August 2008: obs
g) Total precipitation, 1-6 September 2008: obs
h) Total precipitation, 10-15 September 2008: obs
i) Total precipitation, 8-13 December 2008: obs
j) Total precipitation, 24-29 March 2009: obs
k) Total precipitation, 1-6 May 2009: obs
l) Total precipitation, 5-10 October 2009: obs
300
200
150
100
50
25
12.5
6.25

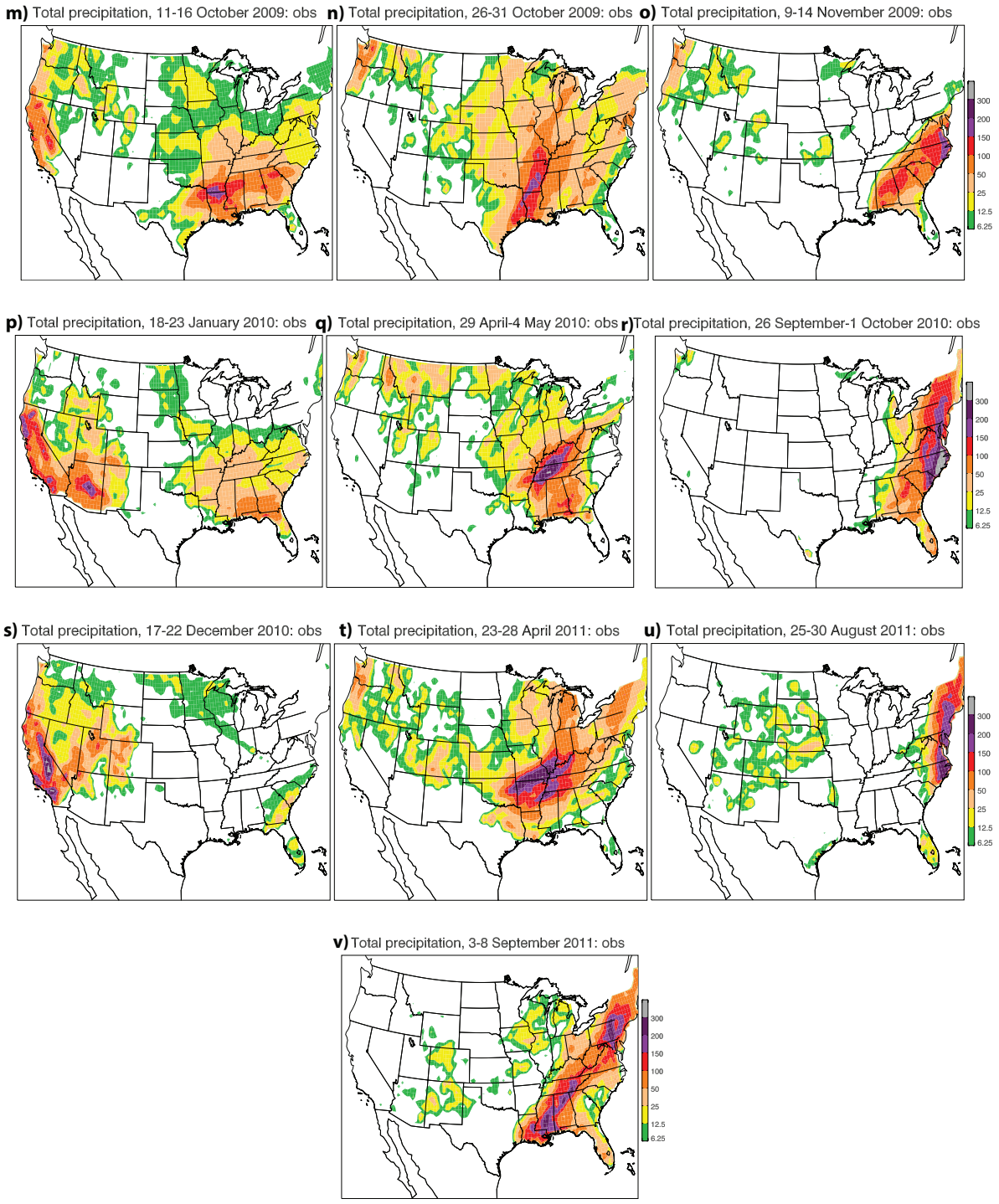

Figure 3.1: Five-day accumulated precipitation (color shading) for each of the 22 widespread precipitation events between 2007-2011 (see also Table 3.1): (a) 25-30 Jun 2007, (b) 18-23 Aug 2007, (c) 22-27 Oct 2007, (d) 15-20 Mar 2008, (e) 4-9 Jun 2008, (f) 22-27 Aug 2008, (g) 1-6 Sep 2008, (h) 10-15 Sep 2008, (i) 8-13 Dec 2008, (j) 24-29 Mar 2009, (k) 1-6 May 2009, (l) 5-10 Oct 2009, (m) 11-16 Oct 2009, (n) 26-31 Oct 2009, (o) 9-14 Nov 2009, (p) 18-23 Jan 2010, (q) 29 Apr-4 May 2010, (r) 26 Sep-1 Oct 2010, (s) 17-22 Dec 2010, (t) 23-28 Apr 2011, (u) 25-30 Aug 2011, and (v) 3-8 Sep 2011.

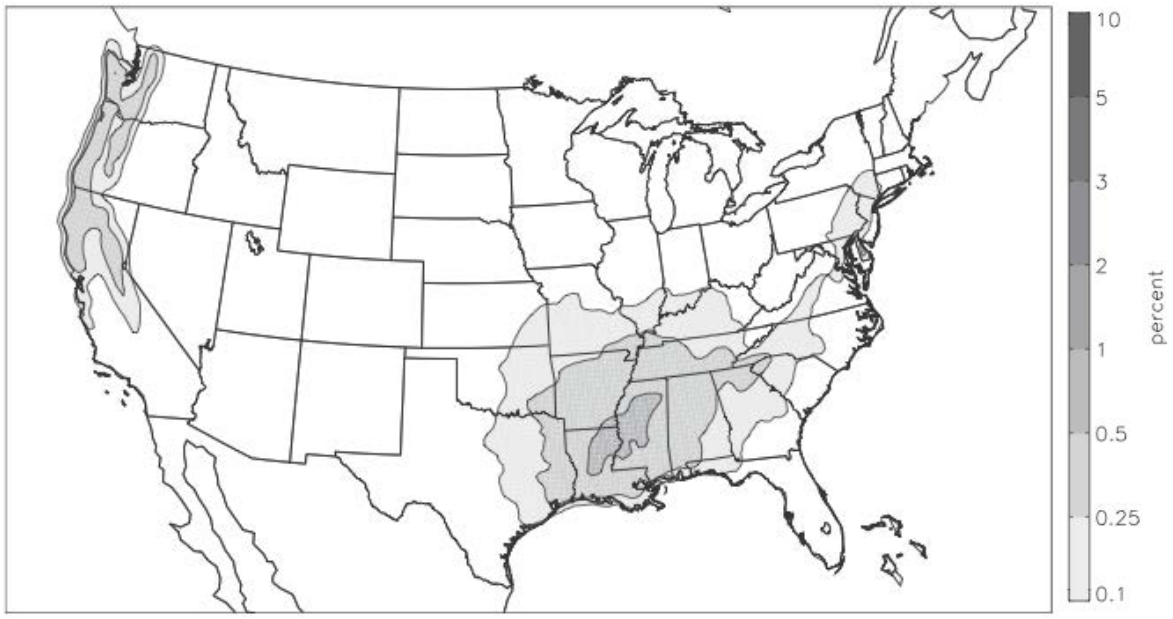

Figure 3.2: Climatological frequency (based on 1948-2006) of 100 mm of rainfall in 5 days only if it occurred as part of a widespread rain event as defined in the text. From Schumacher and Davis (2010).

3.3 Numerical models

Operational ensemble forecasts will then be used to assess the key factors that were favorable for, or detrimental to, the development of widespread, multiple day rainfall for the 29 April-4 May 2010 and 23-28 April 2011 events. To investigate the atmospheric processes associated with these events, a large global ensemble dataset, such as the The Observing System Research and Predictability Experiment (THORPEX) Interactive Grand Global Ensemble (TIGGE, Bougeault et al. 2010), will be used. In 2007, seven global ensembles in the TIGGE data archive became available and accessible to the public, providing an opportunity to explore new dimensions in early flood forecasting and warning (Pappenberger et al. 2008). The TIGGE dataset allows for quantitative analysis of synoptic- and mesoscale factors associated with the development of heavy precipitation.

The models that will be used are the ECMWF EPS, NCEP EPS, and UKMET EPS. Because the ECMWF, NCEP, and UKMET had complete forecast data for the years 2007 to 2011, these were the only three numerical models used in the present study. The ECMWF EPS is a 51-member ensemble with a spectral truncation of T639 (corresponding to approximately 32-km horizontal grid spacing) and 62 vertical levels through 240 forecast hours (10 days) (ECMWF 2010). The ECMWF EPS contains a control run and 50 members that are initially perturbed by singular vectors in pairs (i.e., a positive and negative perturbation) and by stochastic physics (ECMWF 2012). Singular vectors have been studied considerably in weather prediction models (Buizza and Palmer 1995, Palmer 2000). The singular vector perturbations within the ECMWF EPS have a horizontal scale of T42 with 62 vertical levels and are designed so that their impact is maximized over Europe at 48 hours into the forecast. Forecasts for all 51 members were obtained on a 0.5° latitude by 0.5° longitude grid from the TIGGE archive (information online at http://tigge-portal.ecmwf.int). Additional information about the ECMWF EPS can be found in Molteni et al. (1996) and Buizza et al. (2007) and references therein. The NCEP EPS is a 21-member ensemble comprising a control run and 20 members with spectral truncation of T254 (corresponding to approximately 90-km horizontal grid spacing) through 192 forecast hours (8 days) and a spectral truncation of T190 (corresponding to approximately 90-km horizontal grid spacing) through 384 forecast hours (16 days). The NCEP EPS consists of 42 vertical levels. An ensemble transform with rescaling (ETR) method is implemented to create initial perturbations (Wei et al. 2008). The UKMET EPS is a 25-member ensemble, comprising a control run and 24 members, at approximately 60-km resolution with 70 vertical levels through 360 forecast hours (15 days). The local ensemble transform Kalman filter (ETKF) is used to generate the initial condition perturbations within the ensemble, with model uncertainty

perturbations prescribed by stochastic kinetic energy backscatter scheme (SKEB, Bowler et al. 2009). Below is a table of all model upgrades for the three numerical models - ECMWF, NCEP, and UKMET EPS (Table 3.2). Between 2007 and 2011, each of the three models made horizontal resolution upgrades. In January 2010, the ECMWF increased from a resolution of T399 (0.4 degree) to T639 (0.25 degree) for day 1 to 10 forecasts. The NCEP increased horizontal resolution from T126 (1.4 degree) to T190 (0.9 degree) in February 2010. Lastly, in March 2010, the UKMET increased horizontal resolution from 90 km (38 levels) to 60 km (70 levels, Table 3.2).

Table 3.2: Listing of the three numerical models used for this study and all model upgrades associated with each model.

ECMWF		NCEP		UKMET	
Jan-10	•Day 1-10: T639 truncation (0.25 degree) •To day 15: T319 truncation (0.5 degree) •Same upgrades made to control run	**Feb-12**	•0-192 hours: T254 truncation (0.75 degree), 42 levels •192-384 hours: T190 truncation (0.9 degree), 42 levels	**Mar-10**	•60 km resolution (0.56 x 0.83 degree), 70 levels
Nov-06	•Forecast extended to 15 days •Day 1-10: T399 truncation (0.4 degree), 62 levels •To day 15: T255 truncation (0.75 degree), 62 levels •Two constant-resolution forecasts for calibration and validation purposes: at T399 truncation, 62 levels and at T255 truncation, 62 levels for full forecast time day 1-15	**Feb-10**	•T190 truncation (0.9 degree), 28 levels	**Sep-08**	•24 members •90 km resolution, 38 levels •Forecast extended to 15 days
		Mar-07	•20 members		
		May-06	•14 members		
		Aug-05	•T126 truncation (1.4 degree), 28 levels		
		Mar-04	•Day 0-7.5: T126 truncation (1.4 degree), 28 levels •Day 7.5-16: T62 truncation (2.9 degree), 28 levels		
Sep-05	•TL399 linear truncation (0.4 degree), 62 levels •Control run at TL399L62				
		Jan-01	•Day 0-3.5: T126 truncation (1.4 degree), 28 levels •Day 3.5-16: T62 truncation (2.9 degree), 28 levels		
Nov-00	•TL255 linear truncation (0.75 degree), 40 levels •Control run at TL255L40				
Oct-99	•TL159 linear truncation (1.125 degree), 40 levels •Control run at TL159L40	**Jun-00**	•10 members •Day 0-2.5: T126 truncation (1.4 degree), 28 levels •Day 2.5-16: T62 truncation (2.9 degree), 28 levels		
Dec-96	•50 members •TL159 linear truncation (1.125 degree), 31 levels	**Mar-94**	•10 members at 00 UTC •4 members at 12 UTC		
Dec-92	•32 members •T63 truncation (2.8 degree), 19 levels		•T62 truncation (2.9 degree), 28 levels		
		Dec-92	•2 members •T62 truncation (2.9 degree), 18 levels		

3.4 Use of ensemble forecasts

One benefit of using operational forecasts is that they are readily available. Operational forecasts also allow for the opportunity of studying multiple cases with very little computation. A significant disadvantage of using operational forecasts is that it is not possible to run sensitivity tests or experiment with these forecasts; the data are fixed. Considering the countless impacts that heavy rainfall and flooding have on society, there is a need to further research and understand the processes that lead to extreme precipitation events. Following the work of Schumacher (2011), the remainder of the study will use ensemble forecasts in order to analyze the synoptic- and mesoscale factors that led to the development of the 29 April-4 May 2010 and the 23-28 April 2011 widespread rain events. The ECMWF EPS is the primary ensemble forecast that will be used. The ensemble prediction system provides information on the probability of the event occurring and allows an objective risk assessment (Böttger et al. 2011). This would include evaluating model performance and determining how far in advance an event such as the 29 April-4 May 2010 widespread rain event and the 23-28 April 2011 widespread rain event could have been predicted. As pointed out by Lorenz (1963), slightly differing initial states of the atmosphere can evolve into considerably different states of the atmosphere, allowing the use of an ensemble system to be very beneficial by providing multiple outcomes for the atmosphere based on the number of ensemble members. Ensemble forecasts from other centers were considered, notably NCEP. However, the ECMWF EPS was chosen because of its large number of ensemble members and because it has a well tuned ensemble spread (Park et al. 2008). Additionally, Froude et al. (2007) found that the ECMWF EPS has a slightly higher level of skill than does the NCEP EPS in the Northern Hemisphere for predicting extratropical cyclones.

3.5 Evaluation of precipitation forecasts

One metric used in this study is the area under the relative operating characteristic (ROC) curve [hereafter ROC area; Wilks (2005)]. The ROC area is used to evaluate model performance of the 22 widespread rain events. For simplicity, the ROC area is calculated without accounting for the varying climatology, as suggested by Hamil and Juras (2006); it is compared with a random reference forecast with area 0.5. The ROC area is calculated using Eqs. (10)–(12) of Hamill and Juras (2006). The hit rate (HR) for the *i*th sorted member forecast is defined as:

$$HR_i = \frac{a_i}{a_i + c_i} \tag{3.1}$$

Similarly, the false alarm rate (FAR) is defined as:

$$FAR_i = \frac{b_i}{b_i + d_i} \tag{3.2}$$

Then an approximate integral ROC area can be calculated as:

$$\text{ROC area}_f = \sum_{i=1}^{n+1} \frac{(FAR_i - FAR_{i-1})(HR_i + HR_{i-1})}{2} \tag{3.3}$$

A perfect forecast has a ROC area = 1.0, and forecasts that are random draws from climatology are presumed to provide a ROC area = 0.5. The ROC area was calculated for three precipitation thresholds – 50, 100, and 150 mm. Overlaid on the ROC area are error bars. The error bars are calculated using the same methodology of Gallus et al. (2007). Statistical significance testing of differences in the ROC areas associated with each model is performed using a permutation test. For this study, the number of permutations taken was 1000.

For the individual case studies, rather than reviewing the forecasts of all 51 ECMWF ensemble members, subsets of the most accurate and the least accurate ensemble members from each forecast were focused on. In order to determine which ensembles members were most

accurate and least accurate, the spatial distribution of precipitation was analyzed. The forecasted precipitation of each ensemble member was subjectively compared to the CPC precipitation dataset to determine the skill in its forecasts. This comparison focused on the spatial distribution of the heavy rainfall as well as the maximum observed precipitation. Additionally, the observed five-day area-averaged precipitation was calculated within a thick black box encompassing part of the eastern United States and then compared to the five-day area-averaged precipitation of the forecasted ensemble members (shown later in the study).

The equitable threat score (ETS) was the final method used to determine the most accurate and least accurate ensemble members, also known as the Gilbert Skill Score (GS, Schaefer 1990). The ETS measures the fraction of observed and/or forecast events that were correctly predicted over a given threshold, and is adjusted for hits associated with random chance (Eqns. 3.1 and 3.2). A value of 1 is a perfect forecast and a value of zero is a forecast with no skill relative to chance. The absolute minimum ETS is -1/3. The ETS is commonly used to assess the skill of forecasts, in particular, precipitation forecasts (Rogers et al. 1995, Hamill 1999, Bayler et al. 2000, Stensrud et al. 2000, Xu et al. 2001, Ebert 2001, Gallus and Segal 2001, Chien et al. 2002, Accadia et al. 2003, Craig et al. 2011). Hamill and Juras (2006) demonstrate the geographic dependence of the ETS, with the ETSs being much larger in the southeast United States and along the west coast than in the northwestern Great Plains. The ETS is believed to be strongly related to event frequency, with a larger ETS in locations where precipitation events occur more frequently. Additionally, the ETS shows a clear seasonal dependence, with a higher ETS in winter when rain is associated mainly with synoptic-scale systems, while in summer the ETS is lower, reflecting the greater difficulty in forecasting convective rainfall (Ebert et al. 2003). The ETS is defined by:

$$\text{ETS} = \frac{\text{hits} - \text{hits random}}{\text{hits} + \text{misses} + \text{false alarms} - \text{hits random}}, \quad (3.4)$$

$$\text{where hits random} = \frac{(\text{hits} + \text{misses})(\text{hits} + \text{false alarms})}{\text{hits} + \text{misses} + \text{false alarms} + \text{hits random}} \quad (3.5)$$

For further details on the definition of the ETS, see CAWCR (2010).

A single ETS will also be calculated for the entire ECWMF ensemble, in an effort to compare the forecast skill of the two individual case studies. In contrast to before, this will be done by summing all the hits, misses, false alarms, and hits random from each of the ensemble members. These totals will then be used to calculate one ensemble ETS (Eqns. 3.3 and 3.4). The ensemble ETS is defined by:

$$\text{ETS} = \frac{\text{total hits} - \text{total hits random}}{\text{total hits} + \text{total misses} + \text{total false alarms} - \text{total hits random}}, \quad (3.6)$$

$$\text{where total hits random} = \frac{(\text{total hits} + \text{total misses})(\text{total hits} + \text{total false alarms})}{\text{total hits} + \text{total misses} + \text{total false alarms} + \text{total hits random}} \quad (3.7)$$

3.6 Correlations

As an alternate method of analysis, linear correlation plots were created and analyzed for the two selected case studies. The linear correlations relate area-averaged precipitation to several atmospheric variables. The correlation coefficient measures the strength of the linear relationship between area-averaged precipitation and the variable of interest at each grid point and forecast time, on a scale from -1 to 1. If the correlation coefficient is close to 1 (-1), the data are tightly clustered around a line with a positive (negative) slope (Larget 2005). A correlation coefficient near 0 is indicative of a weak linear relationship between the area-averaged precipitation and the variable of interest. Correlations with magnitudes greater than approximately 0.36 are statistically different from zero at the 99% confidence level using a two-tailed significance test, assuming that beyond forecast hour 36 the 51 ensemble members of the ECMWF are equally

likely. The correlation between variables shows the presence of linear relationships that can be used along with physical interpretation to understand the behavior of the ensemble forecasts.

CHAPTER 4

COMPARISON OF THE ECMWF, NCEP, AND UKMET EPS

4.1 Numerical model evaluation

Figs. 4.1a-i show area under the ROC curve for the 22 widespread precipitation events forecasted by each EPS, at precipitation thresholds of 50, 100, and 150 mm. By comparing area under the ROC curve for each forecast, one can determine the type of events that are better predicted by each numerical model, as well as, if the model has improved with time through the 5 year period. It also becomes apparent if one model generally has a better forecast than the others. Looking first at the ROC curve for the ECMWF at a 50 mm threshold, a majority of the events were skillfully forecasted. Ten days prior to the onset of the event, the events 8-13 December 2008, 5-10 October 2009, 18-23 January 2010, 26 September-1 October 2010, and 25-30 August 2011 had a ROC area above 0.9 (Fig. 4.1a). These events were either due to a landfalling tropical cyclone or a synoptic cyclone tracking across the United States. The synoptic cyclone event from 18-23 January 2010 was even better predicted at a threshold of 100 mm (Fig. 4.1b). Also, at the 150 mm threshold the 18-23 January 2010 synoptic scale event was well forecasted, with the exception of the longest lead times (Fig. 4.1c). The other synoptic type events that took place were 15-20 March 2008, 24-29 March 2009, 26-31 October 2009, 29 April-4 May 2010, and 23-28 April 2011, all of which have a relatively good forecast, even 10 days prior to the event taking place. Interestingly, the event that took place 4-9 June 2008, which was a series of MCSs passing through the upper Midwest, had a good forecast at long lead times but then began to worsen at short lead times (Fig. 4.1a). At the 150 mm threshold, the event from 1-6 September 2008 was well predicted at even the longest lead time (Fig. 4.1c). This event was

landfalling Hurricane Gustav that entered the United States through Louisiana, when it then began to slowly track poleward. Again, tropical cyclones appear to be a well-forecasted phenomena by the ECMWF. However, back at the 50 mm threshold, Tropical Storm Fay, 22-27 August 2008, was poorly forecasted at the longest lead time but very well forecasted at all the subsequent lead times (Fig. 4.1a). At each threshold, the event that occurred on 25-30 June 2007 had a forecast of little to no skill at the longest lead time shown, but then showed improvement at short lead times (Figs. 4.1a-c). The cases from 2007 and 2008 are discussed in greater detail in Schumacher and Davis (2010). With time, the ECMWF model appears to show much improvement. The forecasts with the lowest ROC area tend to have occurred prior to 2009, with the best forecasts occurring during the years 2010 and 2011. In January of 2010, the ECMWF upgraded the horizontal resolution of its EPS from a spectral truncation of T399 (0.4 degree) to T639 (0.25 degree), likely contributing to the increased forecast skill in 2010 and 2011 (Table 3.1).

Looking now at the ROC curve for the NCEP at a 50 mm threshold, not a single forecast has done as well as the ECMWF, with an exception of the 23-28 April 2011 widespread rain event. The synoptic cyclone events that took place 18-23 January 2010 and 23-28 April 2011 maintained a skillful forecast throughout the 10 day forecast period (Fig. 4.1d). At the 100 mm threshold, the 18-23 January 2010 synoptic cyclone event was even better predicted. The events from 29 April-4 May 2010 and 23-28 April 2011 were well predicted at a threshold of 100 mm, with the exception of the longest lead time (Fig. 4.1e). Looking back at the 50 mm threshold, the events 15-20 March 2008, 8-13 December 2008, and 26-31 October 2009 were not well predicted (Fig. 4.1d). In February of 2010, the NCEP increased the spectral truncation of their EPS from T126 (1.4 degree) to T190 (0.9 degree), likely helping to better predict synoptic scale

events in 2010 and 2011 (Table 3.1). Tropical Storm Fay, 22-27 August 2008, was very poorly predicted, continually jumping from a decent forecast to a forecast of absolutely no skill relative to chance. Landfalling Hurricane Gustav, 1-6 September 2008, was also poorly predicted by the NCEP EPS. Tropical Storm Nicole, 26 September-1 October 2010, and Hurricane Irene, 25-30 August 2011, were well predicted for the majority of the forecast period, however, appear to have had a few poor initialization times throughout (Fig. 4.1e). It appears that with time, the NCEP has made large improvements to the prediction of tropical cyclone rainfall, likely attributed to the increase in horizontal resolution of the EPS (Table 3.1). As mentioned before, at the 50 mm threshold, the event that occurred on 25-30 June 2007 had a very poor forecast at the longest lead time shown, but then showed improvement at short lead times (Fig. 4.1d). At higher thresholds however, the event was forecasted with almost no skill relative to chance (Figs. 4.1e and 4.1f).

Finally, looking at the ROC curve for the UKMET at a 50 mm threshold, the forecasts appear to be much better than the NCEP EPS, more comparable to the ECMWF EPS. Tropical Storm Nicole, 26 September-1 October 2010, was very well predicted throughout the 10 day forecast period. Tropical Storm Fay, 22-27 August 2008, Hurricane Ida, 9-14 November 2009, Hurricane Irene, 25-30 August 2011, and Tropical Storm Lee, 3-8 September 2011 were also well forecasted with the exception of early initialization times. However, landfalling Hurricane Gustav, 1-6 September 2008, was very poorly predicted throughout the majority of the 10 day forecast period (Fig. 4.1g). Majumdar and Finocchino (2010) studied this case in greater detail using both the ECMWF and UKMET. It appears that the prediction of rainfall from land falling hurricanes and tropical storms by the UKMET has improved over the 5 years of data shown. In September 2008, the UKMET increased the horizontal resolution of their EPS from 90 km (with

38 levels) to 60 km (with 70 levels), likely contributing to the improvements in forecasting land falling hurricanes and tropical storms (Table 3.1). The synoptic cyclone impacting the Mississippi Valley on 5-10 October 2010 remained very well forecasted throughout the entire forecast period. The synoptic cyclone events that took place 24-29 March 2009 and 18-23 January 2010 remained extremely well predicted, with the exception of the longest lead time (Fig. 4.1g). Even at a threshold of 100 mm, the event from 18-23 January 2010 was well forecasted (Fig. 4.1h). Interestingly, at the 50 mm threshold, the widespread rain event from 8-13 December 2008 was extremely well forecasted at the longest lead times, but then the forecast skill decreased at the shortest lead times (Fig. 4.1g). As mentioned before, at each threshold, the event that occurred on 25-30 June 2007 had a very terrible forecast at the longest lead time shown, but then showed improvements at short lead times (Figs. 4.1g-i). This event was poorly forecasted by each of the three models, indicating models might need improvement in resolving MCVs that produce widespread precipitation. On the other hand, high precipitation MCVs may have low predictability overall.

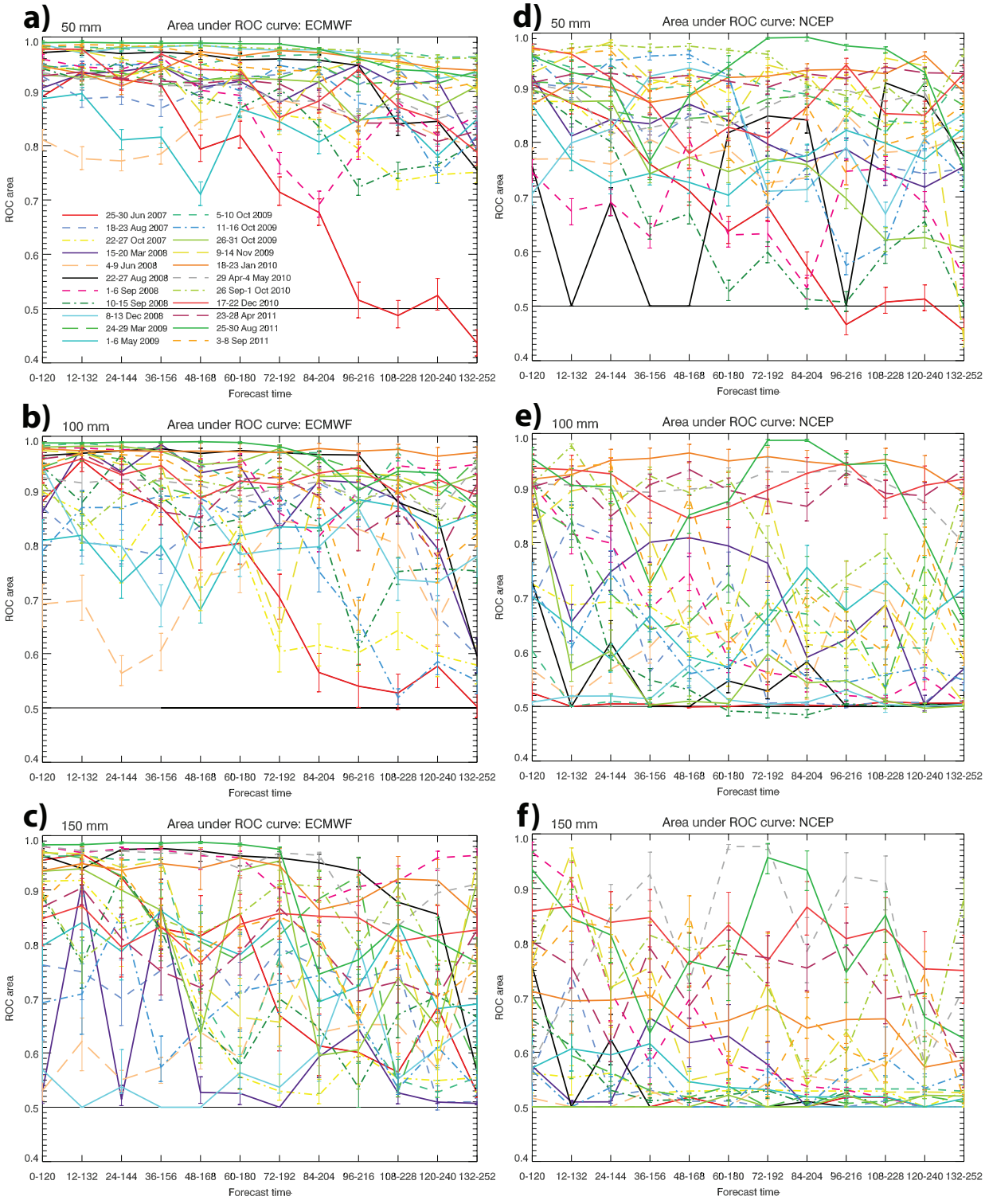
a)
50 mm
Area under ROC curve: ECMWF
ROC area
Forecast time
25-30 Jun 2007
18-23 Aug 2007
22-27 Oct 2007
15-20 Mar 2008
4-9 Jun 2008
22-27 Aug 2008
1-6 Sep 2008
10-15 Sep 2008
8-13 Dec 2008
24-29 Mar 2009
1-6 May 2009
5-10 Oct 2009
11-16 Oct 2009
26-31 Oct 2009
9-14 Nov 2009
18-23 Jan 2010
29 Apr-4 May 2010
26 Sep-1 Oct 2010
17-22 Dec 2010
23-28 Apr 2011
25-30 Aug 2011
3-8 Sep 2011
d)
50 mm
Area under ROC curve: NCEP
b)
100 mm
Area under ROC curve: ECMWF
e)
100 mm
Area under ROC curve: NCEP
c)
150 mm
Area under ROC curve: ECMWF
f)
150 mm
Area under ROC curve: NCEP
0-120 12-132 24-144 36-156 48-168 60-180 72-192 84-204 96-216 108-228 120-240 132-252

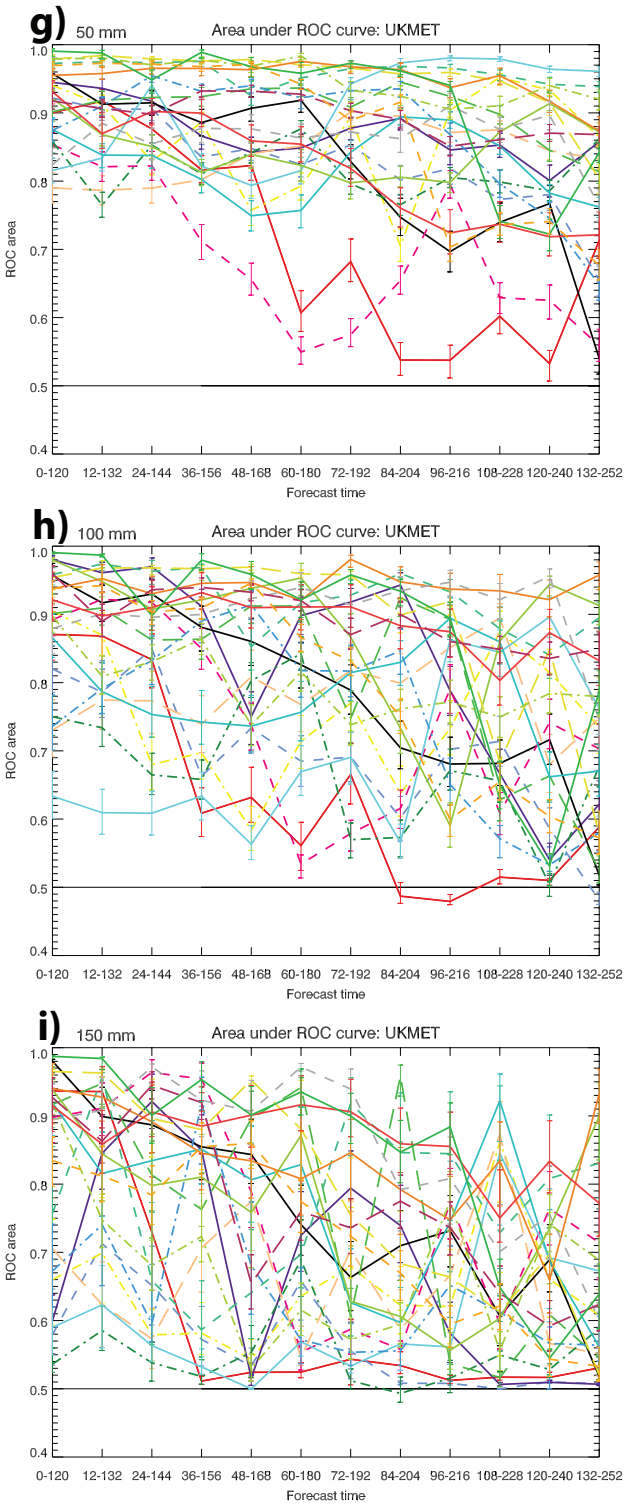

Figure 4.1: Area under the ROC curve for the ECMWF, NCEP, and UKMET ensembles for the 22 widespread 5-day precipitation events. Shown are 120-hr precipitation accumulation thresholds for (a), (d), and (g) 50, (b), (e), and (h) 100, and (c), (f), and (i) 150 mm. The ROC area does not account for seasonal climatology. A perfect forecast has a ROC area of 1; a random reference forecast has an area of 0.5. Note that the legend for ECMWF ensemble is also valid for both the NCEP and UKMET ensemble.

Table 4.1 provides a list of how many of the 22 widespread rain events were most accurately forecasted by each of the ensemble prediction systems at each lead time at a threshold of 50 mm using the ROC area. This table essentially summarizes the results from Fig. 4.1 at a threshold of 50 mm. The most skillful forecasts at both the shortest and longest lead times were from the ECMWF. For many of the widespread rain events, all three ensemble prediction systems were able to accurately forecast the precipitation at the shortest lead time (Table 4.1).

Table 4.1: Listing of how many of the 22 widespread rain events were most accurately forecasted by each of the ensemble prediction systems at each lead time at a threshold of 50 mm. "ECMWF/NCEP/UKMET" means that not one of the ensemble prediction systems was better than another; there was no obvious better forecast. "ECMWF/UKMET","ECMWF/NCEP", and "NCEP/UKMET" means the two listed ensemble prediction systems had the most accurate forecast. The method for the bootstrap error bar calculation was the method used for determining the superior forecasts.

Lead time (hours)	0-120	12-132	24-144	36-156	48-168	60-180	72-192	84-204	96-216	108-228	120-240	132-252
ECWMF	5	9	10	10	10	12	8	7	7	8	6	11
NCEP					1		2	3	2	3	2	2
UKMET		2	1	2	1	1	1	2	4	4	3	5
ECMWF/UKMET	6	4	4	6	6	6	7	8	4	4	1	
ECMWF/NCEP	3	1	1					1	1	1	4	3
NCEP/UKMET			1						2		1	
ECMWF/NCEP/UKMET	8	6	5	4	4	3	4	1	2	2	5	1
TOTAL	22	22	22	22	22	22	22	22	22	22	22	22

4.2 Individual case evaluation

4.2.1 25-30 June 2007

The precipitation producer for this event was a mesoscale convective vortex (MCV, Bartels and Maddox 1991) that up scaled into a much larger warm-core vortex over the southern plains on the United States (Goebbert et al. 2008). Schumacher and Davis (2010) analyzed this event, among eight other events, using the ECMWF to assess forecast skill and uncertainty. Schumacher (2011) used operational global ensemble forecasts from the ECMWF to examine the factors contributing to, or inhibiting, the development of this long-lived continental vortex and

its associated rainfall. At the 50 mm threshold, each of the three models went from having a very poor forecast at the longest lead time, to a good forecast at the shortest lead time. At the longest lead times, both the ECMWF and NCEP had a forecast with absolute no skill relative to chance (Fig. 4.2a). This is due to these models not predicting any heavy rain in the southern plains of the United States. The UKMET forecasted for a chance of 50 mm precipitation 10 days prior to the occurrence of the event (not shown). At a 100 mm threshold, both the ECMWF and UKMET showed improvement in their forecast for this event, however, the NCEP had almost no forecast skill for the entire 10 day period (Fig. 4.2b). The NCEP did not forecast for any precipitation exceeding 100 mm for the entire forecast period (not shown). Lastly, at the 150 mm threshold, the ECMWF was the only model to consistently make improvements throughout the forecast period. The NCEP forecasted with little to no skill, while the UKMET had very little skill with the exception of the shortest lead times (Fig. 4.2c). Again, the NCEP did not forecast for any precipitation exceeding 150 mm for the entire forecast period. At the shortest lead times, the UKMET started to pick up on heavy precipitation in the southern plains of the United States (not shown).

4.2.2 22-27 August 2008

The widespread flooding for this event was a result of Tropical Storm Fay. From 19 to 23 August 2008, Tropical Storm Fay moved slowly across Florida, continued into Alabama and Mississippi from 23 to 25 August 2008, and finally curved northeastward. The slow-moving Fay allowed for large rainfall totals across the southeastern United States. Looking at the 50 mm threshold, the ECMWF had an outstanding forecast with the exception of the longest lead times (Fig. 4.2d). At these longer lead times, the ECMWF had misplaced the heavy precipitation to the east (not shown). The UKMET began with a poor forecast, gradually making improvements at

shorter lead times (Fig. 4.2d). Similar to the ECMWF, the UKMET initially forecasted for the heavier rainfall totals to be too far to the southeast (not shown). The NCEP is missing data for the following forecasts at all three precipitation thresholds: 96-216 hrs, 48-168 hrs, 36-156 hrs, and 12-132 hrs (Fig. 4.2d). Initially, the NCEP had forecasted for heavy precipitation in the southeastern United States, however, at the shorter lead times the NCEP misplaced the large core of heavy precipitation to the south (not shown). At both the 100 and 150 mm thresholds, the ECMWF maintained a great forecast for the majority of the forecast period, except at the longest lead times, again misplacing the heavy precipitation amounts to the east (not shown). The UKMET was very similar with the exception that it took much longer for their model to make advances in the forecast. The NCEP demonstrated little to no skill throughout almost the entire forecast period, having not predicted for high rainfall amounts (Figs. 4.2e and 4.2f). At the shortest lead times, the NCEP forecasted for heavier rainfall totals but they were displaced to the southeast (not shown).

4.2.3 1-6 September 2008

From the 1 to 6 September 2008 Hurricane Gustav made landfall along the Louisiana/Alabama coast, providing the southern United States with high rainfall totals. Looking at the 50 mm threshold, the ECMWF maintained a fairly good forecast for this 10 day forecast period. There appears to be a few bad initialization times within the model, but overall the ECMWF had a good forecast (Fig. 4.2g). At the longest lead times, the ECMWF forecasted the heavier rainfall amounts to be located to far south, largely off the Louisiana coast, possibly under predicting the speed of landfalling Hurricane Gustav (not shown). Both the NCEP and UKMET gave a forecast with very little skill at the longest lead time, showing gradual improvements to their forecasts with time (Fig. 4.2g). At a threshold of 100 and 150 mm, the ECMWF had a great

forecast for Hurricane Gustav. The NCEP had a forecast of absolutely no skill relative to chance at the longest lead time, making steady advances with time throughout the 10 day forecast period. The UKMET began with a moderate forecast at long lead times, worsened for the next couple of lead times, and then finally showed improvements at the shortest lead times (Figs. 4.2h and 4.2i). Both the NCEP and UKMET had strong model agreement among their ensemble members that Hurricane Gustav would be located too far south for almost the entire forecast period (not shown). Again, the speed of this landfalling Hurricane may have been a challenge for all three numerical models.

4.2.4 18-23 January 2010

This event was brought upon the western coast of the United States when a synoptic cyclone swept through, producing heavy rain, both convective and orographic. At the 50 and 100 mm threshold, the ECMWF, NCEP, and UKMET had an outstanding forecast for this event, even 10 days in advance (Figs. 4.2j and 4.2k). It appears that this event was very well predicted with greater than 90% model agreement 10 days prior to the event (not shown). At a threshold of 150 mm, the ECMWF maintained a great forecast throughout this 10 day forecast period, accurately predicting the location of heaviest rainfall totals. The UKMET had a moderate forecast at the longer lead times, showing gradual advances in the forecast at shorter lead times. The NCEP maintained a not-so-great forecast for the entire forecast period at a threshold of 150 mm (Fig. 4.2l). Overall, it appears the NCEP did not anticipate rainfall totals exceeding 150 mm for this widespread rain event (not shown).

4.2.5 29 April -4 May 2010

This widespread precipitation event was characterized by two quasi-stationary mesoscale convective systems passing through Nashville, TN on the 1 and 2 May 2010 (Moore et al. 2012).

At both the 50 and 100 mm threshold, all three of the models maintained a skillful forecast for this precipitation event. The precipitation at a threshold of 100 mm was slightly better predicted than the smaller threshold value of 50 mm. The NCEP and UKMET had a poor forecast at the longest lead time but then demonstrated gradual improvements (Figs. 4.2m and 4.2n). At the longest lead time, both of these models placed the heaviest rainfall totals much too far west of the observed precipitation. The ECMWF extended the spatial distribution of this precipitation event too far west, however, maintained a great forecast overall (not shown). However, at the 150 mm threshold, the ECMWF outshined both the NCEP and UKMET. The ECMWF maintained skill throughout the entire forecast period. With an exception of the longest lead times, the ECMWF had pinpointed exactly where the heaviest rainfall amounts would be located. The UKMET had a poor forecast at the longer lead times, but showed improvements with time (Fig. 4.2o). Initially, the UKMET had forecasted the heaviest rainfall amounts to be much too far south (not shown). The NCEP, on the other hand, had a poor forecast at the longest lead time, showed major improvements at shorter lead times, and then plummeted to very little skill relative to chance at the shortest lead time (Fig. 4.2o). Ten days prior to the onset of the event, the NCEP had very little indication of rainfall exceeding 150 mm. As the event came closer, the NCEP was able to determine a nearly exact location for the heaviest rainfall amounts, with a ROC area of 0.990308 for the 72-192 hrs forecast. Finally, a day prior to the event, the NCEP displaced the 150 mm rainfall too far north, losing skill in their forecast (not shown).

4.2.6 23-28 April 2011

From 23 to 28 April 2011, a series of MCSs passed through the Mississippi Valley producing widespread flooding for the area. At the culmination of this event, violent and destructive tornadoes tore through Alabama, Arkansas, Georgia, Mississippi, North Carolina,

Virginia, Tennessee, and New York. At a threshold of 50 and 100 mm, the ECMWF, NCEP, and UKMET all had a forecast that remained good and steady through the entire forecast period (Figs. 4.2p and 4.2q). The ECMWF and UKMET initially displaced the heaviest precipitation to the northwest, explaining the decreased ROC score at the longest lead times (not shown). At the 150 mm threshold, each of the models demonstrates a lot more uncertainty. The ECMWF had a few poor forecasts throughout the forecast period but ended with a pretty good forecast at the shortest lead time (Fig. 4.2r). At the longest lead times, the ECMWF predicted the heaviest rainfall amounts too far to the west (not shown). The UKMET had a poor forecast at the longest lead time but gradually showed advances, having a great forecast at the shortest lead time (Fig. 4.2r). At these longest lead times, the UKMET had forecasted for the heavier rainfall totals to be located too far northwest (not shown). The NCEP began with a poor forecast, making slight improvements to their forecast throughout the 10 day forecast period (Fig. 4.2r). Overall, the NCEP had displaced the heaviest rainfall totals to the north of the observed 150 mm contour (not shown).

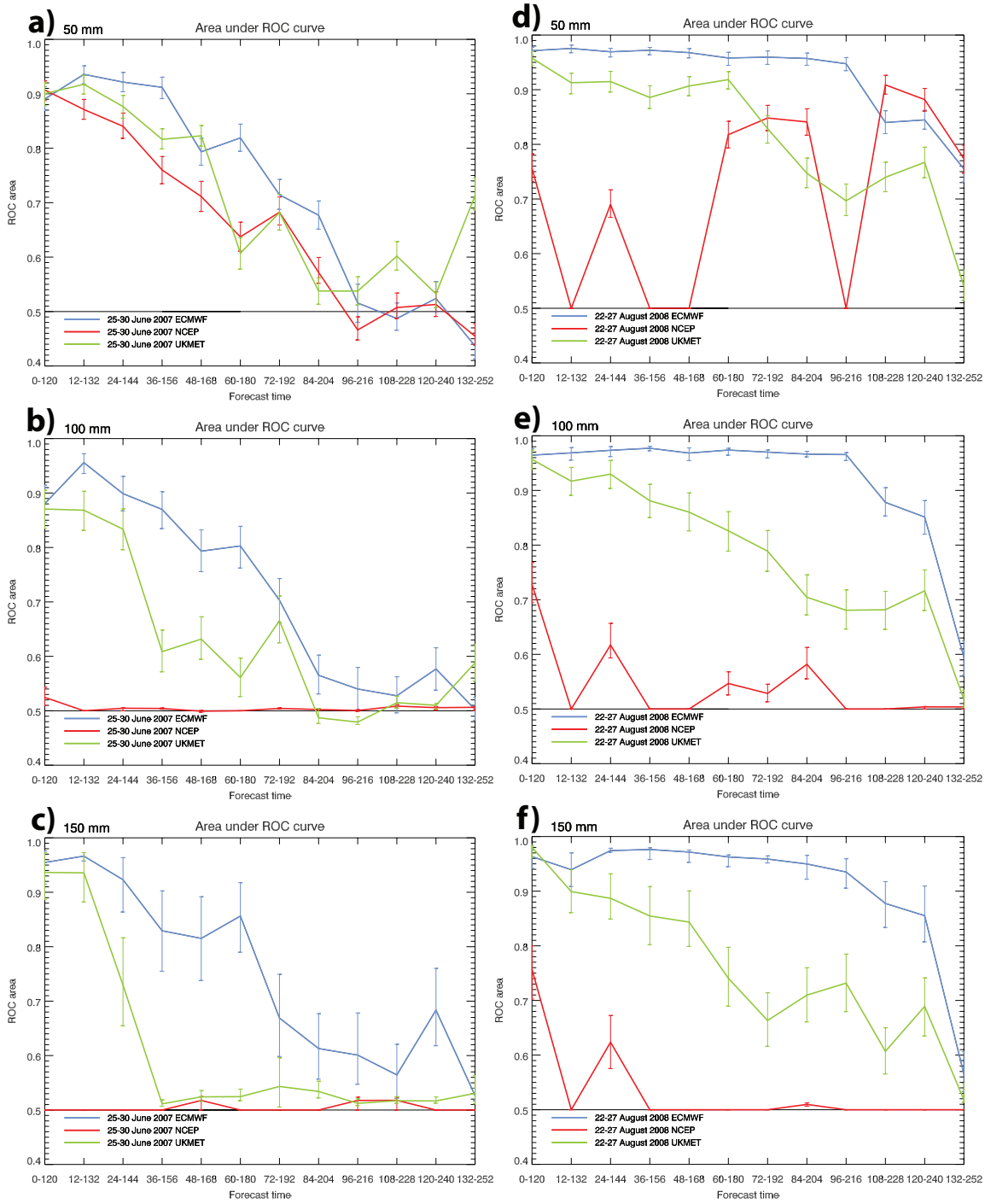
a) 50 mm
Area under ROC curve
ROC area
Forecast time
25-30 June 2007 ECMWF
25-30 June 2007 NCEP
25-30 June 2007 UKMET
d) 50 mm
Area under ROC curve
22-27 August 2008 ECMWF
22-27 August 2008 NCEP
22-27 August 2008 UKMET
b) 100 mm
Area under ROC curve
e) 100 mm
Area under ROC curve
c) 150 mm
Area under ROC curve
f) 150 mm
Area under ROC curve
0-120 12-132 24-144 36-156 48-168 60-180 72-192 84-204 96-216 108-228 120-240 132-252

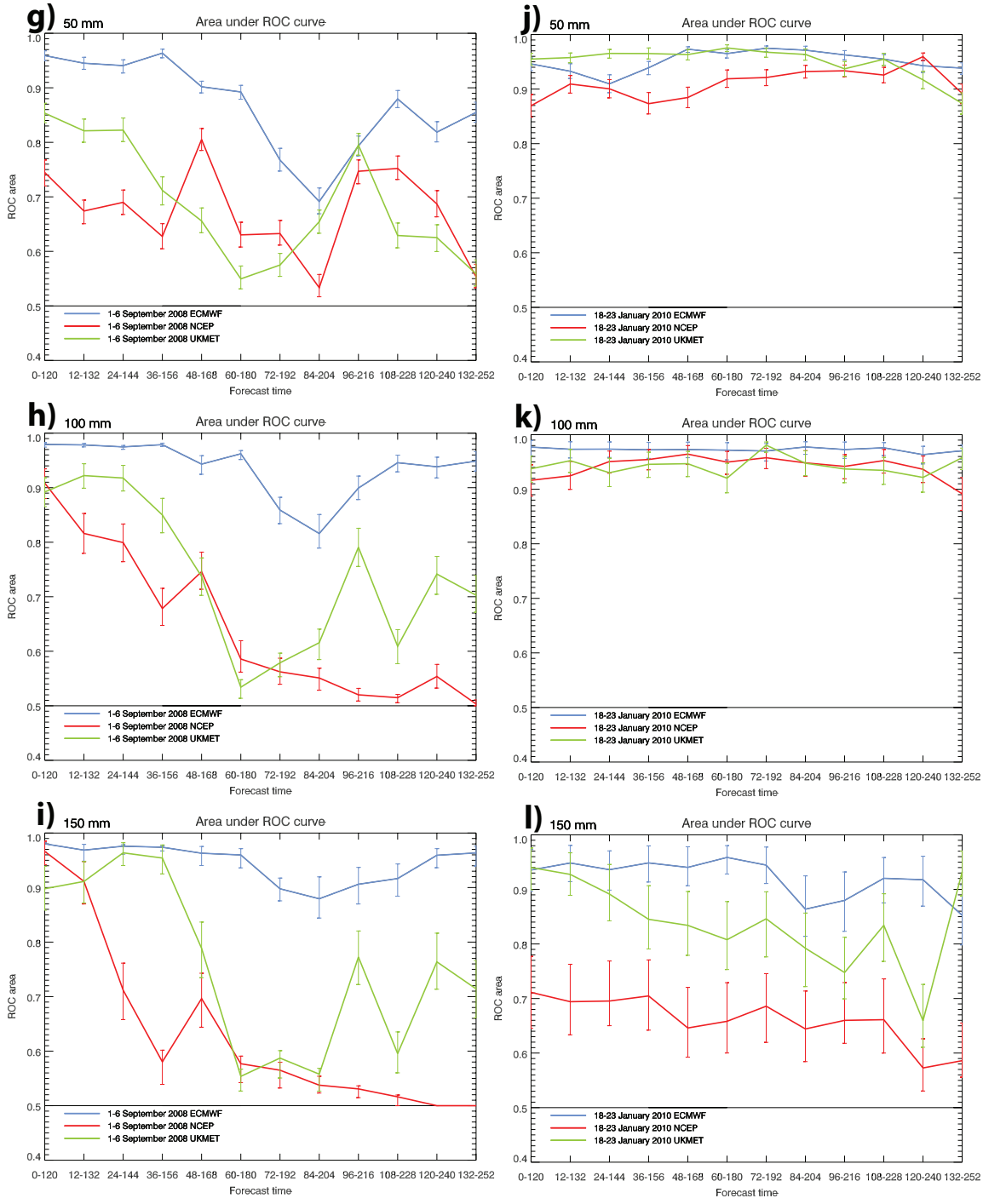
g) 50 mm
Area under ROC curve
ROC area
Forecast time
1-6 September 2008 ECMWF
1-6 September 2008 NCEP
1-6 September 2008 UKMET
j) 50 mm
Area under ROC curve
ROC area
Forecast time
18-23 January 2010 ECMWF
18-23 January 2010 NCEP
18-23 January 2010 UKMET
h) 100 mm
Area under ROC curve
ROC area
Forecast time
1-6 September 2008 ECMWF
1-6 September 2008 NCEP
1-6 September 2008 UKMET
k) 100 mm
Area under ROC curve
ROC area
Forecast time
18-23 January 2010 ECMWF
18-23 January 2010 NCEP
18-23 January 2010 UKMET
i) 150 mm
Area under ROC curve
ROC area
Forecast time
1-6 September 2008 ECMWF
1-6 September 2008 NCEP
1-6 September 2008 UKMET
l) 150 mm
Area under ROC curve
ROC area
Forecast time
18-23 January 2010 ECMWF
18-23 January 2010 NCEP
18-23 January 2010 UKMET

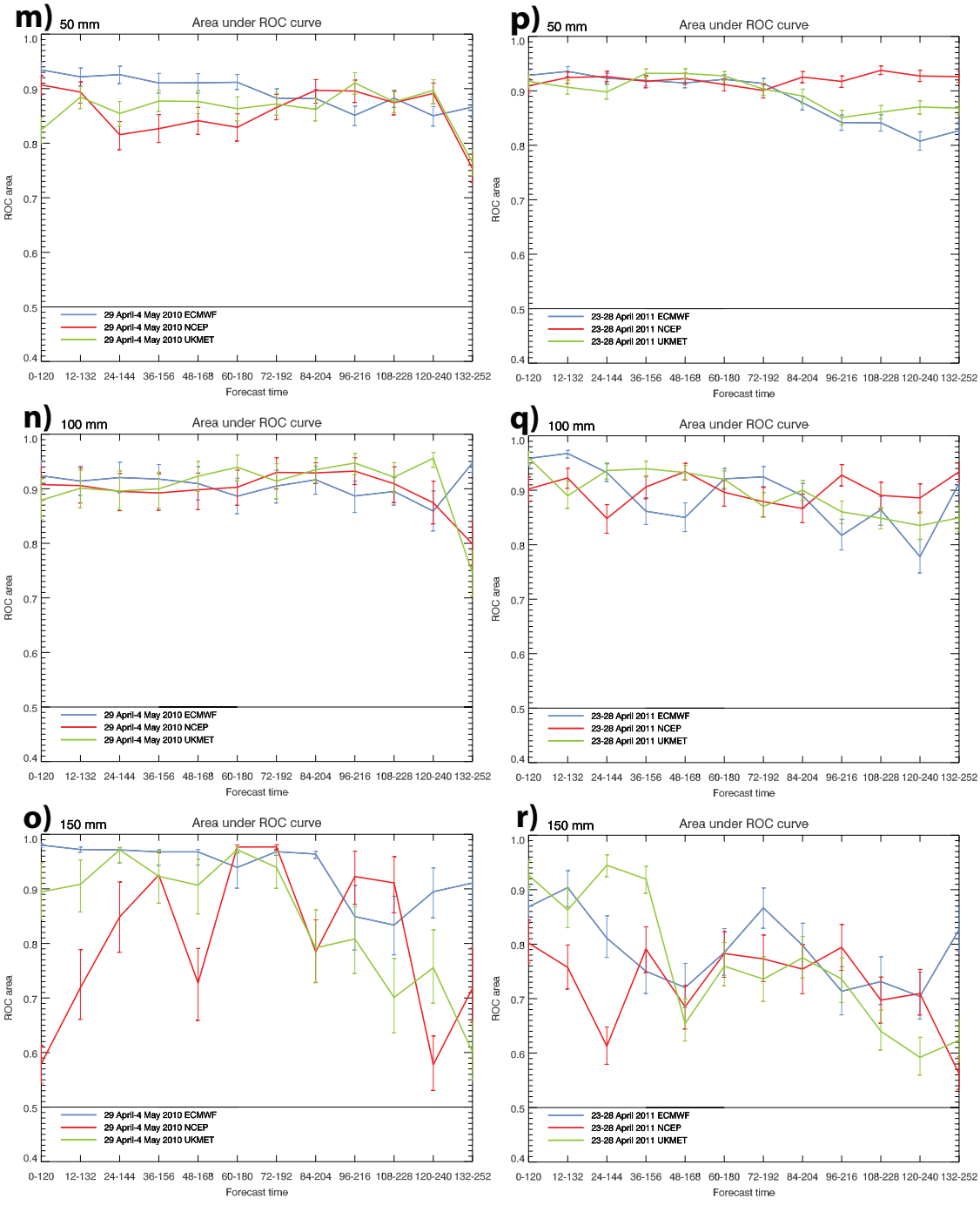

Figure 4.2: Area under the ROC curve for the ECMWF, NCEP, and UKMET ensembles for 6 of the 22 widespread 5-day precipitation events: 25-30 Jun 2007, 22-27 Aug 2008, 1-6 Sep 2008, 18-23 Jan 2010, 29 Apr-4 May 2010, and 23-28 Apr 2011. Shown are 120-hr precipitation accumulation thresholds for (a), (d), (g), (j), (m), and (p) 50, (b), (e), (h), (k), (n), and (q) 100, and (c), (f), (i), (l), (o), and (r) 150 mm. The ROC area does not account for seasonal climatology. A perfect forecast has a ROC area of 1; a random reference forecast has an area of 0.5. Note that the legend for ECMWF ensemble is also valid for both the NCEP and UKMET ensemble.

4.3 Discussion

Twenty-two widespread precipitation events were introduced in this study in an effort to determine which model, the ECMWF, NCEP, or UKMET, is better at predicting multiday, widespread rainfall events. The ECMWF demonstrated a skillful precipitation forecast for many types of events including tropical cyclones, synoptic cyclones, stationary fronts, etc. (Fig. 4.1a-c). The one type of scenario that the ECMWF, NCEP, and UKMET struggled the most with was the MCV in the southern plains (Fig. 4.2a-c). With time, the forecast skill of the ECMWF appears to have improved, likely attributed to the horizontal resolution increase in January 2010 from T399 (0.4 degree) to T639 (0.25 degree) valid out to 10 days (Fig. 4.1a-c, Table 3.1). The NCEP has battled more with maintaining a skillful forecast throughout the entire forecast period. The prediction of both tropical cyclone and synoptic cyclone events has drastically improved with time for the NCEP model, again due to the upgrade in the EPS from a resolution of T126 (1.4 degree) to T190 (0.9 degree, Fig. 4.1d-f, Table 3.1). Lastly, the UKMET has had regularly better forecasts than the NCEP, making this model more comparable to the ECMWF. More recently, forecasts for tropical cyclones have shown advances within the UKMET, likely a result of the spectral resolution increase in September 2008 from 90 km (38 levels) to 60 km (70 levels, Fig. 4.1g-i, Table 3.1). Of the three numerical models, the ECMWF appears to have outshined the other two. This result does not come as a surprise seeing as the ECMWF has consistently maintained a higher horizontal resolution than both the NCEP and the UKMET (Table 3.1). Overall, the ECMWF has produced a skillful forecast for each of the events, with an exception of the 25-30 June 2007 event, the MCV over the southern plains of the United States.

CHAPTER 5

CASE STUDY: 29 APRIL-4 MAY 2010 WIDESPREAD PRECIPITATION EVENT

5.1 Event overview

Beginning 1 May 2010 and lasting until 3 May 2010, Tennessee, Kentucky and Mississippi, experienced an extended period of heavy precipitation, resulting in destructive flooding and record rainfall in many locations. This rainfall was a result of two successive quasi-stationary mesoscale convective systems associated with an upper-level low pressure system that approached the eastern United States, along with a frontal boundary that stalled just west of Tennessee (Figs. 5.1a and 5.1b, Moore et al. 2012). Consistent with the findings of Glass et al. (1995) and Maddox et al. (1979) on heavy precipitation events, most of the heavy rainfall associated with the 29 April-4 May 2010 widespread precipitation event occurred during the overnight hours or occupied a large portion of the nocturnal hours. There was persistent tropical moisture transport from the Gulf of Mexico, feeding the heavy precipitation. The bulk of heavy rainfall pounded the Tennessee area, specifically Nashville. Nashville International Airport recorded over 160 mm (6 inches) of rain on 1 May 2010 and over 183 mm (7 inches) on 2 May 2010. The two-day rainfall total stood at 13.53 inches (Fig. 5.2). This more than doubled the previous two-day record of 6.68 inches set on 13-14 September 1979 (NOAA 2010c). Benton County, just to the west of Nashville, recorded approximately 19.41 inches of precipitation over this two-day period (NOAA 2010a). The Cumberland River, which winds through downtown Nashville, Tennessee, crested at 51.86 feet on 3 May 2010, spilling into the city and surrounding neighborhoods. It was the highest level recorded since the Cumberland River dam system was built in the early 1960s (NOAA 2010b). Property damages were estimated to total into the

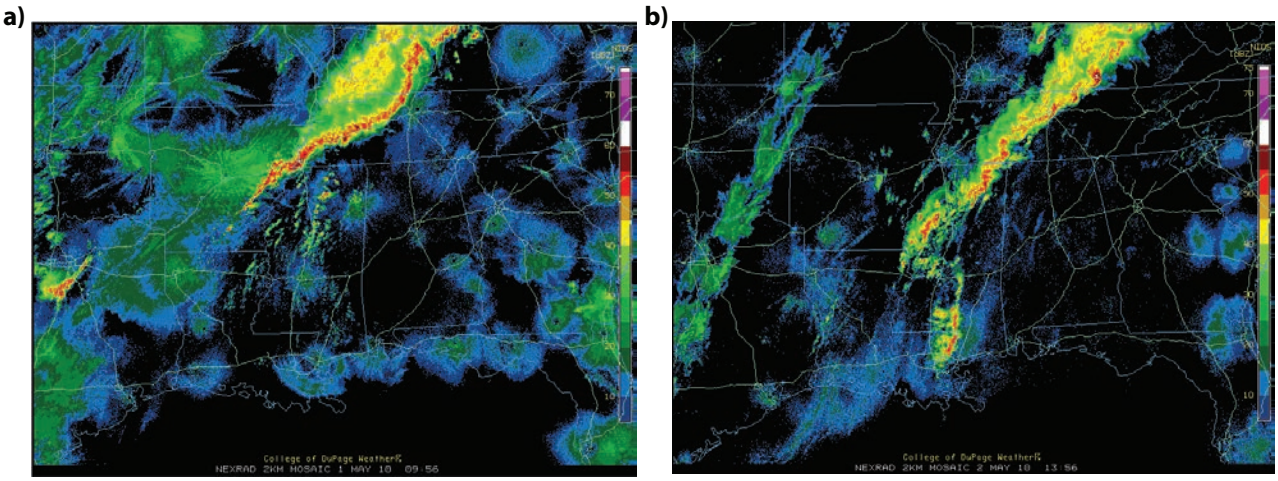

Figure 5.1: Radar reflectivity (color shading in dBZ) at (a) 0956 UTC 1 May 2010 and (b) 1356 UTC 2 May 2010.

hundreds of millions of dollars, which helped to prompt a Presidential Disaster Declaration for many counties in west and middle Tennessee (NOAA 2011b). In Greater Nashville, property damage exceeded $2 billion and 11 fatalities occurred with 18 other fatalities occurring in

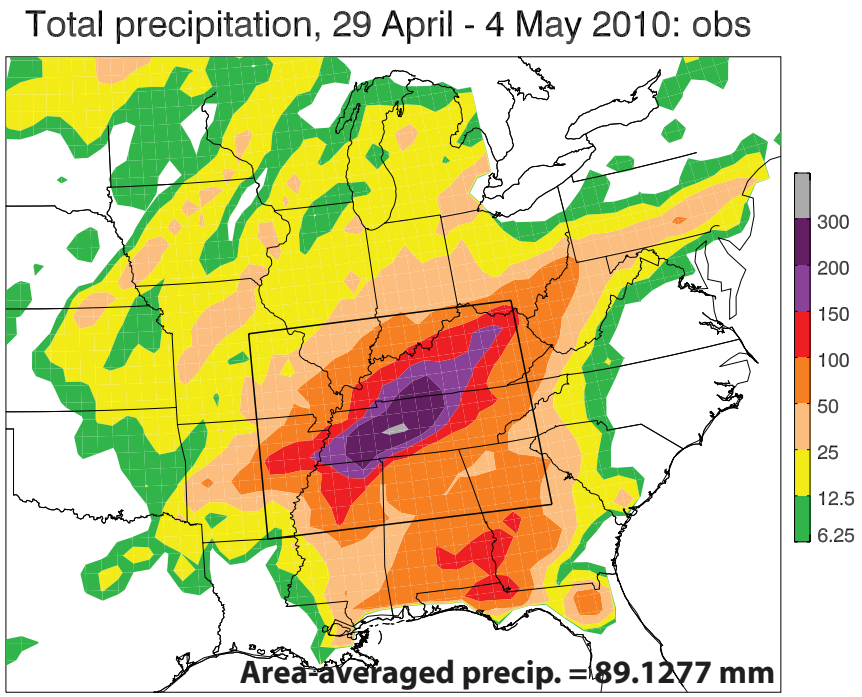

Figure 5.2: Five-day accumulated precipitation (color shading in mm) between 1200 UTC 29 April 2010 – 1200 UTC 4 May 2010. The black rectangle indicates the location for areal averaging of precipitation and other fields.

Middle Tennessee (NOAA 2011c). In the present study, medium-range ensemble forecasts of the 29 April 2010 to 4 May 2010 rain event will be examined to determine the reason why some ensemble members produced a long-lived, slow-moving precipitation system, and others did not. The overlying question is, what were the key factors that were favorable for, or detrimental to, the development of widespread, multiple day rainfall? Looking at the spaghetti plot at a threshold of 100 millimeters, the ECMWF ensemble members did a relatively good job forecasting the location of the event (Fig. 5.3). The remainder of the study will only show forecasts from the ECMWF EPS.

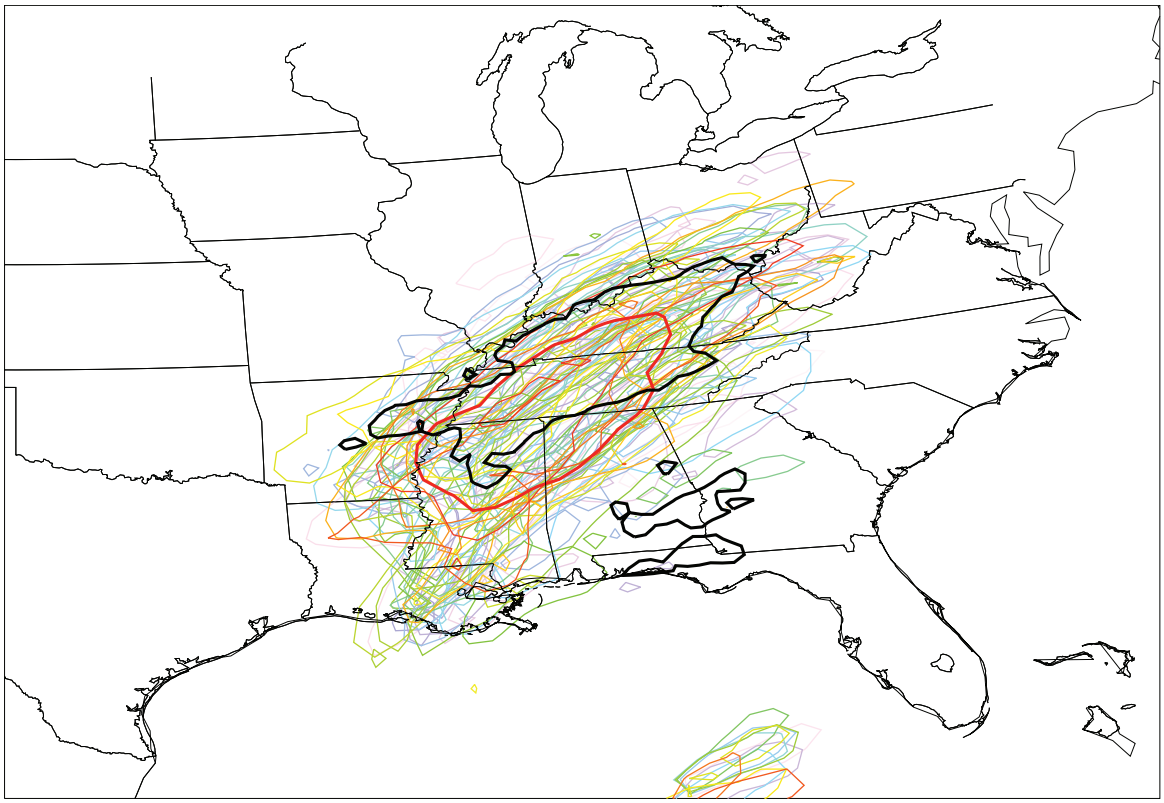

Figure 5.3: "Spaghetti" plot showing the predicted 100-mm rainfall contour from 1200 UTC 29 April 2010 – 1200 UTC 4 May 2010 from each ECMWF ensemble member in a different color. The observed 100-mm contour from 1200 UTC 29 April 2010 – 1200 UTC 4 May 2010 is shown in thick black. The ensemble mean 100-mm contour is shown in thick red. Initialization time of 1200 UTC 29 April 2010.

5.2 Synoptic analysis

The primary source for upper-level atmospheric observations and analyses is the University Corporation for Atmospheric Research (UCAR) image archive. Looking at the upper-level conditions at the time of the event, many factors contributed to the support of heavy precipitation across the eastern United States. At 1200 UTC 2 May 2010 at the 300-hPa level a deep trough stretches across the continental United States. Additionally, there is a jet streak oriented from the southwest to the northeast across the states of Arkansas, Illinois, and Michigan. Relative to the jet streak and the upper-level trough, Nashville, Tennessee is in an area of upper-level divergence, with convergence at the surface (Fig. 5.4a). This provides support for the development of thunderstorms throughout the Tennessee area. At the 500-hPa level, there is an area of absolute cyclonic vorticity being advected to the northeast, into the Kentucky, Tennessee area (Fig. 5.4b). Again, the advection of cyclonic vorticity provides support for convection across Tennessee. At the 700-hPa level, southerly flow is pulling in moisture from the Gulf of Mexico, up into the northeastern United States. Throughout the eastern United States, dew points are high, reaching a value of 12˚C in southern Mississippi and Alabama (Fig. 5.4c). With sufficient moisture present, heavy rainfall is imminent. At the 850-hPa level, slight warm air advection is present in the Tennessee area, and an apparent baroclinic zone exists. Warm coastal temperatures are being advected poleward, into Nashville and nearby areas. There is also indication of a nocturnal low level jet positioned over the southeastern United States, with the strongest winds overhead Alabama, Georgia, and Tennessee (Fig. 5.4d). The presence of a southerly low level jet becomes a key player in the moisture transport into the Mississippi Valley, promoting strong, persistent convection (Doswell 1994). Taking a look at the sounding

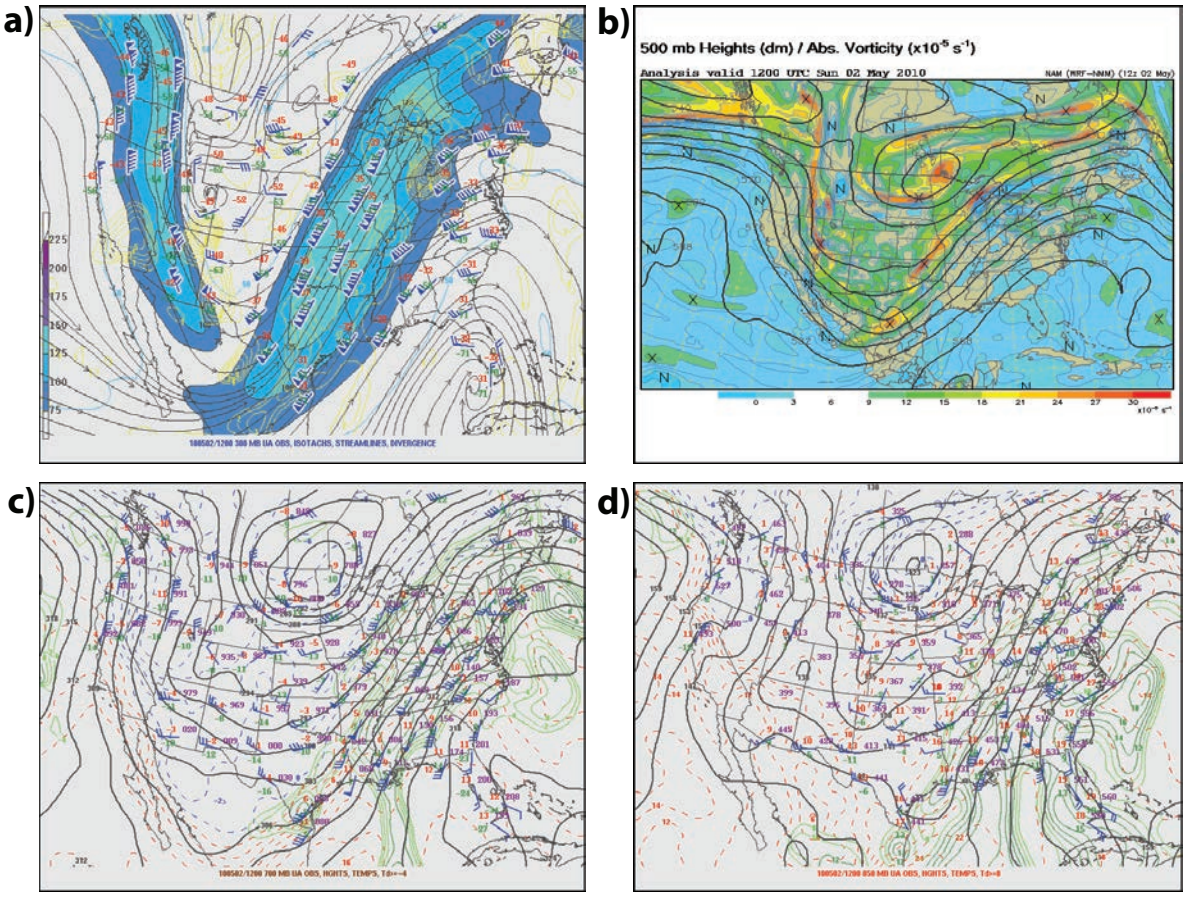

Figure 5.4: (a) 300-hPa wind (vectors in knots), isotachs (color shading in knots), streamlines (black contours), and divergence (yellow contours in x10^{-5} s^{-1}) at 1200 UTC 2 May 2010. (b) 500-hPa height (black contours in dm) and absolute vorticity (color shading in x10^{-5} s^{-1}) at 1200 UTC 2 May 2010. (c) 700-hPa wind (vectors in knots), height (black contours in dm), temperature (dashed red-above freezing and blue-below freezing contours in Celsius), and dew point temperature ≥ -4 (green contours in Celsius) at 1200 UTC 2 May 2010. (d) 850-hPa wind (vectors in knots), height (black contours in dm), temperature (dashed red-above freezing and blue-below freezing contours in Celsius), and dew point temperature ≥ 8 (green contours in Celsius) at 1200 UTC 2 May 2010.

from 1200 UTC 2 May 2010, the atmosphere is saturated from the surface to about 700-hPa. The surface temperature and the dew point are only a few degrees Celsius apart, indicative of extremely moist conditions. The atmosphere has a moderate amount of directional shear at low levels, as well as speed shear. Throughout the atmosphere, wind ranges from 5 m/s (10 knots) at the surface to 50 m/s (95 knots) at the 400-hPa level (Fig. 5.5a). Because both moisture and lift

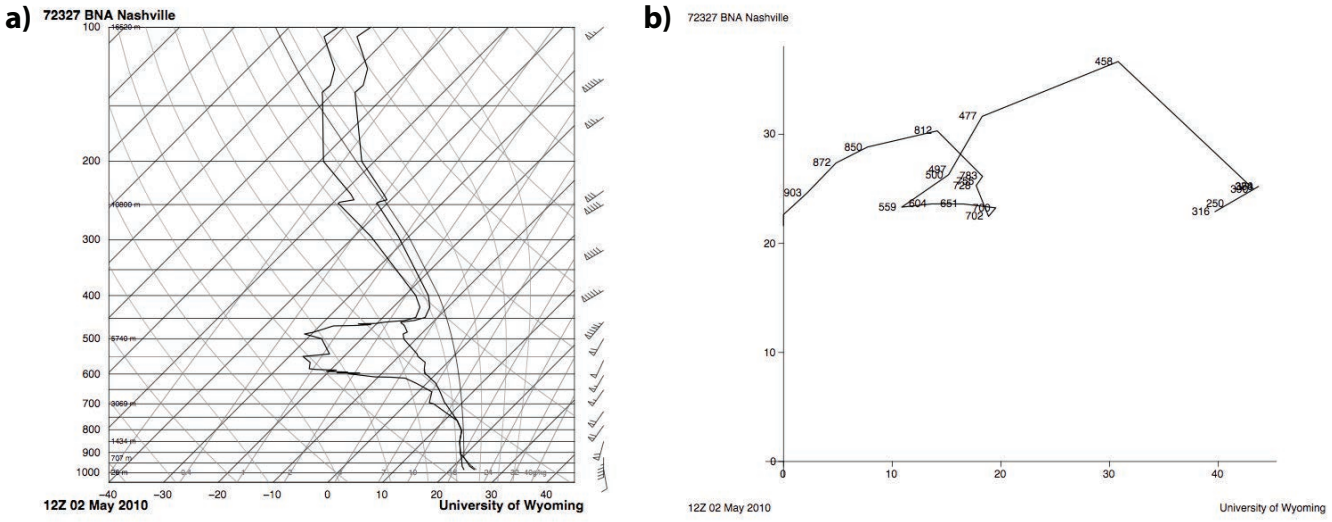

Figure 5.5: (a) Skew-T and (b) hodograph from Nashville International Airport (KBNA) at 1200 UTC 2 May 2010.

are present, the only other ingredient needed for severe weather is instability. With convective available potential energy (CAPE) at 2507 J kg^{-1} (not shown), and a 500-hPa lifted index of -11°C (not shown), the atmosphere is very unstable, capable of producing thunderstorms and severe weather. Looking at the hodograph from 1200 UTC 2 May 2010, between approximately 900 hPa to 700 hPa, a nocturnal low level jet is present. The hodograph turns clockwise at lower levels, with peak winds at around 800 hPa (Fig. 5.5b). For this particular event, all of the ingredients pulled together to produce heavy precipitation for an extended period of time, as well as severe weather.

Maddox et al. (1979) has identified three primary types of synoptic and mesoscale patterns as often producing excessive rain. Both the meso-high and frontal types are primarily mesoscale phenomena, while synoptic forcing drives the synoptic type events, described in detail earlier in the study. The 29 April-4 May 2010 precipitation event occurred in the spring months, between late April and early May. Not only did this widespread rain event happen in the Spring, it occurred in the Mississippi Valley region. As noted by Maddox et al. (1979), the location

where synoptic type flash flood events are most commonly observed in the spring is the Mississippi Valley. At the 500-hPa level, a well-defined trough dug into the central plains and then began to weaken and slide off to the east (Fig. 5.4b). Looking at the surface analysis, a cold front approaching Tennessee from the west stalled as it became parallel to the upper-level flow. The frontal boundary stalled oriented from southwest to northeast (Fig. 5.6). For the duration of the precipitation event, dew point temperatures remained above 70°F in Nashville, Tennessee and nearby areas (Fig. 5.6). Winds at the 850-hPa level reached a wind speed of about 60 knots, with 0 to 6-kilometer wind shear reaching 72 knots (Fig. 5.5a). With that said, the 29 April-4 May 2010 widespread, precipitation event is a classic synoptic type flash flood event.

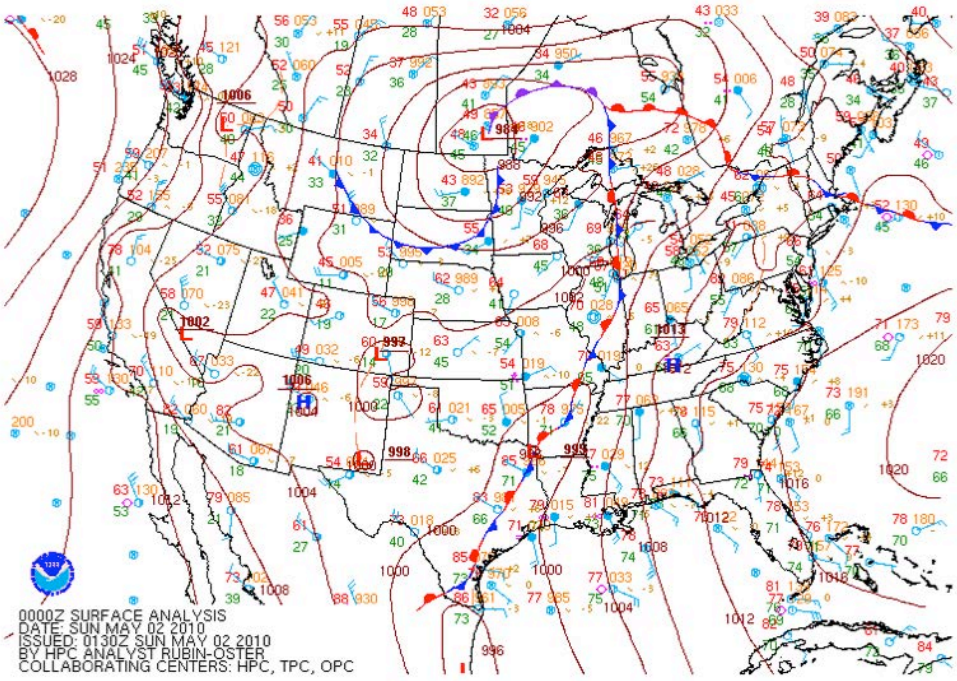

Figure 5.6: Hydrometeorological Prediction Center (HPC) surface analysis for 0000 UTC 2 May 2010.

5.3 Results

5.3.1 Selection of "wet" and "dry" ensemble members

With an initialization time of 1200 UTC 29 April 2010, the 84-hour (0000 UTC 3 May 2010) and 96-hour (1200 UTC 3 May 2010) forecasts were found to be the most useful for this case to look at the synoptic analysis. At forecast hour 84, the second MCS was still training over Nashville, Tennessee when it then began to slide off to the east impacting eastern Tennessee at forecast hour 96. Both the 84-hour and 96-hour forecasts have a large spread in their respective precipitation forecasts, with some members correctly predicting heavy precipitation and others that were not. Whitaker and Loughe (1998) found that spread is much more useful as a predictor of skill when it is extreme (very large or very small). Schumacher and Davis (2010) noted an apparent inverse relationship between spread and skill in the precipitation forecasts. For example, an event with large (small) spread in the forecasts also had the lowest (highest) skill. Looking at the 12-hr accumulated precipitation time series at Nashville, Tennessee, a majority of the ensemble members have forecasted for the heaviest precipitation to occur around forecast hours 84 and 96 (Fig. 5.7). The observed 12-hr accumulated precipitation is shown by the thick black contour. It appears each of the ensemble members largely underpredicted the amount of precipitation Nashville, TN would receive from the first MCS (Fig. 5.7).

A few of the ensemble members realistically reflected the spatial distribution of precipitation and the evolution of the precipitation system. Member 29 and member 31 had a very similar spatial distribution as the observed event, while member 36 and member 5 had little to no resemblance (shown later in the study). Additionally, the five-day area-averaged precipitation was calculated within the thick black box encompassing the Tennessee area and

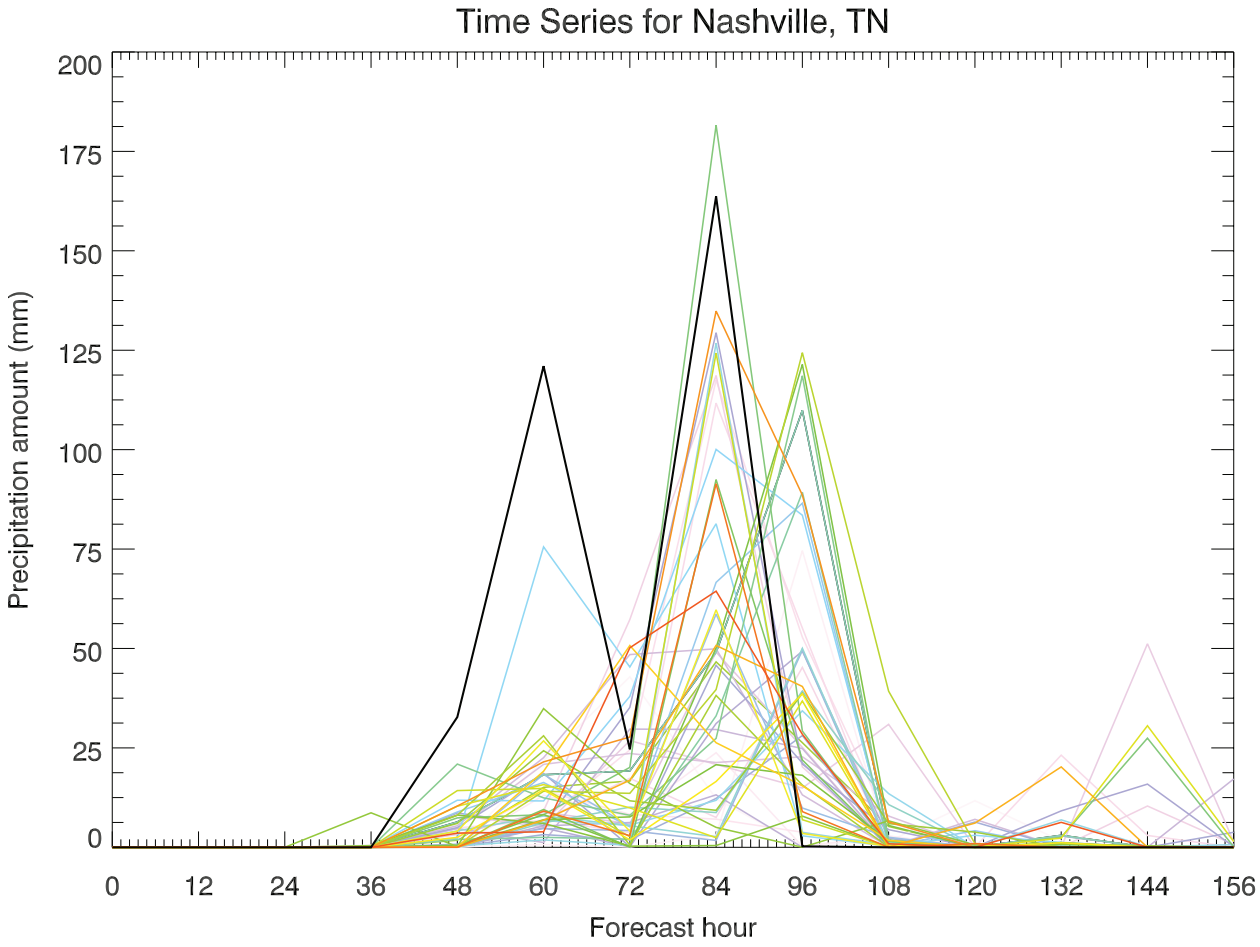

Figure 5.7: Time series plot for Nashville, Tennessee (latitude: 36° N, longitude: 87° W) showing the predicted 12-hr accumulated precipitation from each ensemble member in a different color. Initialization time of 1200 UTC 29 April 2010. The observed 12-hr accumulated precipitation contour is shown in thick black, obtained from the National Climatic Data Center (NCDC).

then compared to the five-day area-averaged precipitation of the forecasted ensemble members. The observed area-averaged precipitation for this event was 89 millimeters. Member 29 had a five-day area-averaged precipitation of 98 millimeters and member 31 had a five-day area-averaged precipitation of 95 millimeters. Interestingly, member 29 and member 31 slightly over-predicted the five-day area-averaged precipitation. Member 36 had an area-averaged precipitation of 48 millimeters and member 5 had a five-day area-averaged precipitation of 49

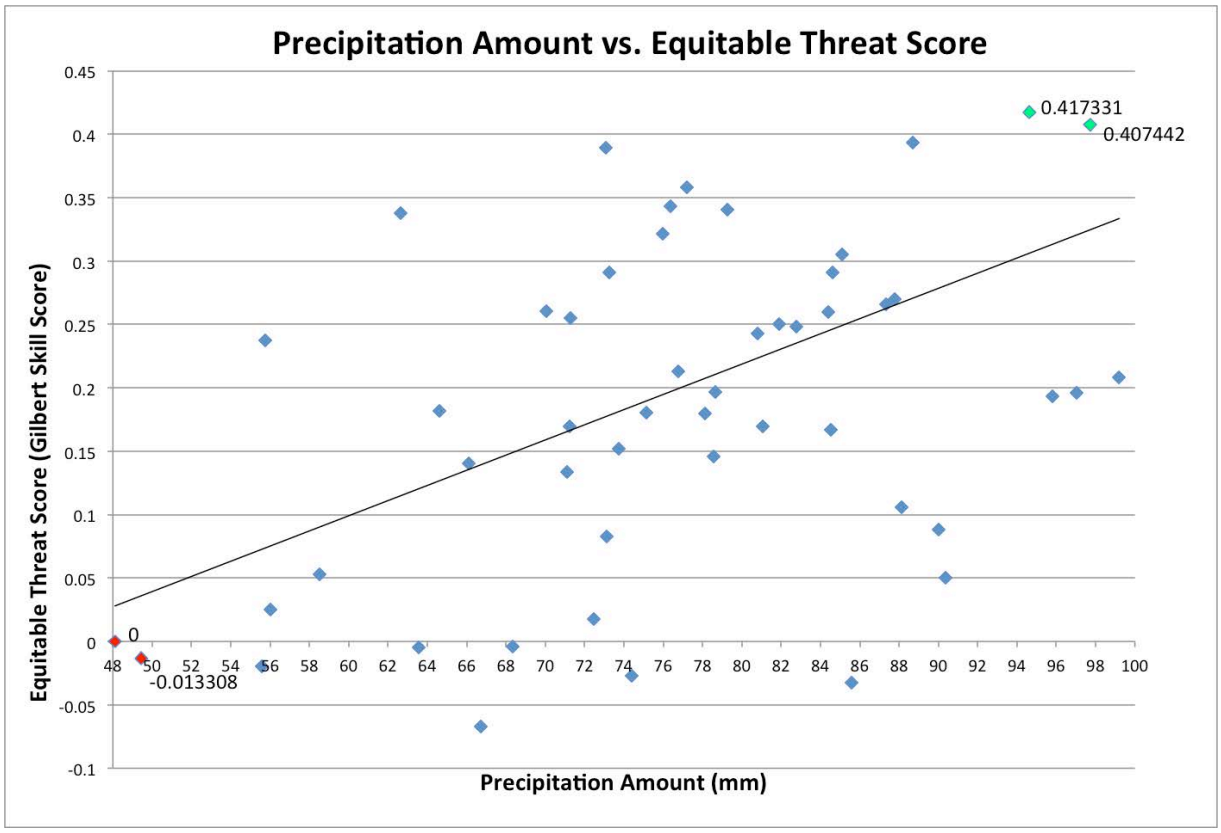

Figure 5.8: Area-averaged precipitation vs. equitable threat score scatter plot at a threshold of 100 mm between 1200 UTC 29 April 2010 – 1200 UTC 4 May 2010. Equitable threat score was calculated within the area-averaged box shown on Fig. 5.2. The wet ensemble members (members 29 and 31) are plotted in green and the dry ensemble members (members 36 and 5) are plotted in red.

millimeters (Fig. 5.8). At a threshold of 100 millimeters, the equitable threat score was calculated for each ensemble member as the final method to determine the most accurate and least accurate ensemble members. Also seen on the area-averaged precipitation vs. equitable threat score scatter plot is the best-fit line. The best-fit line denotes the positive correlation between precipitation amount and equitable threat score. For the Nashville, Tennessee case, the ensemble members have a large spread, however, demonstrate high skill (Fig. 5.8).

Although analyzing the spatial distribution of precipitation and ETS to determine the most accurate and least accurate ensemble members is beneficial, it is not sufficient. As pointed

out by Roulston and Smith (2003), identification of the best ensemble member should be done using multivariate forecasts, even if only univariate forecasts are required. This requires one to analyze all weather variables that all relevant to identifying the best ensemble member. After looking at all 50 members, it was determined that the most accurate forecast was from members 29 and 31 (the wet ensemble members), while the least accurate forecast was from members 36 and 5 (the dry ensemble members).

5.3.2 Correlations

Looking at the 84-hour forecast of the 500-hPa height correlations to area-averaged precipitation, there is a region of positive correlation ($r \approx 0.5$) to the west/northwest of Tennessee, in the Central Plains region (Fig. 5.9). This suggests that higher heights in the Midwest resulted in more precipitation over the area of interest. A large core of positive correlation resides over the Pacific Ocean and western United Sates, indicating the wet ensemble members having a stronger upper-level ridge off the coast of the western United States, than do the dry ensemble members (Fig. 5.9). In central Tennessee, 500-hPa height and area-averaged precipitation are slightly anticorrelated, indicating the ensemble members with lower heights over Tennessee also had more precipitation in that area (Fig. 5.9). A negative correlation ($r \approx -0.4$) also resides along the Texas/Mexico border. This denotes a deep, more elongated upper-level trough is correlated with more precipitation in the area of interest (Fig. 5.9). Taking a look at the 84-hour forecast of the 850-hPa height correlations to area-averaged precipitation, there is a region of positive correlation, with a correlation coefficient around 0.5, just to the northwest of Tennessee, in the Central Planes region (Fig. 5.10). In this region of positive correlation, encompassing Tennessee, as heights increase, area-averaged precipitation increases. When considered along with the maps of the total height field, this suggests that a weaker cyclone over

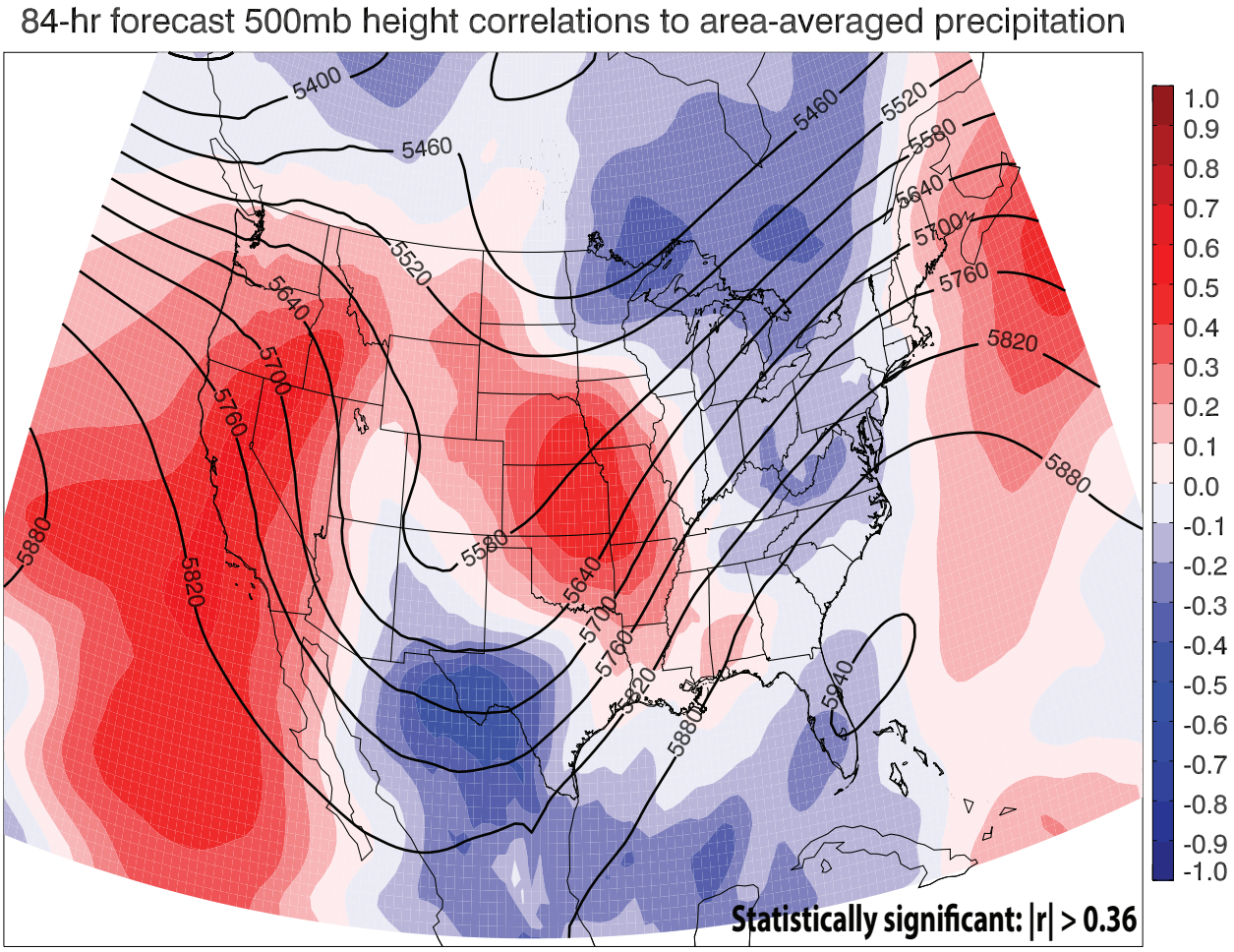

Figure 5.9: Area-averaged precipitation between 1200 UTC 29 April 2010 – 1200 UTC 4 May 2010 correlated to 500-hPa height at 0000 UTC 3 May 2010, corresponding to forecast hour 84. Warm colors represent a positive correlation, while cool colors represent a negative correlation. The ensemble mean 500-hPa height contours are shown in thick black.

the central United States was associated with more precipitation over the area of interest. Another region of positive correlation ($r \approx 0.5$) exists in the western United States and just off the coast into the Pacific Ocean (Fig. 5.10). This strong correlation is due to the wet ensemble members having much higher heights off the coast of the western United States, than do the dry ensemble members. Also, the higher heights are a bit more inland in the wet ensemble members. A strong negative correlation ($r \approx -0.5$) lies just east of Mexico (Fig. 5.10). This negative correlation could denote the presence of a lee trough from the Sierra Madre Oriental Mountains

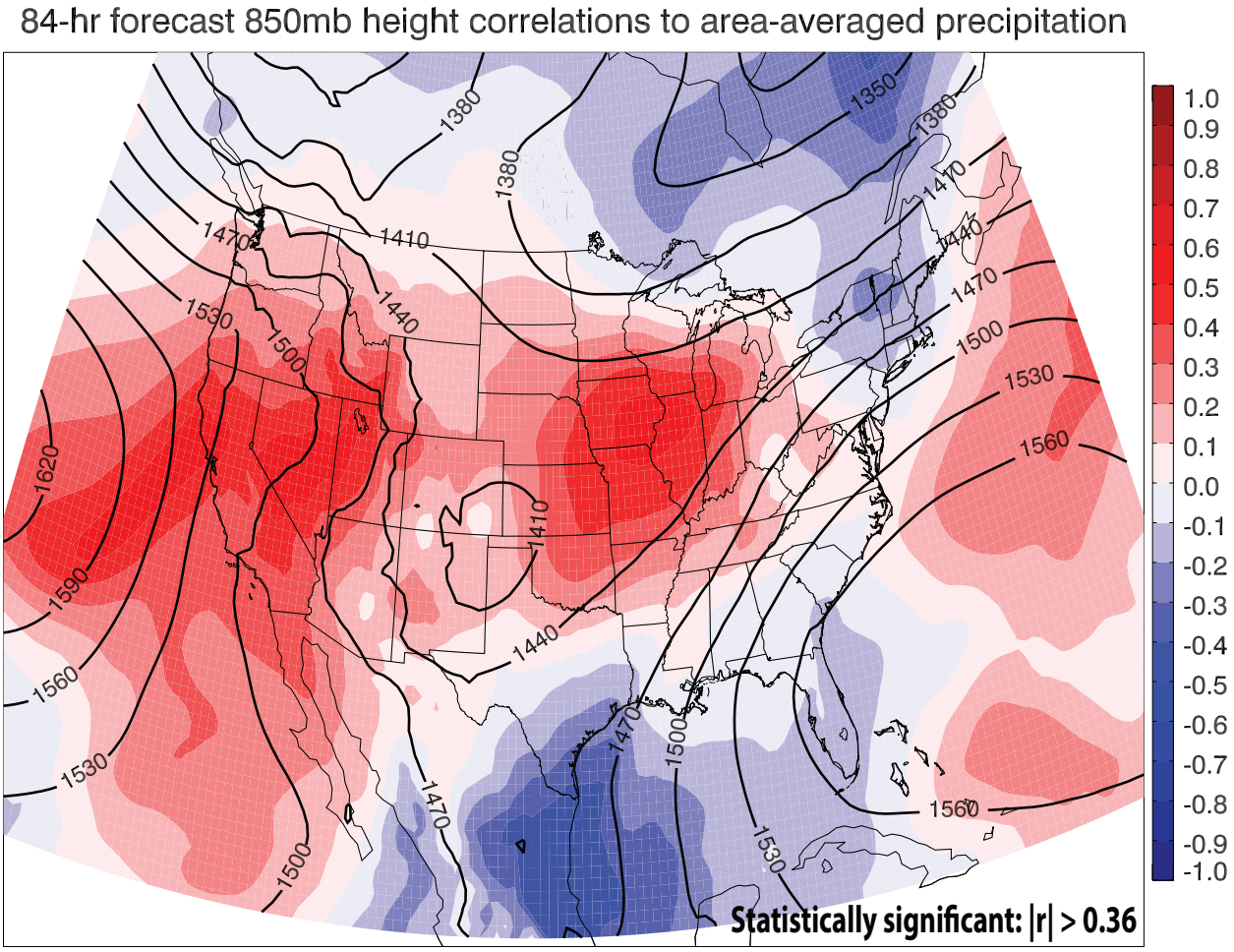

Figure 5.10: Area-averaged precipitation between 1200 UTC 29 April 2010 – 1200 UTC 4 May 2010 correlated to 850-hPa height at 0000 UTC 3 May 2010, corresponding to forecast hour 84. Warm colors represent a positive correlation, while cool colors represent a negative correlation. The ensemble mean 850-hPa height contours are shown in thick black.

in Mexico, with lower heights indicative of more precipitation. Moore et al. (2012) suggest the 850-hPa lee trough positioned along the eastern Mexico coast was likely linked to downslope flow along the Sierra Madre Oriental Mountains of eastern Mexico and a stronger height gradient in the area. Taking a look at the 84-hour forecast of the 850-hPa v-wind correlations to area-averaged precipitation, there is a large negative correlation ($r \approx -0.4$) to the west of Tennessee, encompassing Arkansas, Missouri, Illinois, and Indiana (Fig. 5.11). In this region of negative correlation, as the winds decrease, precipitation increases in the area of interest. It also helps to

explain the position of the low level jet. More specifically, for heavy precipitation to occur in the area of interest, the low level jet shouldn't be positioned to the west of Tennessee. In Tennessee, there is not a very strong correlation, indicating all ensemble members forecasted for strong southerly winds. The location of the ensemble mean low level jet is denoted by the thick black contours, with peak winds around 20 ms^{-1} (Fig. 5.11).

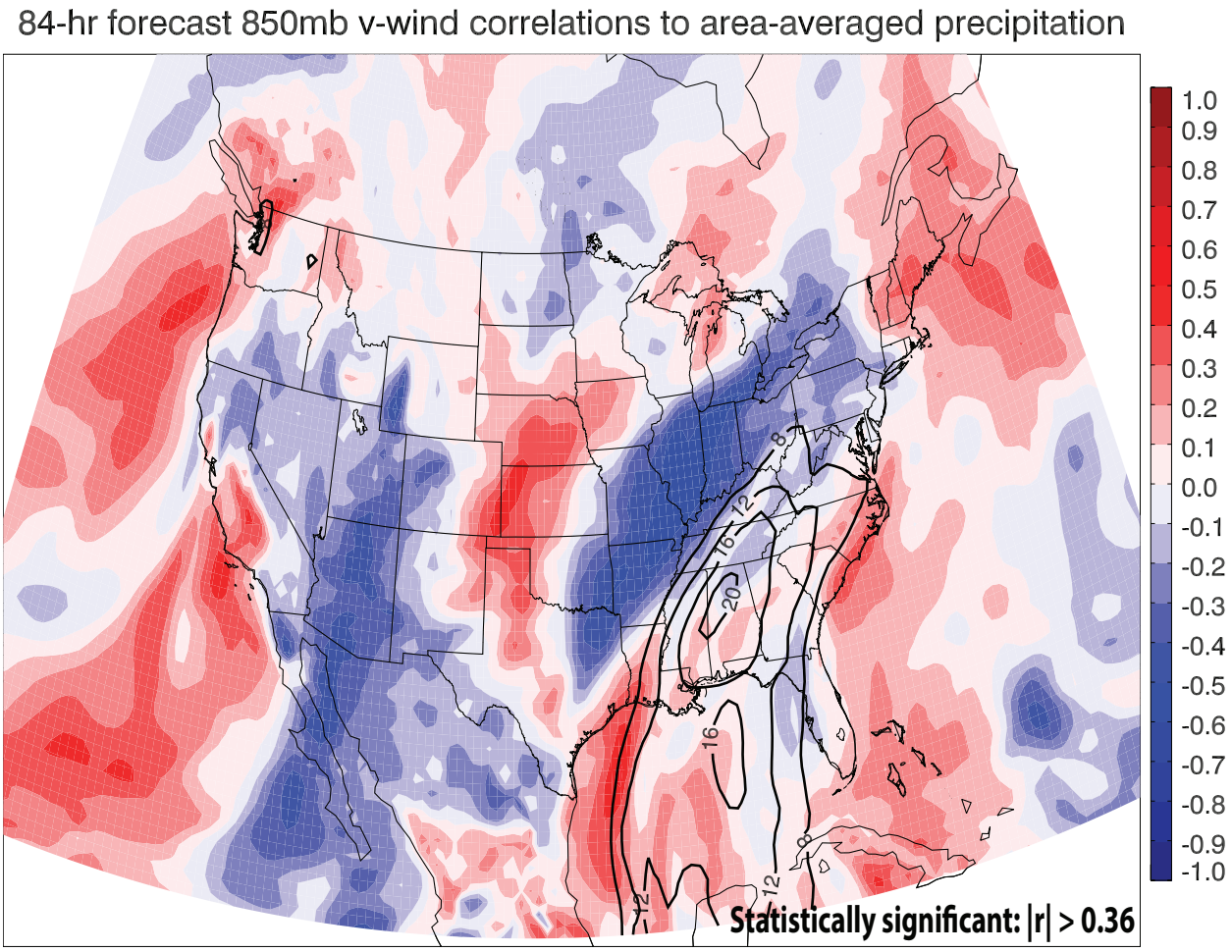

Figure 5.11: Area-averaged precipitation between 1200 UTC 29 April 2010 – 1200 UTC 4 May 2010 correlated to 850-hPa v-wind at 0000 UTC 3 May 2010, corresponding to forecast hour 84. Warm colors represent a positive correlation, while cool colors represent a negative correlation. The ensemble mean 850-hPa v-wind (in ms^{-1}) contours are shown in thick black.

Looking at the 72-hour forecast of the 850-hPa total column water correlations to area-averaged precipitation, there is a slight positive correlation over Tennessee, indicating total

column water is now slightly correlated with area-averaged precipitation, with a correlation coefficient of about 0.2 (Fig. 5.12). At this time the initial quasi-stationary MCS was impacting western Tennessee. To the northwest of Tennessee, in Illinois, Iowa, Missouri, and surrounding areas, 850-hPa total column water and area-averaged precipitation are strongly anticorrelated ($r \approx -0.6$), oriented parallel to the stationary surface boundary (Fig. 5.12). At this time, the stationary surface front appears to have pushed to the east slightly. This is verified by looking at the 72-hour area-averaged precipitation and total column water scatter plot (Fig. 5.13). The scatter plot

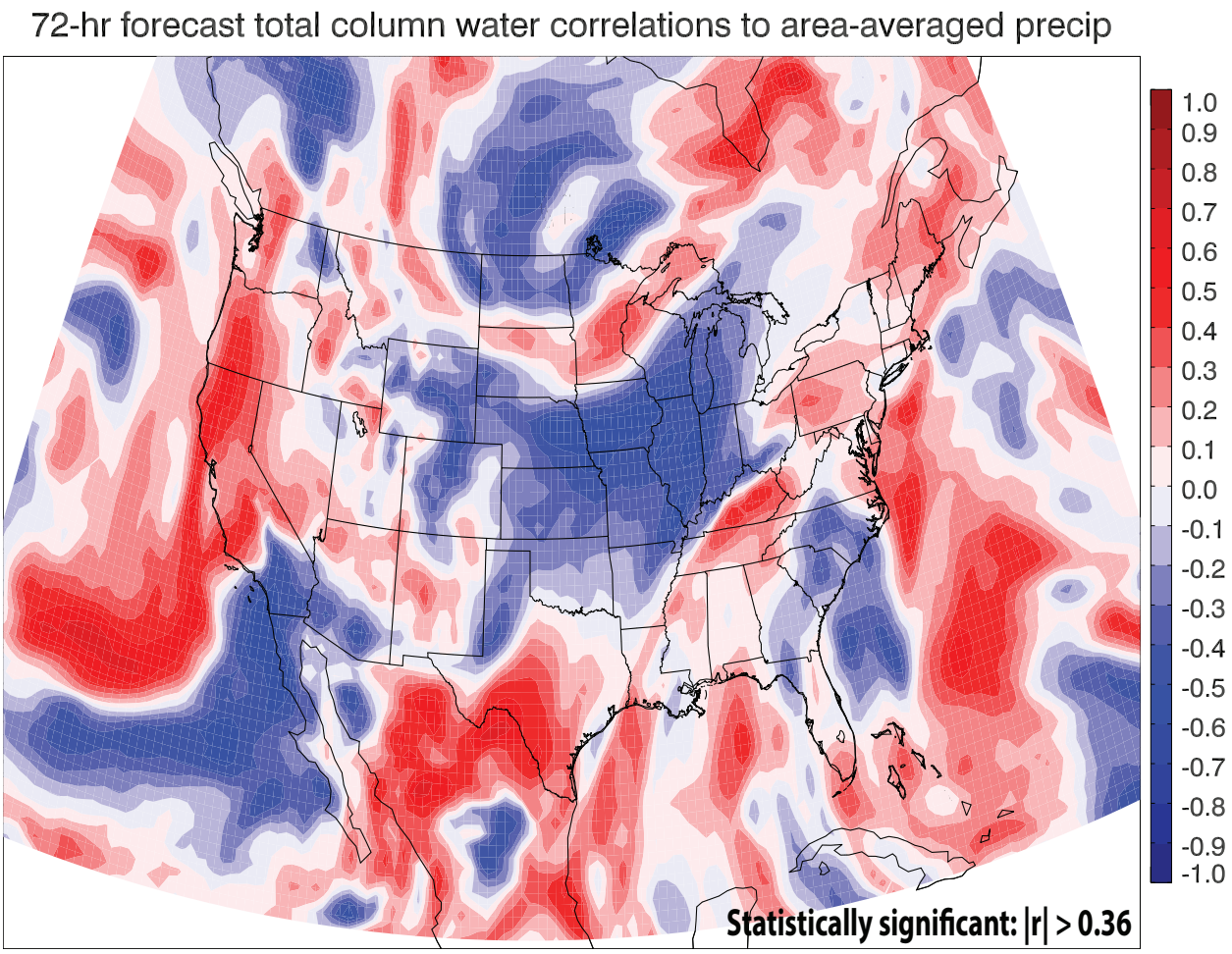

Figure 5.12: Area-averaged precipitation between 1200 UTC 29 April 2010 – 1200 UTC 4 May 2010 correlated to total column water at 1200 UTC 2 May 2010, corresponding to forecast hour 72. Warm colors represent a positive correlation, while cool colors represent a negative correlation.

shows a weak linear relationship between these two variables, as a result of all the ensemble members (both wet and dry) forecasting for a high amount of total column water. The dry ensemble members have a slightly smaller amount of total column water than do the wet ensemble members (Fig. 5.13). Twenty-four hours later, looking at the 96-hour forecast of the 850-hPa total column water correlations to area-averaged precipitation, the large region of negative correlation that was in the Great Lakes slides to the east slightly (Fig. 5.14). In Tennessee, total column water is now strongly correlated with area-averaged precipitation, with a correlation coefficient of about 0.7. This strong positive correlation appears to be oriented parallel to the stationary surface boundary, from southwest to northeast (Fig. 5.14). To the

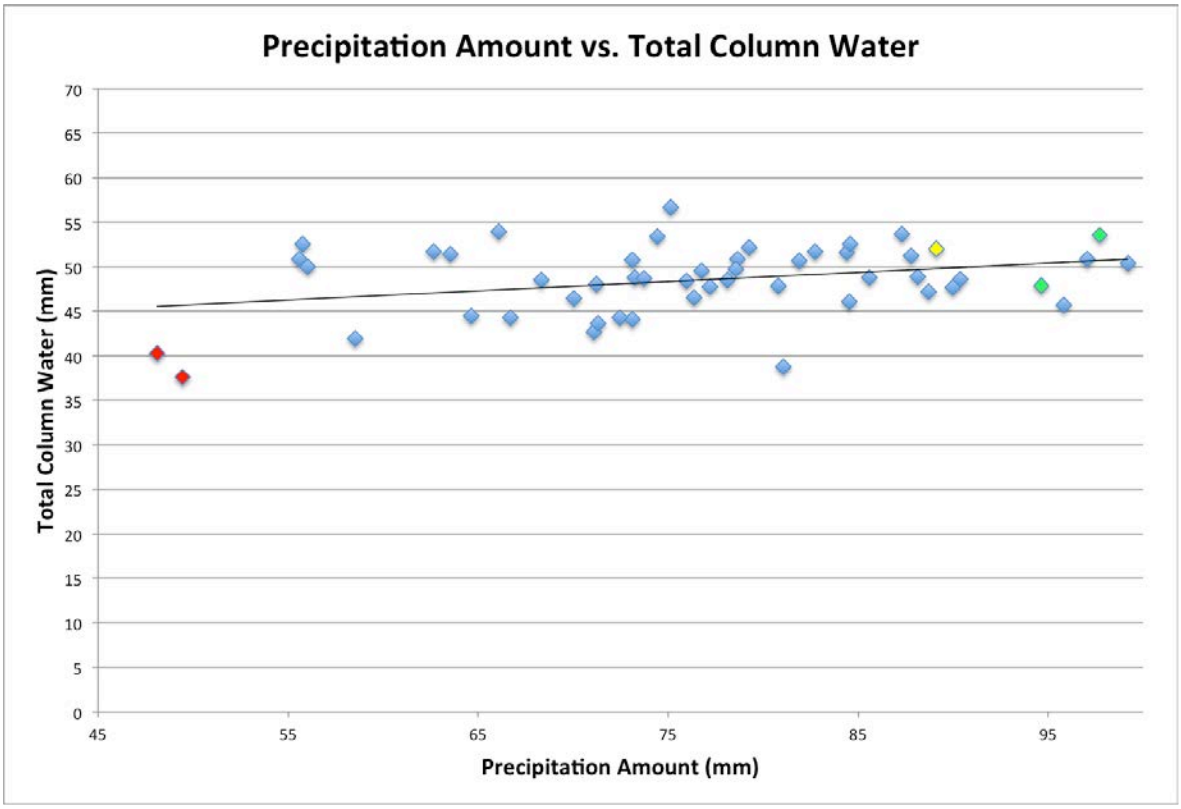

Figure 5.13: Scatter plot of area-averaged precipitation between 1200 UTC 29 April 2010 – 1200 UTC 4 May 2010 vs. total column water at latitude: 36° N and longitude: 87° W at 1200 UTC 2 May 2010, corresponding to forecast hour 72. The wet ensemble members (members 29 and 31) are plotted in green, the dry ensemble members (members 36 and 5) are plotted in red, and the analysis is plotted in yellow.

southeast of Tennessee, 850-hPa total column water and area-averaged precipitation are strongly anticorrelated ($r \approx -0.6$), also oriented parallel to the stationary surface boundary (Fig. 5.14). This is verified by looking at the 96-hour area-averaged precipitation and total column water scatter plot (Fig. 5.15). The scatter plot now exhibits a strong linear relationship between these two variables, with higher (lower) total column water corresponding to more (less) precipitation. The strong anticorrelation in Tennessee indicates the wet ensemble members have advected the

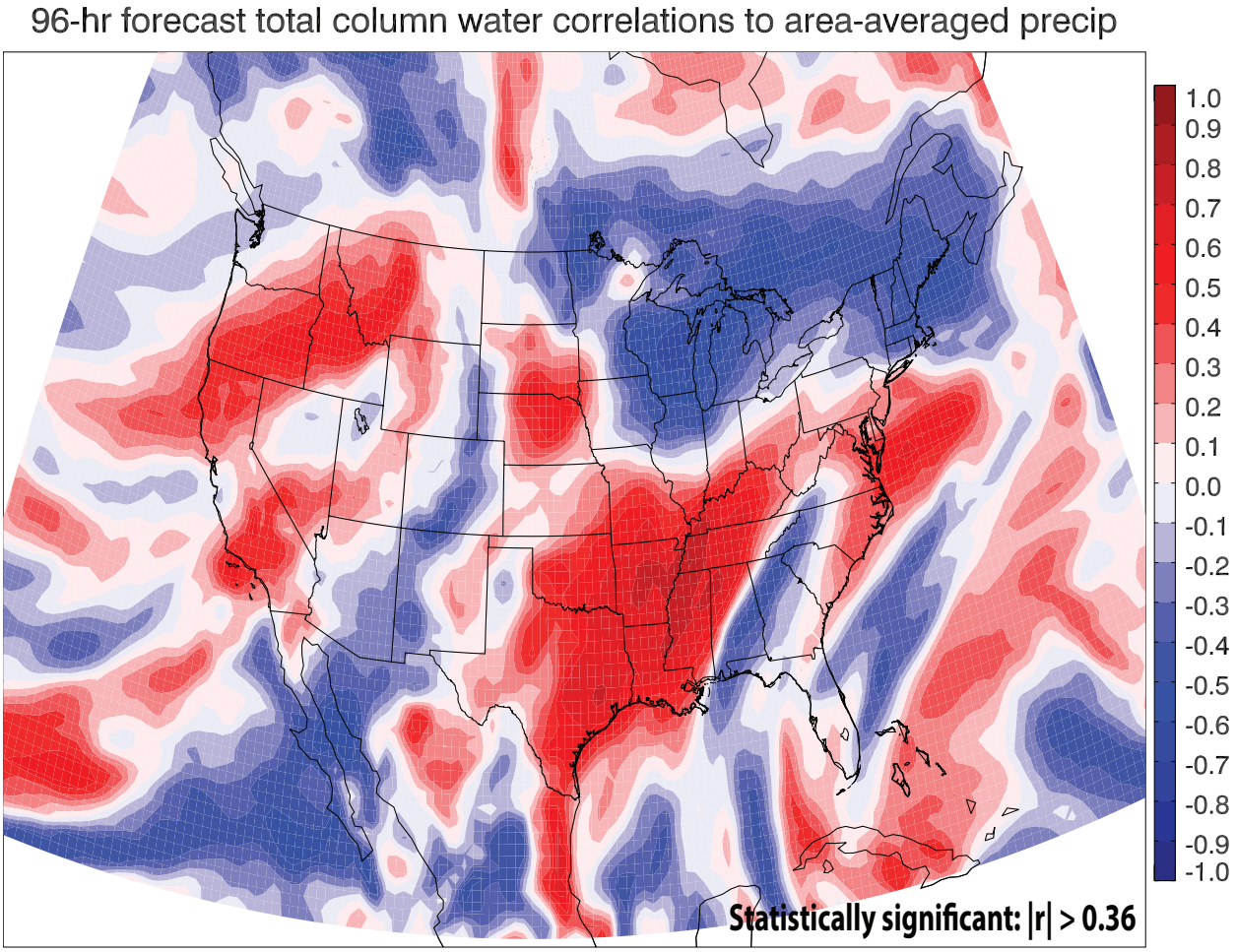

Figure 5.14: As in Fig. 5.12, except for correlated to total column water at 1200 UTC 3 May 2010, corresponding to forecast hour 96.

moisture into Tennessee and nearby areas, however, the strong negative correlation in the Great Lakes region is a result of the dry ensemble members lofting the moisture much farther

poleward. Interestingly, the analysis has one of the smallest amounts of total column water, yet has a large precipitation amount (Fig. 5.15). The loss of total column water over this twelve-hour period is likely associated to condensation and precipitation occurring slightly earlier in reality compared to the forecast.

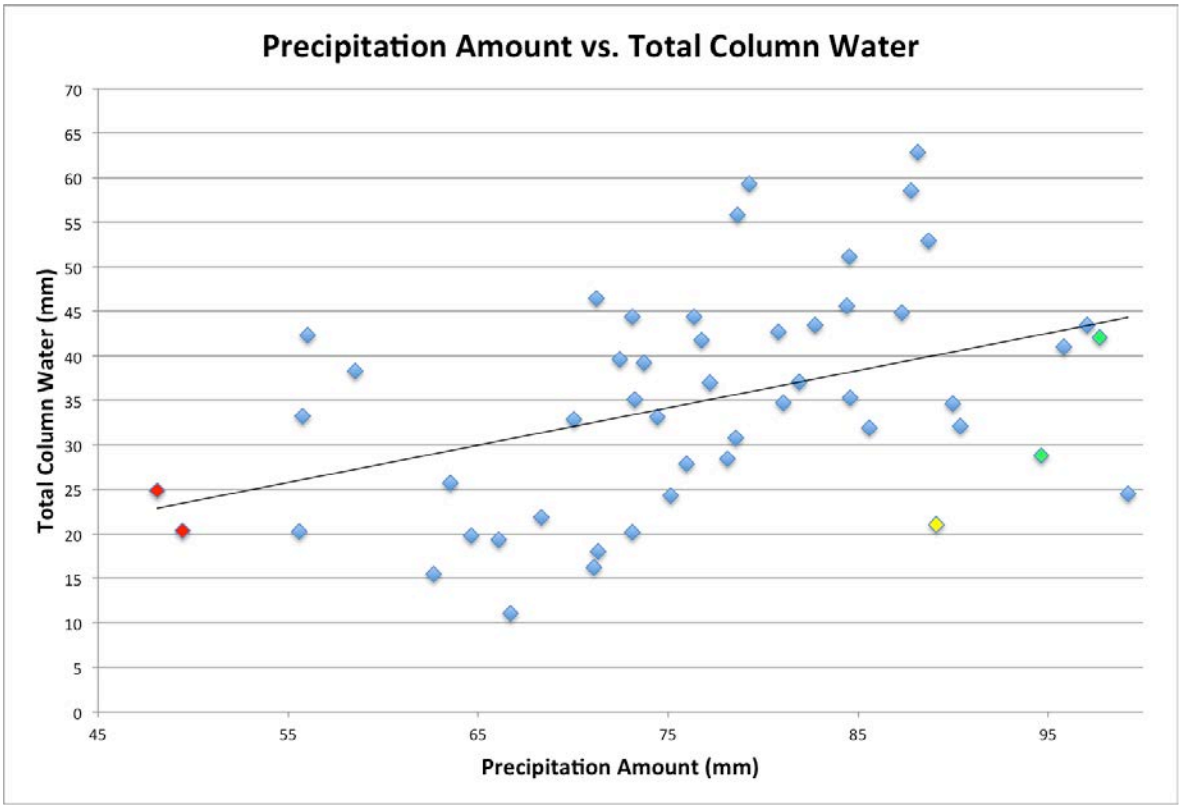

Figure 5.15: Scatter plot of area-averaged precipitation between 1200 UTC 29 April 2010 – 1200 UTC 4 May 2010 vs. total column water at latitude: 36° N and longitude: 87° W at 1200 UTC 3 May 2010, corresponding to forecast hour 96. The wet ensemble members (members 29 and 31) are plotted in green, the dry ensemble members (members 36 and 5) are plotted in red, and the analysis is plotted in yellow.

5.3.2 Ensemble member comparison

To put the previously presented results into physical perspective, plots of the two most accurate members and the two least accurate members, both spatially and temporally, were constructed. As for the forecasted precipitation, member 29 and member 31 (the wet ensemble

members) forecasted for a very strong, linear precipitation area. This area of heavy rainfall was oriented from southwest to northeast and extended from northern Mississippi to northern Kentucky. The system slowly pushed off to the southeast bringing high rainfall amounts to cities in its path (Figs. 5.16a and 5.16c). Member 36 and member 5 (the dry ensemble members) forecasted for much smaller rainfall amounts, with the heavier precipitation displacement slightly to the west. Member 36 over-predicted precipitation in other locations such as Florida and Georgia. Additionally, there is not much of a linear feature in the precipitation for the dry ensemble members (Figs. 5.16b and 5.16d). When comparing the forecasted precipitation to the

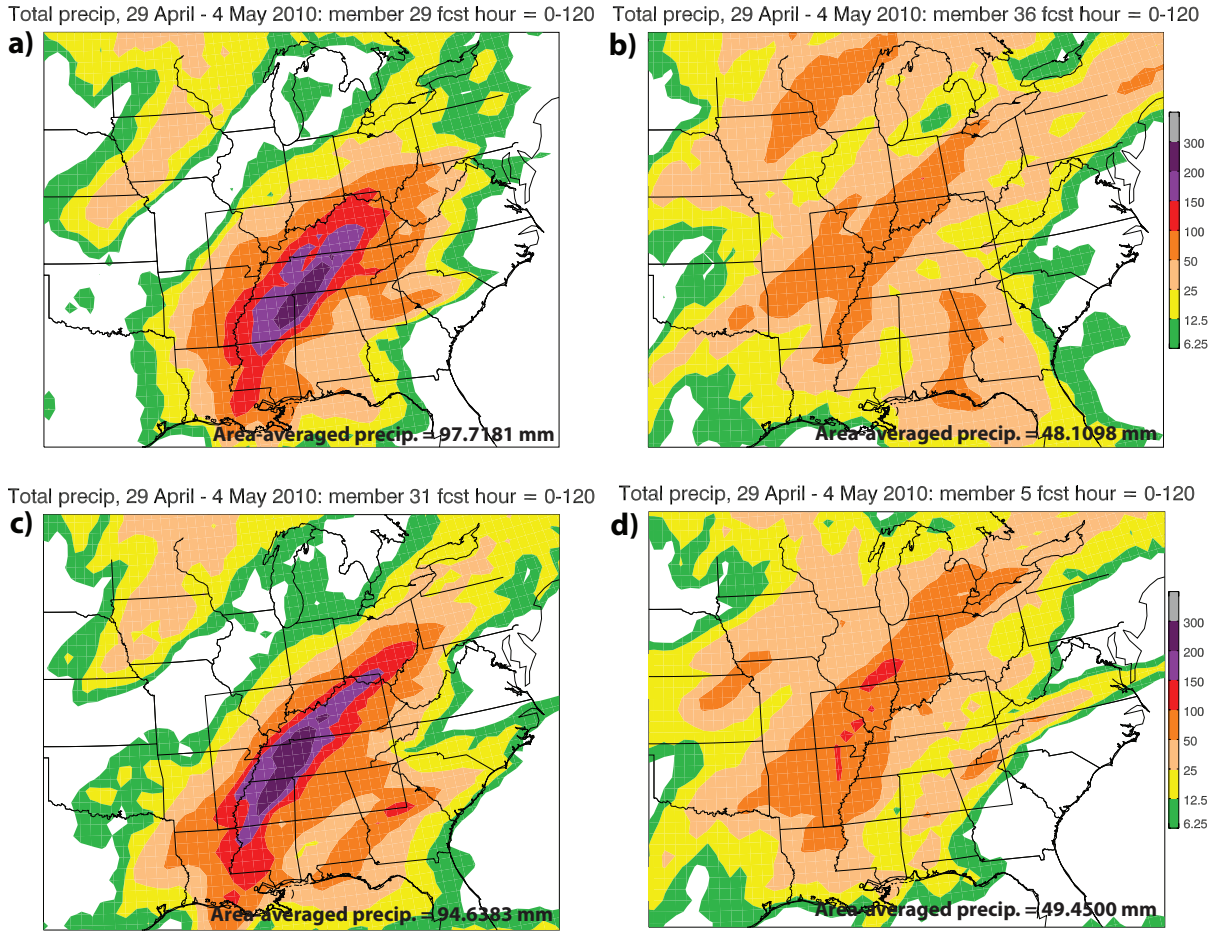

Figure 5.16: Five-day accumulated precipitation (color shading in mm) between 1200 UTC 29 April 2010 – 1200 UTC 4 May 2010: (a) member 29 (wet), (b) member 36 (dry), (c) member 31 (wet), and (d) member 5 (dry). The black rectangle indicates the location for areal averaging of precipitation and other fields.

actual observed precipitation, it is easily seen that member 29 and member 31 (the wet ensemble members) were quite accurate (Figs. 5.16a and 5.16c). However, in member 29, the maximum forecasted precipitation is displaced a bit to the southeast (Fig. 5.16a). The observed precipitation is oriented southwest to northeast, with a linear feature. The bulk of heavy precipitation swept across the state of Tennessee. The resulting precipitation accumulation between the wet ensemble members and the dry ensemble members is very different, with comparable differences also occurring among other individual ensemble members.

Something else to consider when looking at forecasted precipitation is the maximum precipitation amount. From the U.S. Daily Precipitation Analysis dataset, the maximum observed precipitation amount was 321 millimeters (yellow). Member 29 and member 31 (the wet ensemble members, green) each forecasted a maximum precipitation amount of 304 millimeters. Member 36 and member 5 (the dry ensemble members, red) forecasted a maximum precipitation amount of 104 millimeters and 176 millimeters (Fig. 5.17). The wet ensemble members did a much better job at predicting the maximum precipitation amount than did the dry ensemble members, however, even the wet ensemble members slightly underpredicted the maximum precipitation amount. Interestingly, a few of the ensemble members overpredicted the maximum rainfall amount, including ensemble member 2, which forecasted for a maximum precipitation amount of 417 millimeter. Although ensemble member 2 overpredicted the maximum precipitation amount, it had a five-day area-averaged precipitation of 86, which is lower then the chosen wet ensemble members. Ensemble member 2 forecasted for the heavy precipitation to be displaced to far to the southeast in northern Alabama.

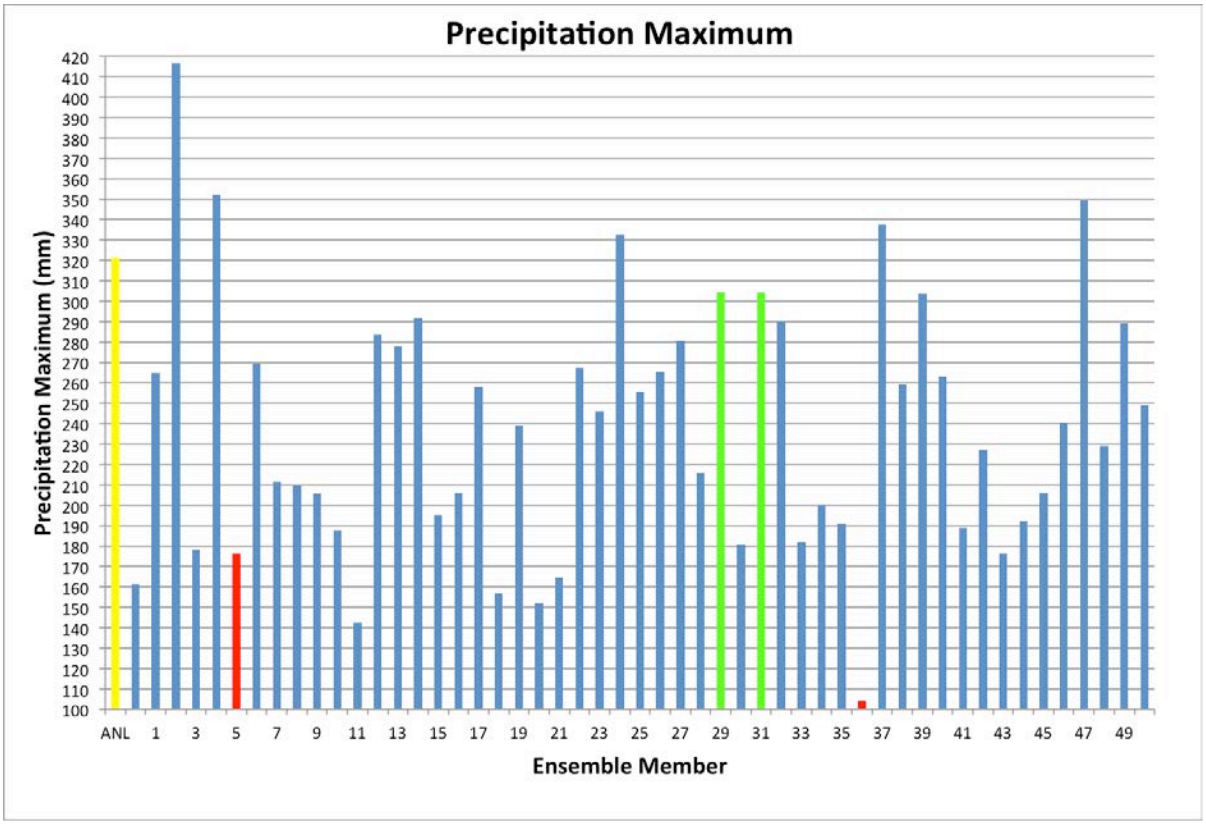

Figure 5.17: Precipitation maximum between the 5-day period 1200 UTC 29 April 2010 – 1200 UTC 4 May 2010. The wet ensemble members (members 29 and 31) are plotted in green, the dry ensemble members (members 36 and 5) are plotted in red, and the analysis is plotted in yellow.

The two main focuses for this precipitation event were the two successive quasi-stationary mesoscale convective systems (MCSs) on 1 and 2 May 2010. On these particular days, most of the ensemble members had a large amount of variability in their forecasts. Looking at the radar composite from 1155 UTC 1 May 2010, the first MCS was seen passing through western central Tennessee. This line of heavy precipitation was oriented from southwest to northeast, extending from southwestern Tennessee to northern Kentucky (Fig. 5.18a). The MCS then trains over central Tennessee for nearly 12 hours (not shown). Twenty-four hours following the initial MCS, at 1154 UTC 2 May 2010, the second MCS was seen passing through western

central Tennessee. This line of heavy precipitation was oriented from southwest to northeast, extending from northeastern Louisiana to southern Ohio (Fig. 5.18b). The MCS then trained over

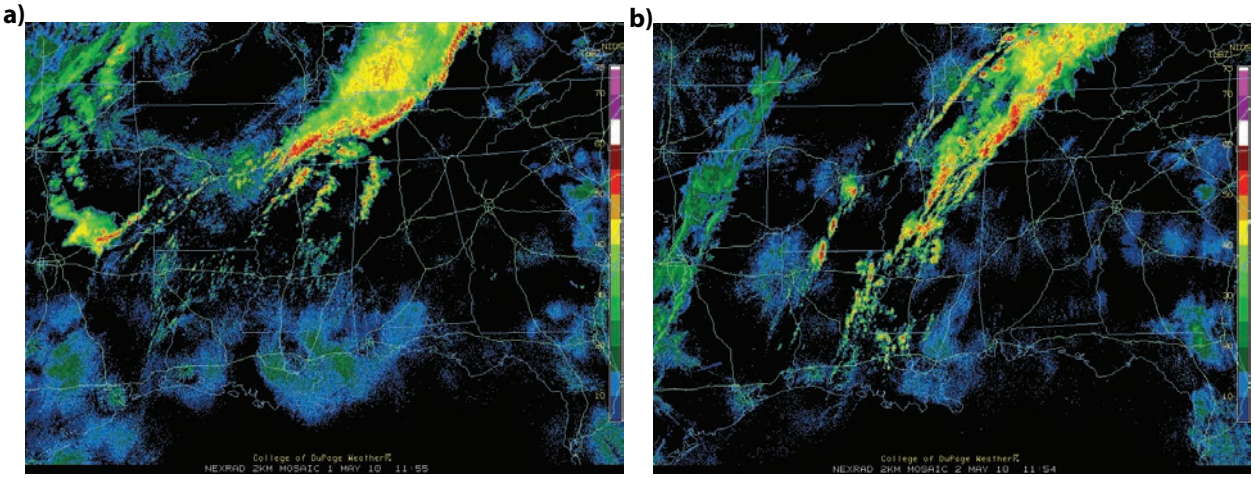

Figure 5.18: Radar reflectivity (color shading in dBZ) at (a) 1155 UTC 1 May 2010 and (b) 1154 UTC 2 May 2010.

central Tennessee for nearly 12 hours (not shown), similar to the previous MCS. As for the accumulated 24-hr precipitation from 1200 UTC 1 May 2010 to 1200 UTC 2 May 2010, rainfall totals exceeding 75 mm were observed in west/central Tennessee, western Kentucky, and northern Mississippi (Fig. 5.19a). Looking at the forecasted 24-hr precipitation at 1200 UTC 2 May 2010, ensemble members 29 and 31 (the wet ensemble members) forecasted for high rainfall totals in western Tennessee, northern Mississippi, and southeast Arkansas, a result of the first quasi-stationary MCS. Each of the wet ensemble members underpredicted the spatial extent of these higher precipitation amounts (Figs. 5.20a and 5.20b). Although member 5 and 36 (the dry ensemble members) forecasted for high rainfall totals, they were displaced to the west, completely voiding Nashville of high precipitation amounts (Figs. 5.20c and 5.20d). Twenty-four

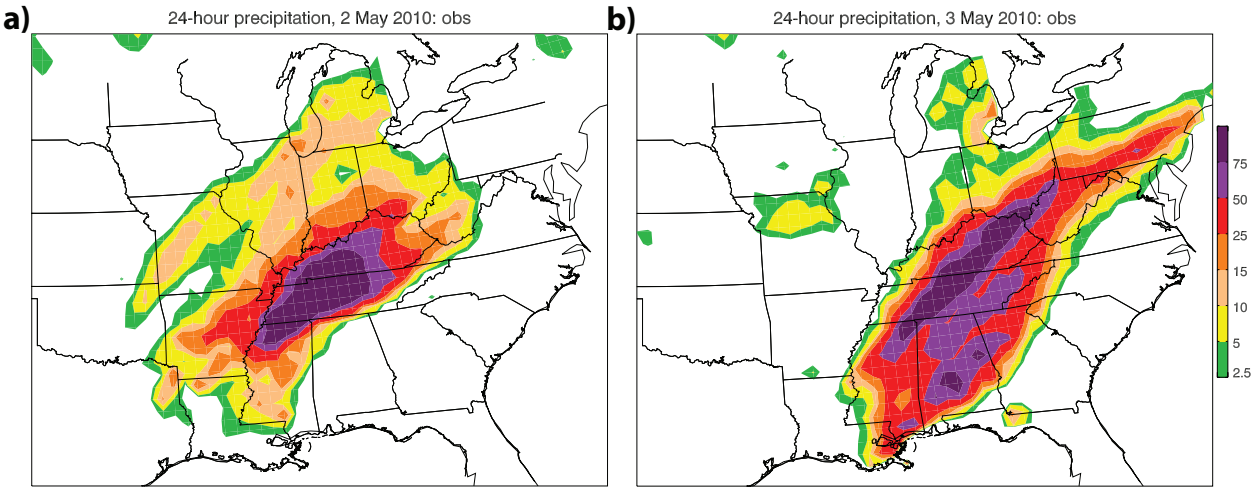

Figure 5.19: Observed 24-hr accumulated precipitation (color shading in mm) (a) from 1200 UTC 1 May 2010 to 1200 UTC 2 May 2010 and (b) from 1200 UTC 2 May 2010 to 1200 UTC 3 May 2010.

hours later, at 1200 UTC 3 May 2010, the second quasi-stationary MCS was impacting Nashville, Tennessee and surrounding areas. The accumulated 24-hr precipitation from 1200 UTC 2 May 2010 to 1200 UTC 3 May 2010 exceeded 75 mm throughout central Tennessee and Kentucky, in the form of a linear feature due to the consistent training/backbuilding of the second MCS. Alabama also received high rainfall totals exceeding 75 mm (Fig. 5.19b). Member 29 and 31 (the wet ensemble members) forecasted for high rainfall totals in central Tennessee, also in the form of a linear feature (Figs. 5.20e and 5.20f). Members 5 and 36 (the dry ensemble members) also forecasted for high rainfall totals, but the highest precipitation amounts were displaced too far north, missing Nashville, Tennessee (Figs. 5.20g and 5.20h). This is consistent with the 96-hour forecast of the 850-hPa total column water correlations to area-averaged precipitation (Fig. 5.14). The dry ensemble members were advecting the high values of total column water to the Great Lakes region, where it would then precipitate out.

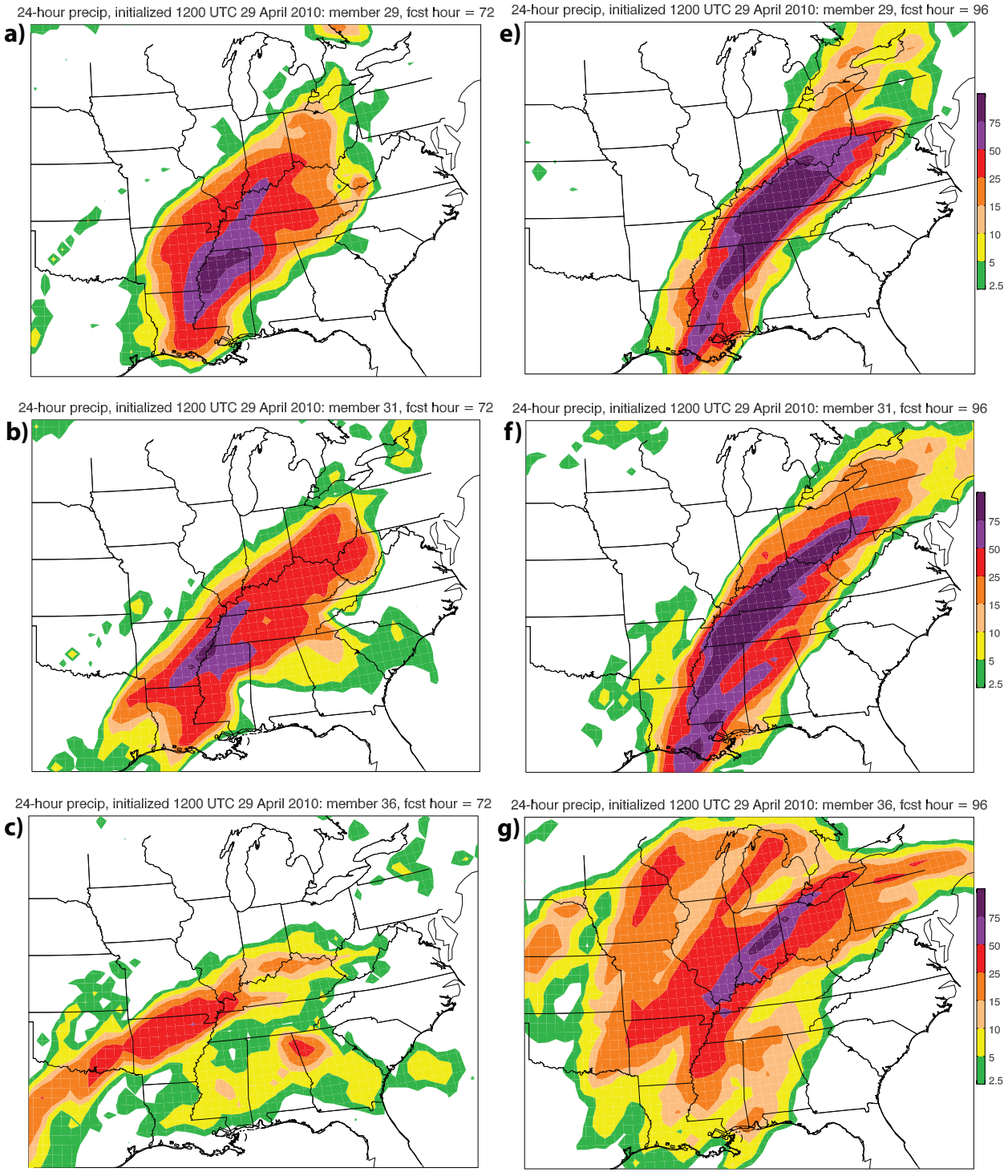
24-hour precip, initialized 1200 UTC 29 April 2010: member 29, fcst hour = 72
a)
24-hour precip, initialized 1200 UTC 29 April 2010: member 29, fcst hour = 96
e)
24-hour precip, initialized 1200 UTC 29 April 2010: member 31, fcst hour = 72
b)
24-hour precip, initialized 1200 UTC 29 April 2010: member 31, fcst hour = 96
f)
24-hour precip, initialized 1200 UTC 29 April 2010: member 36, fcst hour = 72
c)
24-hour precip, initialized 1200 UTC 29 April 2010: member 36, fcst hour = 96
g)
75
50
25
15
10
5
2.5

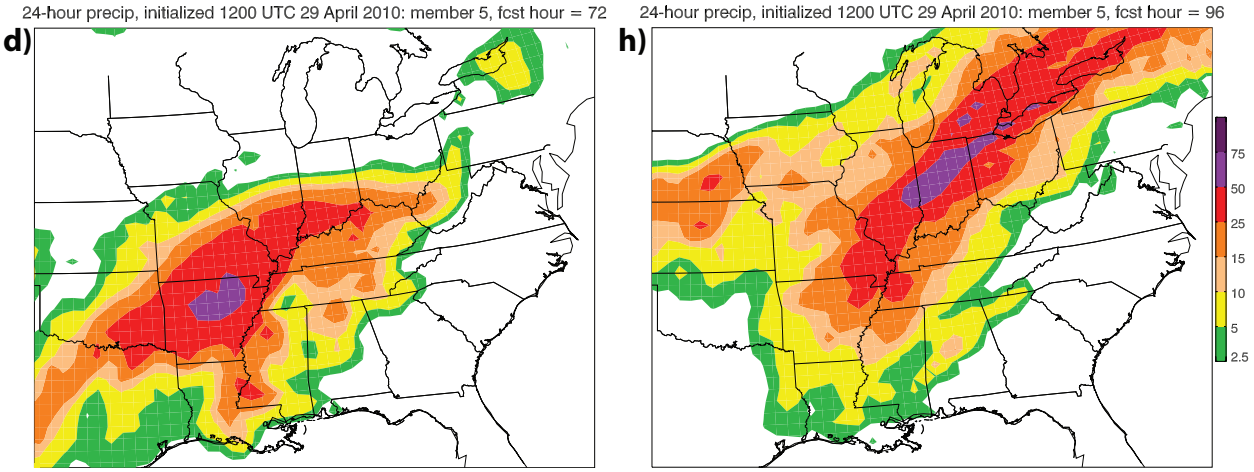

Figure 5.20: Forecasted 24-hr accumulated precipitation (color shading in mm) at 1200 UTC 2 May 2010, corresponding to forecast hour 72: (a) member 29 (wet), (b) member 31 (wet), (c) member 36 (dry), and (d) member 5 (dry), and at 1200 UTC 3 May 2010, corresponding to forecast hour 96: (e) member 29 (wet), (f) member 31 (wet), (g) member 36 (dry), and (h) member 5 (dry).

Looking at the synoptic set-up of the event, one can determine the processes that were favorable or detrimental to the system's development. Beginning at the 500-hPa level, there is a strong upper-level trough digging into the central plains of the United States. The upper-level trough is positively tilted from northeast to southwest (Fig. 5.21a). Twelve hours later, the upper-

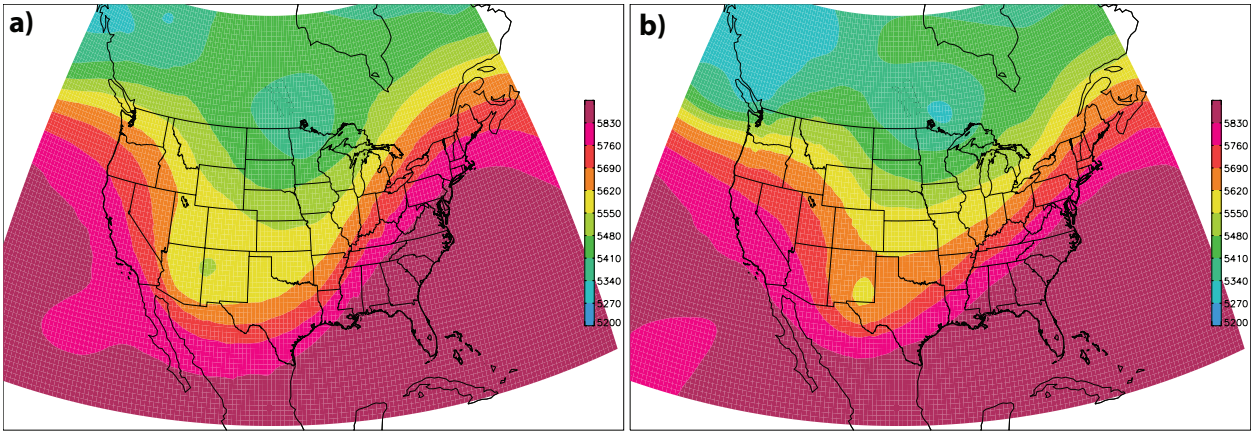

Figure 5.21: ECMWF analysis of 500-hPa height (color shading in m) at (a) 0000 UTC 3 May 2010 and (b) 1200 UTC 3 May 2010.

level trough weakens in strength and begins to move east (Fig. 5.21b). Member 29 and member 31 (the wet ensemble members) forecasted for a strong upper-level trough extending into southern New Mexico. Again, the trough axis is positively tilted from southwest to northeast (Figs. 5.22a and 5.22c). Member 36 and member 5 (the dry ensemble members), however, have a slightly deeper trough plunging into the central United States with its trough axis extending north to south (Figs. 5.22b and 5.22d). This is quite different than member 29 and member 31 (the wet ensemble members), having a positively tilted trough axis (Figs. 5.22a and 5.22c). The dry ensemble members forecasted for an upper-level trough with a tight gradient overhead the state of Tennessee (Figs. 5.22b and 5.22d).

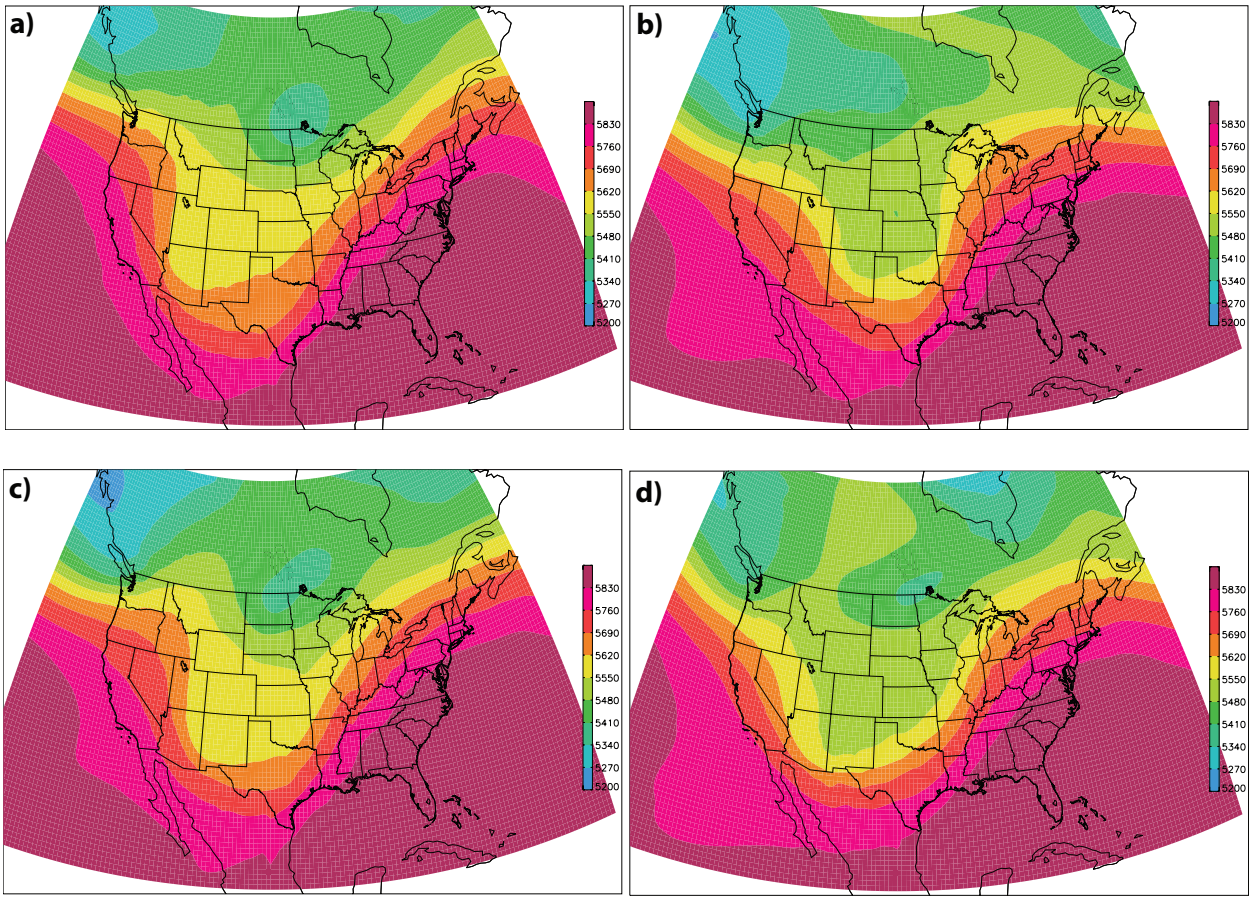

Figure 5.22: Forecasted 500-hPa height (color shading in m) at 0000 UTC 3 May 2010, corresponding to forecast hour 84: (a) member 29 (wet), (b) member 36 (dry), (c) member 31 (wet), and (d) member 5 (dry).

At the 850-hPa level, both the wet and the dry ensemble members forecasted for a low pressure system in the northern United States. However, member 29 and member 31 (the wet ensemble members) forecasted for a weak 850-hPa trough that extends down into the northern United States. The wet ensemble members placed this weak 850-hPa cyclone in Canada. The associated low pressure system is slightly weaker than what was observed (Figs. 5.24a and 5.24c). Contrastingly, member 36 and member 5 (the dry ensemble members) forecasted for a much deeper trough extending down into the state of Texas. This 850-hPa cyclone was forecasted to be located around Missouri for the dry ensemble members. This deep 850-hPa trough has a tight pressure gradient over the state of Tennessee, supporting the aforementioned nocturnal low level jet (Figs. 5.24b and 5.24d). When looking at the observed 850-hPa height, it resembles that of member 29 and member 31 (the wet ensemble members). The trough and associated low pressure system is quite weak (Fig. 5.23a). Progressing through time, only twelve hours later the trough has weakened even more (Fig. 5.23b). Another parameter of interest is the 850-hPa wind speed and direction. On the day of the heavy precipitation event for Nashville,

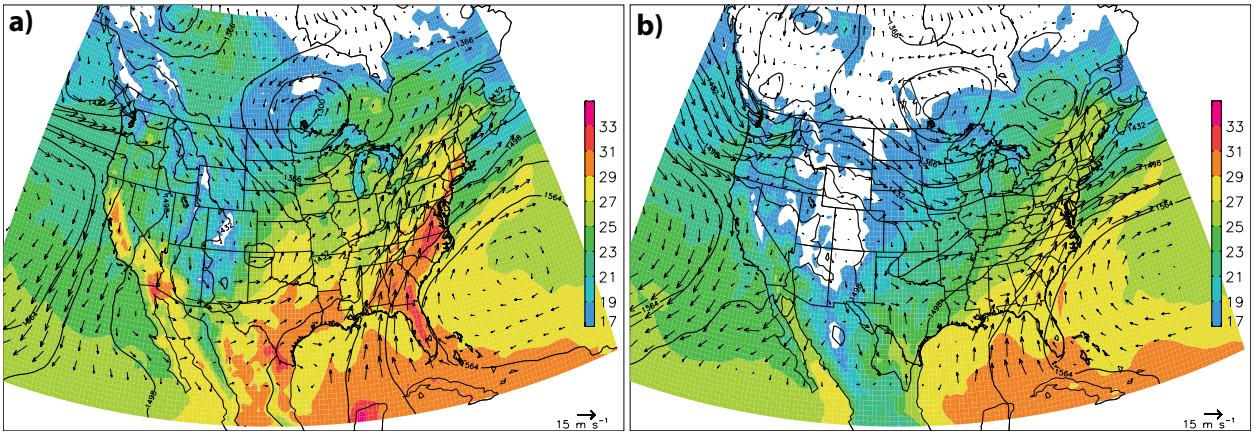

Figure 5.23: ECMWF analysis of 850-hPa temperature (color shading in C), height (black contours overlaid in m), and wind (vectors overlaid, vector scale is shown at bottom right) at (a) 0000 UTC 3 May 2010 and (b) 1200 UTC 3 May 2010.

Tennessee there were consistent southerly winds (Figs. 5.23a and 5.23b). This moisture allowed for precipitation to occur. In time, westerly winds started to prevail, pushing the system off to the east (Fig. 5.23b). Member 29 and member 31 (the wet ensemble members) have strong southerly flow bringing in a surplus of moisture from the Gulf of Mexico (Figs. 5.24a and 5.24c). This was a key component for the heavy precipitation that the Tennessee area received. When looking at the 850-hPa winds for member 36 and member 5 (the dry ensemble members), a very strong cyclonic rotation is present just to the west of Tennessee (Figs. 5.24b and 5.24d). This area of

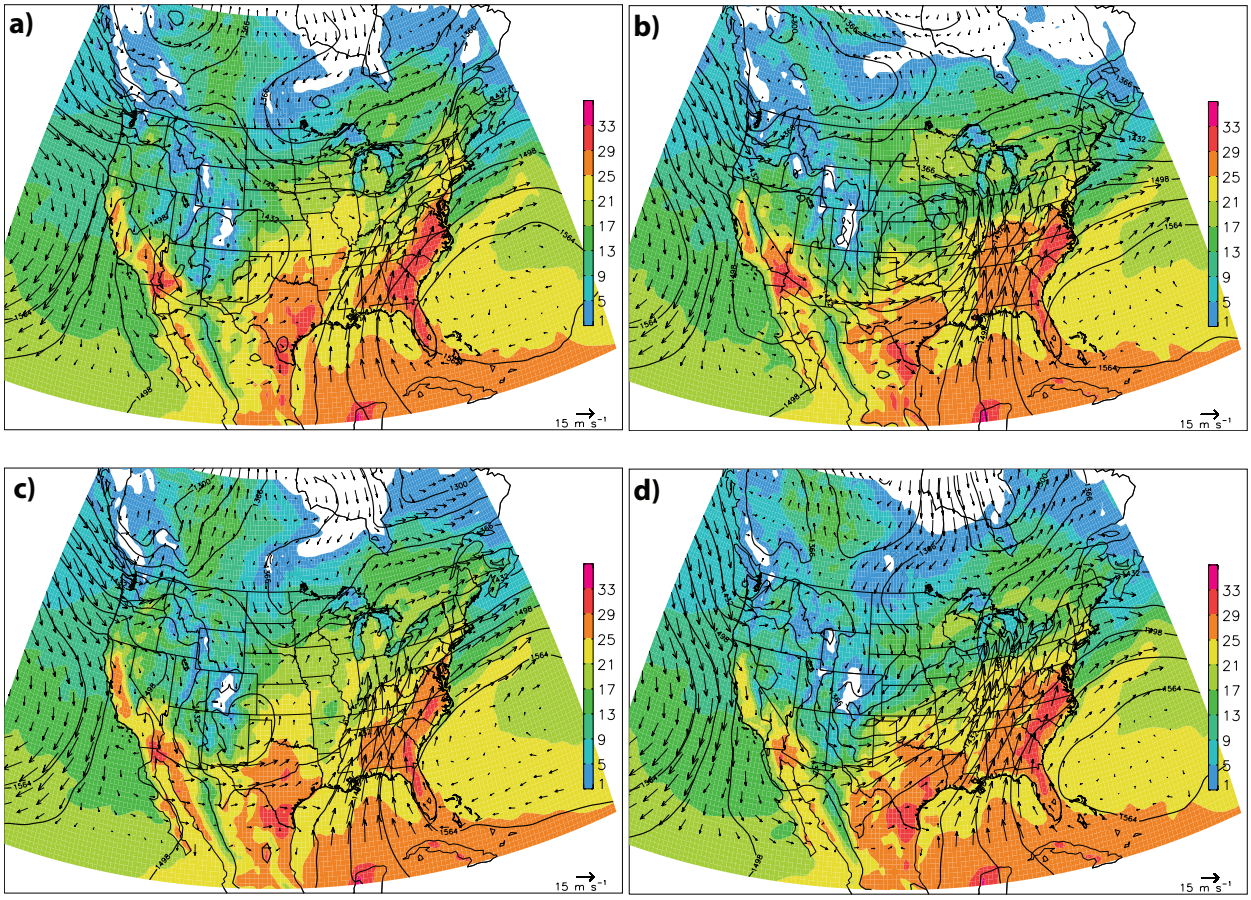

Figure 5.24: Forecasted 850-hPa temperature (color shading in C), height (black contours overlaid in m), and wind (vectors overlaid, vector scale is shown at bottom right) at 0000 UTC 3 May 2010, corresponding to forecast hour 84: (a) member 29 (wet), (b) member 36 (dry), (c) member 31 (wet), and (d) member 5 (dry).

rotation could be carrying drier air from the southwest into the Tennessee area, along with the southerly flow already present. Although the winds are much stronger in the dry ensemble members, this punch of dry air likely hindered the amount of precipitation that member 36 and member 5 forecasted for. Taking a look at the 850-hPa temperature, the stalled frontal boundary is easily distinguished. A fairly strong temperature gradient sits just to the west of Tennessee, along with a stronger gradient to the east (Figs. 5.23a and 5.23b). This stalled frontal boundary provides the necessary lift to initiate the thunderstorms and severe weather of the 29 April-4 May 2010 precipitation event. Member 29 and member 31 (the wet ensemble members) forecasted for temperatures slightly cooler in central Tennessee, with a defined frontal boundary to the west of Tennessee (Figs. 5.24a and 5.24c). Contrastingly, member 36 and member 5 (the dry ensemble members) forecasted for slightly warmer temperatures throughout Tennessee, with a less defined frontal boundary (Figs. 5.24b and 5.24d). This is likely due to strong cyclonic rotation causing warm air advection from Texas and Mexico. Additionally, the dry ensemble members forecasted for the warm front to be too far south, located around northern Kentucky (Figs. 5.24b and 5.24d).

Looking at the 850-hPa equivalent potential temperature, the location of the stationary surface front is denoted by the tight gradient in equivalent potential temperature located in western Tennessee. At 0000 UTC 3 May 2010, the surface frontal boundary is oriented from southwest to northeast, extending as far north as the Great Lakes region (Fig. 5.25a). Twelve hours later, at 1200 UTC 3 May 2010, the surface front is seen slowly pushing off to the east. The warm front associated with this extratropical cyclone is present extending to the east around Massachusetts (Fig. 5.25b). By looking at the forecasted 850-hPa equivalent potential temperature field, the key frontal structure differences become obvious between the wet and dry ensemble members. Ensemble members 29 and 31 (the wet ensemble members) forecasted for

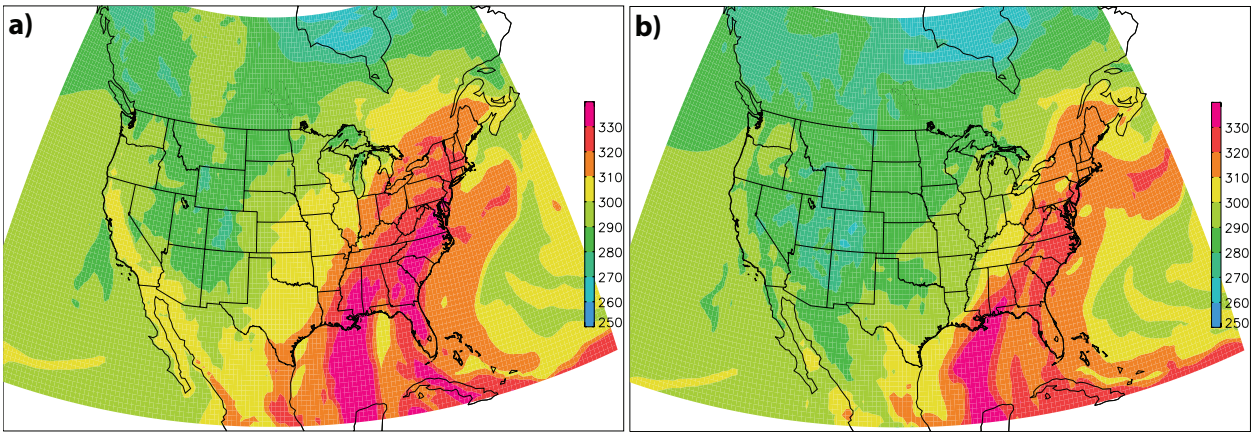

Figure 5.25: ECMWF analysis of 850-hPa equivalent potential temperature (color shading in K) at (a) 0000 UTC 3 May 2010 and (b) 1200 UTC 3 May 2010.

the stationary surface front to be oriented southwest to northeast, extending into the New England region. The wet ensemble members greatly resemble the observed equivalent potential temperature (Figs. 5.26a and 5.26c). As for ensemble members 5 and 36 (the dry ensemble members), the stationary surface front is forecasted to have a north south orientation. The surface front only extends as far north as Illinois. Associated with this extratropical cyclone, the dry ensemble members forecasted for the surface warm front to extend east of Illinois, oriented west to east (Figs. 5.26b and 5.26d). One big difference between the wet and dry ensemble members is the placement of this stationary surface front and associated warm front. The dry ensemble members have forecasted for a much more prominent warm front (Figs. 5.26b and 5.26d).

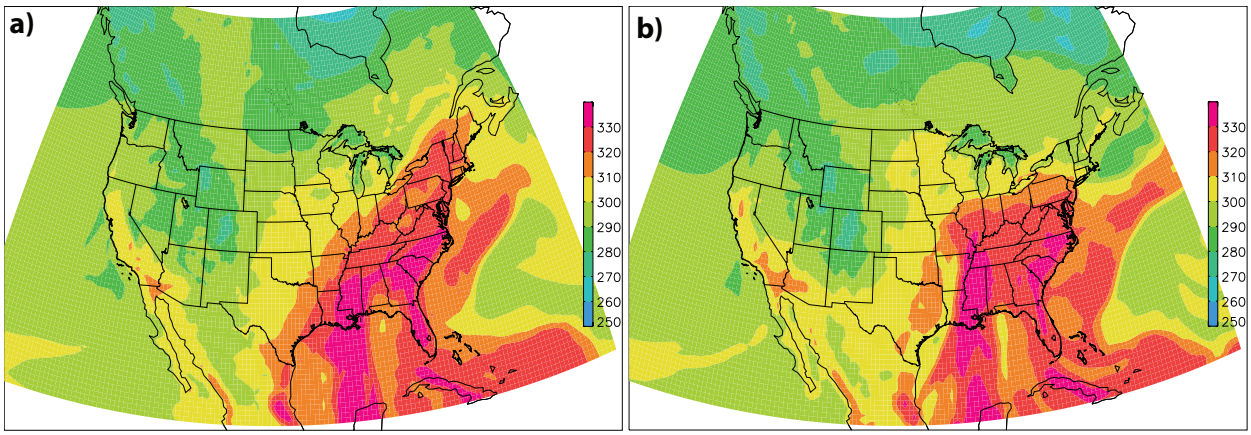

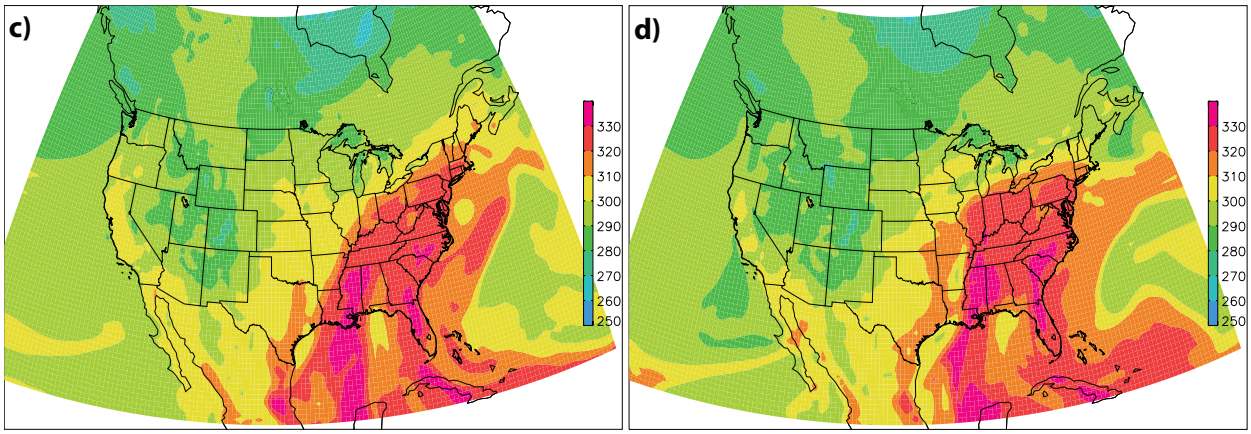

Figure 5.26: Forecasted 850-hPa equivalent potential temperature (color shading in K) at 0000 UTC 3 May 2010, corresponding to forecast hour 84: (a) member 29 (wet), (b) member 36 (dry), (c) member 31 (wet), and (d) member 5 (dry).

When looking at the total column water, an impressive, linear feature is present feeding in moisture from the Gulf of Mexico. The origin of this moisture plume extends farther south and east towards the Caribbean Sea. Just south of Central America, in the eastern Pacific, a large reservoir of tropical moisture resides, with values greater than 60 mm. Twenty-four hours prior, a build up of this tropical moisture occurred, where it then rushed into the Mississippi Valley carrying an exceptionally high value of total column water (Fig. 5.27a-d). Additional moisture is being pulled into the southeastern United States from the deep tropics. The total column water in central Tennessee is around 50 to 55 mm (Fig. 5.27c). This was able to supply Tennessee and the Mid-Atlantic states with sufficient moisture to support heavy precipitation. Twelve hours later, the moisture has pushed off to the east, toward the coast of the United States (Fig. 5.27d). Member 29 and member 31 (the wet ensemble members) forecasted for a very strong inflow of moisture from the Gulf of Mexico. This conveyor belt of moisture extended from the Caribbean Sea up to northern Kentucky (Figs. 5.28a and 5.28c). Member 29 and member 31 (the wet ensemble members) forecasted for central Tennessee to receive a high amount of total column

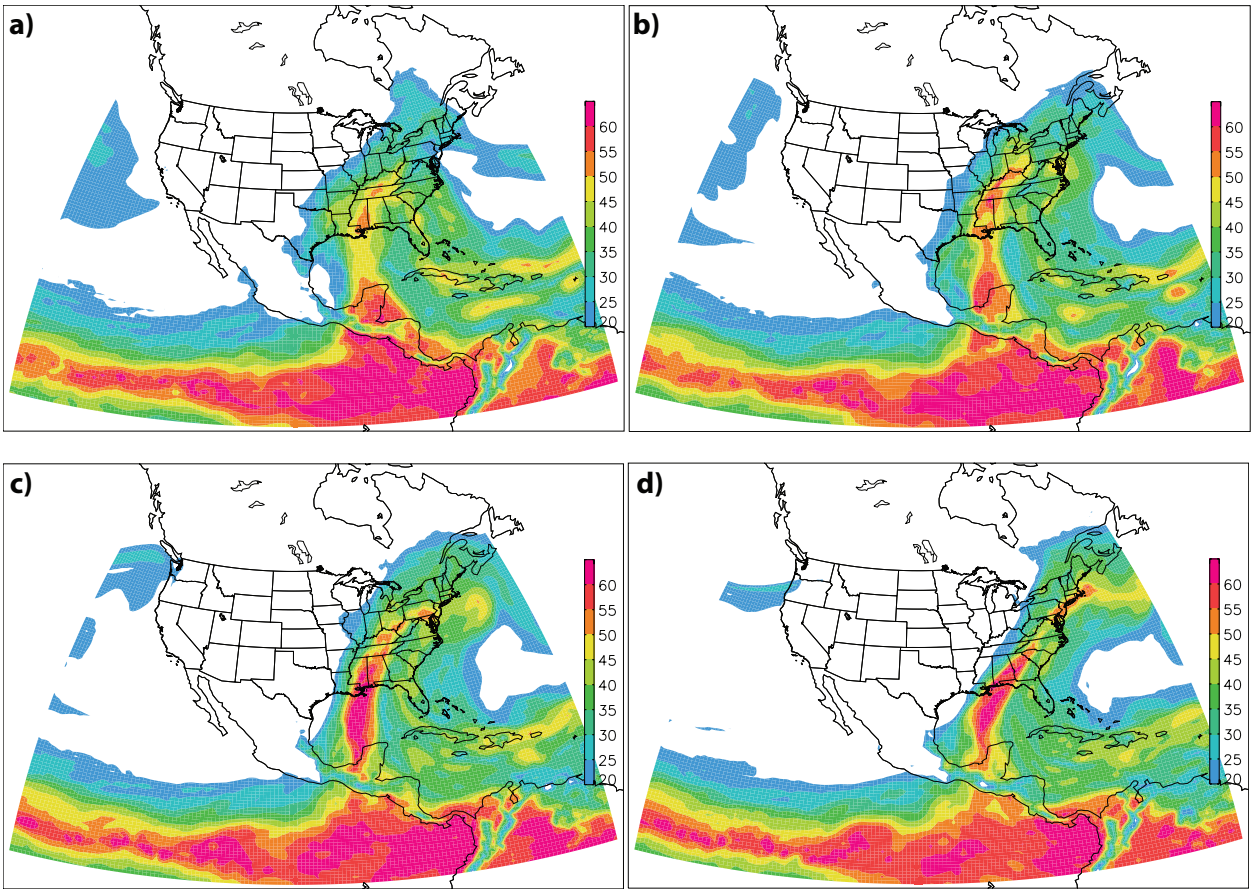

Figure 5.27: ECMWF analysis of total column water (color shading in mm) at (a) 0000 UTC 2 May 2010, (b) 1200 UTC 2 May 2010, (c) 0000 UTC 3 May 2010, and (d) 1200 UTC 3 May 2010.

water, while member 36 (one of the dry ensemble member) forecasted for high total column water to be located in western Tennessee (Figs. 5.28b and 5.28d). Member 5 (one of the dry ensemble members) forecasted quite differently, even from the other dry ensemble member. Member 5 forecasted for moisture to be flowing in from the Gulf of Mexico, however, the amount of such moisture is significantly decreased. Additionally, the bulk of moisture flowing in from the Gulf of Mexico does not extend north of northern Alabama and northern Mississippi (Fig. 5.28d). Therefore, Tennessee and surrounding areas are not receiving the moisture necessary to support heavy precipitation. Although the moisture is displaced in ensemble member 36 and slightly weakened in ensemble member 5, both ensemble members forecasted

for a strong moisture plume (Figs. 5.28b and 5.28d). Overall, both the wet and dry ensemble members accurately forecasted for the transport of deep tropical moisture poleward into the Mississippi Valley. How that tropical moisture interacted with the synoptic scale flow is what caused the forecasts between the wet and dry ensemble member to differ. Boyd and Roberts (2010) examined the same precipitation event and noted the deep moisture plume, which produced record precipitable water over the Nashville area. They found that the depth of the moisture, combined with the duration of moisture transport, produced high rainfall rates and impressive totals over the Nashville, Tennessee area.

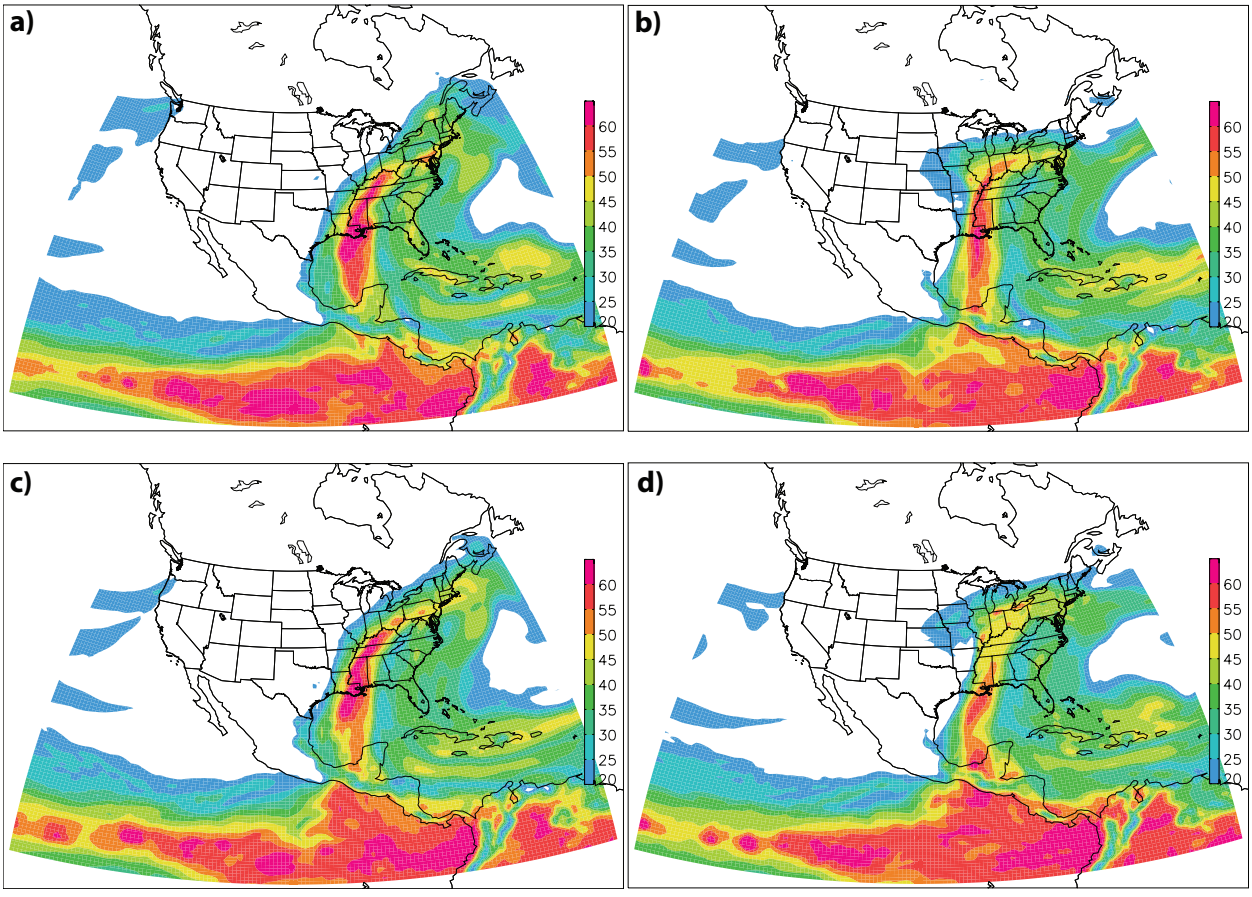

Figure 5.28: Forecasted total column water (color shading in mm) at 0000 UTC 3 May 2010, corresponding to forecast hour 84: (a) member 29 (wet), (b) member 36 (dry), (c) member 31 (wet), and (d) member 5 (dry).

Junker et al. (1999) found that the scale and intensity of rainfall appears to be related to the strength of low-level moisture flux. High values of moisture flux are associated with heavy rainfall potential with convective systems. At the peak of the event, at 1200 UTC 2 May 2010, an exceptionally large swath of moisture is fluxed into the Mississippi Valley, providing impressive moisture for the region (Fig. 5.29a). At 0000 UTC 3 May 2010, 850-hPa moisture flux reaches over 220 g kg^{-1} m s^{-1} extending from the Gulf of Mexico through eastern Tennessee, and then

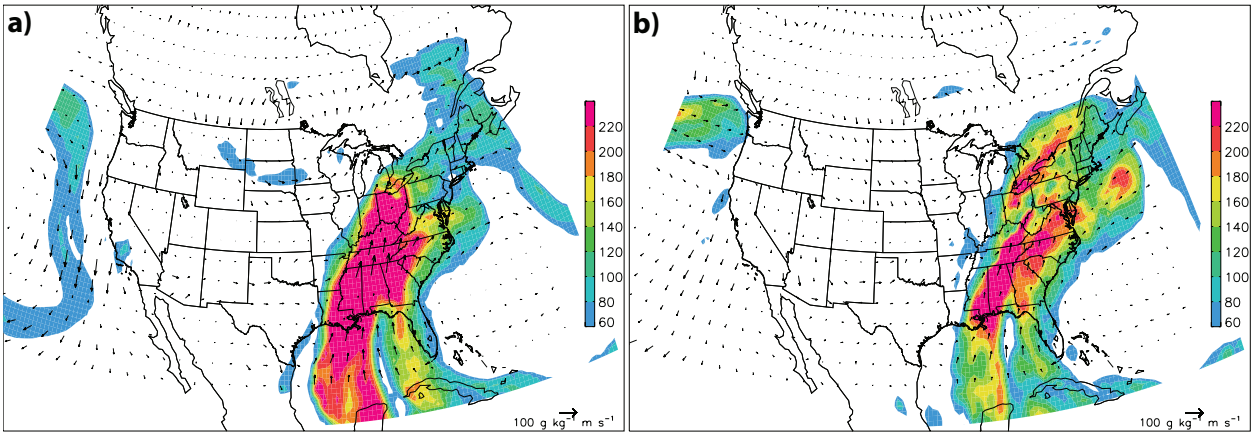

Figure 5.29: ECMWF analysis of 850-hPa moisture flux (color shading in g kg^{-1} m s^{-1} with vectors overlaid, vector scale is shown at bottom right) at (a) 1200 UTC 2 May 2010 and (b) 0000 UTC 3 May 2010.

pushing into the northeastern United States (Fig. 5.29b). Numerous studies have found an axis of 850-hPa moisture flux upstream from MCSs that produced heavy rainfall (Rochette and Moore 1996, Junker and Schneider 1997, Junker et al. 1999, Bodner et al. 2011). Members 29 and 31 (the wet ensemble members) closely resemble the observed 850-hPa moisture flux. Both the wet ensemble members forecasted for a plume of moisture to protrude from the Gulf of Mexico, extending northeastward through Tennessee and into the northeastern United States (Figs. 5.30a and 5.30c). Similar to the wet ensemble members, the dry ensemble members, members 36 and 5, forecasted for a deep plume of moisture to make its way into Tennessee from the Gulf of

Mexico. However, once the plume of moisture reaches the Great Lakes area it spreads out in the horizontal over a large area, likely along the warm front (Figs. 5.30b and 5.30d).

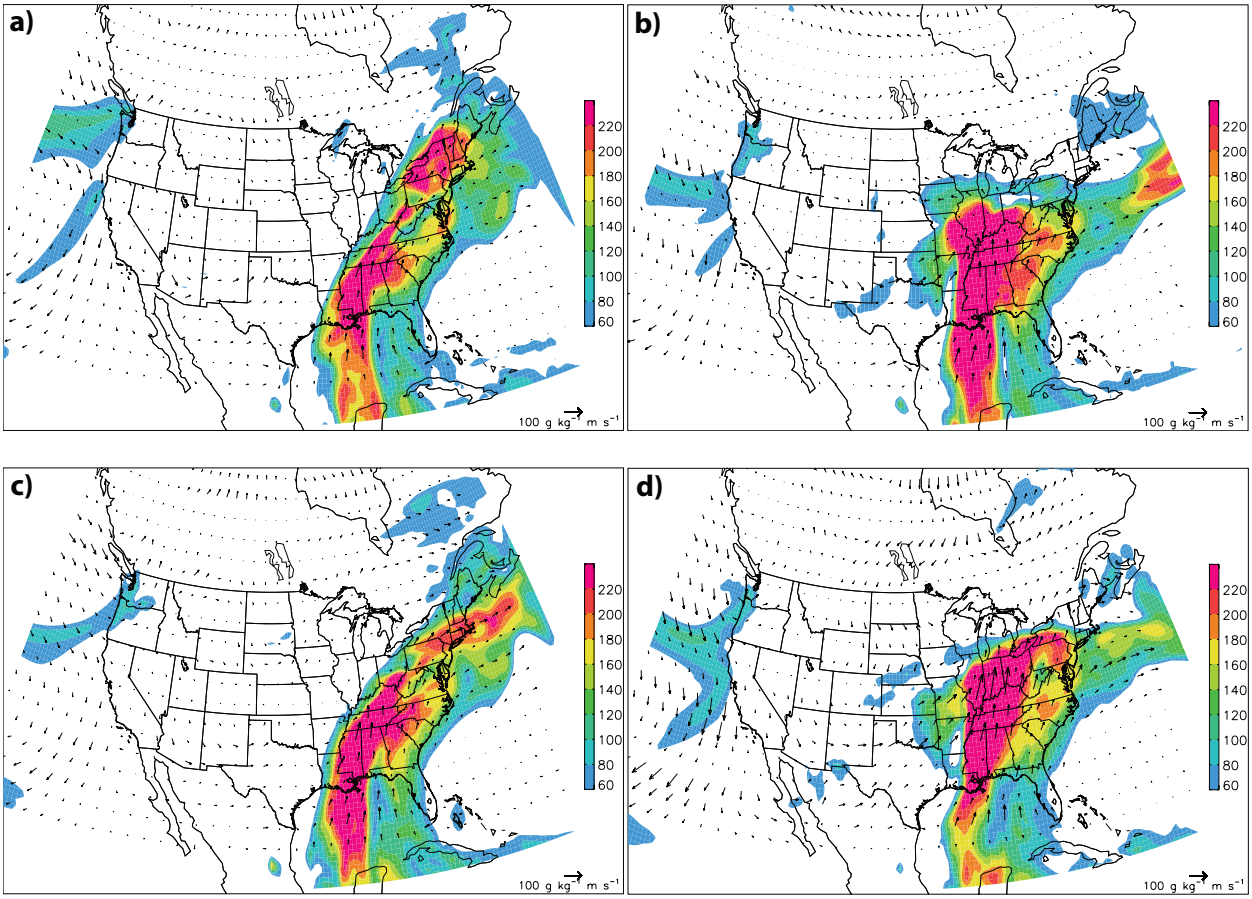

Figure 5.30: Forecasted 850-hPa moisture flux (color shading in g kg^{-1} m s^{-1} with vectors overlaid, vector scale is shown at bottom right) at 0000 UTC 3 May 2010, corresponding to forecast hour 84: (a) member 29 (wet), (b) member 36 (dry), (c) member 31 (wet), and (d) member 5 (dry).

The following figures are the time-integrated moisture flux from 0000 UTC 1 May 2010 to 0000 UTC 3 May 2010 for three different levels of the atmosphere, 925-hPa, 850-hPa, and 700-hPa. Both the quasi-stationary MCSs passed through western Tennessee within this two-day time frame. Starting with the ECMWF analysis of 925-hPa time-integrated moisture flux from 0000 UTC 1 May 2010 to 0000 UTC 3 May 2010, large time-integrated moisture flux values are entering the southeastern United States from the Caribbean Sea. At the lower levels, this time-

integrated flux of moisture reaches over 25 x 10^7 g kg^{-1} m (Fig. 5.31a). As the steady plume of moisture enters the southeastern United States, it begins to get lofted over the stationary surface front. Looking at the 850-hPa level, the highest values of time-integrated moisture flux are overhead Alabama and western Mississippi, reaching 24 x 10^7 g kg^{-1} m (Fig. 5.31b). Finally, looking at the ECMWF analysis of 700-hPa time-integrated moisture flux, large values of time-integrated moisture flux lie in the Tennessee region with values reaching 16 x 10^7 g kg^{-1} m in western Tennessee. The conveyor belt of moisture from the Caribbean Sea has been lofted over the stationary surface front as the moisture was transported poleward, resulting in high amount of time-integrated moisture flux in Tennessee (Fig. 5.31c). Looking at the forecasted 925-hPa time-

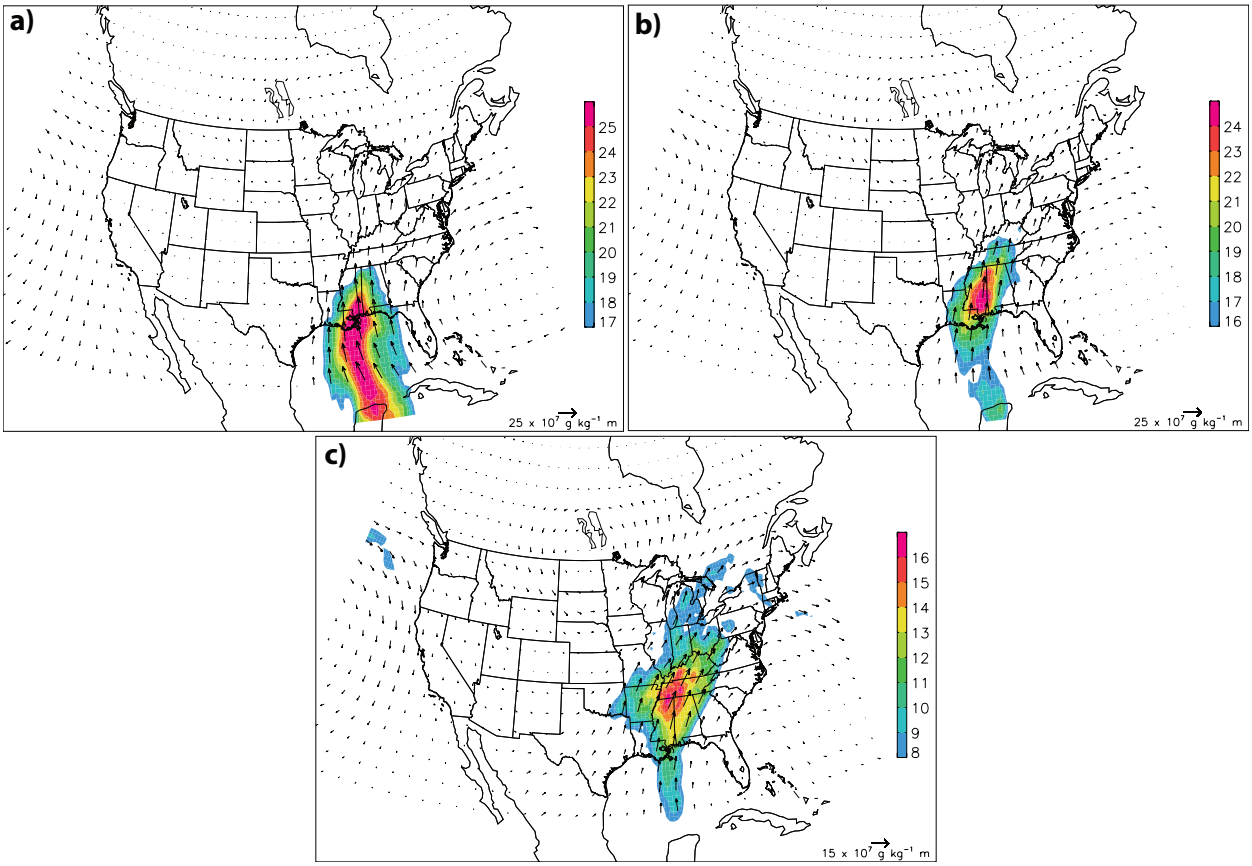

Figure 5.31: ECMWF analysis of (a) 925-hPa, (b) 850-hPa, and (c) 700-hPa time-integrated moisture flux (color shading in 10^7 g kg^{-1} m with vectors overlaid, vector scale is shown at bottom right) from 0000 UTC 1 May 2010 to 0000 UTC 3 May 2010.

integrated moisture flux, both the wet and dry ensemble members have forecasted for a flux of moisture from the Caribbean Sea. However, ensemble members 29 and 31 (the wet ensemble members) have forecasted for a much larger flux of moisture, reaching approximately 25 x 10^7 g kg^{-1} m in the selected two day period (Figs. 5.32a and 5.32c). The dry ensemble members (ensemble members 5 and 36) only forecasted for time-integrated moisture flux values reaching approximately 23 x 10^7 g kg^{-1} m (Figs. 5.32b and 5.32d). At the 850-hPa level, ensemble members 29 and 31 (the wet ensemble members) have forecasted for a large time-integrated moisture flux, exceeding 24 x 10^7 g kg^{-1} m, to enter west/central Tennessee, providing ample moisture to the Nashville, Tennessee area (Figs. 5.33a and 5.33c). On the contrary, ensemble members 36 and 5 (the dry ensemble members) have not forecasted for nearly as much time-integrated moisture flux to impede western Tennessee. Ensemble members 36 and 5 (the dry ensemble members) forecasted for time-integrated moisture flux values in western Tennessee of 19 x 10^7 g kg^{-1} m and 22 x 10^7 g kg^{-1} m (Figs. 5.33b and 5.33d). Finally, looking at the forecasted time-integrated moisture flux at the 700-hPa level, ensemble members 29 and 31 (the wet ensemble members) forecasted for the highest value of time-integrated moisture flux to be located overhead western/central Tennessee. With values reaching 16 x 10^7 g kg^{-1} m, this provides the necessary moisture for heavy precipitation totals in western Tennessee (Figs. 5.34a and 5.34c). Ensemble member 36 (a dry ensemble member) also forecasted for high values of time-integrated moisture flux, exceeding 16 x 10^7 g kg^{-1} m, however this moisture flux is displaced too far to the west, nearly missing Nashville, Tennessee (Fig 5.34b). Ensemble member 5 (a dry ensemble member) only forecasted for time-integrated moisture flux values to reach 14 x 10^7 g kg^{-1} m, also displacing the highest value to the west (Fig. 5.34d). As the

moisture enters the southeastern United States, it is lofted over the stationary surface front, resulting in high amounts of moisture overhead west central Tennessee at the 700-hPa level.

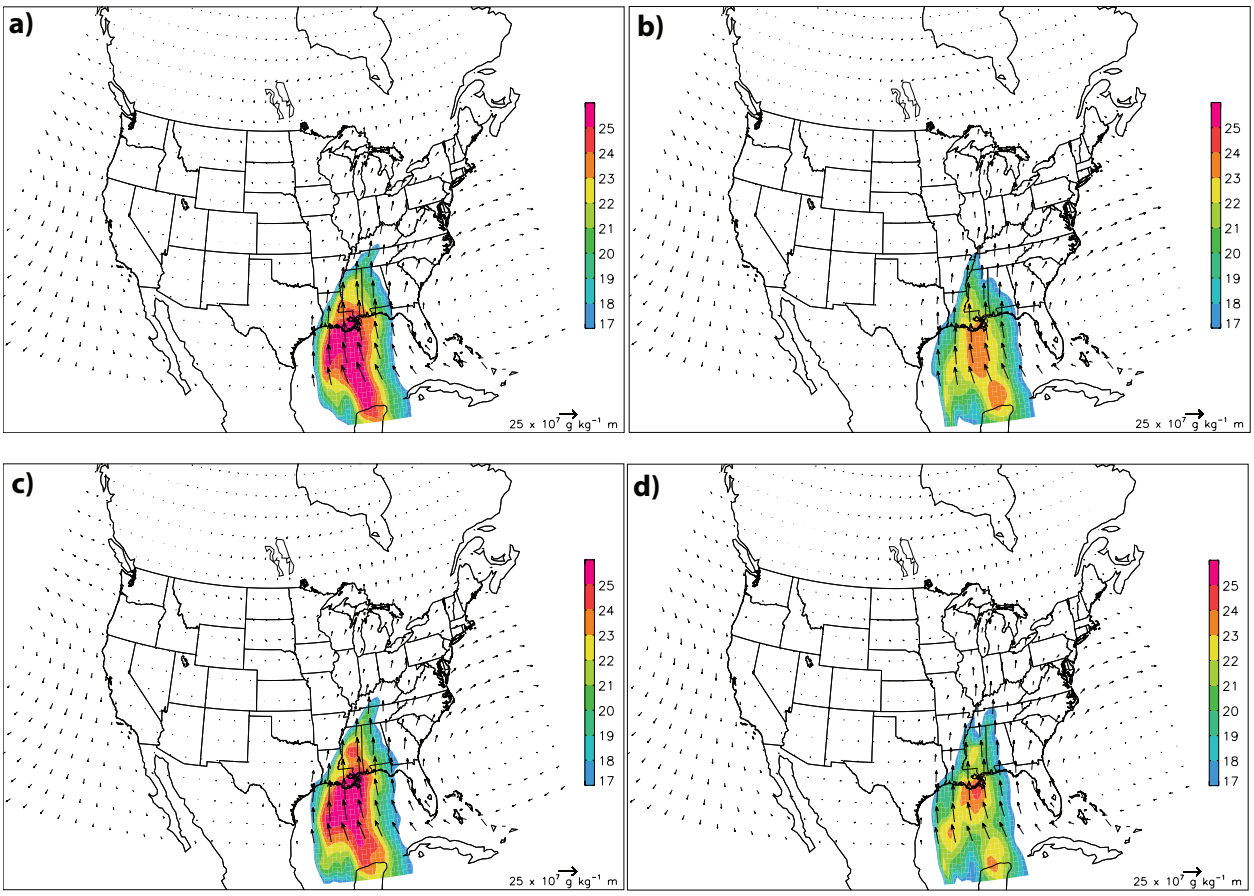

Figure 5.32: Forecasted 925-hPa time-integrated moisture flux (color shading in 10^7 g kg^{-1} m with vectors overlaid, vector scale is shown at bottom right) from 0000 UTC 1 May 2010 to 0000 UTC 3 May 2010, corresponding to forecast hour 36 to forecast hour 84: (a) member 29 (wet), (b) member 36 (dry), (c) member 31 (wet), and (d) member 5 (dry).

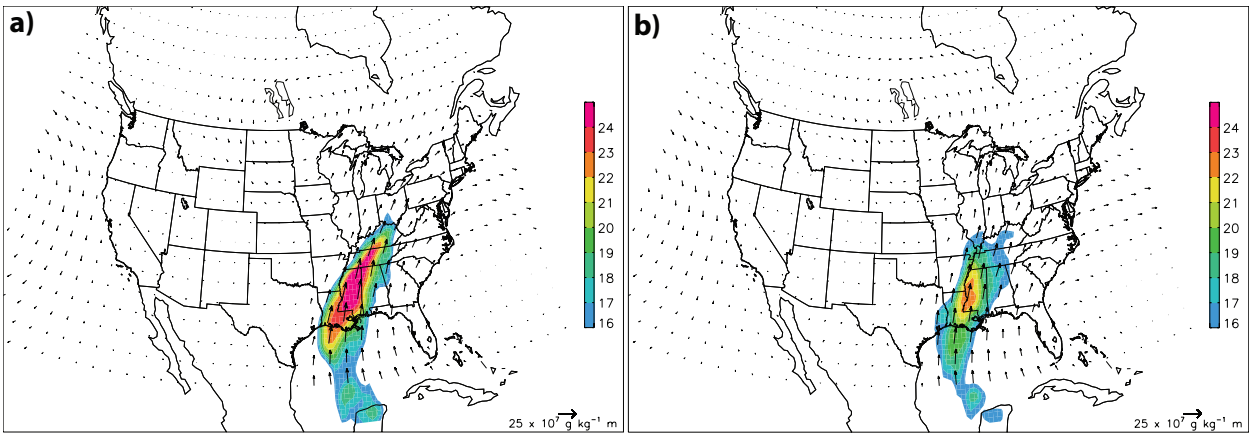

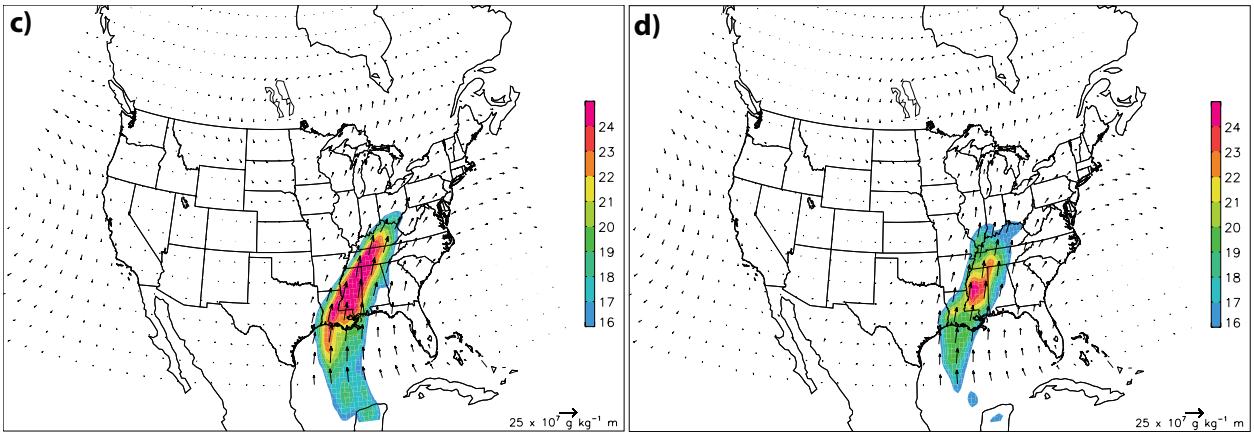

Figure 5.33: As in Fig. 5.32, except for forecasted 850-hPa time-integrated moisture flux.

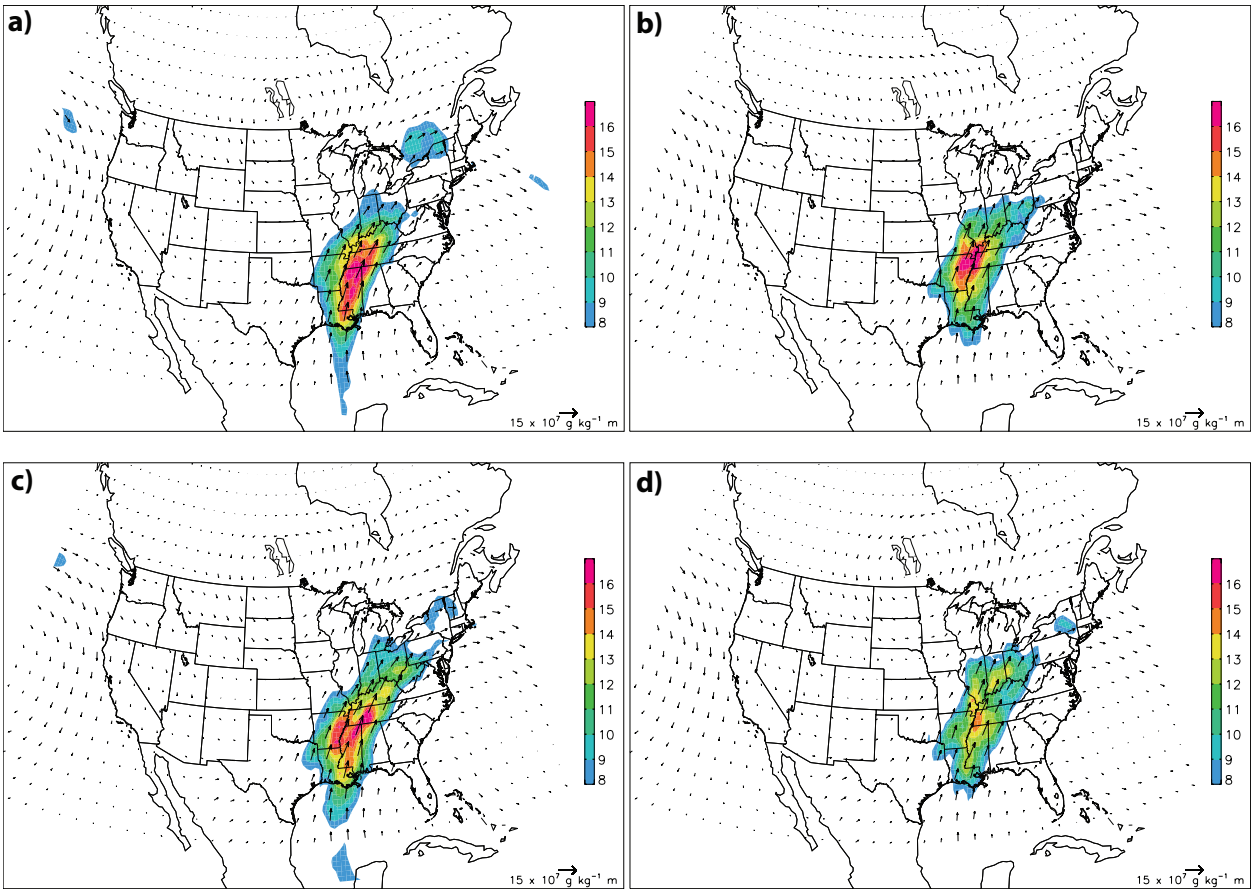

Figure 5.34: As in Fig. 5.32, except for forecasted 700-hPa time-integrated moisture flux.

5.4 Comparison at an alternate initialization time

In order to verify the findings at an initialization time of 1200 UTC 29 April 2010, the same processes were used at a new initialization time of 0000 UTC 29 April 2010, twelve hours prior. At a new initialization time, the selection process of the most accurate and least accurate ensemble members must be repeated. As suggested by Bright and Nutter (2004), the "bad" members may appear as the "best" members at an earlier initialization time. As before, each of the 50 ensemble members was compared to the CPC precipitation dataset to determine the skill in its forecasts. Member 14 and member 45 had a very similar spatial distribution as the observed event, while member 18 and member 26 had little to no resemblance (shown later in the study). After the five-day area-averaged precipitation was calculated within the thick black box encompassing the Tennessee area, it was then compared to the five-day area-averaged precipitation of the forecasted ensemble members (Fig. 5.2; shown later in the study). The observed precipitation for this event had an area-averaged precipitation of 89 millimeters. Member 14 had a five-day area-averaged precipitation of 106 millimeters and member 45 had a five-day area-averaged precipitation of 92 millimeters. Member 18 had an area-averaged precipitation of 68 millimeters and member 26 had a five-day area-averaged precipitation of 65 millimeters (Fig. 5.35). As before, the equitable threat score (ETS) was the final method used to determine the most accurate and least accurate ensemble members at the new initialization time of 0000 UTC 29 April 2010. The two ensemble members plotted in orange will be discussed later as the "displaced ensemble members."

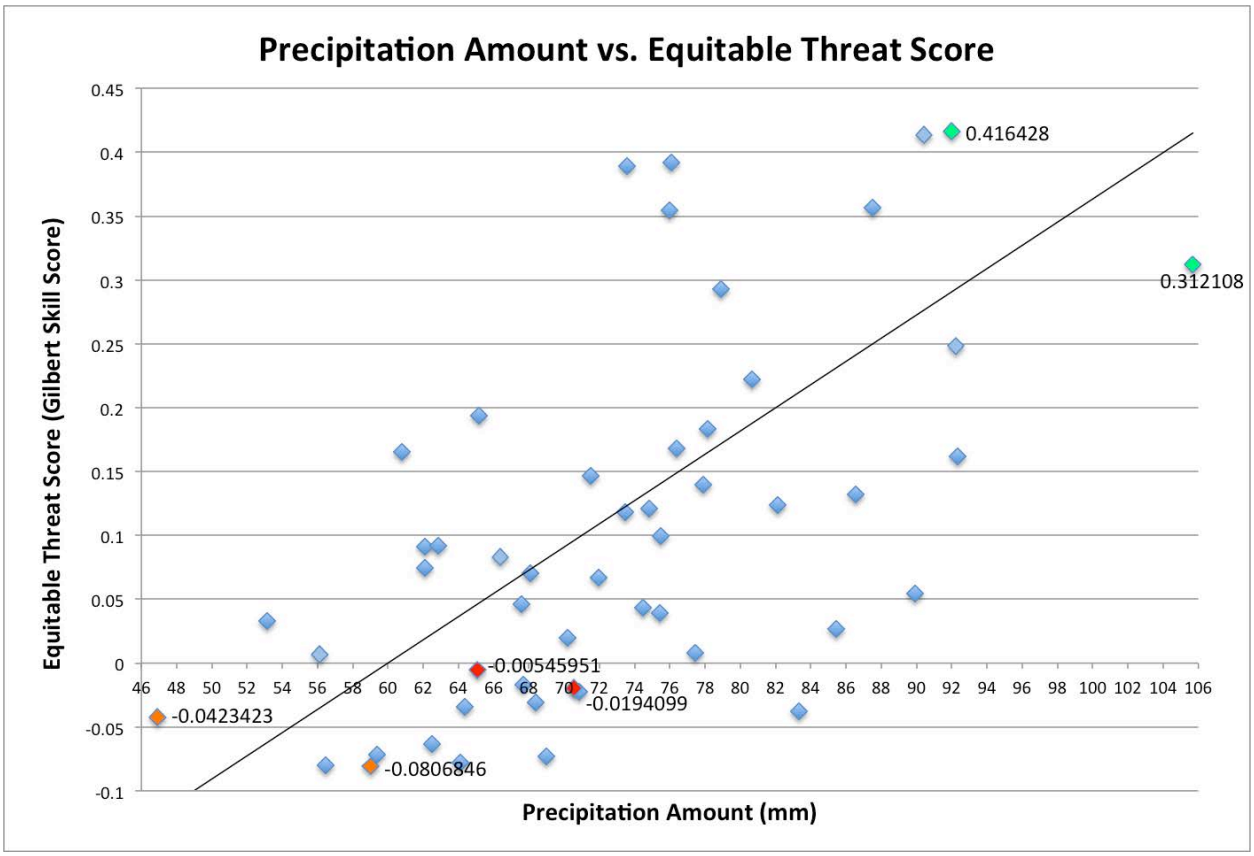

Figure 5.35: Area-averaged precipitation vs. equitable threat score scatter plot at a threshold of 100 mm between 1200 UTC 29 April 2010 – 1200 UTC 4 May 2010. The wet ensemble members (members 14 and 45) are plotted in green, the dry ensemble members (members 18 and 26) are plotted in red, and the displaced ensemble members (members 0 and 37) are plotted in orange.

After looking at all 50 members, it was determined that the most accurate forecast was from members 14 and 45 (the wet ensemble members), while the least accurate forecast was from members 18 and 26 (the dry ensemble members). Once the wet ensemble members and dry ensemble members were selected, correlation plots were created and analyzed. The 96-hour forecast of the 500-hPa height correlations to area-averaged precipitation looks extremely similar to the correlations in the original initialization time of 1200 UTC 29 April 2010. There is a region of positive correlation ($r \approx 0.5$) to the north/northwest of Tennessee indicating higher heights result in more precipitation over the area of interest (Fig. 5.36). Interestingly, at the new

initialization time of 0000 UTC 29 April 2010, the large core of positive correlation residing over the Pacific Ocean and western United States is no longer present. In central Texas, 500-hPa height and area-averaged precipitation are anticorrelated ($r \approx -0.4$), indicating the ensemble members with lower heights over Texas had more precipitation in the area of interest (Fig. 5.36).

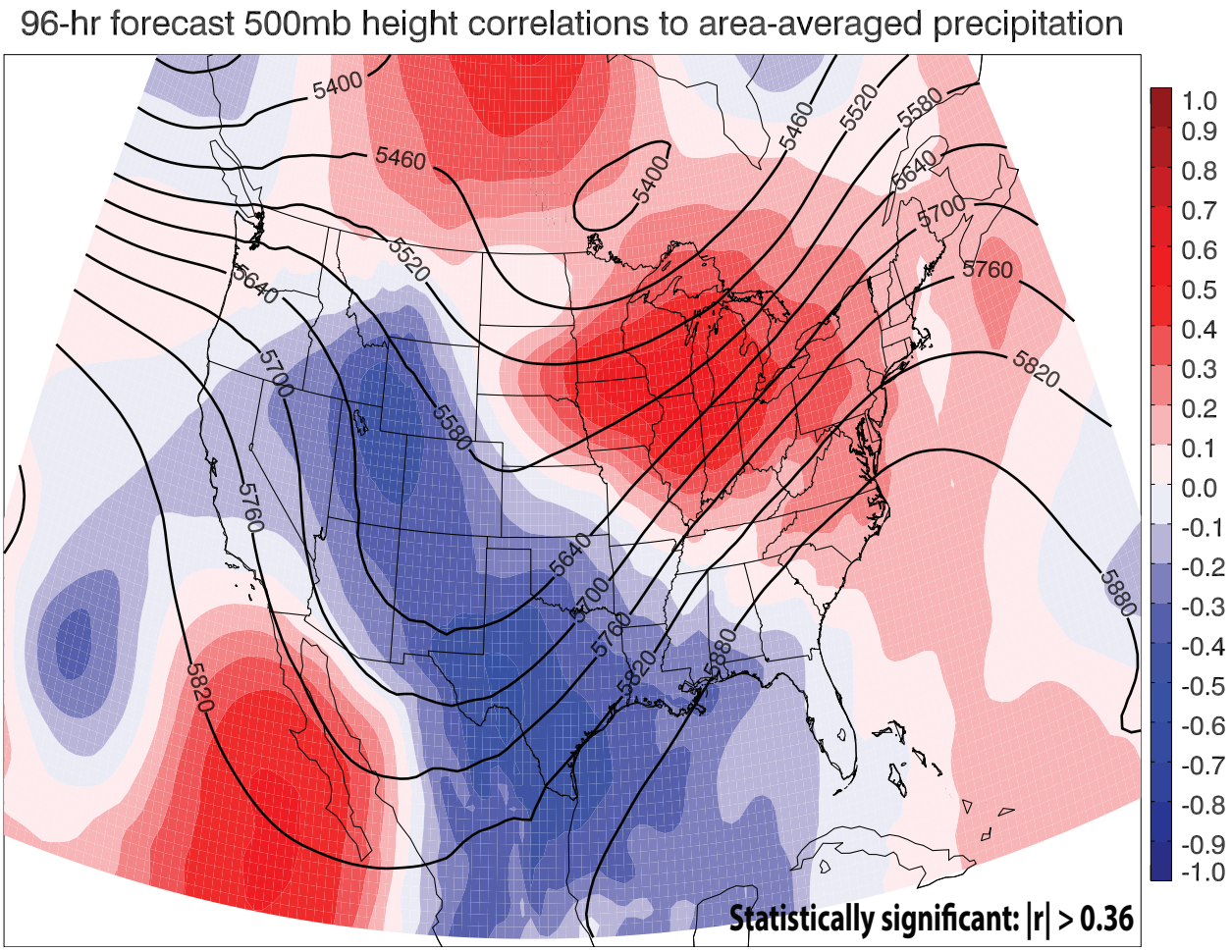

Figure 5.36: Area-averaged precipitation between 1200 UTC 29 April 2010 – 1200 UTC 4 May 2010 correlated to 500-hPa height at 0000 UTC 3 May 2010, corresponding to forecast hour 96. Warm colors represent a positive correlation, while cool colors represent a negative correlation. The ensemble mean 500-hPa height contours are shown in thick black.

Taking a look at the 96-hour forecast of the 850-hPa height correlations to area-averaged precipitation, there is a region of positive correlation, with a correlation coefficient around 0.5, to the north of Tennessee (Fig. 5.37). The position of this positive correlation is noteworthy

because it is now positioned more to the north than in the previous initialization time of 1200 UTC 29 April 2010. Regardless of the slight position difference, this suggests that a weaker trough over the central United States was associated with more precipitation over the area of interest. As noted before, at the new initialization time of 0000 UTC 29 April 2010, the large core of positive correlation residing over the Pacific Ocean and western United Sates is no longer present (Fig. 5.37). A relatively strong negative correlation ($r \approx -0.6$) resides just east of Mexico, suggesting as heights decrease, precipitation increases (Fig. 5.37). Again, this indicates the likely presence of a lee trough from the Sierra Madre Oriental Mountains in Mexico.

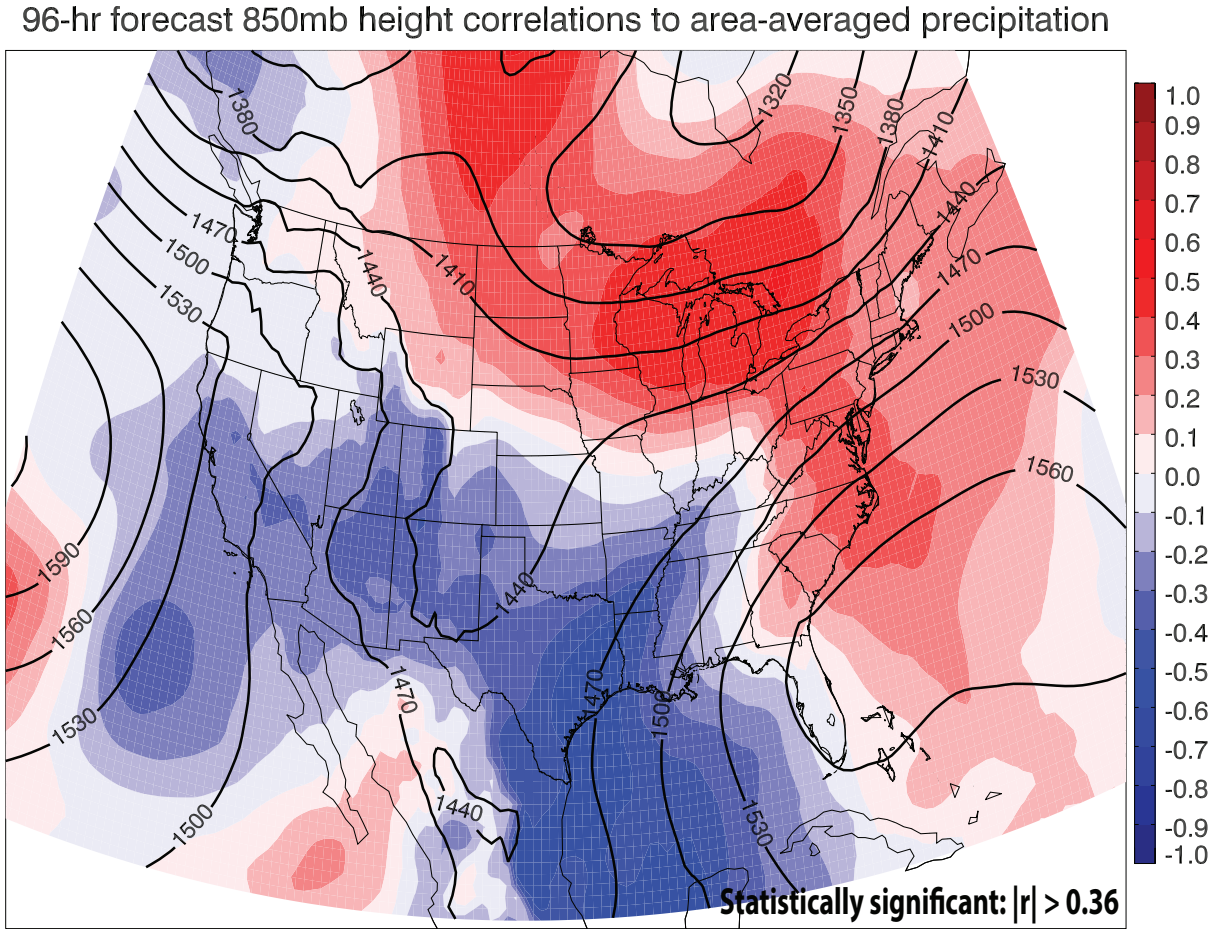

Figure 5.37: Area-averaged precipitation between 1200 UTC 29 April 2010 – 1200 UTC 4 May 2010 correlated to 850-hPa height at 0000 UTC 3 May 2010, corresponding to forecast hour 96. Warm colors represent a positive correlation, while cool colors represent a negative correlation. The ensemble mean 850-hPa height contours are shown in thick black.

Looking at the 96-hour forecast of the 850-hPa v-wind correlations to area-averaged precipitation, a strong positive correlation ($r \approx 0.5$) exists throughout Tennessee, extending south into the Gulf of Mexico (Fig. 5.38). This indicates as the strength of the low level jet increases, the amount of precipitation in the area of interest increases, likely allowing for more moisture transport. In contrast to the results from an initialization time of 1200 UTC 29 April 2010, the strong correlation indicates the wet ensemble members forecasted for a stronger low level jet, while the dry ensemble members forecasted for a weaker low level jet. Consistent with the findings found at an initialization time of 1200 UTC 29 April 2010, there is a region of

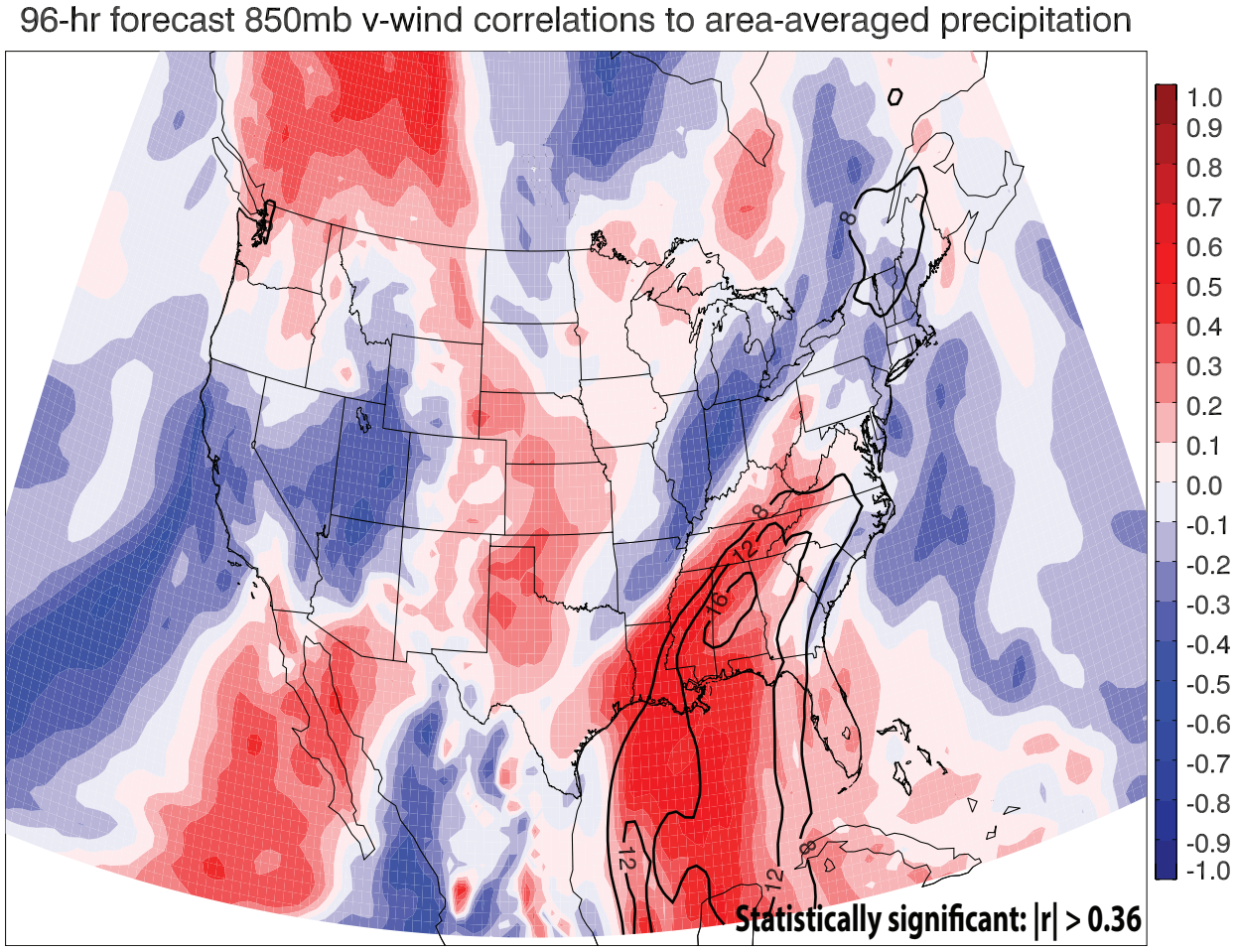

Figure 5.38: Area-averaged precipitation between 1200 UTC 29 April 2010 – 1200 UTC 4 May 2010 correlated to 850-hPa v-wind at 0000 UTC 3 May 2010, corresponding to forecast hour 96. Warm colors represent a positive correlation, while cool colors represent a negative correlation. The ensemble mean 850-hPa v-wind contours (in ms^{-1}) are shown in thick black.

anticorrelation (r ≈ -0.3) to the northwest of Tennessee, in the Midwestern United States. The ensemble mean low level jet, in the thick black contours, is slightly weaker than predicted at the later initialization time only peaking at about 16 ms^{-1} (Fig. 5.38).

Looking at the 84-hour forecast of the 850-hPa total column water correlations to area-averaged precipitation, there is a region of positive correlation (r ≈ 0.3) in central Tennessee, extending southwest into Texas (Fig. 5.39). This positive correlation appears to be oriented along

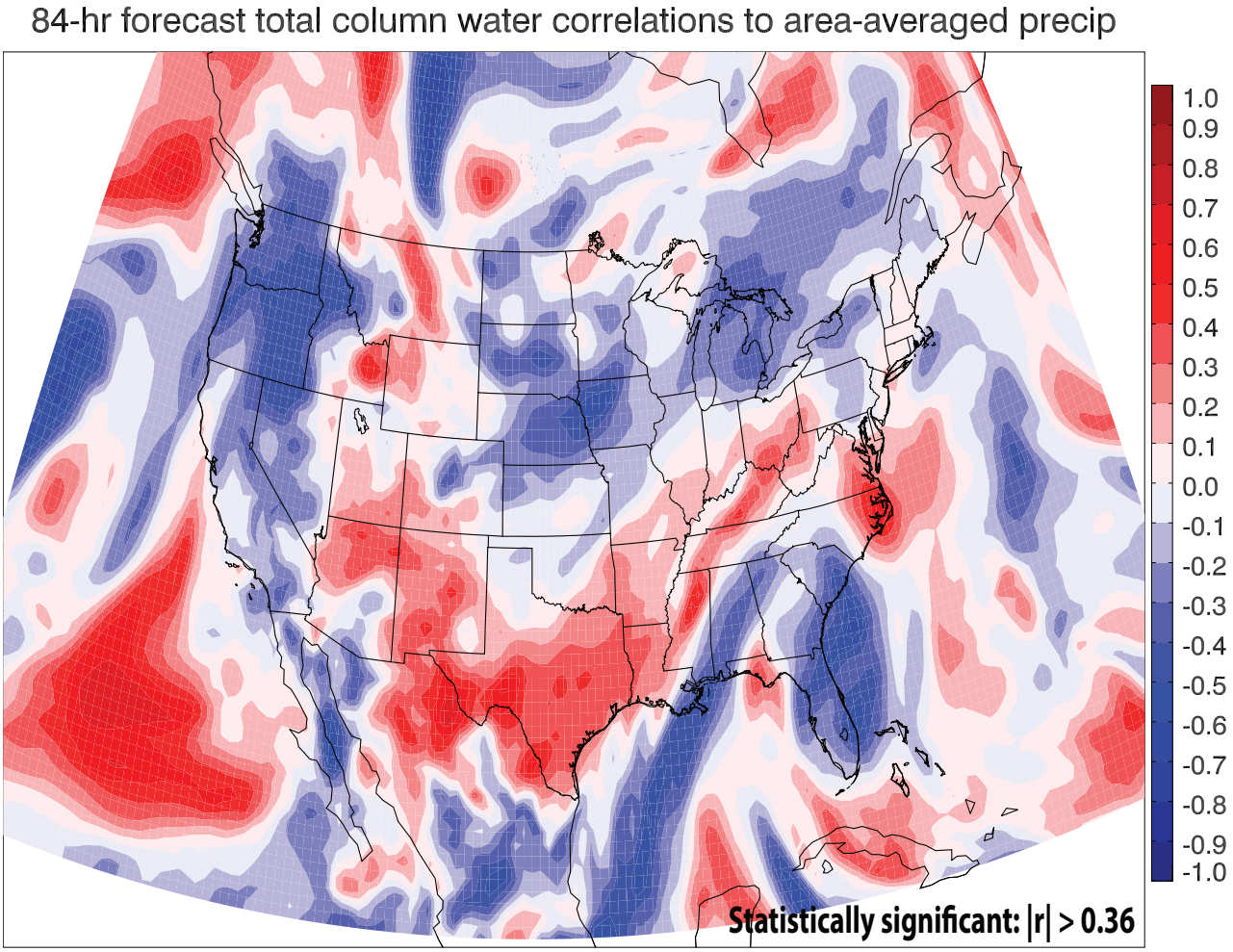

Figure 5.39: Area-averaged precipitation between 1200 UTC 29 April 2010 – 1200 UTC 4 May 2010 correlated to total column water at 1200 UTC 2 May 2010, corresponding to forecast hour 84. Warm colors represent a positive correlation, while cool colors represent a negative correlation.

the stationary surface front in central Tennessee. At this time, the initial MCS was impacting Nashville, Tennessee and surrounding areas. Directly southeast of Tennessee, 850-hPa total column water and area-averaged precipitation are anticorrelated ($r \approx -0.4$, Fig. 5.39). The scatter plot relating the forecast total column water at a point in central Tennessee to 84-hour area-averaged precipitation exhibits little to no relationship between these two variables. This is an indication that all the ensemble members forecasted for a high amount of total column water in Nashville, Tennessee. One of the dry ensemble members has more total column water than both of the wet ensemble members. However, both the dry ensemble members have a much smaller amount of precipitation (Fig. 5.40). As noted before, the two ensemble members plotted in

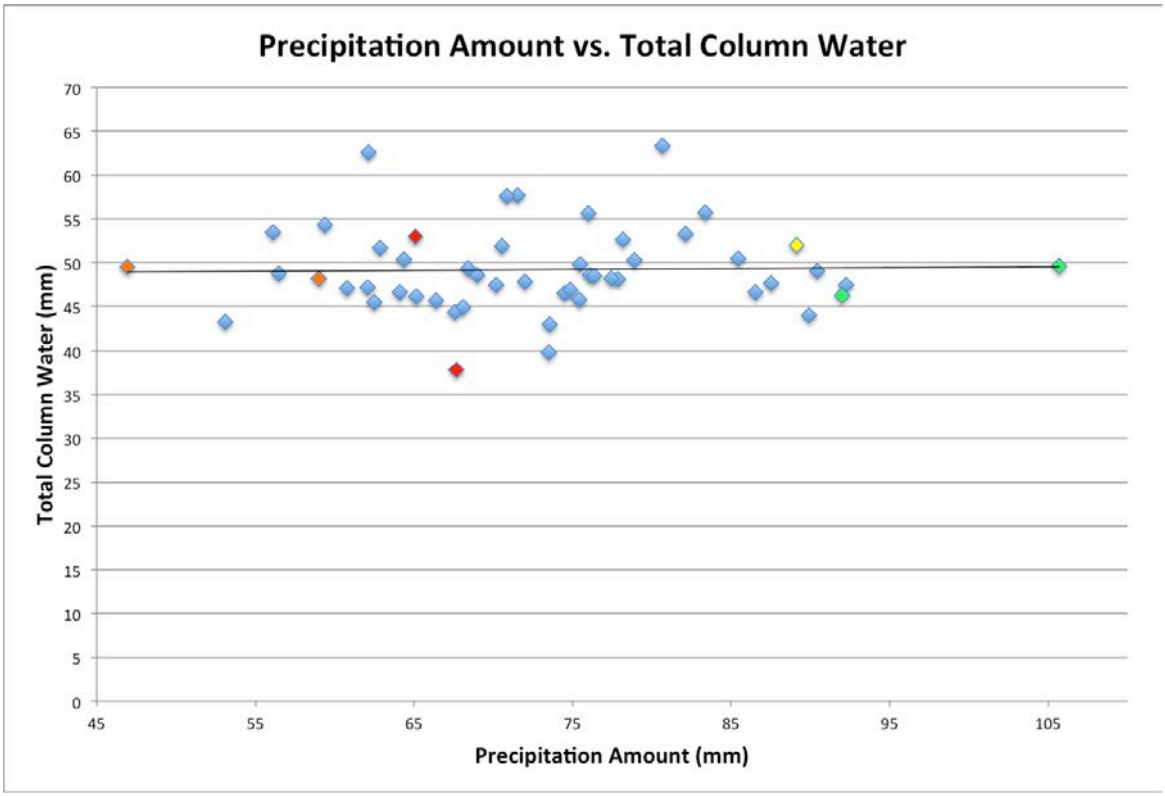

Figure 5.40: Scatter plot of area-averaged precipitation between 1200 UTC 29 April 2010 – 1200 UTC 4 May 2010 vs. total column water at latitude: 36° N and longitude: 87° W at 1200 UTC 2 May 2010, corresponding to forecast hour 84. The wet ensemble members (members 14 and 45) are plotted in green, the dry ensemble members (members 18 and 26) are plotted in red, the displaced ensemble members (members 0 and 37), and the analysis is plotted in yellow.

orange will be discussed in greater detail later in the paper. Twenty-four hours later, the second quasi-stationary MCS was affecting Tennessee. Looking at the 108-hour forecast of the 850-hPa total column water correlations to area-averaged precipitation, there is a large core of positive correlation ($r \approx 0.7$) centered to the west of Tennessee, but also encompassing a majority of Tennessee (Fig. 5.41). This positive correlation appears to be oriented along the stationary surface front, from southwest to northeast. Directly southeast of Tennessee, 850-hPa total column water and area-averaged precipitation are anticorrelated ($r \approx -0.5$), also oriented parallel to the stationary surface boundary (Fig. 5.41). The scatter plot relating the forecast total column water at a point in central Tennessee to 108-hour area-averaged precipitation exhibits a strong

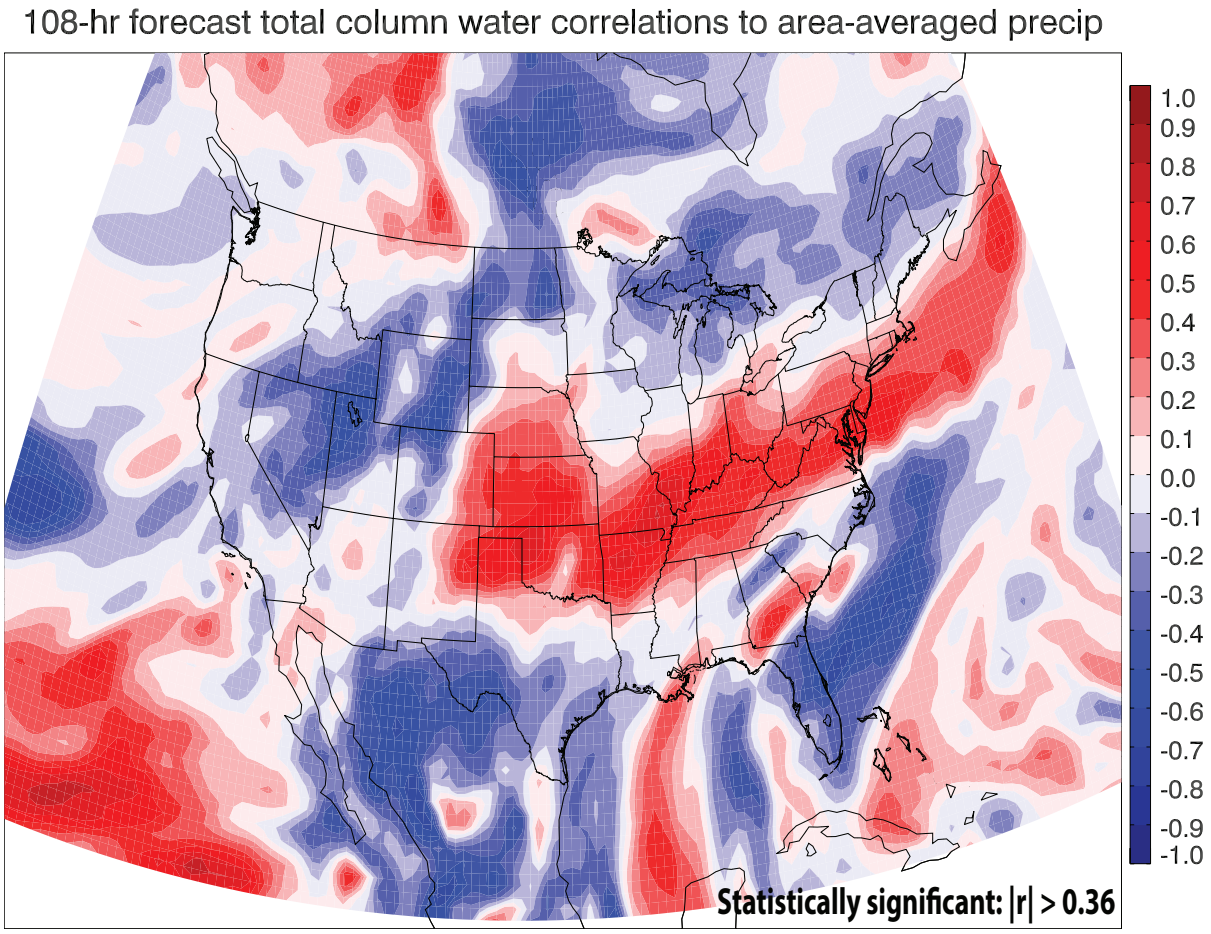

Figure 5.41: As in Fig. 5.39, except for correlated to total column water at 1200 UTC 3 May 2010, corresponding to forecast hour 108.

linear relationship between these two variables, with higher (lower) total column water corresponding to more (less) precipitation. On the scatter plot, the analysis, and the 50 ensemble members are plotted. Both of the dry ensemble members have much less total column water than do the wet ensemble members, resulting in a smaller amount of precipitation (Fig. 5.42). As noted before, the two ensemble members plotted in orange will be discussed in greater detail later in the paper.

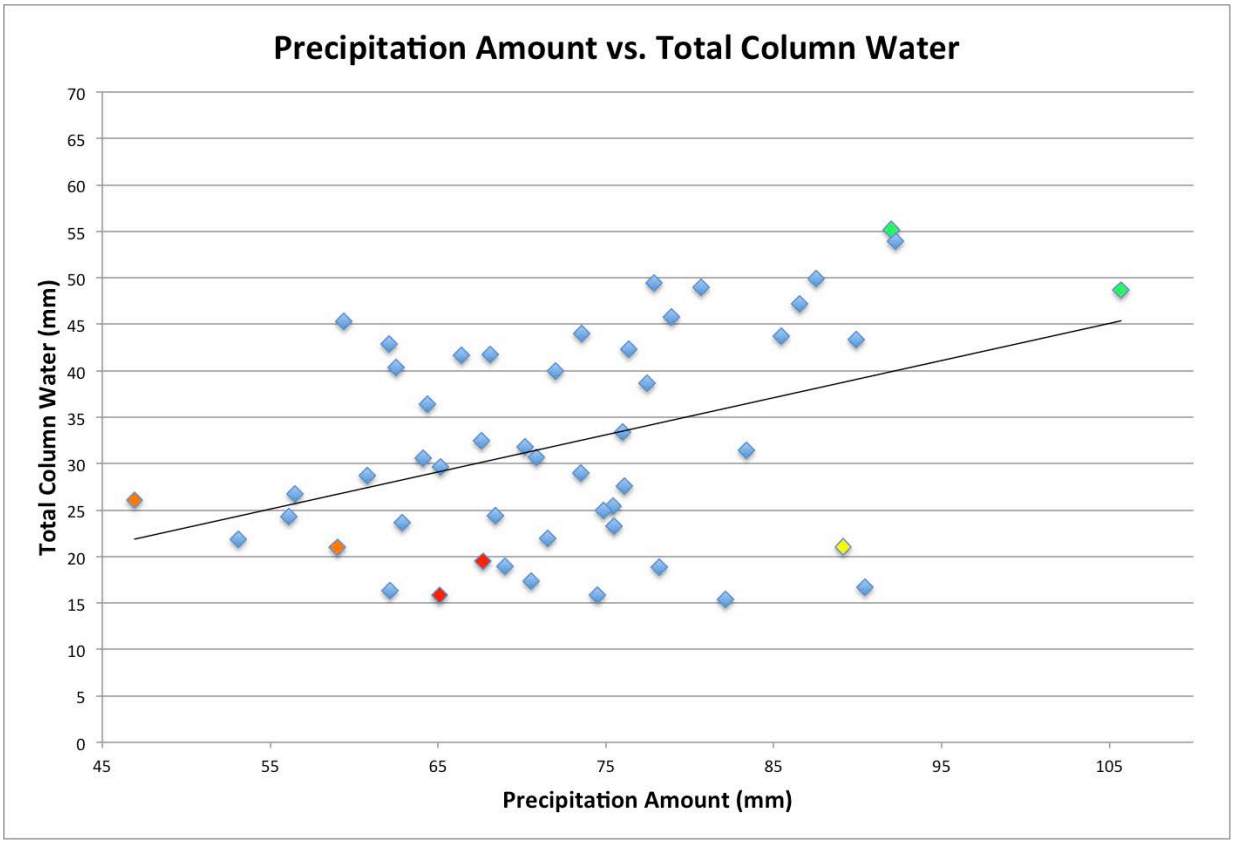

Figure 5.42: Scatter plot of area-averaged precipitation between 1200 UTC 29 April 2010 – 1200 UTC 4 May 2010 vs. total column water at latitude: 36° N and longitude: 87° W at 1200 UTC 3 May 2010, corresponding to forecast hour 108. The wet ensemble members (members 14 and 45) are plotted in green, the dry ensemble members (members 18 and 26) are plotted in red, the displaced ensemble members (members 0 and 37), and the analysis is plotted in yellow.

As seen before, plots of the two most accurate members and the two least accurate members, both spatially and temporally, were constructed. As for the forecasted precipitation,

member 14 and member 45 (the wet ensemble members) forecasted for a very strong, linear precipitation area over Nashville, TN and nearby areas (Figs. 5.43a and 5.43c). Member 18 and member 26 (the dry ensemble members) forecasted for smaller rainfall amounts, over the entire eastern United States (Figs. 5.43b and 5.43d). The dry ensemble members from an initialization time of 1200 UTC 29 April 2010 resembled a very similar spatial distribution of precipitation as ensemble members 18 and 26 (the dry ensemble members).

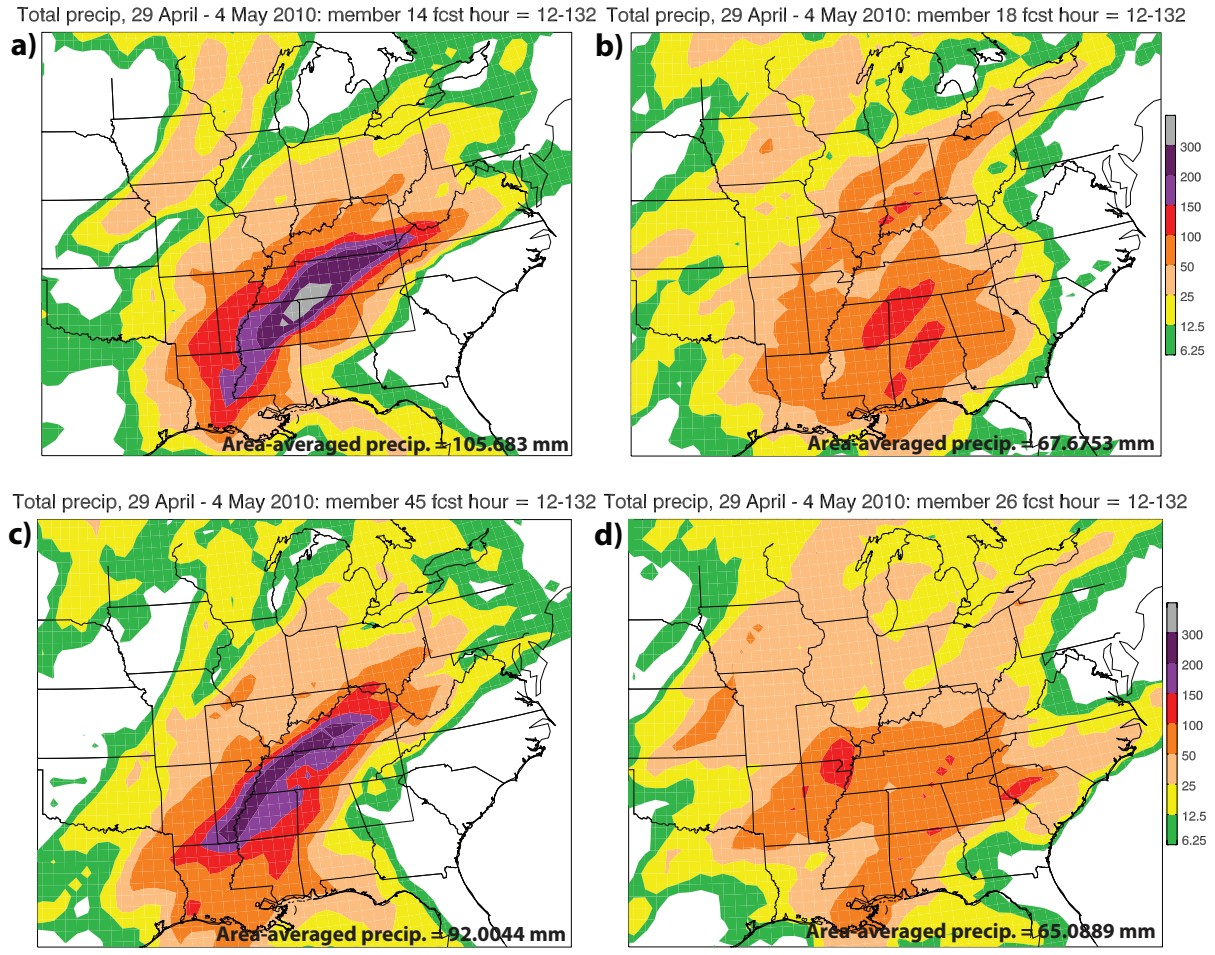

Figure 5.43: Five-day accumulated precipitation (color shading in mm) between 1200 UTC 29 April 2010 - 1200 UTC 4 May 2010: (a) member 14 (wet), (b) member 18 (dry), (c) member 45 (wet), and (d) member 26 (dry). The black rectangle indicates the location for areal averaging of precipitation and other fields.

From the U.S. Daily Precipitation Analysis dataset, the maximum observed precipitation amount was 321 millimeters (yellow). Member 14 and member 45 (the wet ensemble members, green) forecasted a maximum precipitation amount of 380 millimeters and 264 millimeters. Member 18 and member 26 (the dry ensemble members, red) forecasted a maximum precipitation amount of 137 millimeters and 140 millimeters (Fig. 5.44). The wet ensemble members did a much better job at predicting the maximum precipitation amount than did the dry ensemble members. Ensemble member 14 (a wet ensemble member) even overpredicted the maximum precipitation amount by over 50 millimeters (Fig. 5.44). Again, the ensemble members plotted in orange will be discussed later.

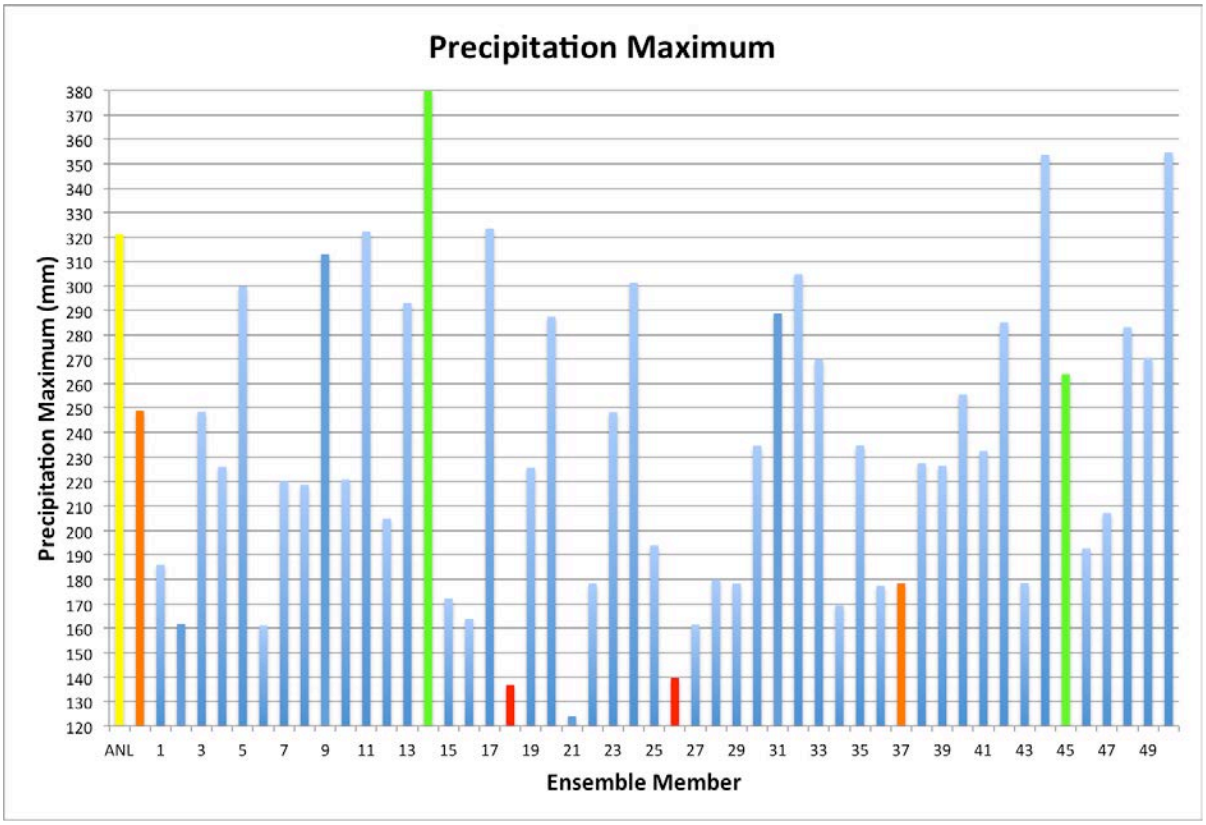

Figure 5.44: Precipitation maximum between the 5-day period 1200 UTC 29 April 2010 – 1200 UTC 4 May 2010. The wet ensemble members (members 14 and 45) are plotted in green, the dry ensemble members (members 18 and 26) are plotted in red, the displaced ensemble members (members 0 and 37), and the analysis is plotted in yellow.

Looking at the 500-hPa level, members 14 and 45 (the wet ensemble members) forecasted for a shallow upper-level trough with a slight positive tilt (Figs. 5.45a and 5.45c). Associated with a shallow upper-level trough is a weaker cyclone with less prominent southerly flow. Members 18 and 26 (the dry ensemble members) forecasted for a much deeper upper-level trough plunging into the southern plains. The dry ensemble members maintain a neutral tilt of the trough axis (Figs. 5.45b and 5.45d). Associated with a stronger cyclone, robust southerly flow bringing in ample moisture from the Gulf of Mexico is present.

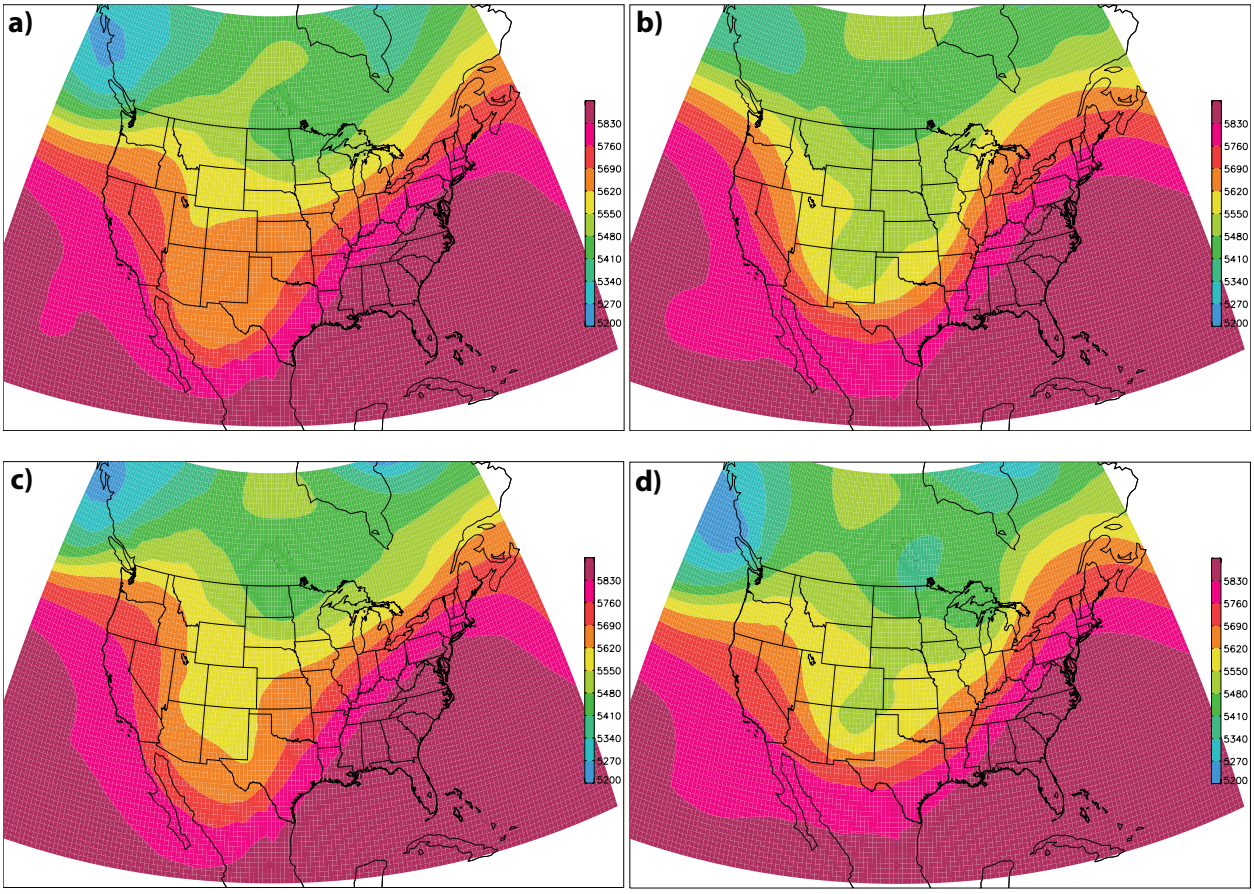

Figure 5.45: Forecasted 500-hPa height (color shading in m) at 0000 UTC 3 May 2010, corresponding to forecast hour 96: (a) member 14 (wet), (b) member 18 (dry), (c) member 45 (wet), and (d) member 26 (dry).

Looking at the 850-hPa moisture flux, members 14 and 45 (the wet ensemble members) forecasted for a large flux of moisture from the Caribbean Sea, extending northeastward into

Tennessee and nearby areas (Figs. 5.46a and 5.46c). This allowed for very localized precipitation in Nashville, Tennessee. On the other hand, members 18 and 26 (the dry ensemble members) forecasted for a plume of moisture from the Caribbean Sea to make its way poleward to the northeast United States. Once the plume of moisture reaches the Great Lakes region, it spreads out in the horizontal over a large area, distributing the rainfall over a wide spatial scale (Figs. 5.46b and 5.46d).

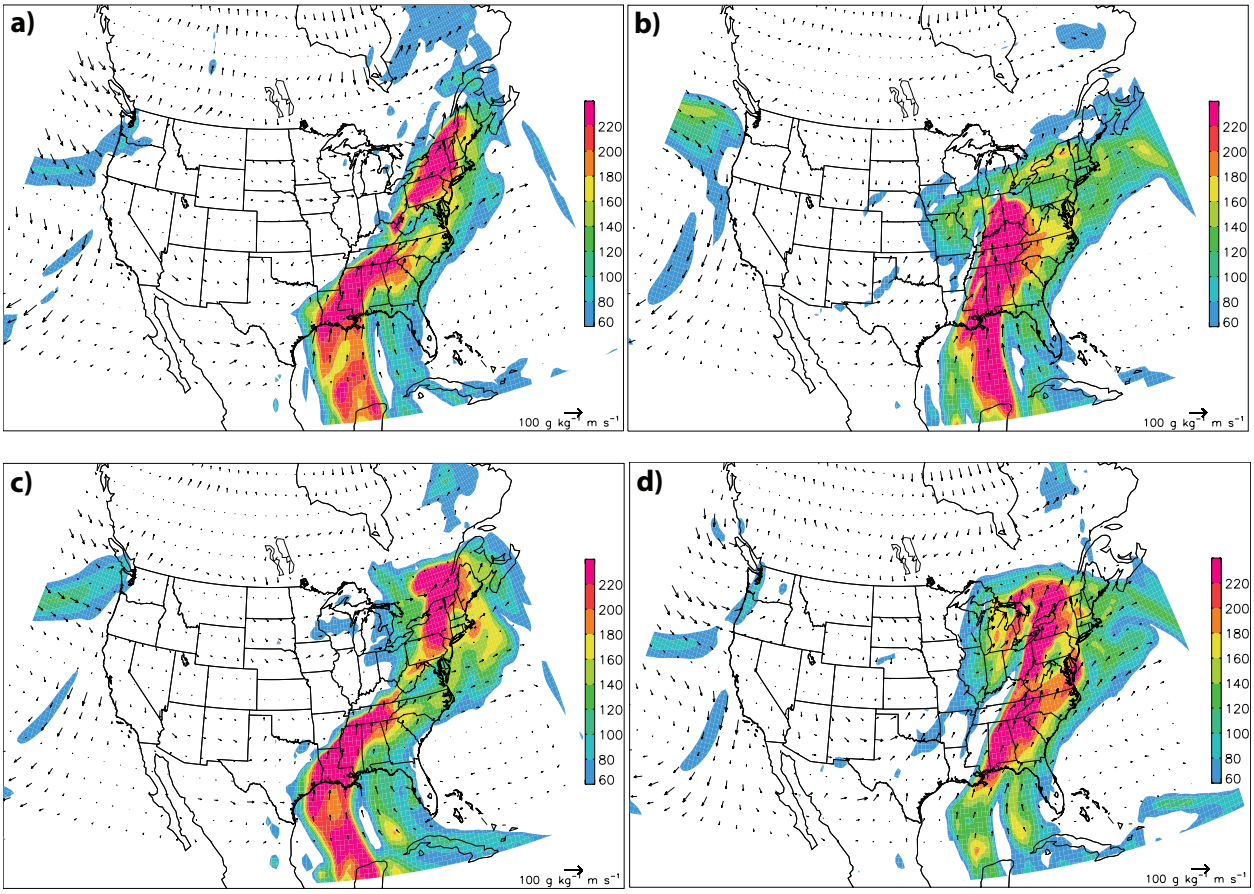

Figure 5.46: Forecasted 850-hPa moisture flux (color shading in g kg^{-1} m s^{-1} with vectors overlaid, vector scale is shown at bottom right) at 0000 UTC 3 May 2010, corresponding to forecast hour 96: (a) member 14 (wet), (b) member 18 (dry), (c) member 45 (wet), and (d) member 26 (dry).

Interestingly, many of the ensemble members displaced this line of heavy precipitation much too far south. With this trend appearing in many of the ensemble members, two ensemble

members will be analyzed in order to determine why they displaced this heavy line of precipitation. Ensemble member 0 and 37 (the displaced ensemble members, orange) displaced the line of heavy precipitation much too far to the south. They forecasted for the area of heavy rainfall to be oriented from southwest to northeast, extending from southern Louisiana to northern Georgia (Figs. 5.47a and 5.47b).

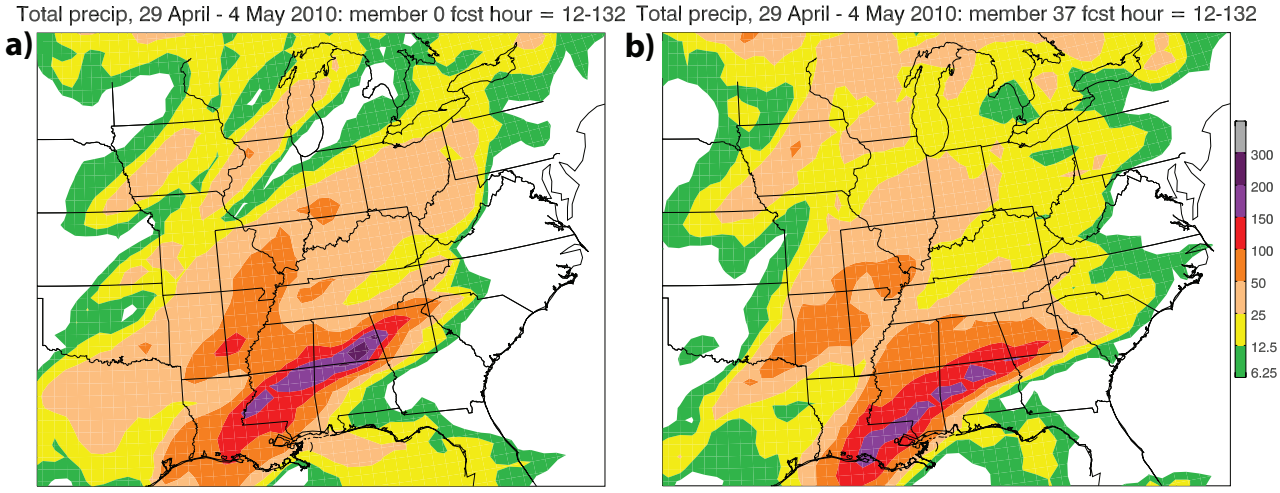

Figure 5.47: Five-day accumulated precipitation (color shading in mm) between 1200 UTC 29 April 2010 – 1200 UTC 4 May 2010: (a) member 0 (displaced), and (b) member 37 (displaced). The black rectangle indicates the location for areal averaging of precipitation and other fields.

Beginning with the 500-hpa level, both the displaced members (member 0 and member 37) forecasted for a very weak upper-level trough extending only as far south as northern Kansas, with an exceptionally strong positive tilt (Figs. 5.48a and 5.48b). This is much different than the other members we have analyzed who extend the upper-level trough much farther south into Texas. Another striking difference is ensemble member 0 (a displaced ensemble member) forecasted for a cutoff low over northwestern Mexico (Fig. 5.48a).

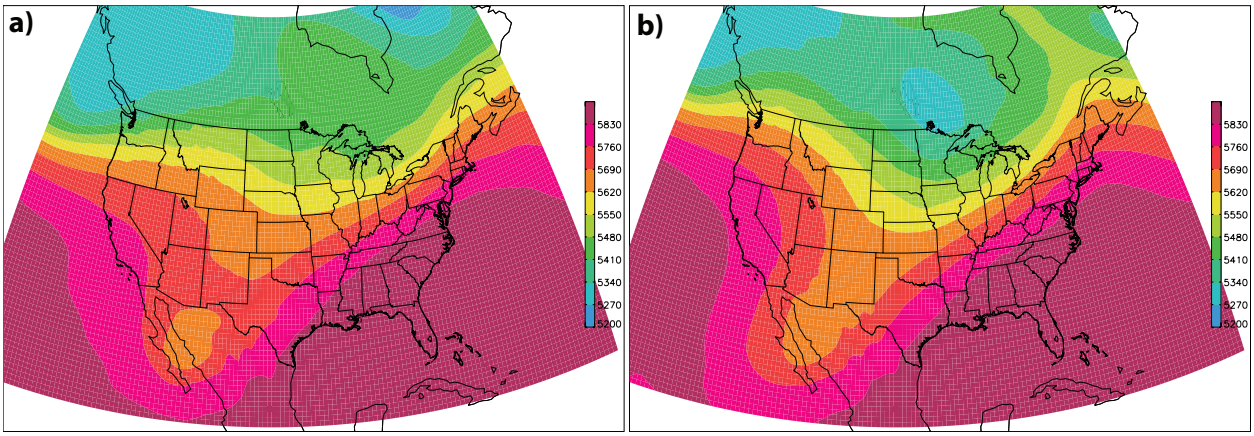

Figure 5.48: Forecasted 500-hPa height (color shading in m) at 0000 UTC 3 May 2010, corresponding to forecast hour 96: (a) member 0 (displaced), and (b) member 37 (displaced).

Looking at the 850-hPa height, member 0 and member 37 (the displaced ensemble members) forecasted for the 850-hPa trough to be much weaker than any of the other ensemble members, only extending as far south as northern Kansas (Figs. 5.49a and 5.49b). Associated with this weak trough is weak cyclonic flow and therefore slightly weaker southerly flow. Looking at 850-hPa temperature, the displaced ensemble members forecasted for slightly cooler temperatures in the Nashville, Tennessee area than what was observed. It appears the displaced

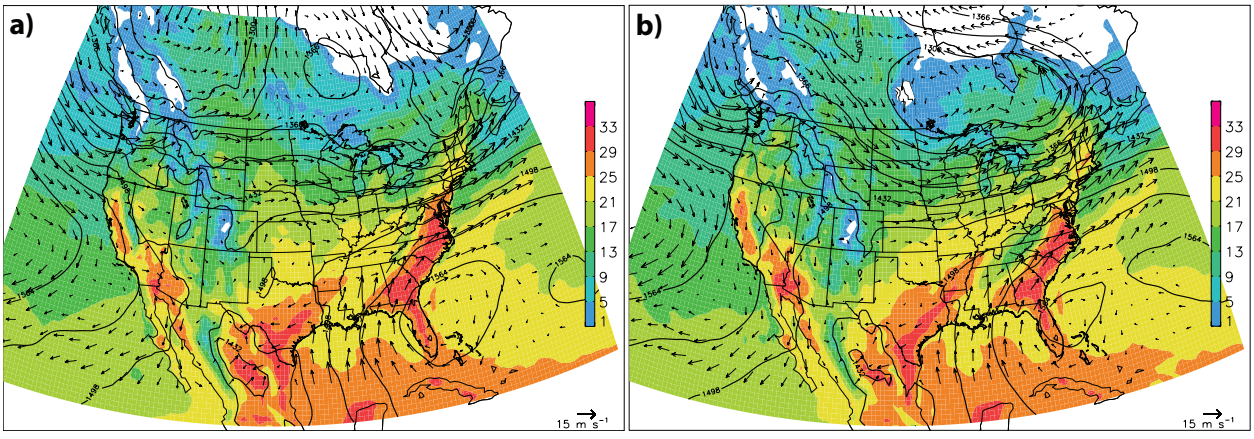

Figure 5.49: Forecasted 850-hPa temperature (color shading in C), height (black contours overlaid in m), and wind (vectors overlaid, vector scale is shown at bottom right) at 0000 UTC 3 May 2010, corresponding to forecast hour 96: (a) member 0 (displaced), and (b) member 37 (displaced).

ensemble members were forecasting for a much stronger cold front extending across the Mississippi Valley. Additionally, ensemble member 0 and 37 (the displaced ensemble members) have the frontal boundary located too far to the southeast, placing it in eastern Tennessee extending as far south as Alabama. The highest temperatures were forecasted for Alabama and Georgia, reaching a value of approximately 29˚C (Figs. 5.49a and 5.49b).

Taking a look at the 850-hPa equivalent potential temperature, both ensemble member 0 and 37 (the displaced ensemble members) have forecasted for a strong frontal boundary extending from the New England region to southern Texas. However, it appears both of the displaced ensemble members have pushed this frontal boundary off to the east much to quickly (Figs. 5.50a and 5.50b).

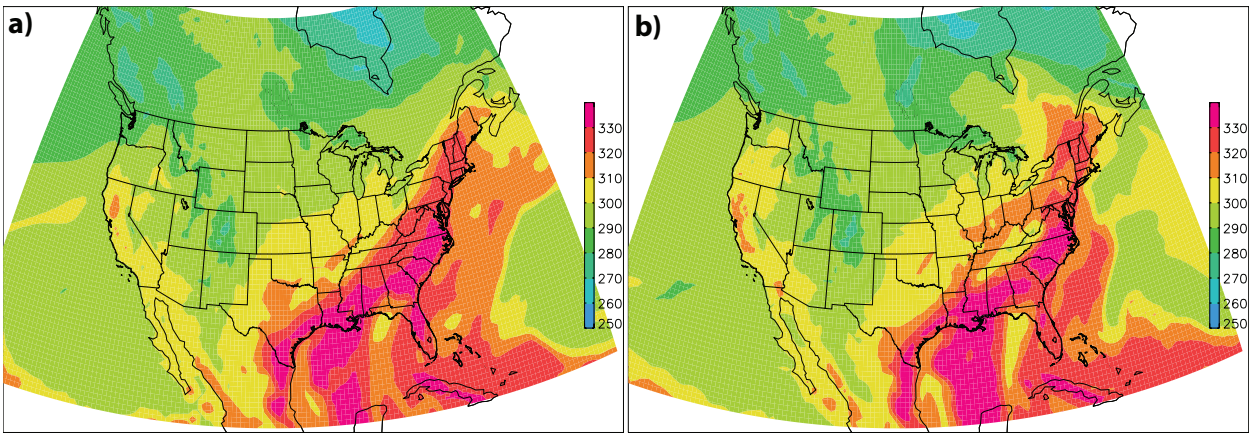

Figure 5.50: Forecasted 850-hPa equivalent potential temperature (color shading in K) at 0000 UTC 3 May 2010, corresponding to forecast hour 96: (a) member 0 (displaced), and (b) member 37 (displaced).

As for the total column water, both member 0 and member 37 (the displaced members) forecasted for a feed of moisture from the Gulf of Mexico, originating near the Yucatan Peninsula. However, the moisture plume only extends as far north as northern Alabama and Georgia (Figs. 5.51a and 5.51b). Nashville, Tennessee appears to be on the outskirts of this moisture plume, reducing the support for heavy precipitation in the area.

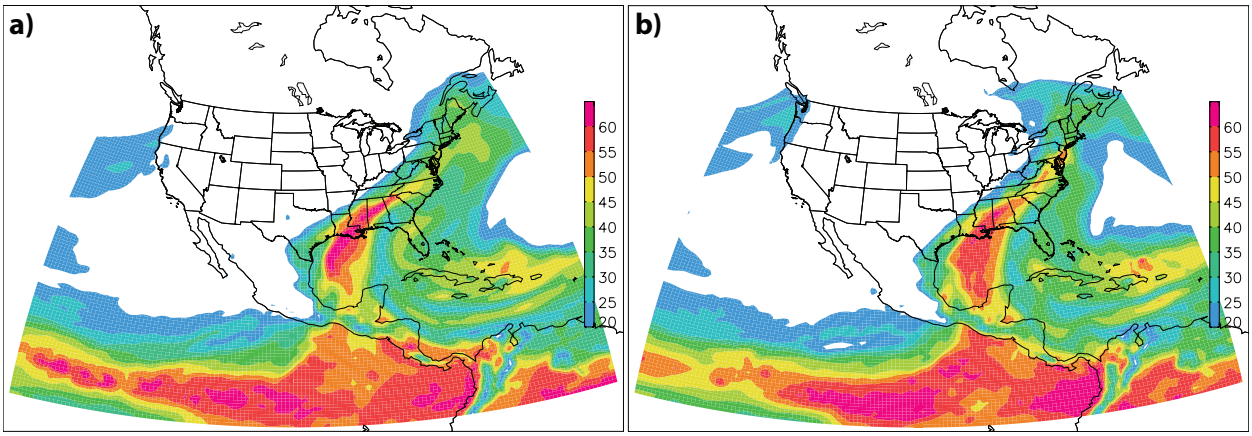

Figure 5.51: Forecasted total column water (color shading in mm) at 0000 UTC 3 May 2010, corresponding to forecast hour 96: (a) member 0 (displaced), and (b) member 37 (displaced).

The final parameter of interest is moisture flux. At the 850-hPa level, both member 0 and member 37 (the displaced ensemble members) forecasted for a plume of moisture to protrude from the Gulf of Mexico, extending northeastward through Alabama and Georgia, on into the northeastern United States. Both the displaced ensemble members forecasted for moisture flux values to reach around 220 g kg^{-1} m s^{-1} in Alabama and Georgia, providing support for heavy rainfall totals in the region. As seen before, the plume of moisture was forecasted too far east, leaving Nashville, Tennessee with very little moisture (Figs. 5.52a and 5.52b).

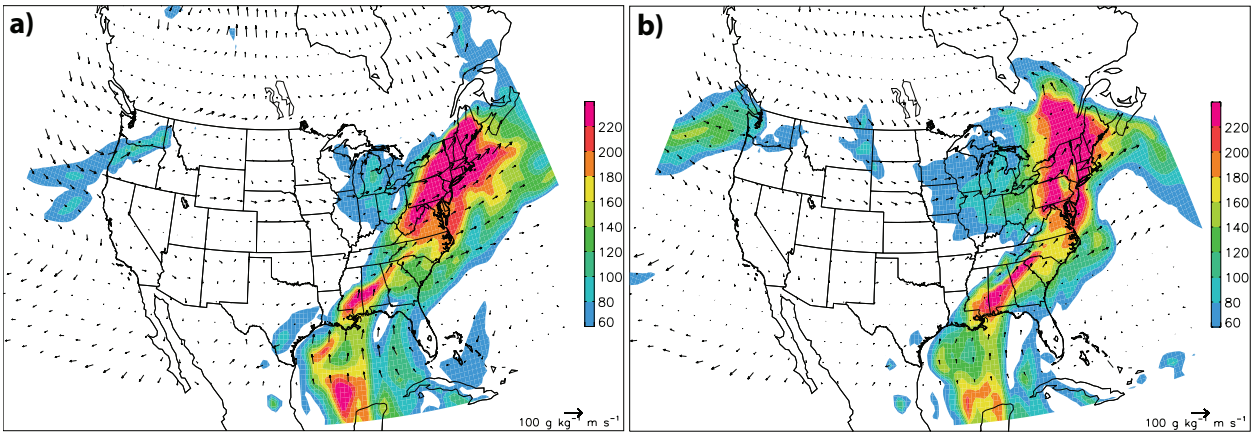

Figure 5.52: Forecasted 850-hPa moisture flux (color shading in g kg^{-1} m s^{-1} with vectors overlaid, vector scale is shown at bottom right) at 0000 UTC 3 May 2010, corresponding to forecast hour 96: (a) member 0 (displaced), and (b) member 37 (displaced).

Overall, it appears that member 0 and member 37 (the displaced ensemble members) forecasted for the heaviest precipitation to be located in northern Alabama and Georgia for a variety of reasons. Namely, the 850-hPa trough was forecasted to be much weaker than the observed 850-hPa trough. As expected with a weak 850-hPa trough, cyclonic flow around the trough is weaker, causing southerly flow to be less robust. With weakened southerly flow, moisture from the Gulf of Mexico was not able to make it as far north as Nashville, Tennessee. This localized the heavy rainfall in northern Alabama and Georgia (Figs. 5.53a and 5.53b). This event, among many others, reinstates the need for improving quantitative precipitation forecasts (QPFs) in the warm season (Fritsch and Carbone 2004).

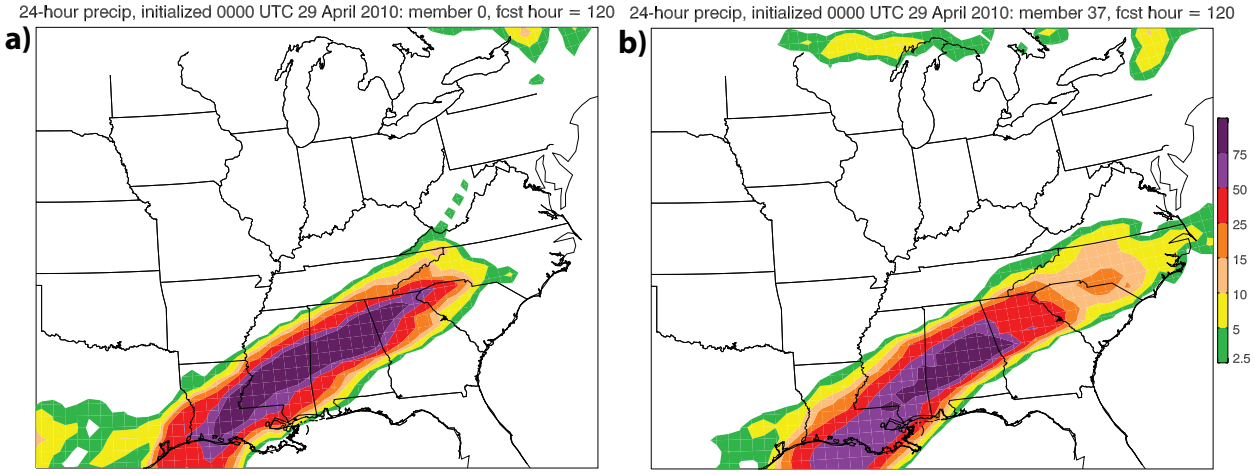

Figure 5.53: Forecasted 24-hr accumulated precipitation (color shading in mm) at (a) 0000 UTC 4 May 2010, corresponding to forecast hour 72: (a) member 0 (displaced), and (b) member 37 (displaced).

5.5 Discussion

This case study provides a way of estimating the predictability of a widespread heavy precipitation event. The analysis in this case study does provide some insight into the uncertainty

in medium-range predictions of this event. Relatively small differences in the structure of the height and wind field translated into vastly different precipitation predictions over Tennessee and surrounding areas for multiple days. The wet ensemble members had forecasted for a much weaker upper-level trough and associated low pressure system, which allowed for southerly winds. Although the winds from the south were not exceptionally strong, they were able to pull moisture from the Gulf of Mexico as far north as Tennessee, where it rained out (Fig. 5.54a). The dry ensemble members, however, had forecasted for a strong upper-level trough and associated low pressure system in the central United States. The cyclonic rotation of this low pressure system caused much stronger winds out of the south. These southerly winds pushed moisture at midlevels much farther to the north, into the Great Lakes. This caused moisture to spread over a larger area across the eastern United States. With a smaller amount of midlevel moisture overhead Tennessee, less precipitation was in the forecast (Fig. 5.54b). With the results being very similar at both an initialization time of 1200 UTC 29 April 2010 and 0000 UTC 29 April 2010, much confidence goes into these findings.

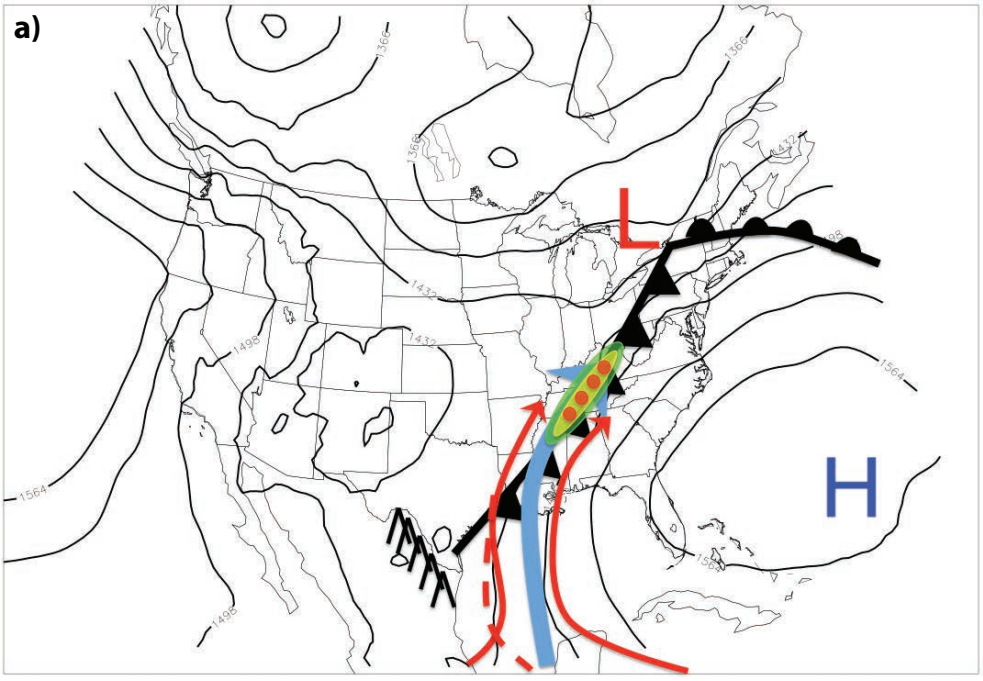

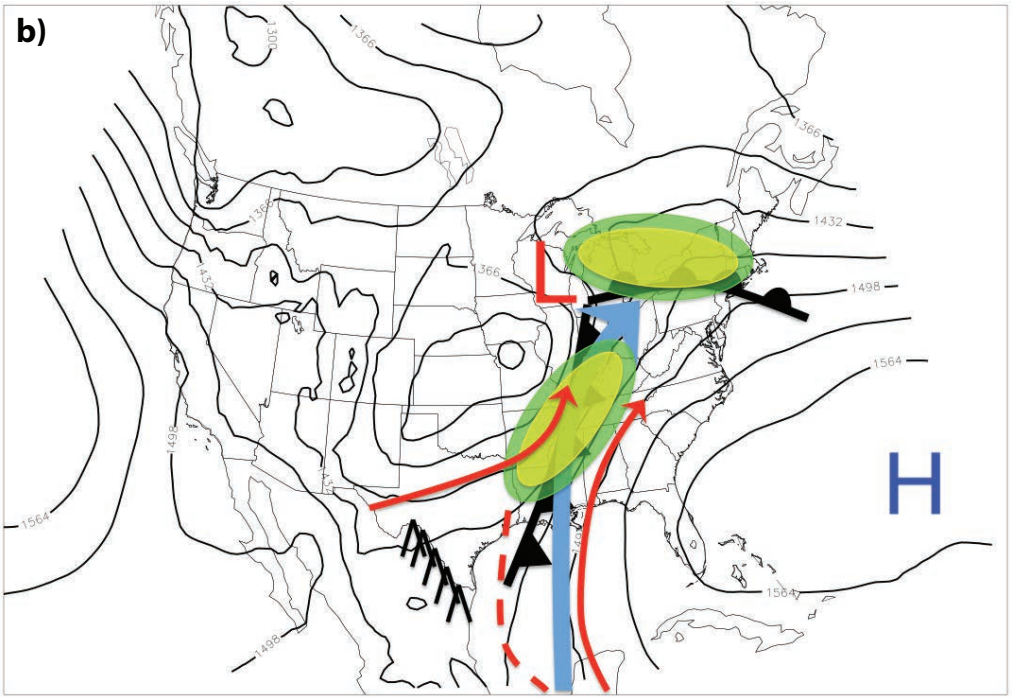

Figure 5.54: Schematic illustration of the key features and processes for (a) the wet ensemble members and (b) the dry ensemble members (Black contours – 850-hPa geopotential height distribution at 0000 UTC 3 May 2010, red arrows – 850-hPa streamlines, surface fronts are shown in standard frontal notation, “H” and “L” symbols – position of the maxima and minima in surface height, dashed red line – axis of the 850-hPa lee trough, thick blue arrow – “atmospheric river”, ∧ symbols – location of the Sierra Madre Oriental Mountains, dark green, yellow, and red shaded regions – represent the radar reflectivity, respectively).

CHAPTER 6

CASE STUDY: 23-28 APRIL 2011 WIDESPREAD PRECIPITATION EVENT

6.1 Event overview

From 23 April 2011 to 28 April 2011, the eastern United States was pounded by heavy precipitation and severe weather, which were caused by an upper-level trough that moved into the Southern Plains on 25 April 2011 (Figs. 6.1a and 6.1b). Ahead of this upper-level trough, an extratropical cyclone developed. With continuous moisture feeding in from the Gulf of Mexico, plenty of support was available for the production of heavy rainfall. More than six states lining the Mississippi River were affected by flooding, including Missouri, Arkansas, Illinois, Tennessee, Kentucky, and Mississippi. With heavy rainfall and snowmelt making its way down the Mississippi River, the southern United States was being inundated with historic floods (Fig. 6.2). For the first time since 1973, the floodgates of the Morganza Spillway were opened, spilling water out of the Mississippi River into the Atchafalaya River Basin (US Army Corps of

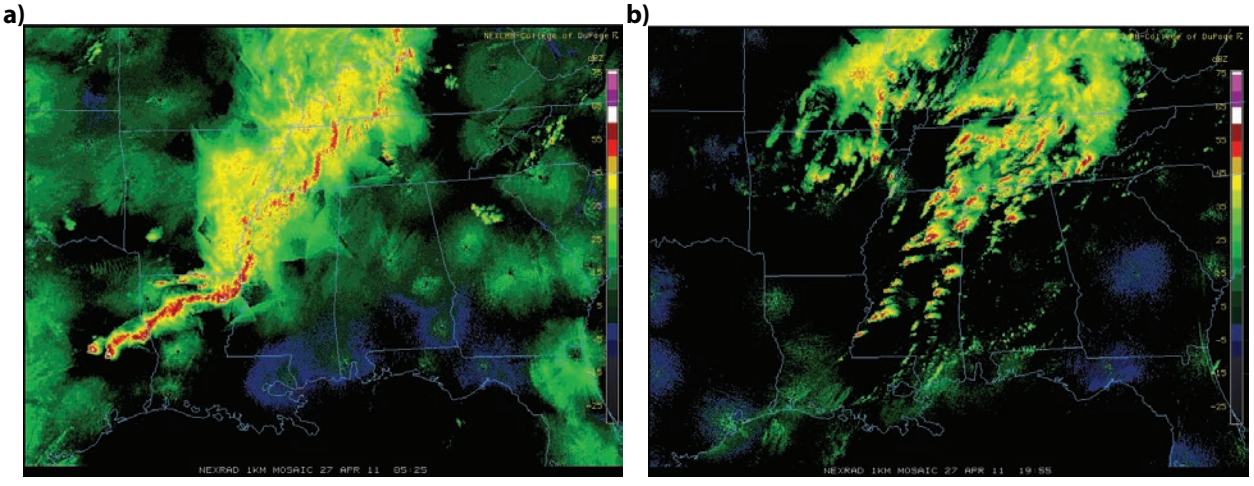

Figure 6.1: Radar reflectivity (color shading in dBZ) at (a) 0525 UTC 27 April 2011 and (b) 1955 UTC 27 April 2011.

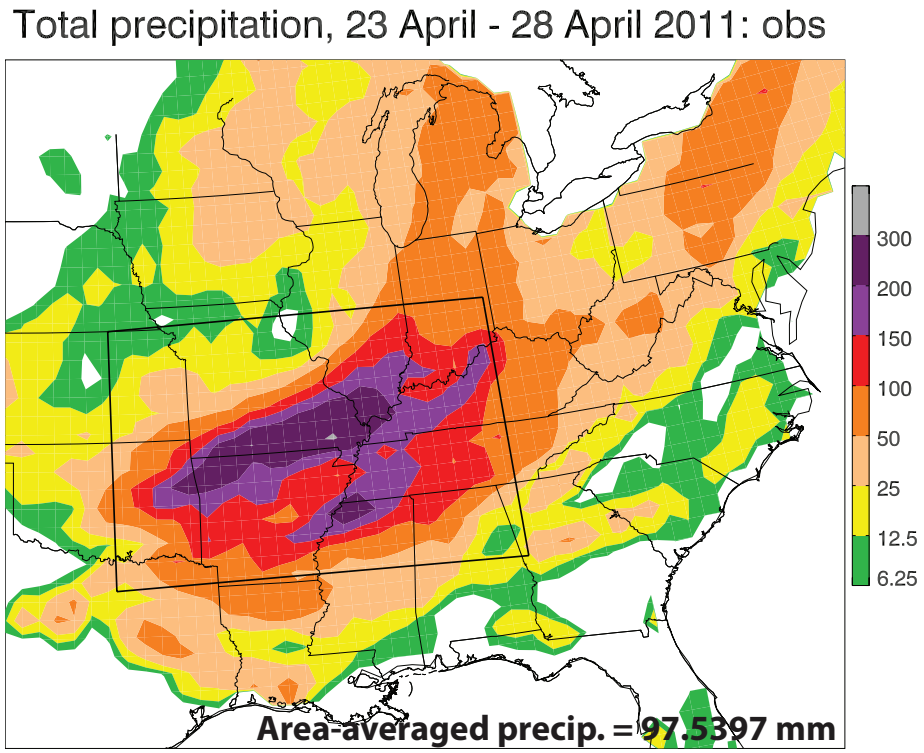

Figure 6.2: Five-day accumulated precipitation (color shading in mm) between 1200 UTC 23 April 2011 – 1200 UTC 28 April 2011. The black rectangle indicates the location for areal averaging of precipitation and other fields.

Engineers). This was done in order to prevent flooding in both Baton Rouge and New Orleans, Louisiana. However, flooding was not the only threat for this weather event. Violent tornadoes tore through Alabama, Arkansas, Georgia, Mississippi, North Carolina, Virginia, Tennessee, and New York. On 27 April 2011, there were 316 tragic fatalities during a particularly destructive tornado outbreak over the southern parts of the country (Fig. 6.1b, Doswell et al. 2012, Carbin and Guyer 2012). In Alabama alone, there were 62 tornadoes, 8 of which were EF4 tornadoes and 3 of which were EF5 tornadoes (NOAA 2011d). Damages from this outbreak totaled over $4.2 billion with more than 2,400 injuries (NOAA 2012). In 2011, a confirmed 550 people lost their lives to 59 killer tornadoes, making 2011 the fourth-deadliest year for tornadoes in United States history (Carbin and Guyer 2012, Doswell et al. 2012). All tornado numbers for 2011

remain preliminary pending further review by SPC and the NOAA National Climatic Data Center. The numbers given here are the best estimated at the time of writing. In the present study, medium-range ensemble forecasts of the 23 April 2011 to 28 April 2011 rain event will be examined to determine the reasons why some ensemble members produced a long-lived, slow-moving precipitation system, and others did not. The overlying question is, how accurately was the flooding of the Mississippi River and the eastern United States predicted? Looking at the spaghetti plot at a threshold of 100 millimeters, the ensemble members did a relatively good job forecasting the location of the event (Fig. 6.3). The ensemble mean axis of heavy precipitation was displaced slightly northward/northeastward, while also missing the southeastern extent of the heavy precipitation (Fig. 6.3). Although not shown in the spaghetti plot, the observed maximum amount of rainfall for this event was not well forecasted.

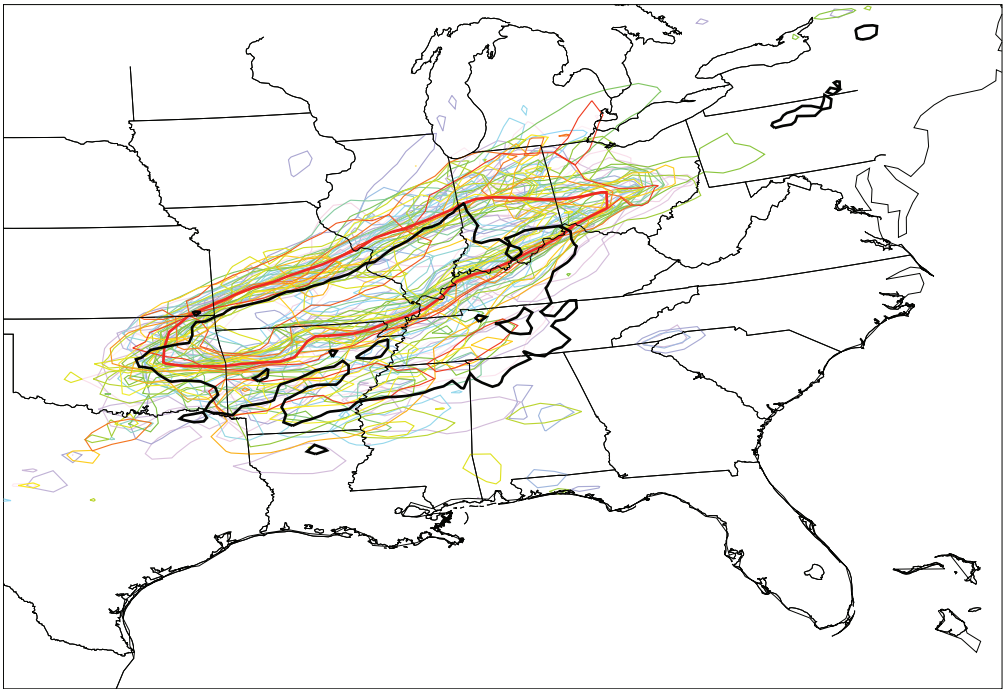

Figure 6.3: “Spaghetti” plot showing the predicted 100-mm rainfall contour from 1200 UTC 23 April 2011 – 1200 UTC 28 April 2011 from each ensemble member in a different color. The observed 100-mm contour from 1200 UTC 23 April 2011 – 1200 UTC 28 April 2011 is shown in thick black. The ensemble mean 100-mm contour is shown in thick red. Initialization time of 1200 UTC 23 April 2011.

6.2 Synoptic analysis

The primary source for upper-level atmospheric information is the Earth System Research Laboratory (ESRL) of NOAA. Composite anomalies will be used for the synoptic analysis of the 23-28 April 2011 widespread rain event because this event occurred over the whole five day period. Looking at the upper levels of the atmosphere, many factors contributed to the support of long-lived, heavy precipitation and convection across the eastern United States. At the 500-hPa level, there was an anomalously deep upper-level trough positioned over the central United States. Cyclonic flow around the upper-level trough resulted in strong southerly flow into the Mississippi River Valley. There was also an anomalously strong ridge just off the coast of the eastern United States (Fig.6.4a). At the 850-hPa level, a strong occluded low pressure system was positioned over the upper Midwest, extending south into the Mississippi Valley (Fig. 6.4b). This occluded low also helped to enhance southerly flow from the Gulf of Mexico. Finally, looking at the columnar precipitable water, there was a large region of anomalously high moisture in the eastern United States, a result of the southerly flow from the anomalous upper-level trough (Fig. 6.4c). This anomalous moisture present in the eastern United States provided support for heavy rainfall amounts. Looking at the upper air sounding from Nashville International Airport (KBNA) at 0000 UTC 27 April 2011, the atmosphere is saturated at the 800-hPa level and then begins to dry out aloft. The surface temperature and dew point temperature are only a few degrees apart, indicative of moist conditions at the surface. There is very little directional shear throughout the atmosphere, except at the lower levels. Speed shear exists throughout the atmosphere with wind speeds ranging from 5 knots at the surface to 80 knots at upper levels. Passage of the cold front has not yet occurred in Nashville, Tennessee, with winds still out of the south (Fig. 6.5a). Prior to the passage of the cold front, the atmosphere

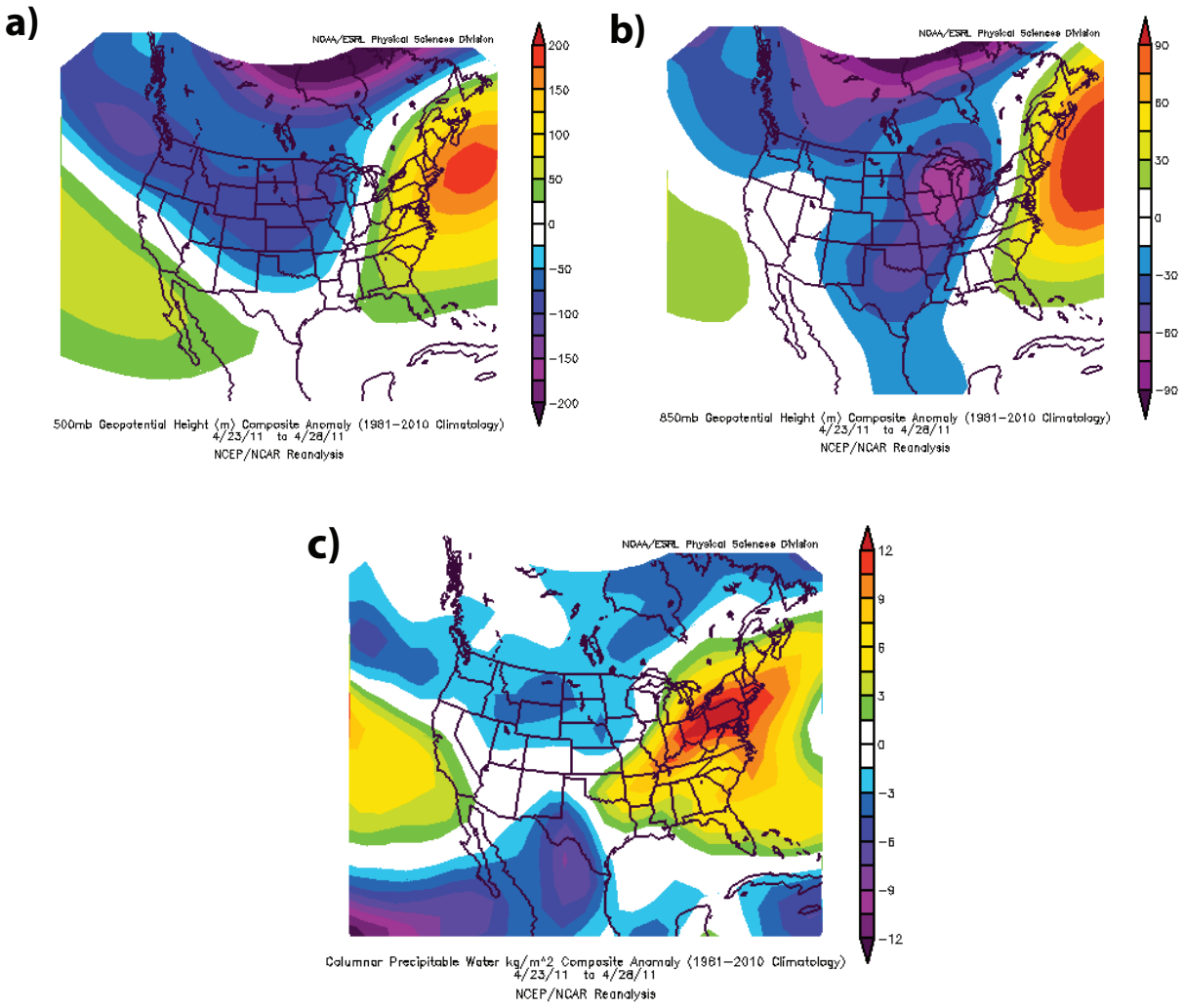

Figure 6.4: (a) 500mb geopotential height (m) composite anomaly (1981-2010 climatology) from 23 April 2011 to 28 April 2011. (b) 850mb geopotential height (m) composite anomaly (1981-2010 climatology) from 23 April 2011 to 28 April 2011. (c) Columnar precipitable water (kg m^{-2}) composite anomaly (1981-2010 climatology) from 23 April 2011 to 28 April 2011.

is quite unstable. In Nashville, convective available potential energy (CAPE) reaches 3094 J kg^{-1} (not shown), with a 500-hPa lifted index (LI) of -7°C (not shown), indicative of a very unstable atmosphere where severe thunderstorms are likely with the presence of a lifting mechanism. Looking farther south at a sounding from Jackson-Evers International Airport (KJAN) at 1800 UTC 27 April 2011, the atmosphere is very conducive to severe weather. There is little to no directional shear throughout the atmosphere, with an exception for the lower levels. Speed shear

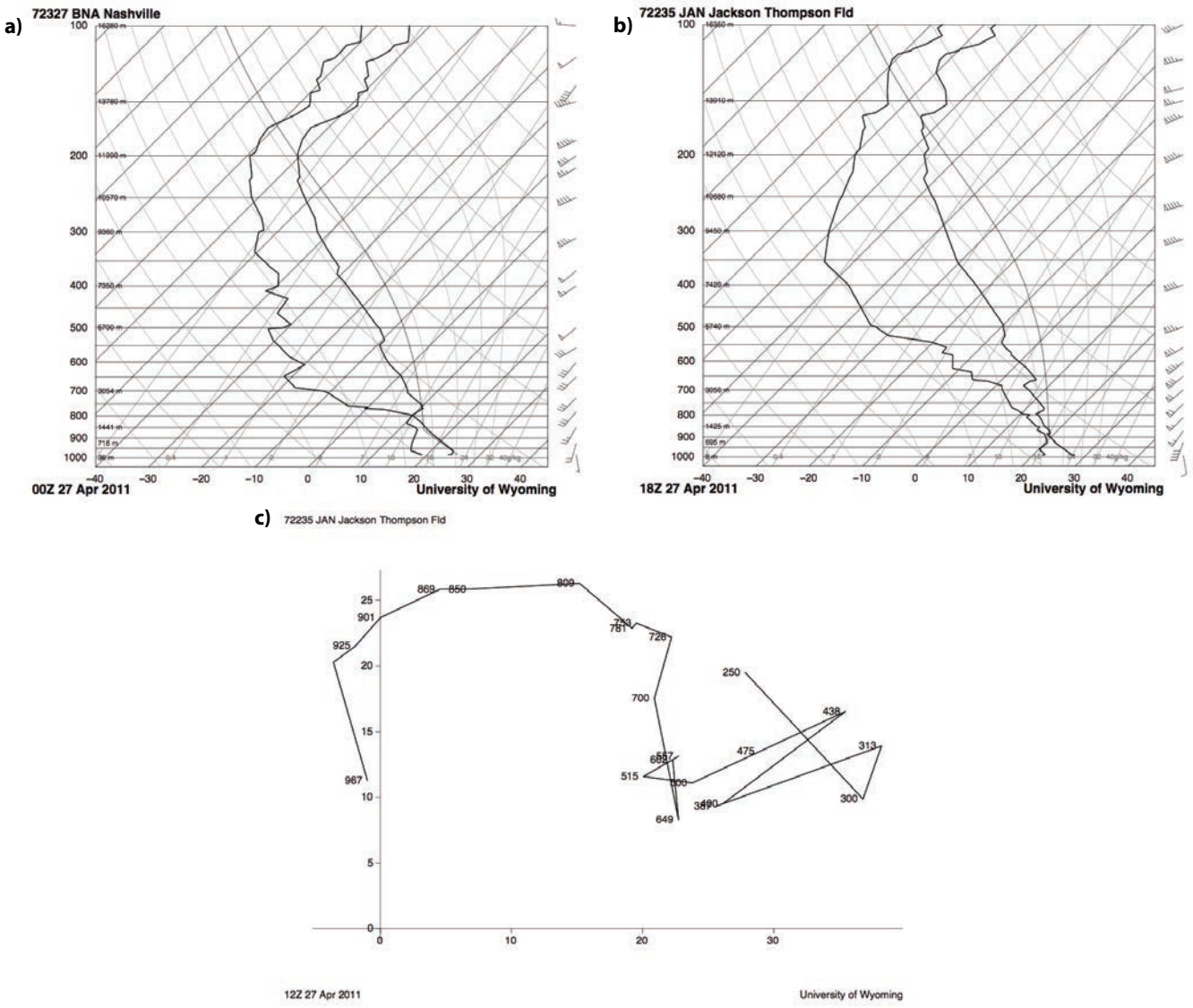

Figure 6.5: Skew-T from (a) Nashville International Airport (KBNA) at 0000 UTC 27 April 2011 and (b) Jackson-Evers International Airport (KJAN) at 1800 UTC 27 April 2011. (c) Hodograph from Jackson-Evers International Airport (KJAN) at 1200 UTC 27 April 2011.

exists with wind speeds ranging from about 10 knots at the surface to about 90 knots at the upper levels. Remarkable speed shear exists at the lower levels, between approximately 950 – 750-hPa, reaching 60-knots. Winds at the surface are coming from the south at about 10 knots (Fig. 6.5b). Convective available potential energy (CAPE) is exceptionally high at 4012 J kg^{-1} (not shown), indicative of an extremely unstable atmosphere. Additionally, a 500- hPa lifted index

(LI) value of -9°C indicates an unstable atmosphere where thunderstorms are likely (not shown). Severe weather is probable assuming a lifting mechanism is available, in this case the frontal boundary. Looking at the hodograph from 1200 UTC 27 April 2011, between approximately 950 hPa to 650 hPa, a nocturnal low level jet is present. The hodograph turns clockwise at lower levels, with peak winds at around 800 hPa (Fig. 6.5c). Throughout this 5-day event, a relatively strong and persistent nocturnal low level jet existed, providing the Mid-Mississippi Valley with ample moisture from the Gulf of Mexico.

Maddox et al. (1979) has identified three primary types of synoptic and mesoscale patterns as often producing excessive rain. Both the meso-high and frontal types are primarily mesoscale phenomena, while synoptic forcing drives the synoptic type events, described in detail earlier in the study. The flooding as a result of the 23-28 April 2011 widespread rain event occurred in the spring months, in late April (Fig. 5.6). At the 500-hPa level, a well-defined trough dug into the central plains and then began to weaken and slide off to the east (Fig. 6.4a). Looking at the surface analysis, a cold front approaching the eastern United States from the west stalled as it became parallel to the upper-level flow. The frontal boundary stalled oriented from southwest to northeast (Fig. 6.6). For the duration of the precipitation event, dew point temperatures remained slightly above 70°F in Alabama and nearby areas (Fig. 6.6). Winds at the 850-hPa level reached a wind speed of about 55 knots, with very strong vertical wind shear at lower levels (Fig. 6.5b). With that said, the widespread rain event of 23-28 April 2011 is a classic synoptic type heavy rainfall event.

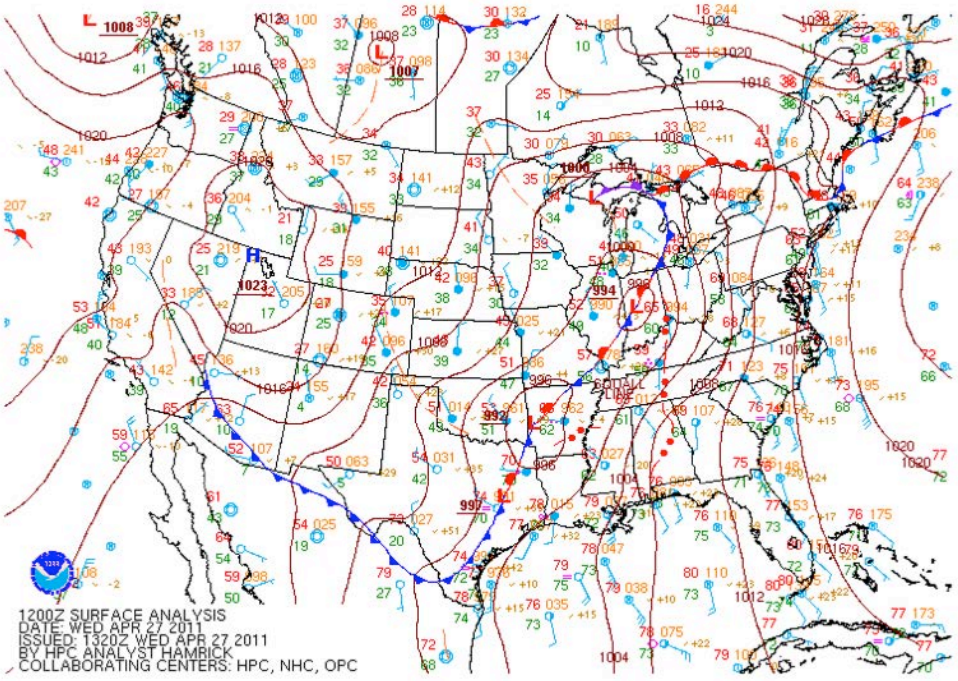

Figure 6.6: Hydrometeorological Prediction Center (HPC) surface analysis for 1200 UTC 27 April 2011.

6.3 Results

6.3.1 Selection of "wet" and "dry" ensemble members

With an initialization time of 1200 UTC 23 April 2011, the 84-hour (0000 UTC 27 April 2011) and 96-hour (1200 UTC 27 April 2011) forecasts were found to be the most useful for this case to look at the synoptic analysis. On this particular day, 27 April 2011, a squall line was seen passing through central Tennessee, as well as, a cluster of strong thunderstorms in southeast Arkansas (shown later in the study). Both the 84-hour and 96-hour forecasts have a large spread in their respective precipitation forecasts and a large portion of the heaviest precipitation fell around these times.

A majority of the ensemble members realistically reflected the spatial distribution of

precipitation and the evolution of the precipitation system (shown later in the study). The area-averaged precipitation for this event was 98 millimeters. Member 10 had a five-day area-averaged precipitation of 85 millimeters, member 37 had a five-day area-averaged precipitation of 86 millimeters, member 39 had a five-day area-averaged precipitation of 85 millimeters and member 46 had a five-day area-averaged precipitation of 92 millimeters. Member 0 had a five-day area-averaged precipitation of 64 millimeters, member 9 had a five-day area-averaged precipitation of 63 millimeters, member 21 had a five-day area-averaged precipitation of 59 millimeters and member 23 had a five-day area-averaged precipitation of 62 millimeters (Fig. 6.7). All 50 members underpredicted the observed amount of precipitation over this five-day period. The ETS was also calculated as a final measure of determining the least and most accurate ensemble members.

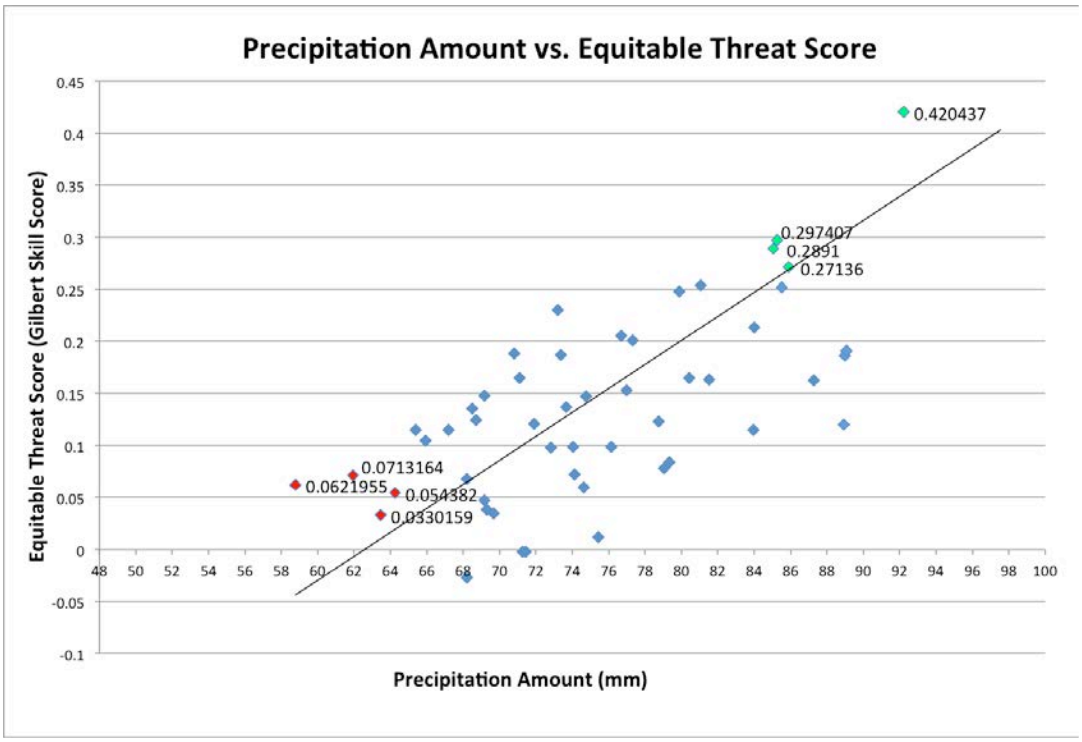

Figure 6.7: Area-averaged precipitation vs. equitable threat score scatter plot at a threshold of 100 mm between 1200 UTC 23 April 2011 – 1200 UTC 28 April 2011. The wet ensemble members (members 10, 37, 39, and 46) are plotted in green and the dry ensemble members (members 0, 9, 21, and 23) are plotted in red.

Although analyzing the spatial distribution of precipitation and ETS to determine the most accurate and least accurate ensemble members is beneficial, it is not sufficient. This requires one to analyze all weather variables that all relevant to identifying the best ensemble member. After looking at all 50 members, it was determined that the most accurate forecast was from members 10, 37, 39, and 46 (the wet ensemble members), while the least accurate forecast was from members 0, 9, 21, and 23 (the dry ensemble members). Also seen on the area-averaged precipitation vs. equitable threat score scatter plot is the best-fit line. The best-fit line denotes the positive correlation between precipitation amount and equitable threat score (Fig. 6.7). In relation to other heavy rain events of similar spatial and temporal scales, the 23-28 April 2011 widespread rain event had remarkably large agreement between the ensemble members, demonstrating high skill and small spread.

6.3.2 Correlations

Looking at the 96-hr forecast of the 500-hPa height correlations to area-averaged precipitation, there is a large core of positive correlation ($r \approx 0.4$) encompassing a majority of the eastern United States, indicating that as heights increase, area-averaged precipitation increases (Fig. 6.8). This would suggest a stronger ridge over the eastern United States was favorable for more precipitation. In Texas, there is a core of negative correlation with a correlation coefficient around -0.5, indicating that as heights decrease, area-averaged precipitation increases (Fig. 6.8). The negative correlation in Texas appears to play an important role in the southern extent of the 500-hPa trough.

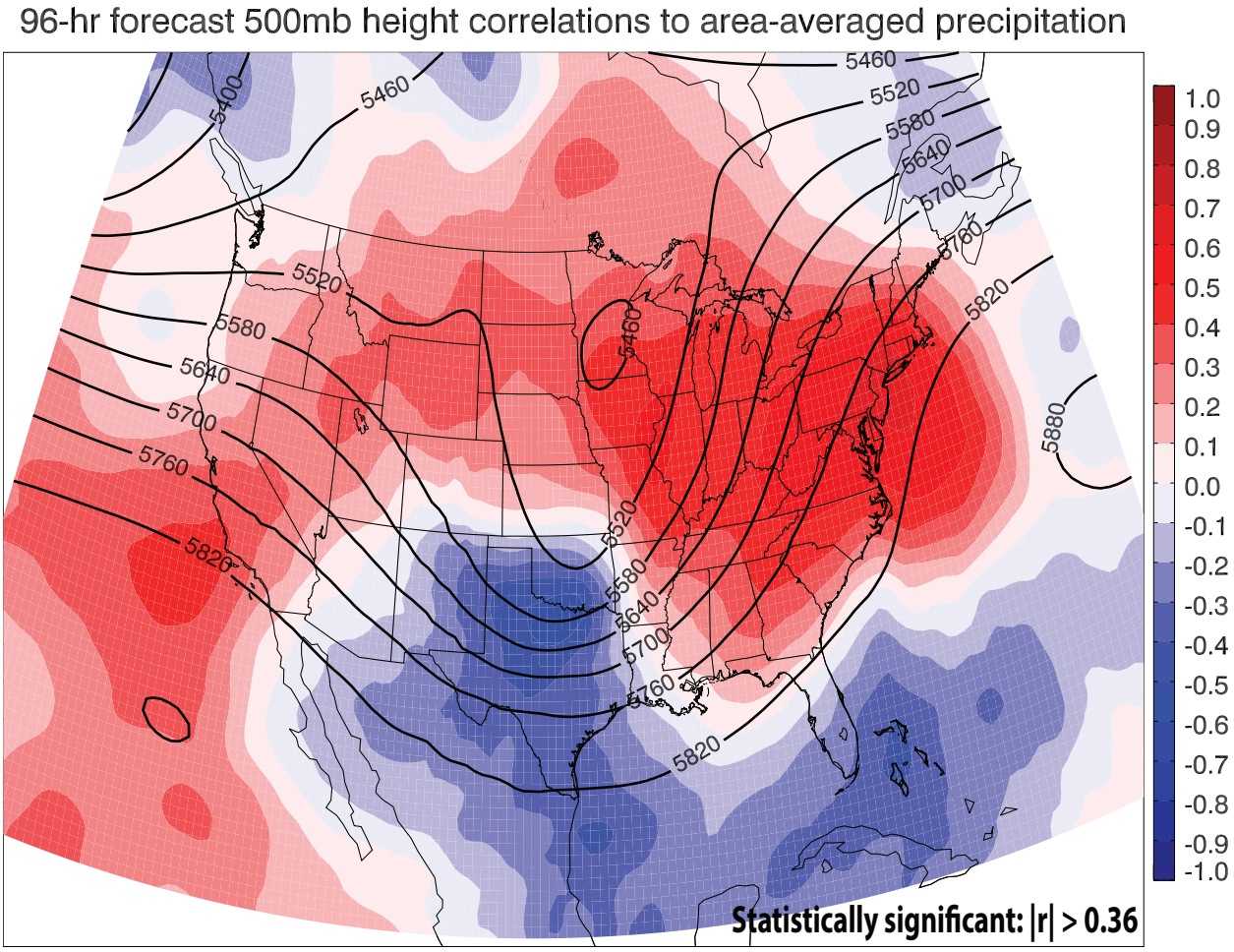

Figure 6.8: Area-averaged precipitation between 1200 UTC 23 April 2011 – 1200 UTC 28 April 2011 correlated to 500-hPa height at 1200 UTC 27 April 2011, corresponding to forecast hour 96. Warm colors represent a positive correlation, while cool colors represent a negative correlation. The ensemble mean 500-hPa height contours are shown in thick black.

Taking a look at the 96-hr forecast of the 850-hPa height correlations to area-averaged precipitation, there is a large core of positive correlation, with a correlation coefficient around 0.7, along the east coast of the United States (Fig. 6.9). In this region of positive correlation, as heights increase, area-averaged precipitation increases. This could suggest importance in the position of the Bermuda High pressure. If the Bermuda High were positioned more westward, more moisture would be drawn into the Mississippi Valley resulting in more precipitation. Another region of positive correlation exists in the western United States and just off the coast

into the Pacific Ocean (Fig. 6.9). There is a core of negative correlation (r ≈ -0.5) in Texas and surrounding areas, suggesting as heights decrease, area-averaged precipitation increases (Fig. 6.9). The negative correlation in Texas appears to play a critical role in the southern extent of the 850-hPa occluded low pressure. The farther south the 850-hPa low pressure core digs, the more precipitation associated.

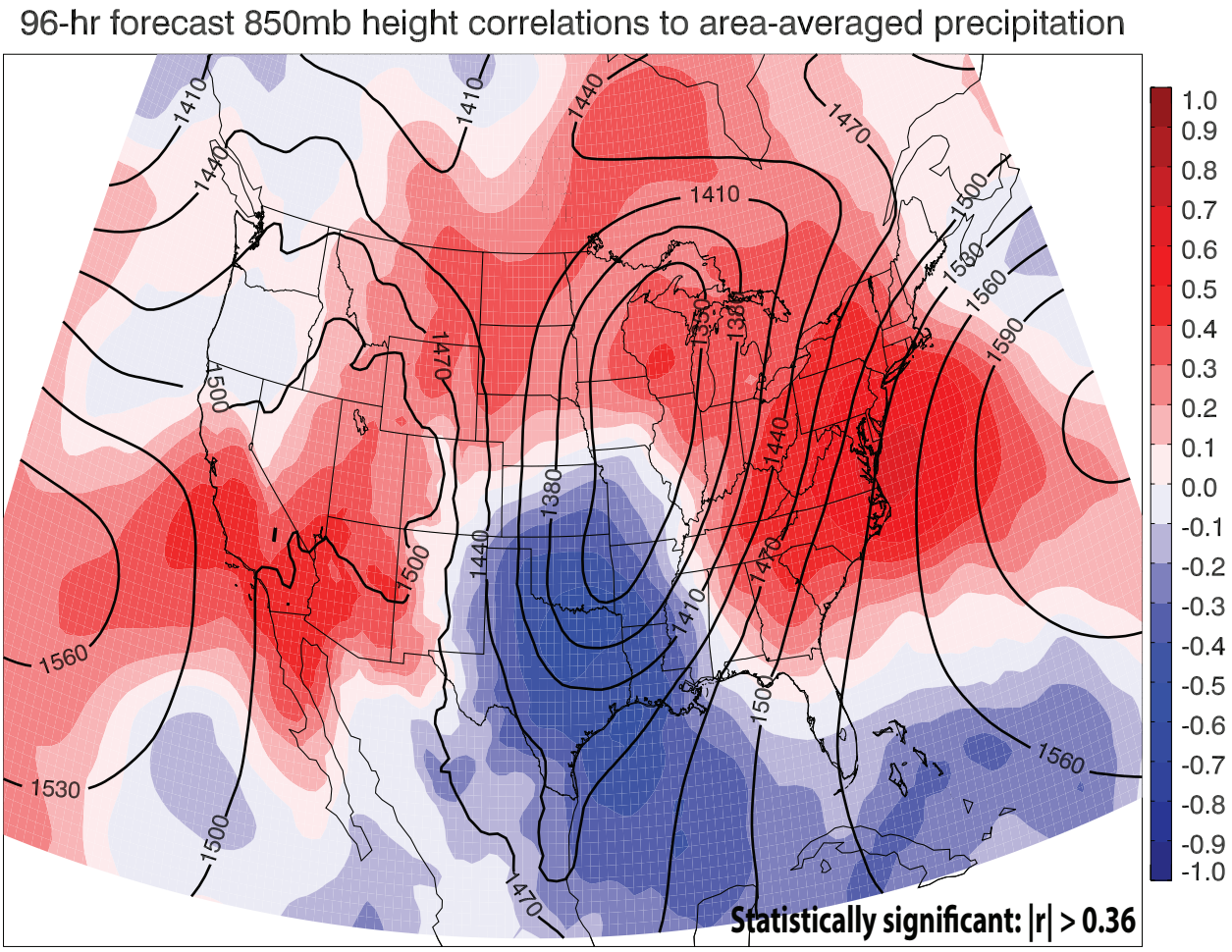

Figure 6.9: Area-averaged precipitation between 1200 UTC 23 April 2011 – 1200 UTC 28 April 2011 correlated to 850-hPa height at 1200 UTC 27 April 2011, corresponding to forecast hour 96. Warm colors represent a positive correlation, while cool colors represent a negative correlation. The ensemble mean 850-hPa height contours are shown in thick black.

Looking at the 96-hour forecast of the 850-hPa v-wind correlations to area-averaged precipitation, there is a large positive correlation (r ≈ 0.5) extending from the Gulf of Mexico

into the Mississippi River Valley (Fig. 6.10). In this region of positive correlation, as the winds increase, precipitation increases in the area of interest. This correlation indicates the wet members had a much stronger low level jet present, supplying the southeastern United States with ample moisture transport. The location of the low level jet is denoted by the thick black contours, with peak winds around 20ms^{-1} (Fig. 6.10).

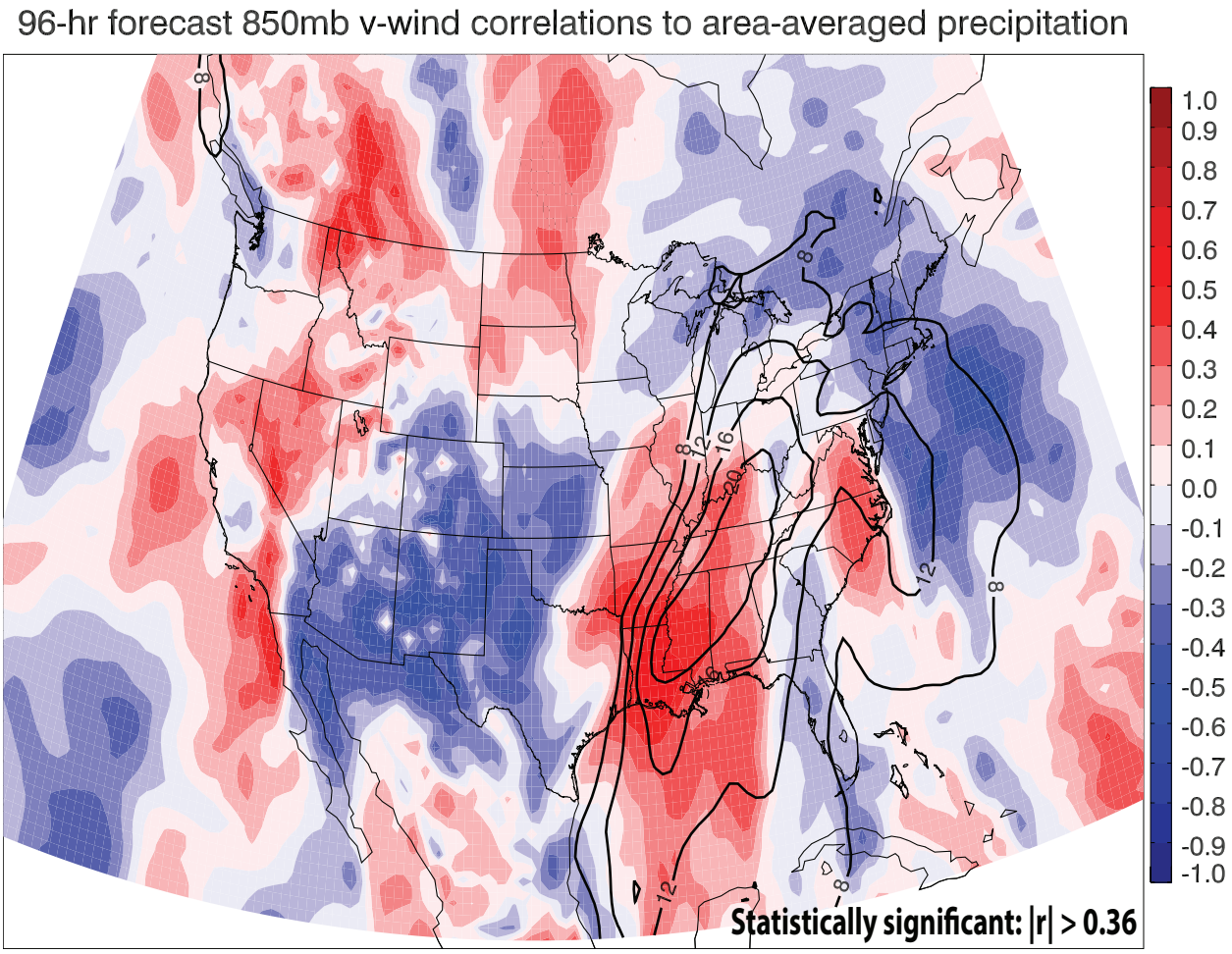

Figure 6.10: Area-averaged precipitation between 1200 UTC 23 April 2011 – 1200 UTC 28 April 2011 correlated to 850-hPa v-wind at 1200 UTC 27 April 2011, corresponding to forecast hour 96. Warm colors represent a positive correlation, while cool colors represent a negative correlation. The ensemble mean 850-hPa v-wind (in ms^{-1}) contours are shown in thick black.

Looking at the 96-hr forecast of the 850-hPa total column water correlations to area-averaged precipitation, there is a large region of positive correlation ($r \approx 0.5$) encompassing

Illinois, Arkansas, Missouri, Iowa, western Tennessee and nearby areas (Fig. 6.11). As expected for the region where the maximum precipitation fell, the more total column water, the more rainfall. Additionally, there is an area of negative correlation extending from southeastern Alabama to Ohio, oriented south-southwest to north-northeast, with a correlation coefficient around -0.4 (Fig. 6.11).

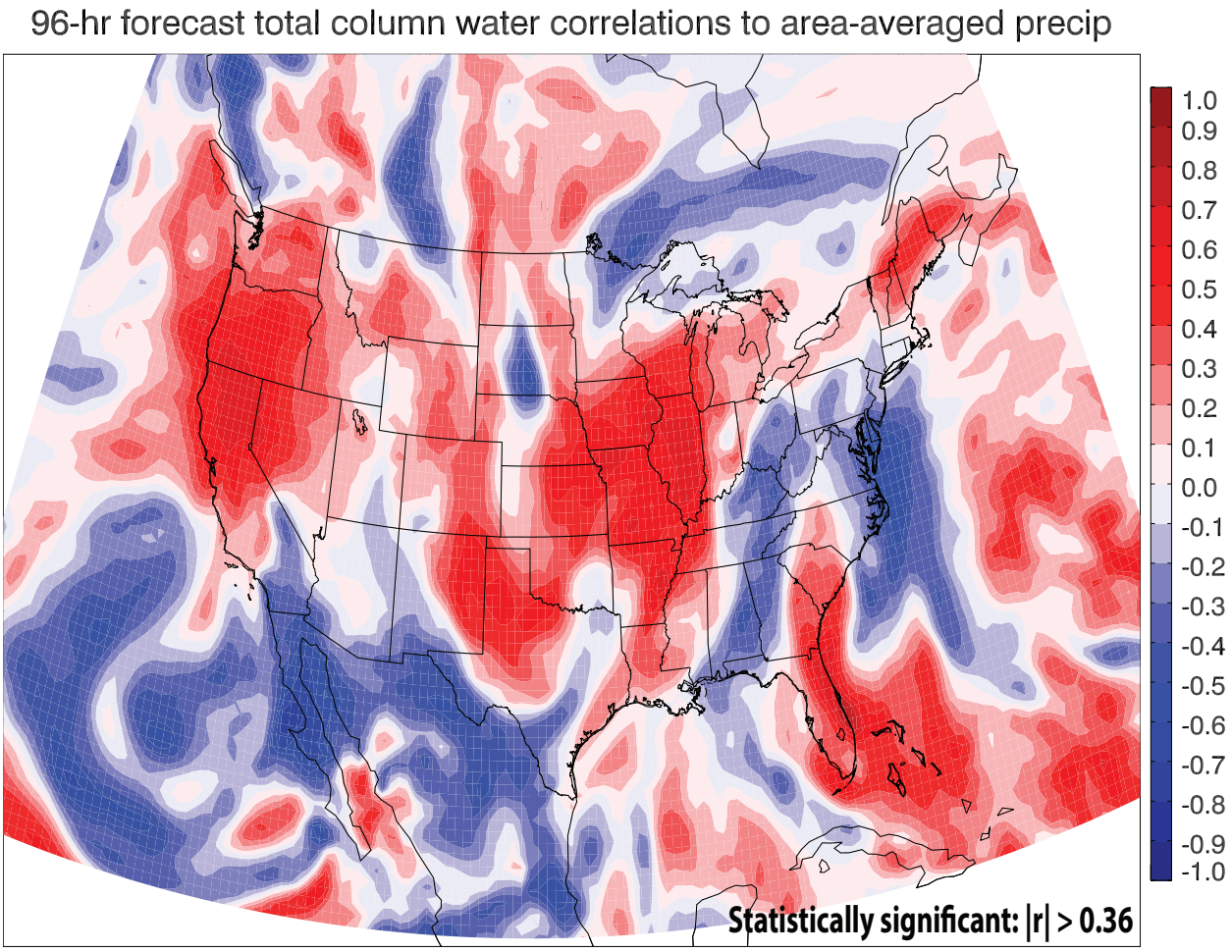

Figure 6.11: Area-averaged precipitation between 1200 UTC 23 April 2011 – 1200 UTC 28 April 2011 correlated to total column water at 1200 UTC 27 April 2011, corresponding to forecast hour 96. Warm colors represent a positive correlation, while cool colors represent a negative correlation.

6.3.2 Ensemble member comparison

To put the previously presented results into physical perspective, plots of the four most accurate members and the four least accurate members, both spatially and temporally, were constructed. Prior to looking at the forecasted precipitation, radar composites were reviewed to analyze the precipitation event. The heavy precipitation that flooded parts of the eastern United States and the Mississippi River lasted for several days. On 23 April 2011 and 24 April 2011, the precipitation area kept back building, continuously pounding southern Missouri with heavy precipitation (not shown). On 25 April 201l, a squall line started to form in eastern Oklahoma, and began to slowly push off to the east (Fig. 6.12a). The squall line continued to push east and slowly dissipated on 26 April 2011 (Fig. 6.12b). On the 27 April 2011, a secondary squall line formed, swept across eastern United States, dissipated, and then supercells began to form in Alabama and nearby areas (Fig. 6.12c). Numerous supercell thunderstorms produced long-lived,

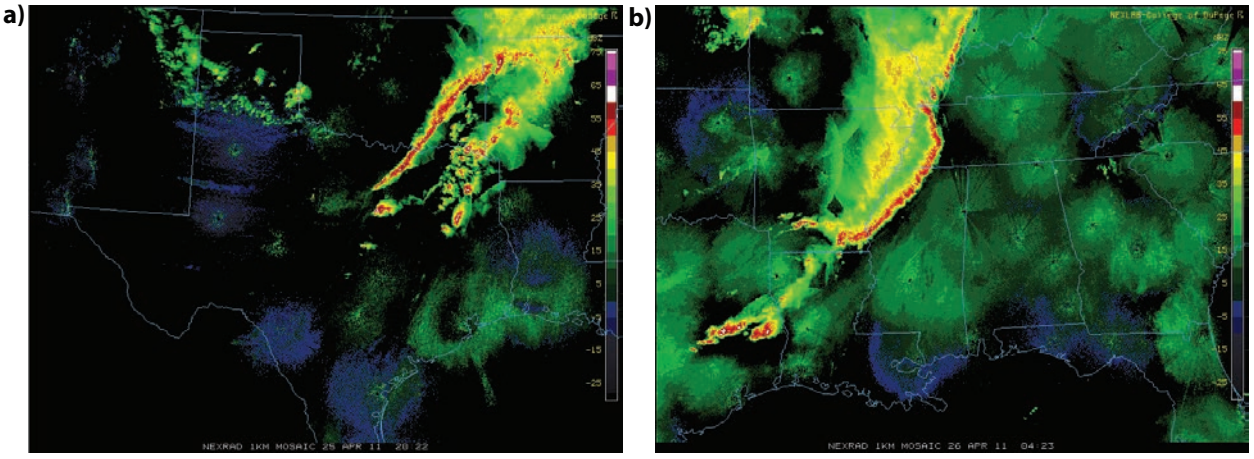

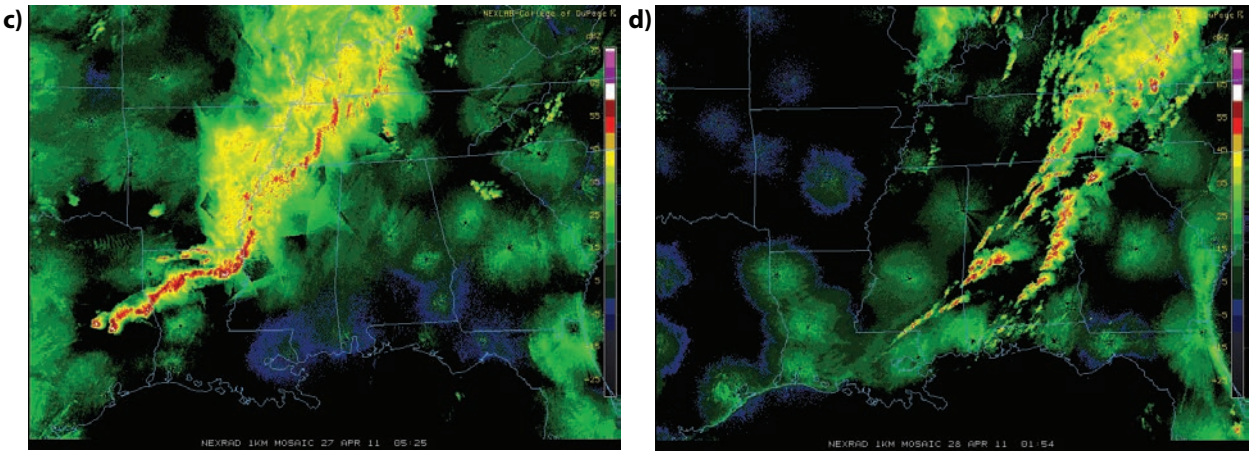

Figure 6.12: Radar reflectivity (color shading in dBZ) at (a) 2022 UTC 25 April. 2011, (b) 0423 UTC 26 April 2011, (c) 0525 UTC 27 April 2011, and (d) 0154 UTC 28 April 2011.

strong to violent tornadoes across Alabama. (NOAA 2011e) Finally, on 28 April 2011, the supercells took the formation of a linear feature and pushed east, off the coast of the United States (Fig. 6.12d). With consecutive days of heavy precipitation, rainfall amounts accumulated. Looking at forecasted precipitation, almost every ensemble member accurately predicted the location of precipitation. However, many of the ensemble members were unable to accurately forecast the quantity of rainfall the eastern United States received. Ensemble members 10, 37, 39, and 46 (the wet ensemble members) forecasted for heavy precipitation amounts in southern Missouri and surrounding areas. The wet ensemble members were very accurate when forecasting for locally high rainfall totals in southeast Arkansas, having done a remarkable job forecasting a squall line in this location 4 days in advance. The precipitation takes on a linear pattern oriented from west/southwest to east/northeast (Fig. 6.13a-d). This linear feature of precipitation was likely due to training, also known as backbuilding. Training occurs when thunderstorms align in a linear fashion and repeatedly move over the same areas in a relatively short period of time. Often, training causes rainfall amounts to accumulate producing a flash flood (Bluestein and Jain 1985, Chappell 1986, Doswell 1994, Doswell et al. 1996, Schumacher

and Johnson 2005, NOAA 2011a). As for members 0, 9, 21, and 23 (the dry ensemble members), the location of precipitation was accurately predicted but the amount of precipitation was far from exact (Fig. 6.13e-h). The overall location of heavy rainfall was well predicted by both the wet and dry ensemble members, resulting in the 23-28 April 2011 widespread rain event being well predicted. However, the amount of precipitation to fall appears to have been a challenge.

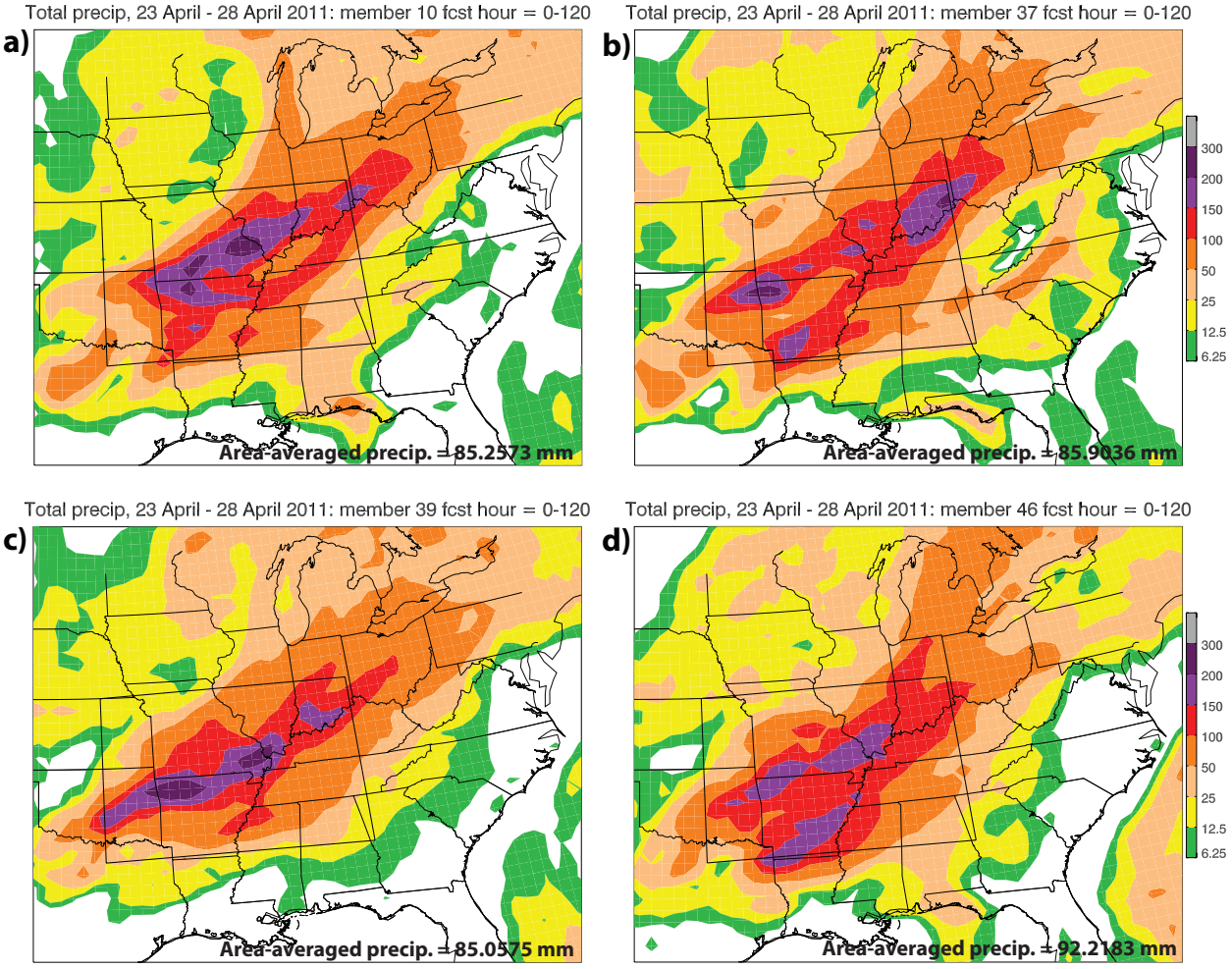

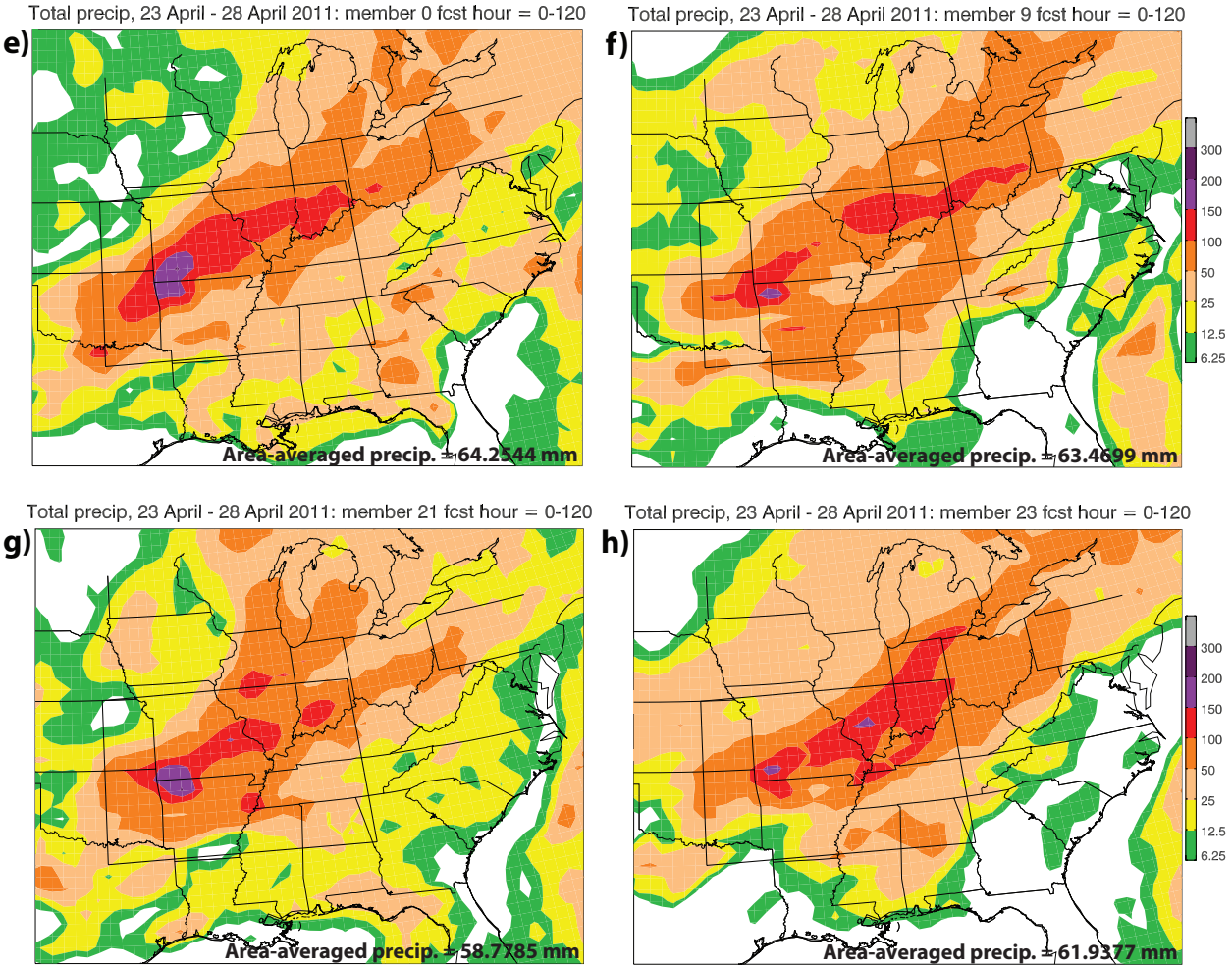

Figure 6.13: Five-day accumulated precipitation (color shading in mm) between 1200 UTC 23 April 2011 – 1200 UTC 28 April 2011: (a) member 10 (wet), (b) member 37 (wet), (c) member 39 (wet), (d) member 46 (wet), (e) member 0 (dry), (f) member 9 (dry), (g) member 21 (dry), and (h) member 23 (dry). The black rectangle indicates the location for areal averaging of precipitation and other fields.

As mentioned earlier, the ensemble members did a very good job at forecasting the location of this precipitation event. However, most ensemble members were far from accurate when predicting the maximum observed precipitation. From the U.S. Daily Precipitation Analysis dataset, the maximum observed precipitation amount was 310 millimeters. Member 10, member 37, member 39, and member 46 (the wet ensemble members) forecasted a maximum precipitation amount of 234 millimeters, 258 millimeters, 295 millimeters, and 208 millimeters.

Ensemble member 39 did an exceptional job forecasting for the maximum precipitation in this event. Member 0, member 9, member 21, and member 23 (the dry ensemble members) forecasted a maximum precipitation amount of 217 millimeters, 203 millimeters, 210 millimeters, and 190 millimeters (Fig. 6.14). Generally speaking, this is a great distribution for an ensemble system; there are members that overpredicted, underpredicted, and accurately forecasted the maximum observed precipitation.

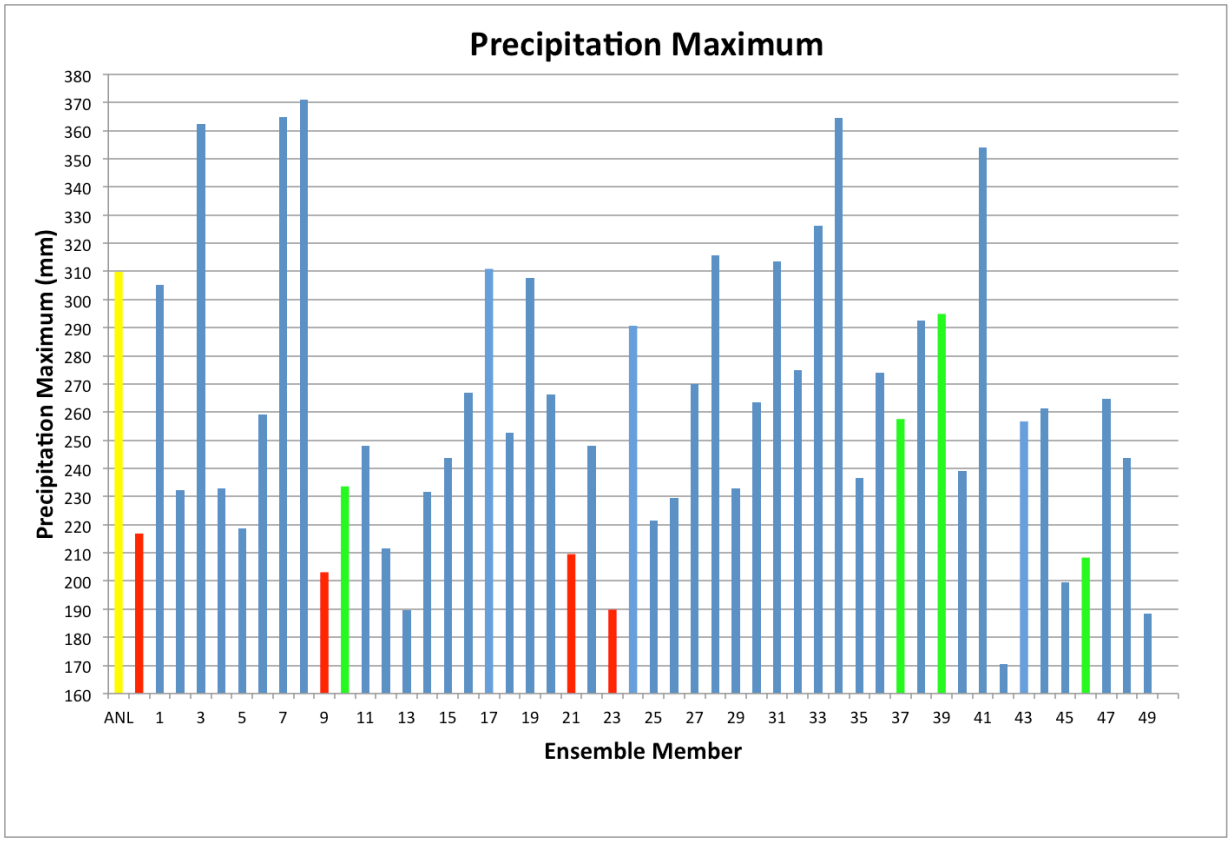

Figure 6.14: Precipitation maximum between the 5-day period 1200 UTC 23 April 2011 – 1200 UTC 28 April 2011. The wet ensemble members (members 10, 37, 39, and 46) are plotted in green, the dry ensemble members (members 0, 9, 21, and 23) are plotted in red, and the analysis is plotted in yellow.

Looking at the radar composite from 1155 UTC 27 April 2011, a squall line was seen passing through central Tennessee. This line of heavy precipitation was oriented from north to south, extending from northern Kentucky to central Alabama. There is also a cluster of strong

thunderstorms in southeast Arkansas, in the form of a squall line (Fig. 6.15a). Both the squall line and cluster of strong thunderstorms are slowly propagating to the northeast (not shown). As for the accumulated 12-hr precipitation from 0000 UTC 27 April 2011 to 1200 UTC 27 April 2011, rainfall totals exceeding 150 mm were observed in northern Louisiana, as well as in southeastern Arkansas. Western Tennessee recorded over 75 mm in this 12-hr time period (Fig.

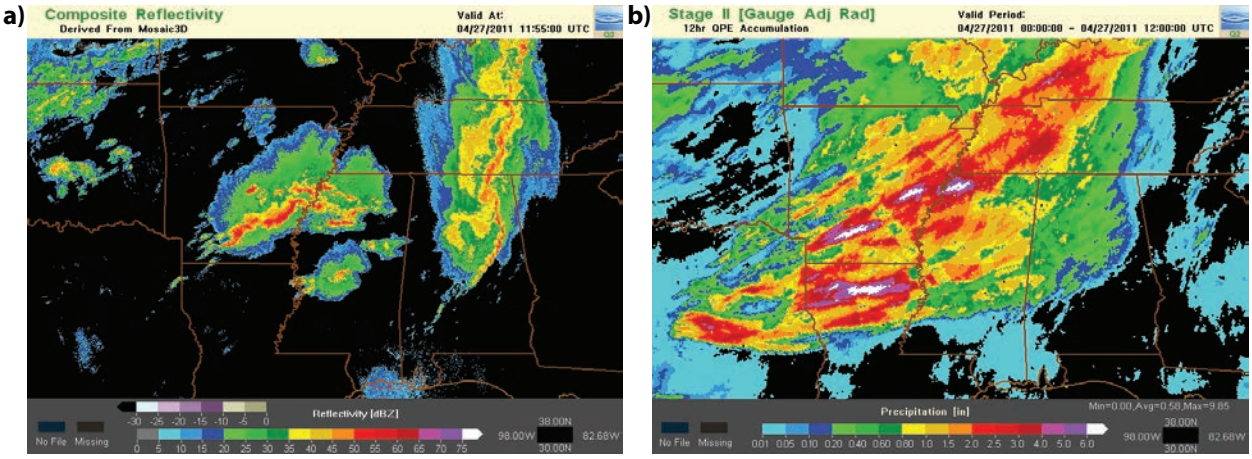

Figure 6.15: (a) Radar reflectivity (color shading in dBZ) at 1155 UTC 27 April 2011 and (b) Quantitative Precipitation Estimation (QPE) accumulation from the National Mosaic & Multi-Sensor QPE (NMQ) valid for the period from 0000 UTC 27 April 2011 to 1200 UTC 27 April 2011 (color shading in in).

6.15b). Ensemble members 10, 37, and 46 (the wet ensemble members) were very accurate when forecasting for a bulls eye of precipitation in southeast Arkansas, having done a remarkable job forecasting a squall line in this location 4 days in advance (Figs. 6.16a, 6.16b, and 6.16d). Ensemble member 39 (the wet ensemble member) also forecasted for localized heavy rainfall in southeastern Arkansas, however the strength and spatial scale of the squall line was greatly underpredicted (Fig. 6.16c). Ensemble members 37, 39, and 46 (the wet ensemble members) also placed a line of heavier precipitation in central Tennessee (Figs. 6.16b, 6.16c, and 6.16d). Each of the wet ensemble members underpredicted the total amount of precipitation for this 12-hr time period, having only forecasted for a maximum rainfall amount of approximately 50 to 75 mm.

As for the dry ensemble members, ensemble member 0 completely missed the squall line in southeast Arkansas, moving the precipitation system off to the east much to quickly (Fig. 6.16e). Ensemble member 9 (a dry ensemble member) forecasted for a squall line in southern Arkansas, although the strength of the squall line was underpredicted (Fig. 6.16f). Ensemble members 0 and 9 (the dry ensemble members) also placed a cluster of heavier rainfall totals in central Tennessee, representative of the squall line that was present (Figs. 6.16e and 6.16f). Ensemble member 23 (a dry ensemble member) forecasted for a very strong squall line, however, it was forecasted to be too far north, in northeastern Arkansas (Fig. 6.16h). Interestingly, ensemble member 21 (the dry ensemble member) more closely resembles the wet ensemble members, forecasting for a squall line in south central Arkansas (Fig. 6.16g). The 12-hr accumulation rainfall was even more underpredicted by the dry ensemble members, having predicted approximately 25 to 50 mm.

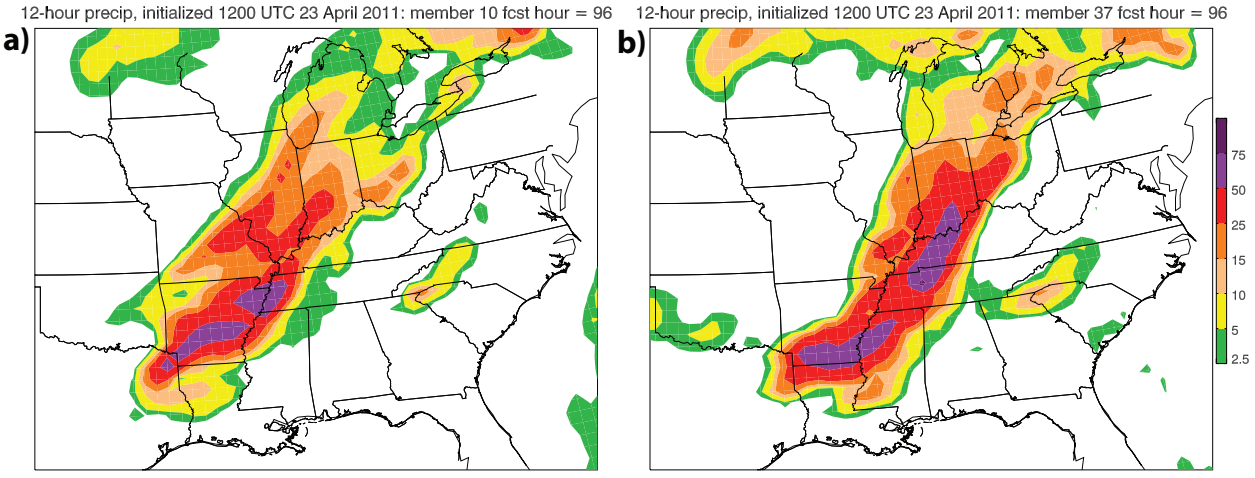

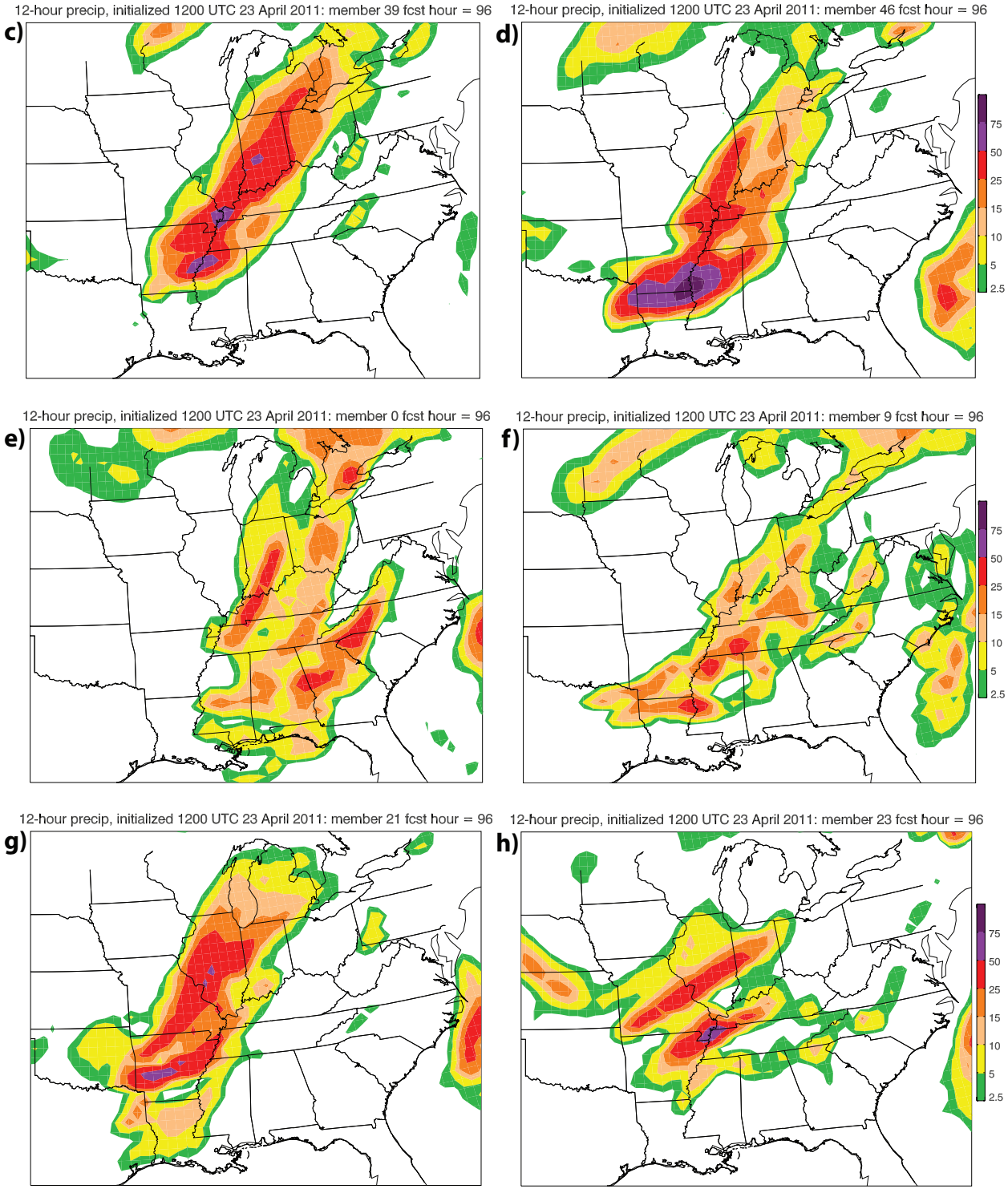

Figure 6.16: Forecasted precipitation (color shading in mm) for 1200 UTC 27 April 2011, corresponding to forecast hour 96: (a) member 10 (wet), (b) member 37 (wet), (c) member 39 (wet), (d) member 46 (wet), (e) member 0 (dry), (f) member 9 (dry), (g) member 21 (dry), and (h) member 23 (dry).

Looking at the synoptic set-up of the event, one can determine the processes that were favorable or detrimental to the system's development. Beginning at the 500-hPa level, there is a strong upper-level trough digging into the southern United States, along with a prominent ridge to the east. A tight pressure gradient exists over central Texas, with the trough axis oriented north to south. Cyclonic flow around the upper-level trough produces robust southerly flow, allowing for transport of deep moisture from the Gulf of Mexico into the southeastern United States. Additionally, an occluded low pressure center has formed in Minnesota (Fig. 6.17a). Twelve hours later, the upper-level trough begins to recede and push to the east (Fig. 6.17b). The forecasts from ensemble members 10, 37, 39, and 46 (the wet ensemble members) look nearly identical to the observed 500-hPa pressure. The wet ensemble members forecasted for an upper-level trough to extend down into central Texas, with a tight pressure gradient at the base of the trough. Additionally, the trough axis is oriented from

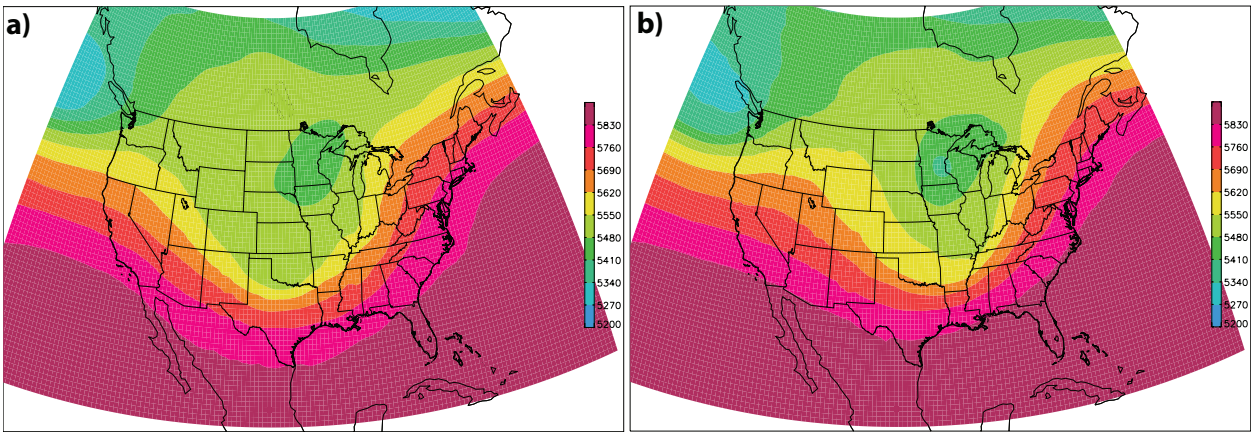

Figure 6.17: ECMWF analysis of 500-hPa height (color shading in m) at (a) 1200 UTC 27 April 2011 and (b) 0000 UTC 28 April 2011.

north to south. Each of the wet ensemble members also forecasted for an occluded low pressure in Minnesota (Fig. 6.18a-d). The dry ensemble members forecasted slightly different. Member 0 (the dry ensemble member) forecasted for an upper-level trough with a strong negative tilt. The

trough axis is oriented from northwest to southeast. The base of the trough is located around Mississippi and Alabama (Fig. 6.18e). It appears ensemble 0 has pushed the trough off to the east approximately 12 hours too soon. Member 9 and 23 (the dry ensemble members) forecasted for a slightly shallower trough than what was observed (Figs. 6.18f and 6.18h). However, ensemble member 23 misplaced the occluded low pressure center, placing it too far southwest of Minnesota extending as far south as Oklahoma (Fig. 6.18h). Lastly, member 21 (the dry ensemble member) forecasted for the base of the trough to be located around the Texas/Louisiana border, again seeming to push the upper-level trough through much too quickly (Fig. 6.18g).

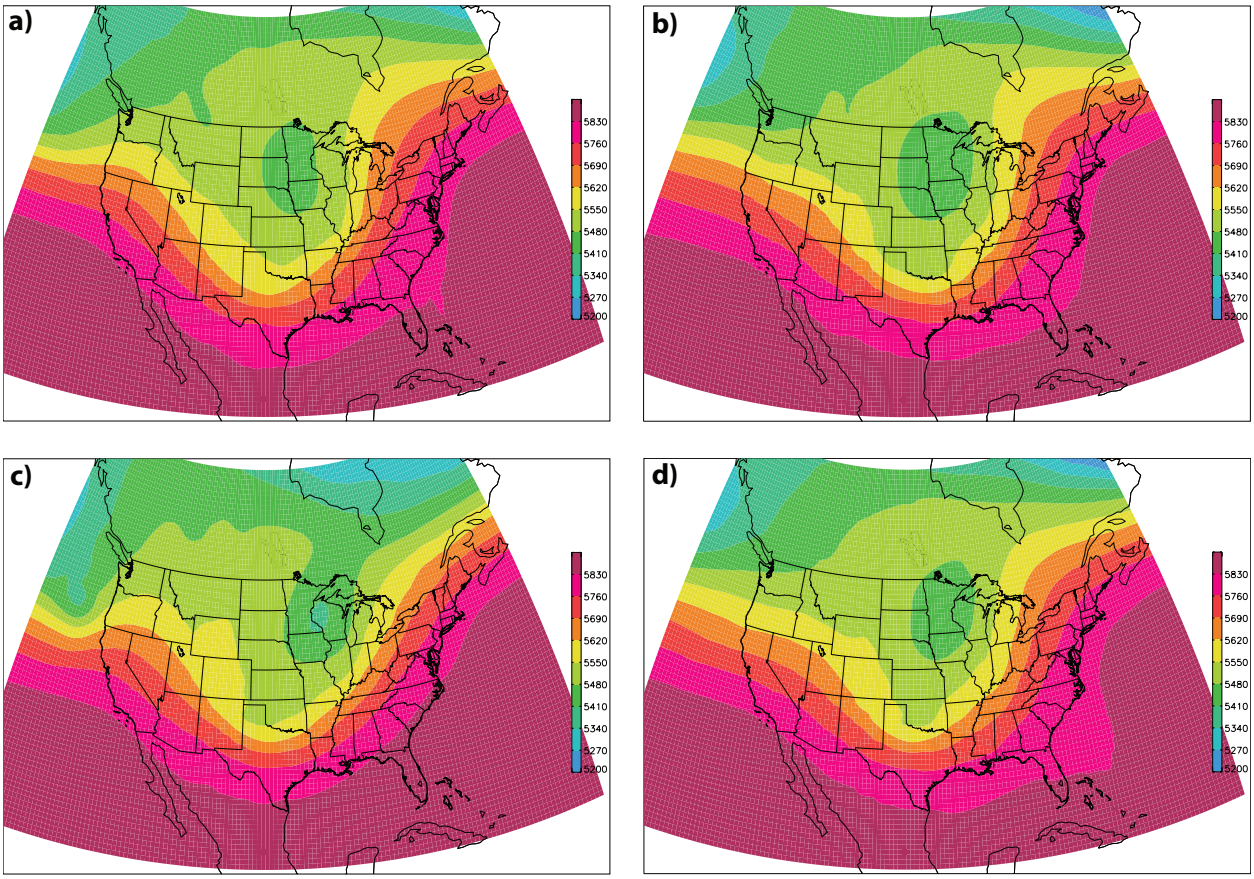

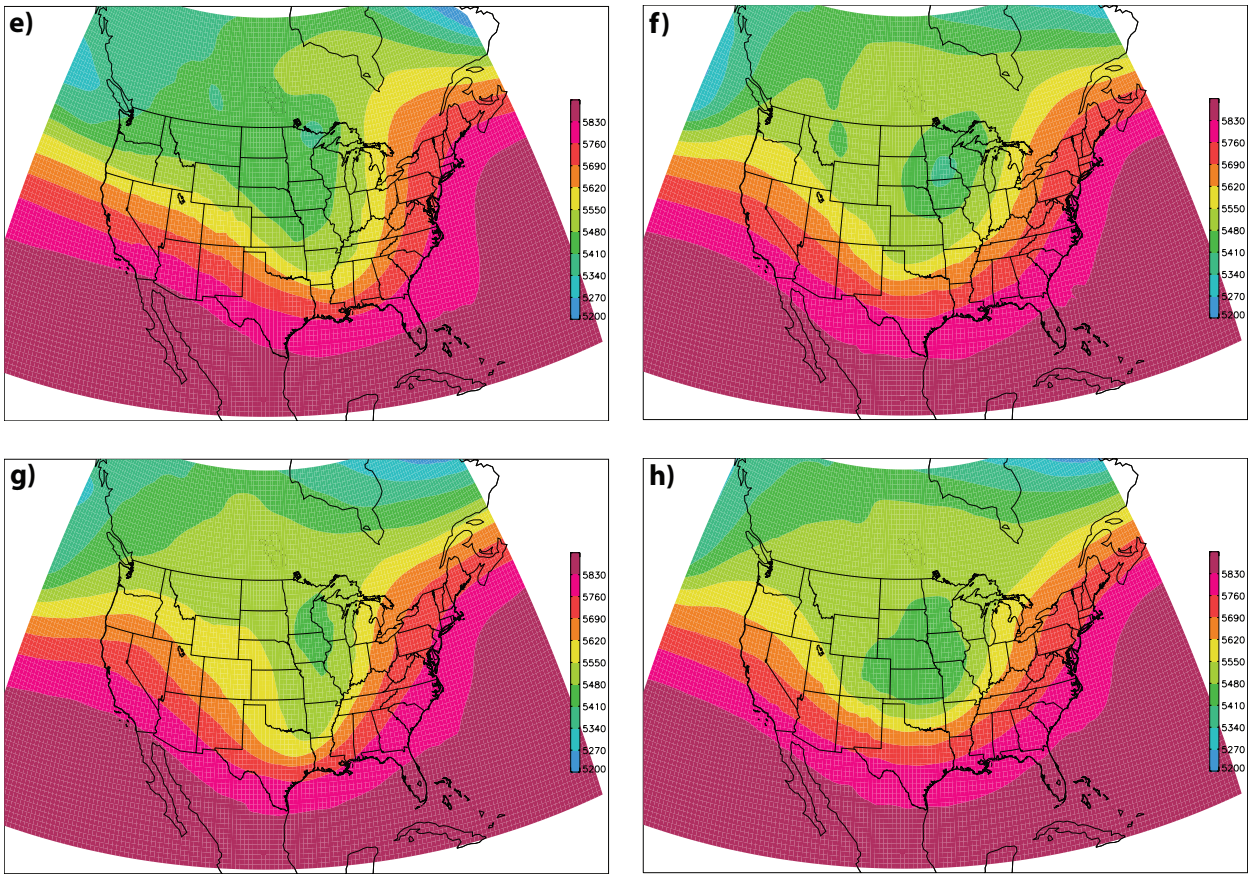

Figure 6.18: Forecasted 500-hPa height (color shading in m) at 1200 UTC 27 April 2011, corresponding to forecast hour 96: (a) member 10 (wet), (b) member 37 (wet), (c) member 39 (wet), (d) member 46 (wet), (e) member 0 (dry), (f) member 9 (dry), (g) member 21 (dry), and (h) member 23 (dry).

On the 27 April 2011, a very strong cyclone at the 850-hPa level was present over the Midwest (Fig. 6.19a). This area of rotation brought strong southerly flow into the Mississippi Valley, supplying sufficient moisture to support heavy precipitation. Both the wet and the dry ensemble members forecasted for a low pressure system in the Midwest United States. Ensemble members 10, 37, 39, and 46 (the wet ensemble members) forecasted for an elongated occluded low pressure center to be located in Wisconsin, digging south into eastern Texas (Fig. 6.20a-d). Member 46 (the wet ensemble member) most accurately forecasted for the 850-hPa pressure field, placing a second, weaker occluded low pressure center in eastern Oklahoma (Fig. 6.20d).

Although the remaining wet ensemble members did not forecasts for the second, weaker low pressure center in northeastern Texas/Oklahoma, the core of low pressure extends far enough southwest to encompass eastern Texas. Associated with the deep digging occluded low each of the wet ensemble members forecasted for is strong cyclonic rotation. The cyclonic rotation caused strong southerly flow, supplying the Mississippi Valley with increased moisture from the Gulf of Mexico. Additionally, the wet ensemble members forecasted for the Bermuda High to be positioned more to the west, helping to draw ample moisture into the southeastern United States (Fig. 6.20a-d). Members 0, 9, and 23 (the dry ensemble members) also forecasted for a low pressure center to be located around Wisconsin, however these ensemble members did not

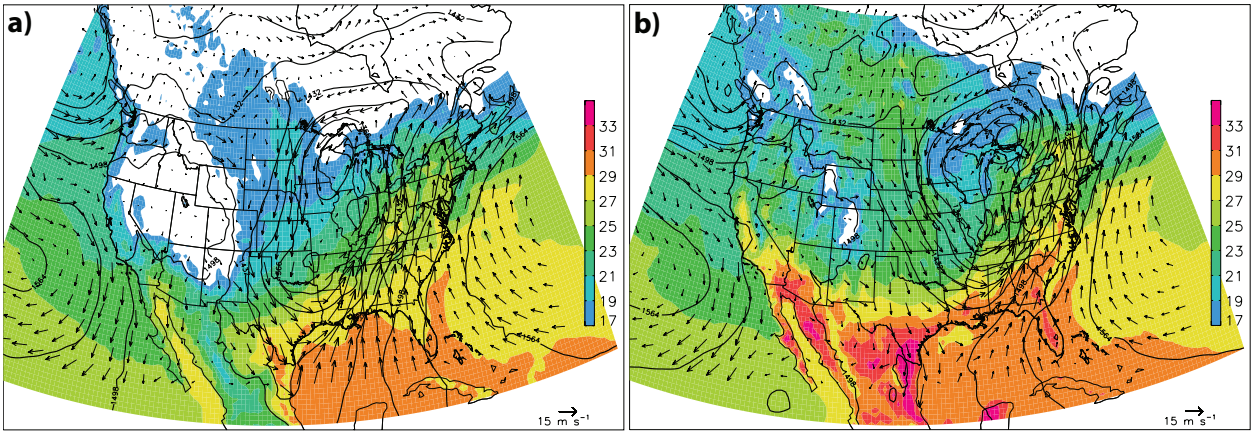

Figure 6.19: ECMWF analysis of 850-hPa temperature (color shading in C), height (black contours overlaid in m), and wind (vectors overlaid, vector scale is shown at bottom right) at (a) 1200 UTC 27 April 2011 and (b) 0000 UTC 28 April 2011.

include the southern extension of the occluded low (Figs. 6.20e, 6.20f, and 6.20h). The cyclonic flow around the occluded low did not extend far enough south to provide ample moisture from the Gulf of Mexico, rather bringing in more dry air from the southern plains region. Ensemble member 21 (the dry ensemble member) forecasted for the occluded low to be centered in Illinois, extending down into northern Louisiana. Ensemble member 21 (a dry ensemble member) created a better forecast when including the southern extension of the occluded low, however, the center

of the occluded low is placed too far south and it appears the cyclone has tracked off to the east too quickly (Fig. 6.20g). The southern extent of the forecasted occluded low allowed for strong cyclonic rotation to supply moisture to the southeastern United States, however, with the system moving off to the east too quickly the moisture supply was cut off too soon. None of the dry ensemble members forecasted for the second low pressure center in the Oklahoma area. The dry ensemble members forecasted for the Bermuda High to be farther off the eastern coast of the United States, suppressing the moisture transport into the southeastern United States (Fig. 6.20e-h). Twelve hours later, the cyclone receded and tracked off to the northeast, sitting overhead the Great Lakes region. Westerly winds started to prevail, pushing the system off to the east (Fig. 6.19b). As the low pressure system slides off to the east, the southerly flow bringing in moisture from the Gulf of Mexico starts to diminish. Both the wet ensemble members and the dry ensemble members forecasted for warm air advection throughout southeast United States. However, the wet ensemble members forecasted for much stronger warm air advection. The cyclonic rotation in north Texas causing strong southerly flow is allowing the transport of warm temperatures inland from the Gulf of Mexico (Fig. 6.20a-d). The dry ensemble members do not have the support of the surface cyclone in eastern Texas, weakening the southerly flow and therefore the temperature transport (Fig. 6.20e-h).

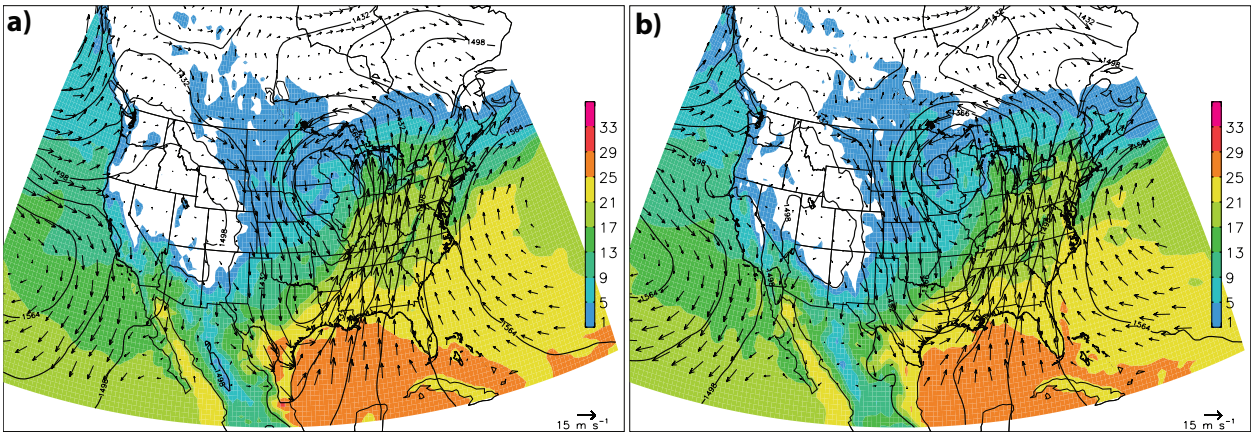

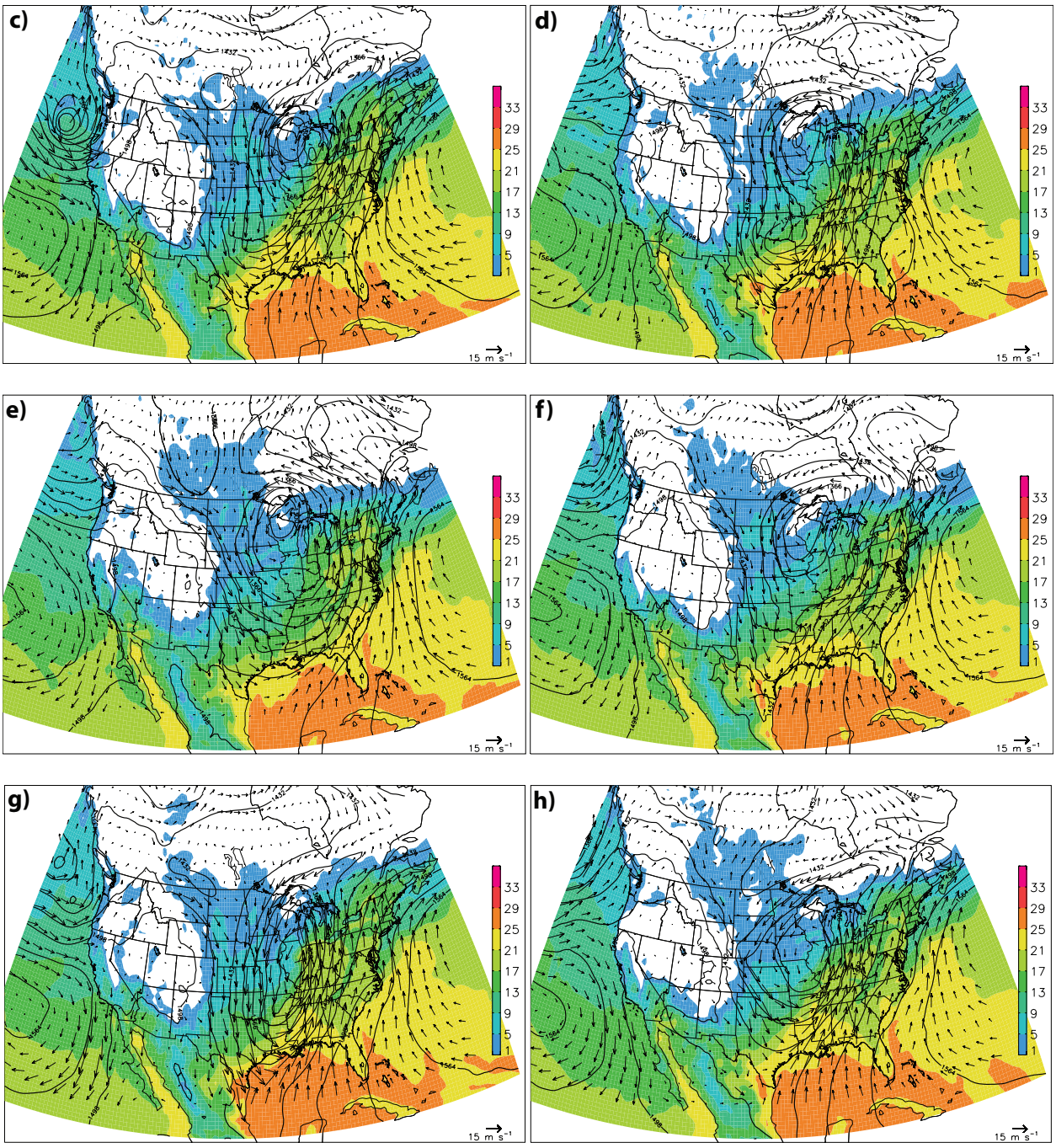

Figure 6.20: Forecasted 850-hPa temperature (color shading in C), height (black contours overlaid in m), and wind (vectors overlaid, vector scale is shown at bottom right) at 1200 UTC 27 April 2011, corresponding to forecast hour 96: (a) member 10 (wet), (b) member 37 (wet), (c) member 39 (wet), (d) member 46 (wet), (e) member 0 (dry), (f) member 9 (dry), (g) member 21 (dry), and (h) member 23 (dry).

Taking a look at the total column water, there is an area of high total column water located over northern Mississippi and Alabama, and extending to the north through central Tennessee and Kentucky. The total column water in northern Mississippi and southeastern Arkansas is greater than 50 mm (Fig. 6.21a). This is able to supply the Mississippi Valley with sufficient moisture to support heavy precipitation. Twelve hours later, the region of high total

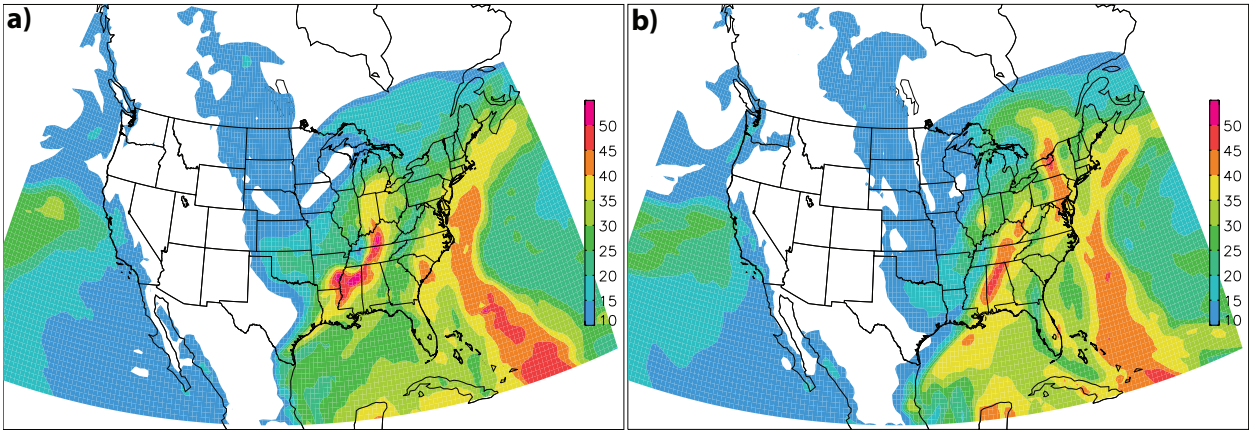

Figure 6.21: ECMWF analysis of total column water (color shading in mm) at (a) 1200 UTC 27 April 2011 and (b) 0000 UTC 28 April 2011.

column water weakens and begins to slide eastward (Fig. 6.21b). Ensemble members 10, 37, 39, and 46 (the wet ensemble members) have forecasted for localized high total column water within the area, however the abundance of total column water was underpredicted (Fig. 6.22a-d). Members 10 and 46 (the wet ensemble members) forecasted for an area of high total column water over northern Mississippi and southeastern Arkansas, however, both of these ensemble members missed the arm of high total column water extending northward through central Tennessee (Figs. 6.22a and 6.22d). Ensemble members 37 and 39 (the wet ensemble members) forecasted for a narrow strip of moisture extending from northern Alabama to the Great Lake region, similar to the observed total column water. However, these ensemble members greatly under forecasted the amount of total column water in northern Mississippi and southeastern

Arkansas, only forecasting for about 35 to 40 mm (Figs. 6.22b and 6.22c). Not only is there a feed of moisture from the Gulf of Mexico, there is a plume of deep moisture from the southwestern Atlantic Ocean pushing up the coast of the eastern United States (Figs. 6.21a and 6.21b). Each of the wet ensemble members forecasted for this plume of moisture to impinge upon the southeastern United States, however its strength was slightly underpredicted (Fig. 6.22a-d). As for member 0 (a dry ensemble member), very little total column water was forecasted for southeast Arkansas and central Tennessee, leaving minimal support for heavy precipitation (Fig. 6.22e). For ensemble member 9 (a dry ensemble member), the region of highest total column water seems to be placed in approximately the right location, however the amount of total column water was underpredicted (Fig. 6.22f). The total column water associated with member 21 (the dry ensemble member) has a linear feature extending from southern Texas to northern Mississippi. The stream of moisture is feeding in from the Gulf of Mexico (Fig. 6.22g). Member 23 (the dry ensemble member) has an area of higher total column water located just overhead Louisiana and Alabama, however, the value of total column water only reaches about 35 mm (Fig. 6.22h). Although each of the dry ensemble members have also forecasted for a plume of moisture from the southwestern Atlantic Ocean, the plume of moisture impinges the northeastern United States, hindering the moisture transport to the Mississippi Valley (Fig. 6.22e-h). This is likely a result of an eastward positioned Bermuda High, shown previously.

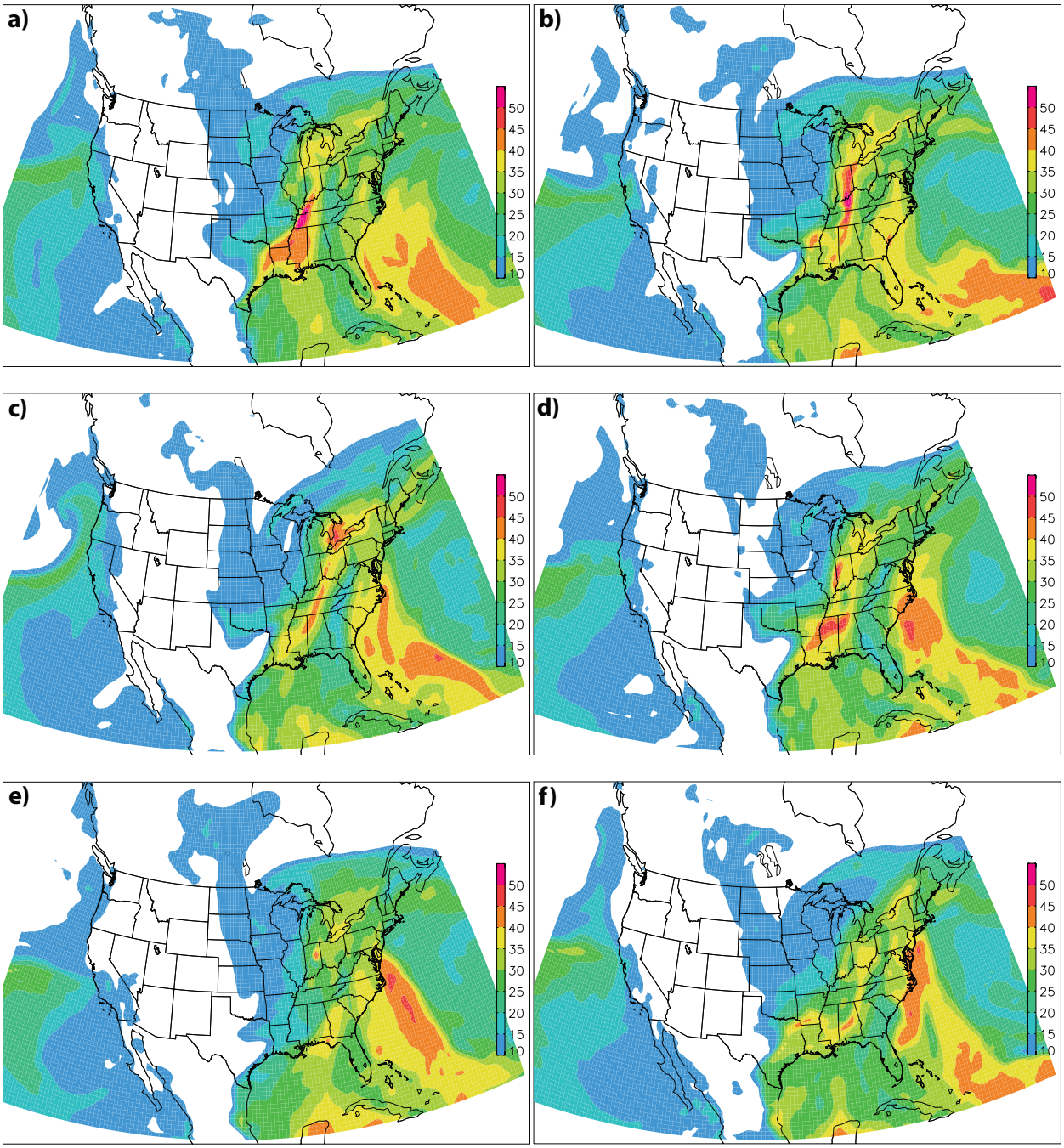
a)
b)
c)
d)
e)
f)
50
45
40
35
30
25
20
15
10

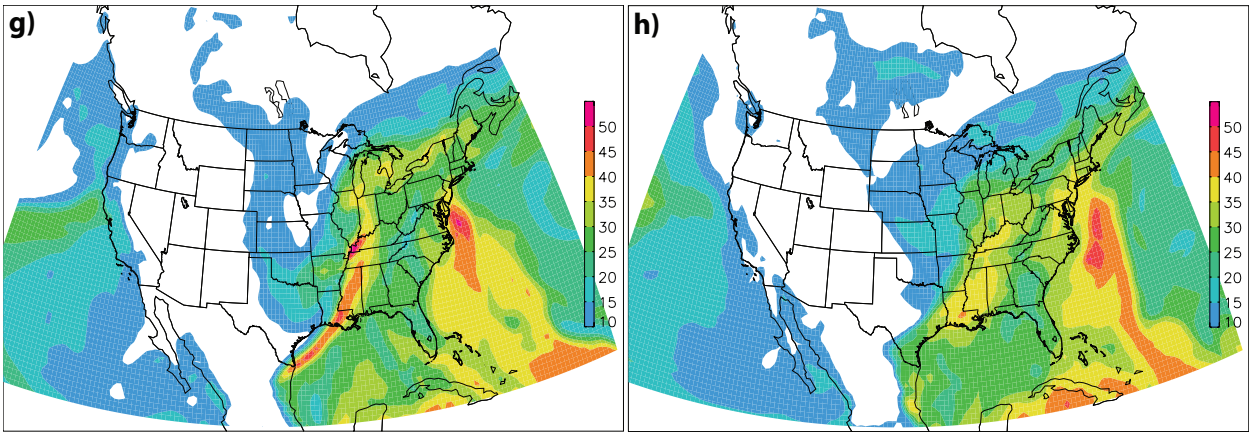

Figure 6.22: Forecasted total column water (color shading in mm) at 1200 UTC 27 April 2011, corresponding to forecast hour 96: (a) member 10 (wet), (b) member 37 (wet), (c) member 39 (wet), (d) member 46 (wet), (e) member 0 (dry), (f) member 9 (dry), (g) member 21 (dry), and (h) member 23 (dry).

Junker et al. (1999) found that the scale and intensity of rainfall appears to be related to the strength of low-level moisture flux convergence. High values of moisture transport are associated with heavy rainfall potential with convective systems. At 1200 UTC 27 April 2011, 850-hPa moisture transport reaches over 220 g kg^{-1} m s^{-1} throughout the eastern United States. Moisture is beginning to push northwards from the Gulf of Mexico into the coastal region. There is also a deep plume of moisture from the Atlantic Ocean, pushing up the coast of the eastern United States, providing the Mississippi Valley with excess moisture (Fig. 6.23a). Twelve hours later, at 0000 UTC 28 April 2011, the moisture transport begins to increase over a larger area, pushing as far north as the Great Lakes region (Fig. 6.23b). Members 10, 37, 39, and 46 (the wet ensemble members) closely resemble the observed 850-hPa moisture flux. However, the wet ensemble members slightly overpredicted the amount of moisture transport at 1200 UTC 27 April 2011. Similar to the observed 850-hPa moisture flux, moisture is entering the United States through the Louisiana/Mississippi region, and then extending northeastward. The wet ensemble members also forecasted for a flux of moisture from the Atlantic Ocean to impinge on the

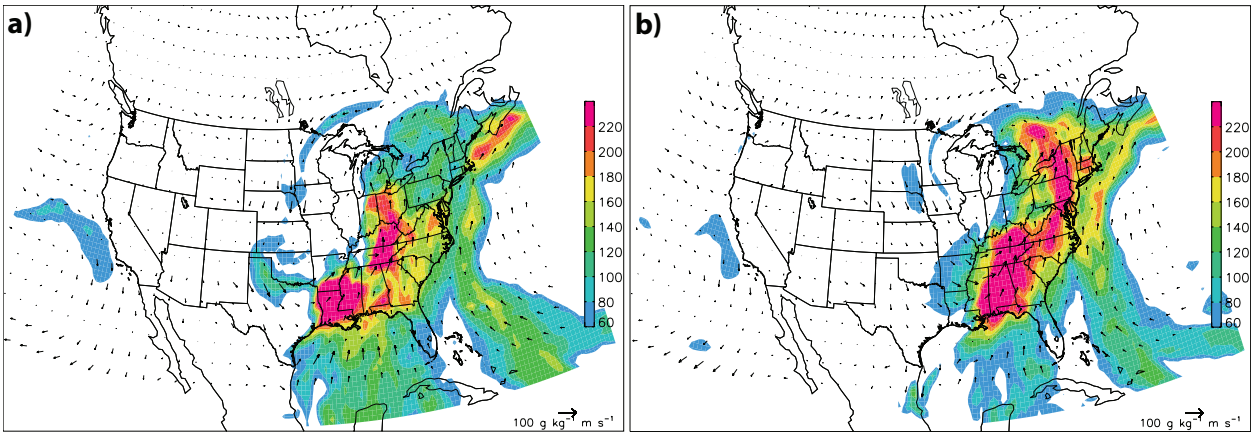

Figure 6.23: ECMWF analysis of 850-hPa moisture flux (color shading in g kg^{-1} m s^{-1} with vectors overlaid, vector scale is shown at bottom right) at (a) 1200 UTC 27 April 2011 and (b) 0000 UTC 28 April 2011.

southeastern coast, supplying moisture to the Mississippi Valley (Fig. 6.24a-d). Members 0 and 9 (the dry ensemble members) underpredicted the amount of moisture transport from the Gulf of Mexico (Figs. 6.24e and 6.24f). Ensemble member 0 has forecasted for higher values of moisture transport too far to the east entering the United States through Alabama and Georgia (Fig. 6.24e). Members 21 and 23 (the dry ensemble members) did a much better job of predicting the moisture trasnport at 1200 UTC 27 April 2011. Both forecasted for a strong plume of moisture entering the United States through Louisiana and Mississippi, with moisture transport reaching a value over 220 g kg^{-1} m s^{-1} throughout the eastern United States (Figs. 6.24g and 6.24h). Ensemble member 21 (a dry ensemble member) appears to have pushed the large plume of moisture off to the east too early, likely cutting short the moisture supply to the Mississippi Valley (Fig. 6.24g). Each of the dry ensemble members also forecasted for a flux of moisture from the Atlantic Ocean, however, the moisture enters the northeastern United States not supplying additional support for heavy precipitation in the Mississippi Valley (Fig. 6.24e-h).

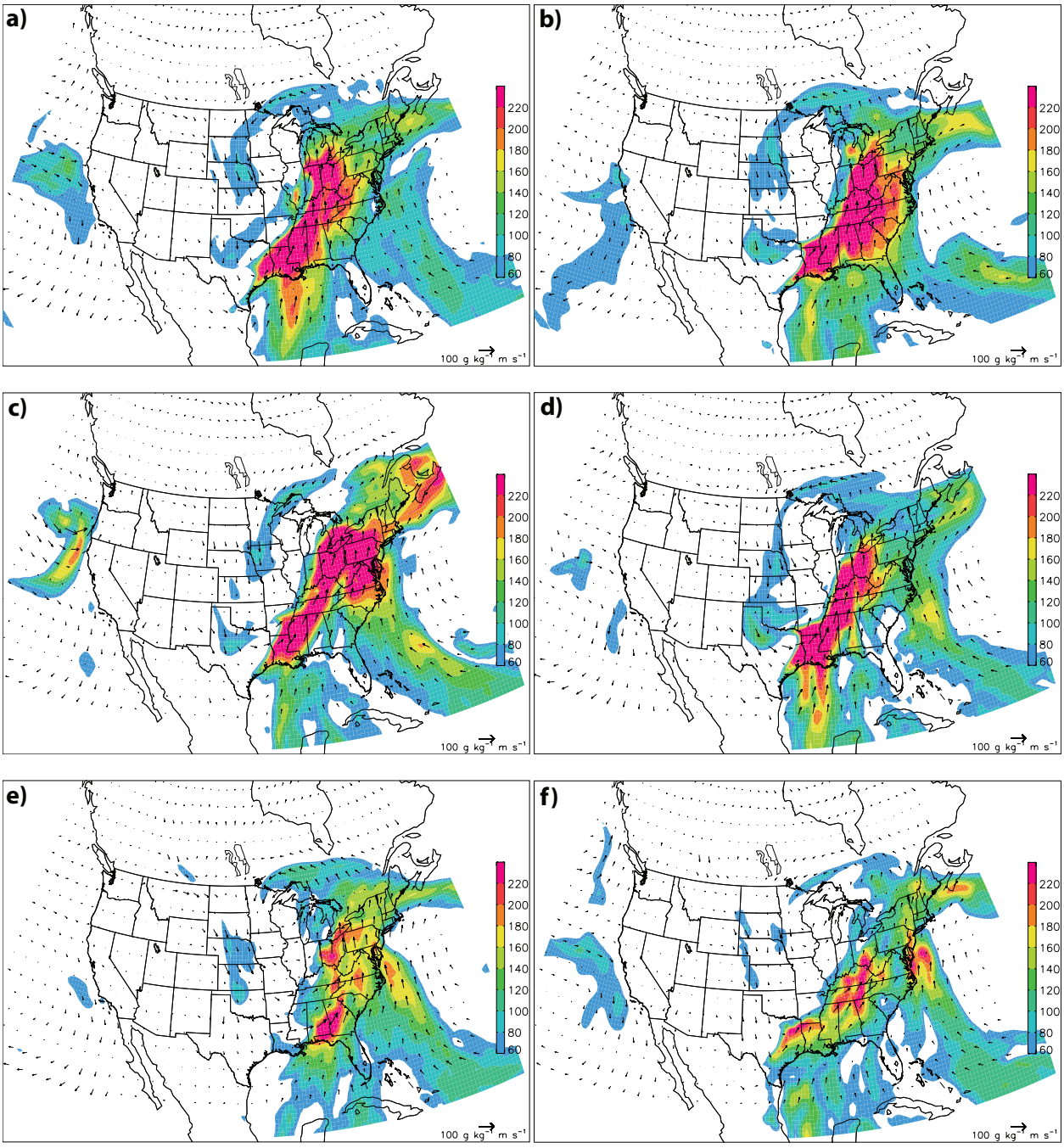
a)
b)
c)
d)
e)
f)
220
200
180
160
140
120
100
80
60
100 g kg⁻¹ m s⁻¹

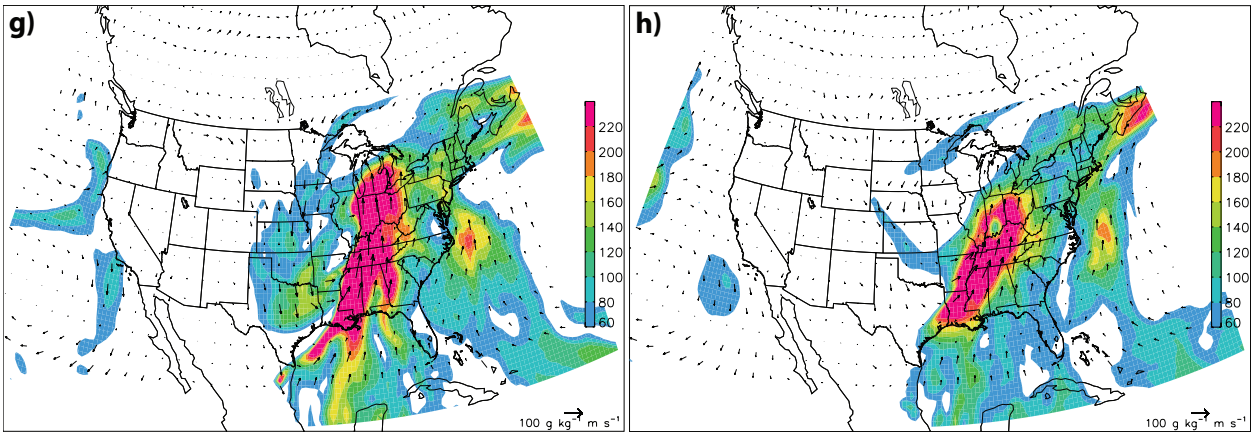

Figure 6.24: Forecasted 850-hPa moisture flux (color shading in g kg^{-1} m s^{-1} with vectors overlaid, vector scale is shown at bottom right) at 1200 UTC 27 April 2011, corresponding to forecast hour 96: (a) member 10 (wet), (b) member 37 (wet), (c) member 39 (wet), (d) member 46 (wet), (e) member 0 (dry), (f) member 9 (dry), (g) member 21 (dry), and (h) member 23 (dry).

The following figure is the time-integrated moisture flux from 0000 UTC 24 April 2011 to 0000 UTC 28 April 2011 at the 850-hPa level. During this four-day time period, a series of mesoscale convective systems passed through the Mississippi Valley. At the 850-hPa level, the highest values of moisture flux are located in central Tennessee and northern Louisiana/southern Arkansas. Moisture flux values exceed 50 x 10^7 g kg^{-1} m on the Arkansas/Louisiana border, as well as in west central Tennessee and Kentucky. As the moisture entered the southeastern United States, it was lofted over the surface frontal boundary, resulting in high amounts of moisture in the Mississippi Valley at the 850-hPa level (Fig. 6.25). Looking at the forecasted 850-hPa time-integrated moisture flux, ensemble members 10, 37, 39, and 46 (the wet ensemble members) forecasted for a high value of time-integrated moisture flux, 50 x 10^7 g kg^{-1} m, just east of Texas extending northeast into Ohio. Although the wet ensemble members appear to have overpredicted the amount of time-integrated moisture flux, the spatial distribution of these higher values is correct (Fig. 6.26a-d). At this point it is still unknown why the wet ensemble members

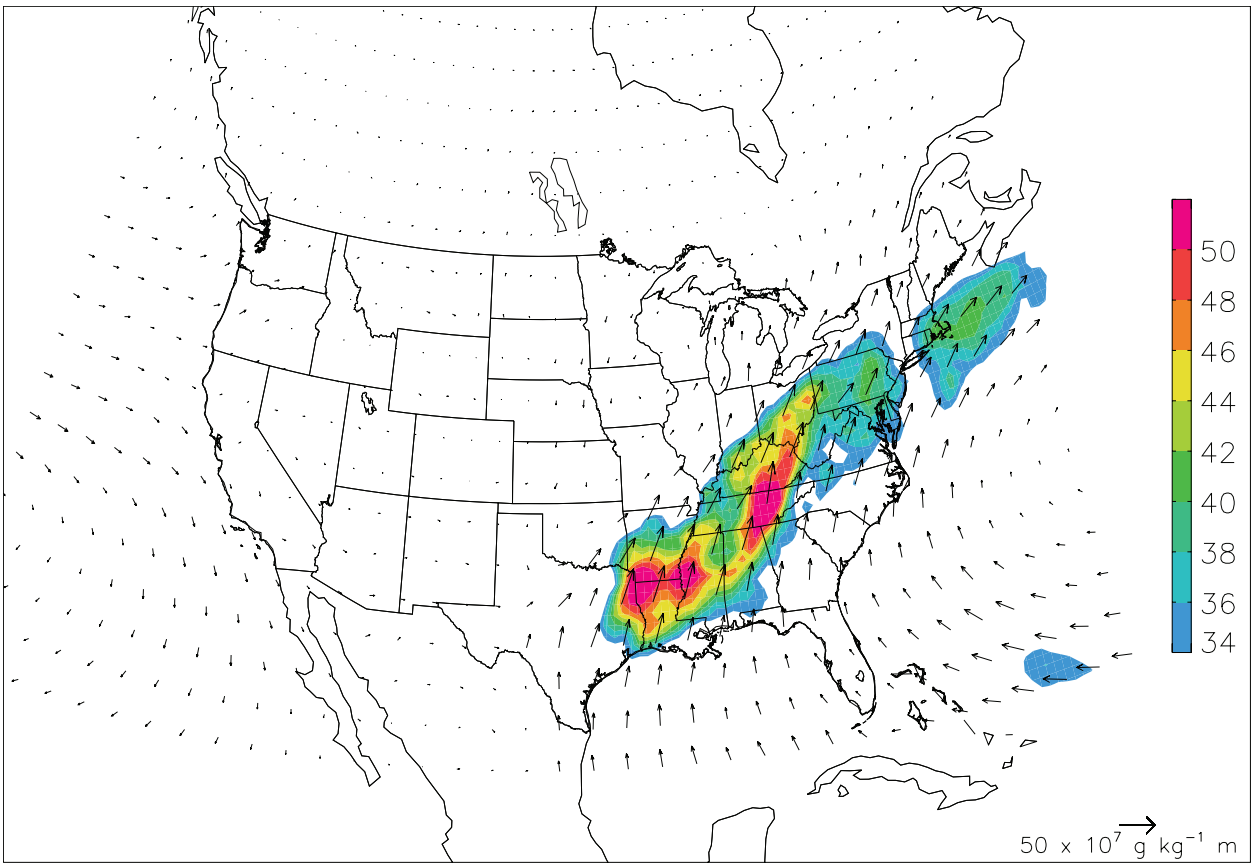

Figure 6.25: ECMWF analysis of 850-hPa time-integrated moisture flux (color shading in 10^7 g kg^{-1} m with vectors overlaid, vector scale is shown at bottom right) from 0000 UTC 24 Apr 2011 to 0000 UTC 28 Apr 2011.

overpredicted the amount of time-integrated moisture flux yet underpredicted the total amount of precipitation for this widespread, multiday precipitation event. Ensemble member 0 (a dry ensemble member) greatly underpredicted the amount of time-integrated moisture flux, only calling for 46 x 10^7 g kg^{-1} m in northern Kentucky (Fig. 6.26e). Ensemble members 9, 21, and 23 (the dry ensemble members) forecasted for higher values of time-integrated moisture flux, however, they missed the bulls eye of higher values in southern Arkansas (Fig. 6.26f-h).

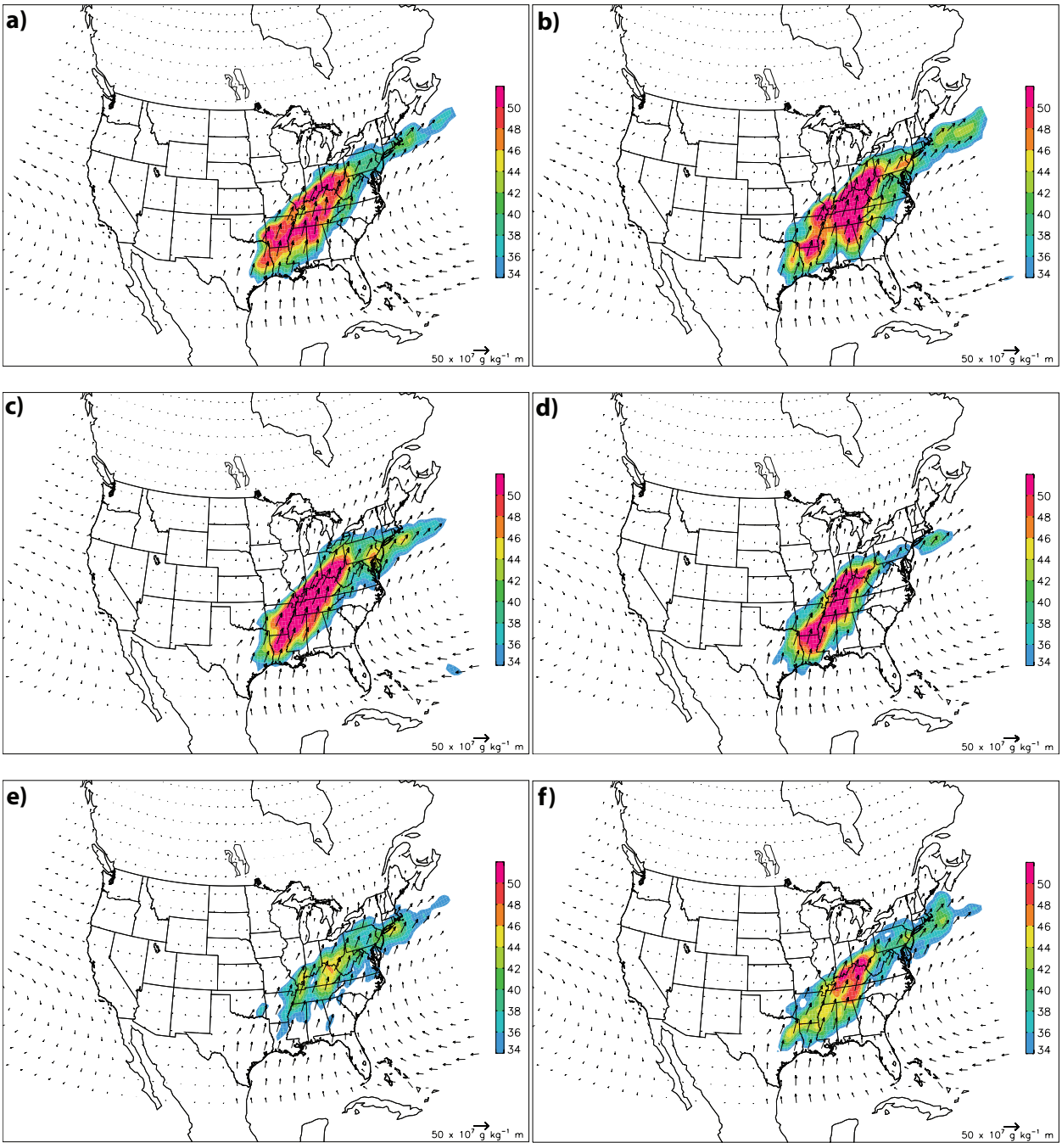
a)
b)
c)
d)
e)
f)
50
48
46
44
42
40
38
36
34
50 x 10^7 g kg^-1 m

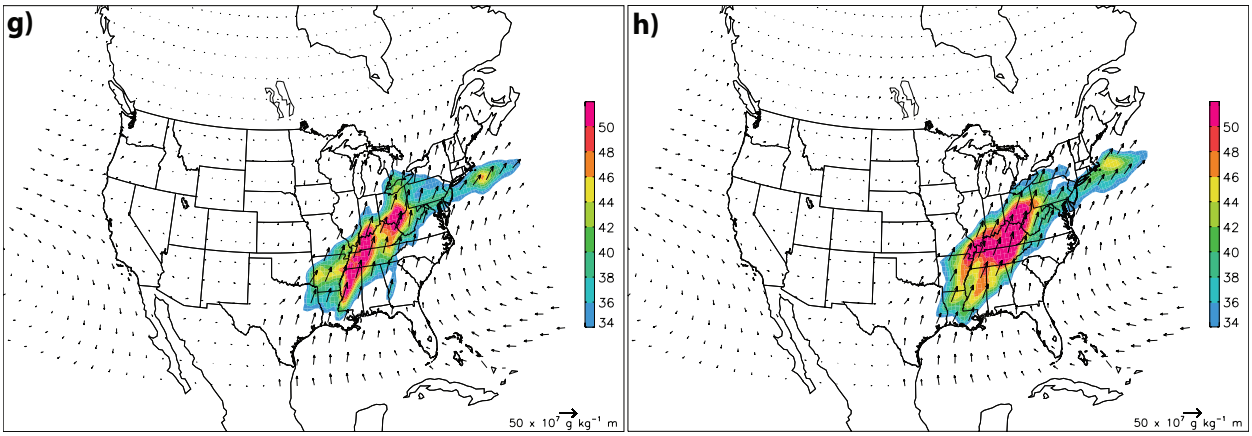

Figure 6.26: Forecasted 850-hPa time-integrated moisture flux (color shading in 10^7 g kg^{-1} m with vectors overlaid, vector scale is shown at bottom right) from 0000 UTC 24 April 2011 to 0000 UTC 28 April 2011, corresponding to forecast hour 12 to forecast hour 108: (a) member 10 (wet), (b) member 37 (wet), (c) member 39 (wet), (d) member 46 (wet), (e) member 0 (dry), (f) member 9 (dry), (g) member 21 (dry), and (h) member 23 (dry).

6.4 Discussion

This case study provides a way of estimating the predictability of a widespread heavy rain event capable of producing not only high precipitation amounts, but also destructive tornadoes (Figs. 6.27a and 6.27b). Relatively small differences in the structure of the height field

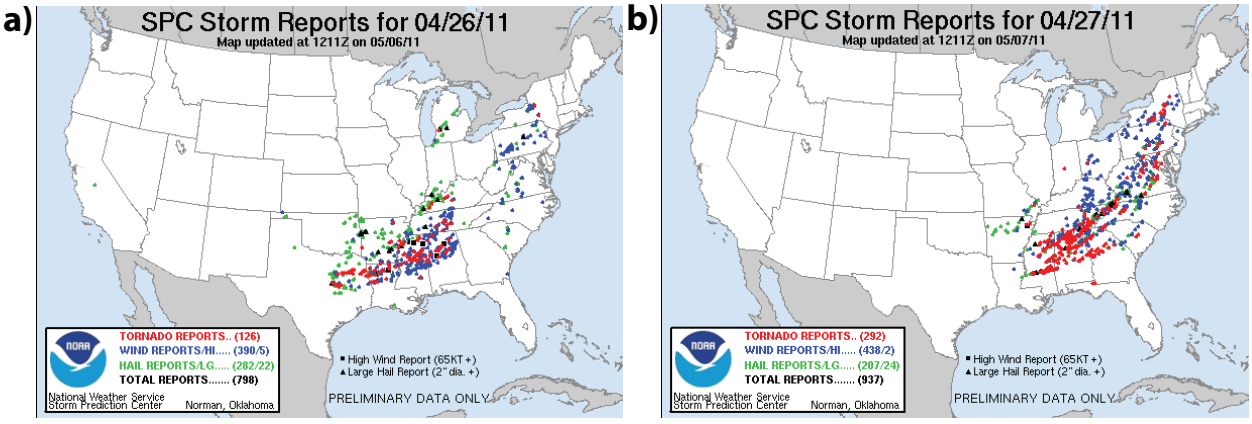

Figure 6.27: Storm Prediction Center (SPC) storm reports for (a) 26 April 2011 and (b) 27 April 2011.

translated into different precipitation predictions over the Mississippi Valley for multiple days. The dry ensemble members forecasted for a shallower upper-level trough, with an associated occluded low pressure system not extending deep into the southern plains. With the cyclone not digging into the deep southern plains, the supply of moisture from the Gulf of Mexico was suppressed, also pulling in drier air from the southern plains. The dry ensemble members also forecasted for the Bermuda High to be farther off the eastern coast of the United States, pulling very little additional moisture into the southeastern United States. Additionally, two of the dry ensemble members forecasted for the system to push through the Mississippi Valley too quickly. Ensemble member 21 (a dry ensemble member) had sufficient moisture to support heavy precipitation however, the upper-level trough was forecasted to move to the east much too quickly. This prevented heavy rainfall from occurring across the Mississippi Valley, causing ensemble member 21 to be one of the driest of the 50 ensemble members. The wet ensemble members forecasted the upper-level trough to push down into central Texas with the occluded low pressure center digging deep into the southern plains. The cyclonic rotation associated with this occluded low caused robust southerly flow from the Gulf of Mexico, supplying moisture to the Mississippi Valley. Additionally, the wet ensemble members forecasted for the Bermuda High to be positioned more to the west, helping to draw additional moisture into the southeastern United States. With sufficient moisture and a frontal boundary to provide lift, heavy precipitation and severe weather affected the eastern United States. For this precipitation event, the strength of the upper-level trough and associated occluded low pressure center was the determining factor in the ensemble members' forecasts.

CHAPTER 7

COMPARISON BETWEEN CASE STUDIES 29 APRIL-4 MAY 2010 and 23-28 APRIL 2011

7.1 Standard deviation of area-averaged precipitation

In an effort to compare the two events, the forecast skill of both the 29 April-4 May 2010 and the 23-28 April 2011 widespread precipitation events are intercompared. The first means of comparison is to calculate the standard deviation of the area-averaged precipitation. After taking the standard deviation of the area-averaged precipitation for both the 29 April-4 May 2010 and 23-28 April 2011 widespread rain events, it becomes clear that the 23-28 April 2011 widespread rain event was forecasted with more certainty. The 23-28 April 2011 widespread rain event had a standard deviation of 7.83, while the 29 April-4 May 2010 widespread rain event had a standard deviation of 12.19.

7.2 Ensemble equitable threat score and ROC area

The ensemble ETS at different initialization times is then calculated, as well as at multiple rainfall thresholds. Table 7.1 summarizes the different model runs, lead times, and initialization times for the two widespread rain events of interest. Looking at the ensemble ETS results in Table 7.2, with an initialization time of 1200 UTC 29 April 2010, the 29 April-4 May 2010 widespread precipitation event was better forecasted at a threshold of 100 and 150 mm. However, with an initialization time of 1200 UTC 23 April 2011, the 23-28 April 2011 event was better predicted at a threshold of 50 mm. At the other initialization times shown in Table 7.2, it appears the heavy precipitation from the 29 April-4 May 2010 event was better forecasted, specifically at the longer lead times. This may be due to the presence of an “atmospheric river,” giving the ensemble confidence that this event would bring extreme rainfall totals.

Table 7.1: Listing of the different initialization times, lead times, and model runs for the 29 April-4 May 2010 and 23-28 April 2011 widespread rain events.

		29 April-4 May 2010	23-28 April 2011
Run	Lead time (hrs)	Initialization time	Initialization time
11	0-120	1200 UTC 29 April 2010	1200 UTC 23 April 2011
10	12-132	0000 UTC 29 April 2010	0000 UTC 23 April 2011
9	24-144	1200 UTC 28 April 2010	1200 UTC 22 April 2011
8	36-156	0000 UTC 28 April 2010	0000 UTC 22 April 2011
7	48-168	1200 UTC 27 April 2010	1200 UTC 21 April 2011
6	60-180	0000 UTC 27 April 2010	0000 UTC 21 April 2011
5	72-192	1200 UTC 26 April 2010	1200 UTC 20 April 2011
4	84-204	0000 UTC 26 April 2010	0000 UTC 20 April 2011
3	96-216	1200 UTC 25 April 2010	1200 UTC 19 April 2011
2	108-228	0000 UTC 25 April 2010	0000 UTC 19 April 2011
1	120-240	1200 UTC 24 April 2010	1200 UTC 18 April 2011
0	132-252	0000 UTC 24 April 2010	0000 UTC 18 April 2011

Table 7.2: Listing of the ensemble ETS for the 29 April-4 May 2010 and 23-28 April 2011 widespread rain events, at thresholds of 50, 100, and 150 mm, as well as the number of points within the area-averaged box exceeding the given threshold.

		29 April-4 May 2010	23-28 April 2011
	Threshold	Ensemble ETS	Ensemble ETS
Run 11	50 mm	0.198	0.204
	100 mm	0.176	0.130
	150 mm	0.109	0.101
Run 10	50 mm	0.200	0.165
	100 mm	0.094	0.113
	150 mm	0.067	0.084
Run 9	50 mm	0.153	0.109
	100 mm	0.084	0.050
	150 mm	0.039	0.035
Run 8	50 mm	0.100	0.028
	100 mm	0.058	-0.016
	150 mm	0.028	0.001

	29 April-4 May 2010	23-28 April 2011
Threshold	Points exceeding threshold	Points exceeding threshold
50 mm	174	253
100 mm	76	169
150 mm	37	93
200 mm	16	35
250 mm	10	14
300 mm	2	2

Now looking at the ROC area for the two widespread precipitation events, one can assess the forecast skill at each lead time prior to the onset of each event. One noteworthy comment is the exceptional ROC area for the 29 April- 4 May 2010 widespread precipitation event at a threshold of 150 mm. 252 hours prior to the event, the ROC area was 0.911005, steadily improving to 0.993241 at the shortest lead time (Table 7.3). This is an extremely good forecast 5 days prior to the actual occurrence. The 150 mm ROC area for the 23-28 April 2011 widespread rain event was not nearly as good, indicating that heavier precipitation for this event was not nearly as well forecasted. This finding is consistent with the results from calculating the ensemble ETS. At a threshold of 50 and 100 mm, the ROC area for both the widespread rain events was about the same (Table 7.3).

Table 7.3: Listing of the area under the relative operating characteristic (ROC) curve "ROC area" for the 29 April- 4 May 2010 and 23-28 April 2011 widespread rain events, at thresholds of 50, 100, and 150 mm.

	29 April-4 May 2010			23-28 April 2011		
ROC area threshold	50 mm	100 mm	150 mm	50 mm	100 mm	150 mm
0-120 hrs	0.935347	0.922842	0.993241	0.928556	0.959187	0.867572
12-132 hrs	0.922365	0.912244	0.984434	0.935789	0.968793	0.903919
24-144 hrs	0.926364	0.919769	0.969450	0.923400	0.931114	0.809482
36-156 hrs	0.910965	0.917694	0.966019	0.919106	0.856841	0.734343
48-168 hrs	0.910608	0.908739	0.966264	0.914594	0.848474	0.714573
60-180 hrs	0.912639	0.884457	0.935847	0.922466	0.922585	0.784894
72-192 hrs	0.882648	0.903813	0.980683	0.914965	0.925238	0.867273
84-204 hrs	0.882284	0.915714	0.978598	0.879394	0.889733	0.795670
96-216 hrs	0.851098	0.885551	0.849258	0.841796	0.816109	0.714270
108-228 hrs	0.883517	0.889395	0.811488	0.842617	0.864486	0.731406
120-240 hrs	0.848834	0.858629	0.886346	0.806594	0.776965	0.697741
132-252 hrs	0.868016	0.947877	0.911005	0.827369	0.912204	0.825028

7.3 500-hPa "spaghetti" plot and standard deviation

Digging further into the 29 April-4 May 2010 event, the 500-hPa height spaghetti plot will be examined at 0000 UTC 3 May 2010, corresponding to forecast hour 84, and at 1200 UTC

3 May 2010, corresponding to forecast hour 96. Looking now at the spaghetti plot of 500-hPa heights for 0000 UTC 3 May 2010, there does not appear to be much agreement between ensemble members (Fig. 7.1a). In an effort to better visualize the spread between the ensemble members, standard deviation will be analyzed. Looking at the standard deviation for 0000 UTC 3 May 2010, the most spread appears to be related to the strength of the ridge along the western coast of the United States. Additionally, there appears to be a lot of uncertainty in the strength of the upper-level trough digging into the central United States (Fig. 7.1b). Twelve hours later, at 1200 UTC 3 May 2010, uncertainty in the forecast for 500-hPa heights has increased. The spaghetti plot indicates little agreement between the ensemble members (Fig. 7.2a). As before, on the standard deviation plots, the most spread lies in the northwestern United States due to the strength of the upper-level ridge. A second peak in spread exists near the base of the trough plunging into the central United States (Fig. 7.2b). Now looking at the 23-28 April 2011 event, the 500-hPa height spaghetti plot will be examined at 0000 UTC 27 April 2011, corresponding to forecast hour 84, and at 1200 UTC 27 April 2011, corresponding to forecast hour 96. Starting with the spaghetti plot of 500-hPa heights for 0000 UTC 27 April 2011, there appears to be more agreement among the ensemble members (Fig. 7.3a). As for the standard deviation plot, the spread is noticeably less for the 23-28 April 2011 event than for the 29 April-4 May 2010 event. The most spread lies at the base of the 500-hPa trough digging into the south central United States (Fig. 7.3b). Twelve hours later, at 1200 UTC 27 April 2011, the agreement between ensemble members has decreased slightly, as expected with time (Fig. 7.4a). The highest spread among ensemble members now lies at the base of the upper-level trough, the placement of the occluded low in the Upper-Midwest, and the strength of the upper-level ridge off the western coast of the United States (Fig. 7.4b). Overall, it appears the widespread precipitation event of

23-28 April 2011 was better predicted, with more agreement among the ensemble members. In order to put there results into a qualitative perspective, the area-average of standard deviation of 500-hPa heights was taken. The area-averaged box had dimensions 20 N to 55 N and 60 W to 130 W. As one would expect, the area-averaged 500-hPa standard deviation increased for both of the widespread rain events from the 84-hr to the 96-hr forecast. However, the area-averaged standard deviation of 500-hPa heights is much larger for the 29 April-4 May 2010 widespread rain event, indicating this event was forecasted with far more uncertainty in comparison to the 23-28 April 2011 event (Table 7.4).

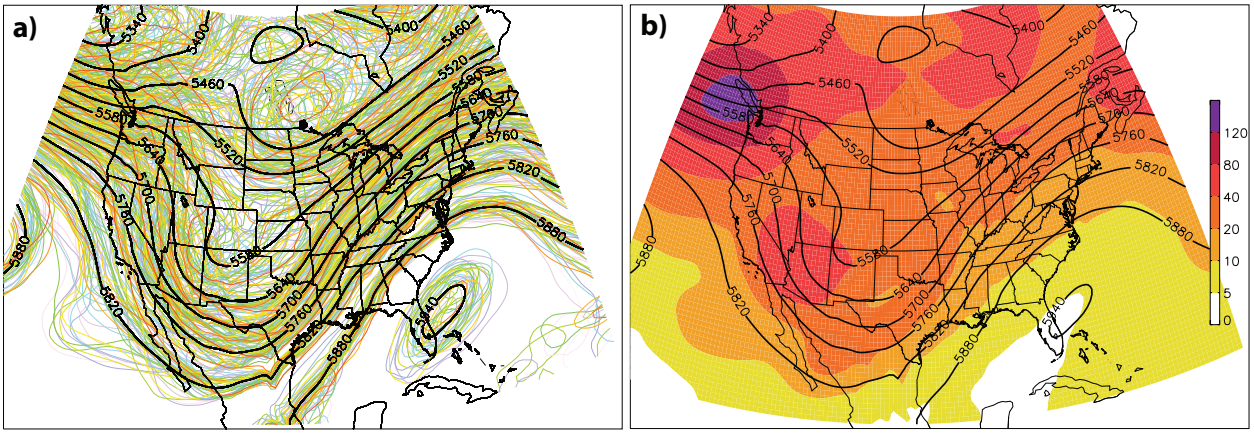

Figure 7.1: (a) "Spaghetti" plot showing the predicted 500-hPa height contours from each ensemble member in a different color and (b) standard deviation in 500-hPa heights at 0000 UTC 3 May 2010, corresponding to forecast hour 84 of the 29 April-4 May 2010 widespread rain event. The ensemble mean 500-hPa height contours are shown in thick black. Initialization time of 1200 UTC 29 April 2010.

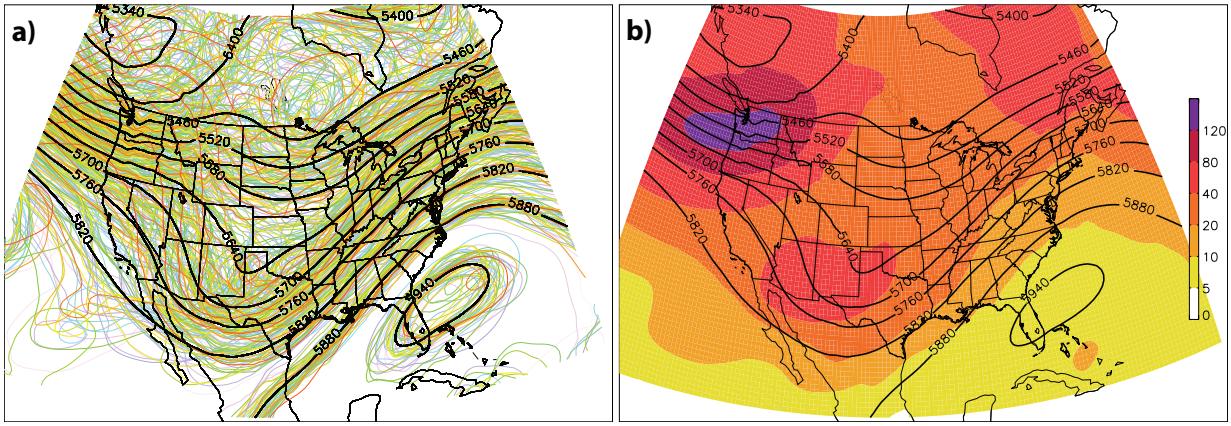

Figure 7.2: As in Fig. 7.1, except for at 1200 UTC 3 May 2010, corresponding to forecast hour 96 of the 29 April-4 May 2010 widespread rain event.

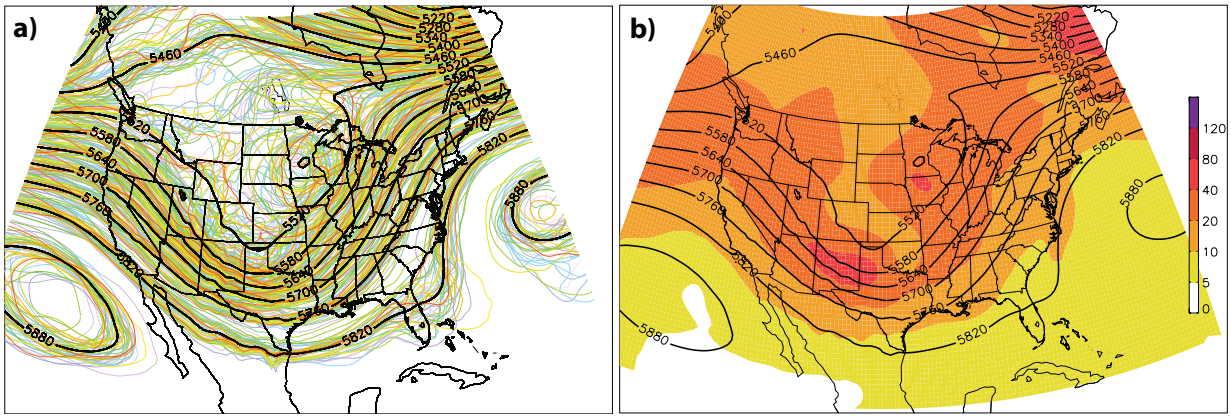

Figure 7.3: As in Fig. 7.1, except for at 0000 UTC 27 April 2011, corresponding to forecast hour 84 of the 23-28 April 2011 widespread rain event. Initialization time of 1200 UTC 23 April 2011.

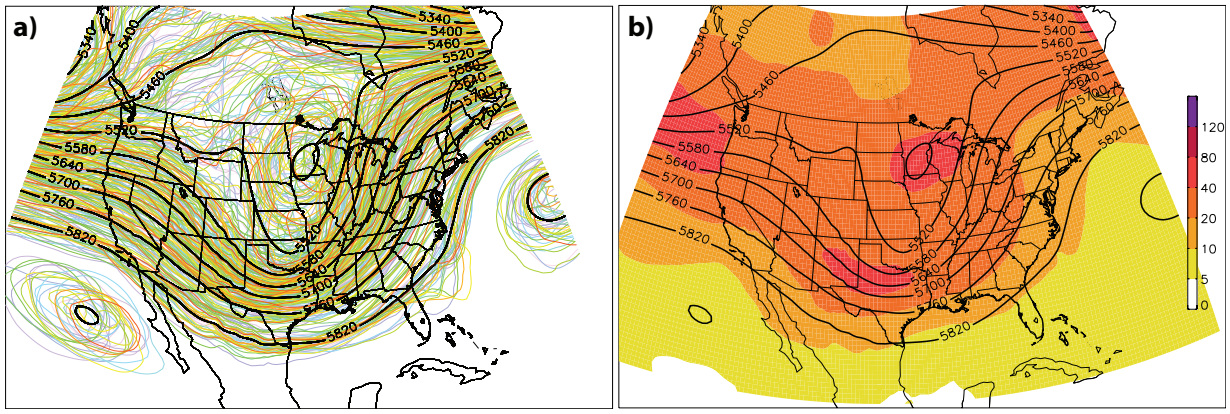

Figure 7.4: As in Fig. 7.3, except for at 1200 UTC 27 April 2011, corresponding to forecast hour 96 of the 23-28 April 2011 widespread rain event.

Table 7.4: Table of the 84-hr and 96-hr area-averaged standard deviation of 500-hPa heights for the 29 April- 4 May 2010 and 23-28 April 2011 widespread rain events. The area-averaged box has dimensions 20 N to 55 N and 60 W to 130 W.

	29 April-4 May 2010	23-28 April 2011
84-hr	25.9311	16.1366
96-hr	31.1477	19.5186

7.4 Forecast error

Assessing the 500-hPa forecast error will allow one to gain insight into what regions of the United States were the most and least well forecasted by the ECMWF ensemble members. Beginning with the 29 April-4 May 2010 widespread rain event, many of the same regions of error exist at both 0000 UTC 3 May 2010 and 1200 UTC 3 May 2010. There is a large area of positive error in the upper Midwest and Mississippi Valley, indicating that many of the ensemble members over predicted heights in these regions, not forecasting for the 500-hPa trough to be deep enough through the central United States. Additionally, there is negative error along the northeast Canadian coast, as well as, along the northwest coast of the United States (Fig. 7.5a,b). Many of the ensemble members must have underpredicted the 500-hPa heights in these regions, not building a strong enough upper-level ridge on either side of the upper-level trough. Now looking at the 23-28 April 2011 widespread rain event, again, many of the same errors exist between 0000 UTC 27 April 2011 and 1200 UTC 27 April 2011. One error that stands out is the slight positive forecast error along the trough in the central United States (Fig. 7.6a,b). Again, this positive error is indicative that many of the ensemble members over predicted 500-hPa heights, not forecasting the upper-level trough to be deep enough into the central United States. Although forecast error is seen for both of the widespread rain events, it is very apparent the 29 April-4 May 2010 widespread rain event had far more forecast error and therefore was forecasted with a lot less certainty.

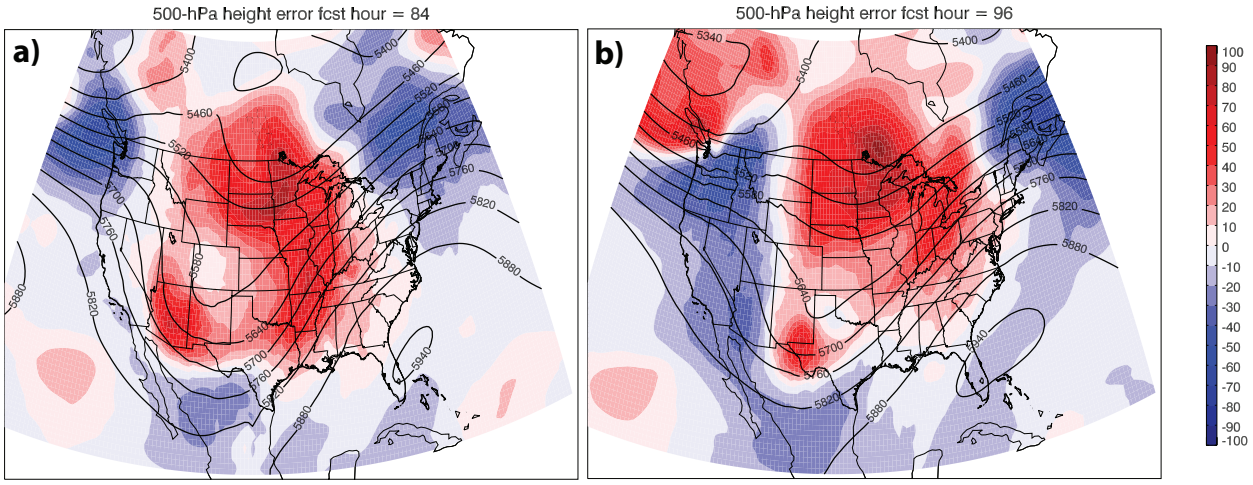

Figure 7.5: 500-hPa height forecast error (ensemble mean – analysis) at (a) 0000 UTC 3 May 2010, corresponding to forecast hour 84 and (b) 1200 UTC 3 May 2010, corresponding to forecast hour 96 of the 29 April-4 May 2010 widespread rain event. The ensemble mean 500-hPa height contours are shown in thick black. Initialization time of 1200 UTC 29 April 2010.

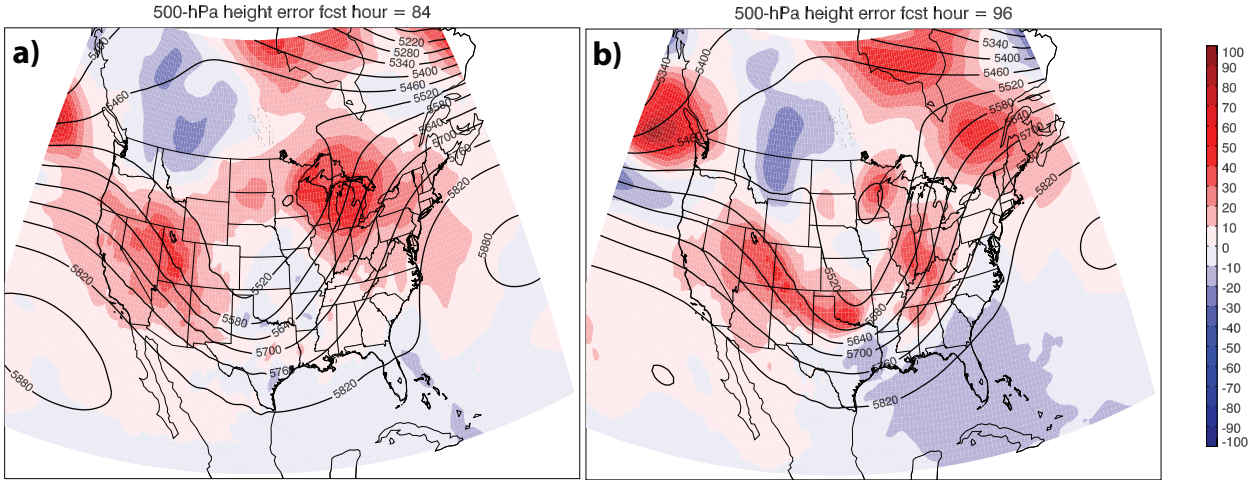

Figure 7.6: As in Fig. 7.5, except for at (a) 0000 UTC 27 April 2011, corresponding to forecast hour 84 and (b) 1200 UTC 27 April 2011, corresponding to forecast hour 96 of the 23-28 April 2011 widespread rain event. Initialization time of 1200 UTC 23 April 2011.

7.5 Raw ensemble probabilities

The following plots display the raw ensemble probabilities, at increasing lead times, for a specified threshold of precipitation. Beginning with the 29 April-4 May 2010 event at a threshold of 50 mm, for the longest lead time shown there was over 50% agreement among the ensemble

members that Nashville, TN and nearby areas would receive 50 mm of precipitation. As the event approached, the ensemble member began to agree more on the location of precipitation, with over 90% agreement among the ensemble members (Fig. 7.7a). At higher rainfall thresholds of 100 and 150 mm, for the longest lead time shown, there was very little indication that this event would be one capable of producing over 480 mm of precipitation. With time, the ensemble members began to agree more on the location of these high rainfall amounts. Over 50% of the ensemble members agreed on the location that would receive at least 100 mm of precipitation (Fig. 7.7b). Additionally, at a threshold of 150 mm, at the shortest lead time shown the ROC area was 0.993241, indicating an exceptional forecast (Fig. 7.7c). Now looking at the 23-28 April 2011 event at a threshold of 50 mm, for the longest lead time shown there was over 70% agreement among the ensemble members when forecasting for the location of 50 mm of precipitation. As the event approached, the ensemble member began to agree more on the location of precipitation, with over 90% agreement among the ensemble members (Fig. 7.8a). Over 70% of the ensemble members agreed on the location that would receive at least 100 mm of precipitation (Fig. 7.8b). At a threshold of 150 mm, at the shortest lead time shown the ROC area was 0.867572, however, at the second longest lead time shown the ROC area was 0.697741 (Fig. 7.8c). The 150 mm threshold was much better predicted for the 29 April-4 May 2010 event.

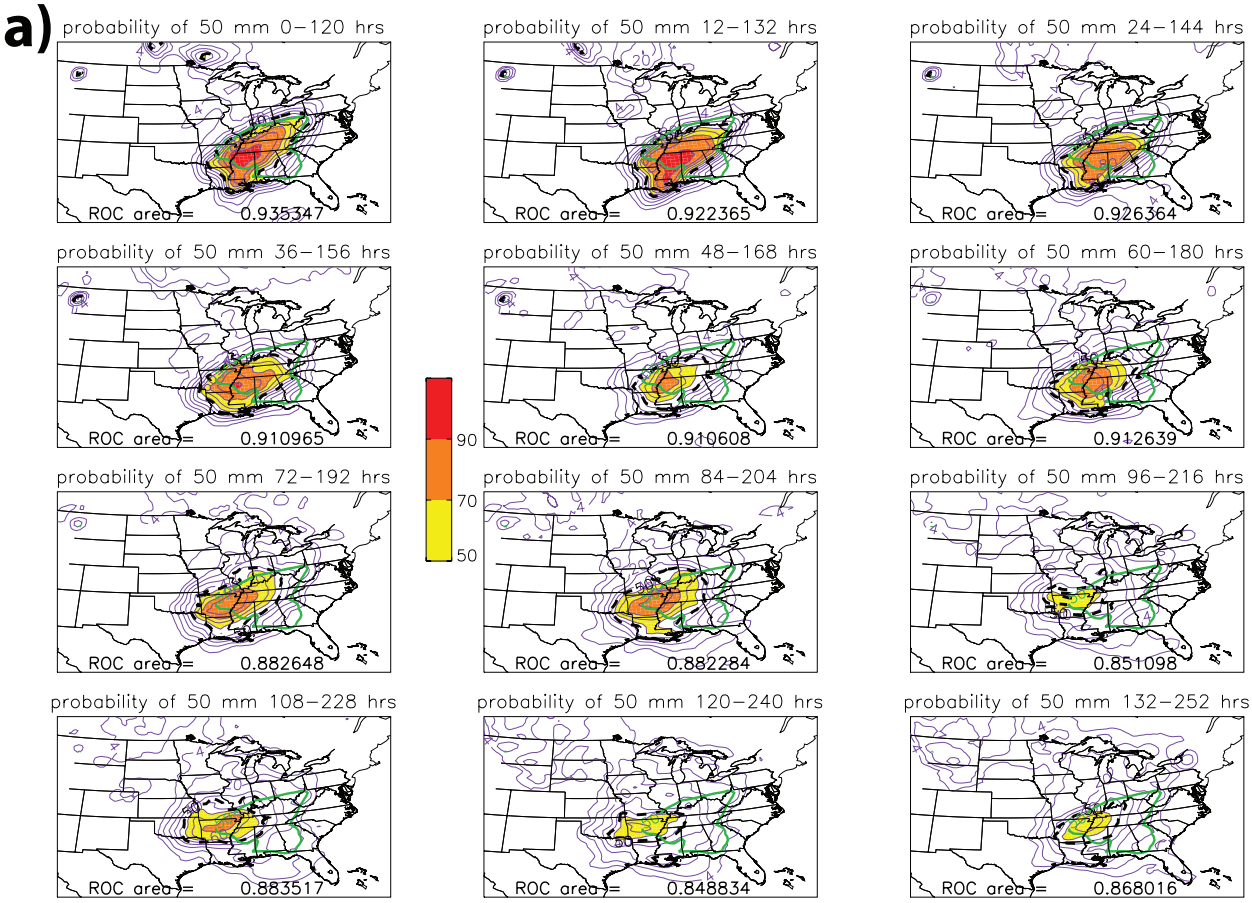
a)
probability of 50 mm 0–120 hrs
ROC area = 0.935347
probability of 50 mm 12–132 hrs
ROC area = 0.922365
probability of 50 mm 24–144 hrs
ROC area = 0.926364
probability of 50 mm 36–156 hrs
ROC area = 0.910965
probability of 50 mm 48–168 hrs
ROC area = 0.910608
probability of 50 mm 60–180 hrs
ROC area = 0.912639
90
70
50
probability of 50 mm 72–192 hrs
ROC area = 0.882648
probability of 50 mm 84–204 hrs
ROC area = 0.882284
probability of 50 mm 96–216 hrs
ROC area = 0.851098
probability of 50 mm 108–228 hrs
ROC area = 0.883517
probability of 50 mm 120–240 hrs
ROC area = 0.848834
probability of 50 mm 132–252 hrs
ROC area = 0.868016

b)

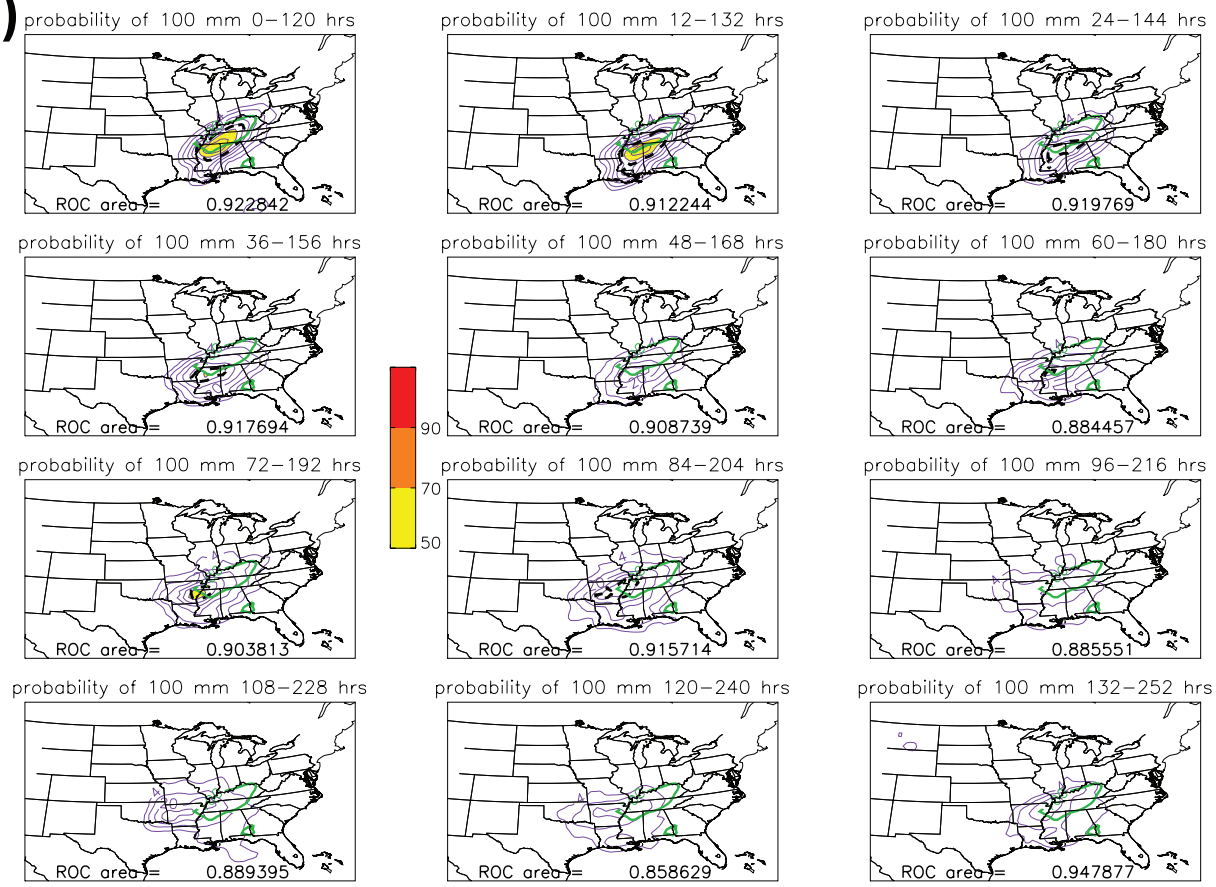
probability of 100 mm 0–120 hrs
ROC area = 0.922842
probability of 100 mm 12–132 hrs
ROC area = 0.912244
probability of 100 mm 24–144 hrs
ROC area = 0.919769
probability of 100 mm 36–156 hrs
ROC area = 0.917694
probability of 100 mm 48–168 hrs
ROC area = 0.908739
probability of 100 mm 60–180 hrs
ROC area = 0.884457
90
70
50
probability of 100 mm 72–192 hrs
ROC area = 0.903813
probability of 100 mm 84–204 hrs
ROC area = 0.915714
probability of 100 mm 96–216 hrs
ROC area = 0.885551
probability of 100 mm 108–228 hrs
ROC area = 0.889395
probability of 100 mm 120–240 hrs
ROC area = 0.858629
probability of 100 mm 132–252 hrs
ROC area = 0.947877

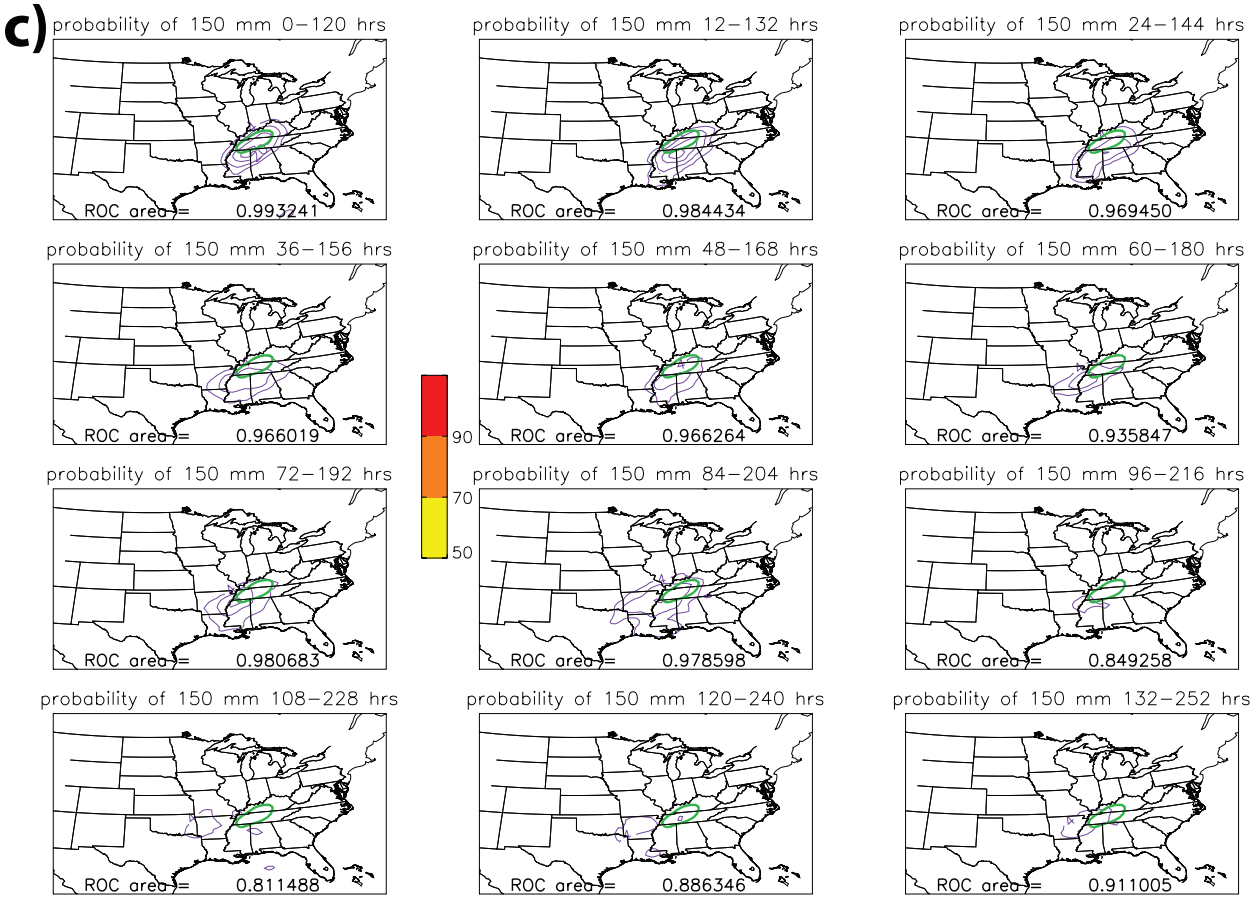

Figure 7.7: Raw ensemble probabilities, at increasing lead times, of (a) 50, (b) 100, and (c) 150 mm of precipitation in the 252-hr period between 1200 UTC 29 April and 1200 UTC 4 May 2010. Probabilities are contoured at 4% (i.e., two ensemble members), 10%, and every 10% above that. The ensemble mean is shown by the thick black dashed line. Areas where (a) 50, (b) 100, and (c) 150 mm of precipitation was observed are contoured in thick green. Red shading indicates at least 90% of the ensemble members were in agreement when forecasting the location of (a) 50, (b) 100, and (c) 150 mm of precipitation, orange shading indicates at least 70% of the ensemble members were in agreement, etc. Area under the relative operating characteristic (ROC) curve is printed on each figure as "ROC area".

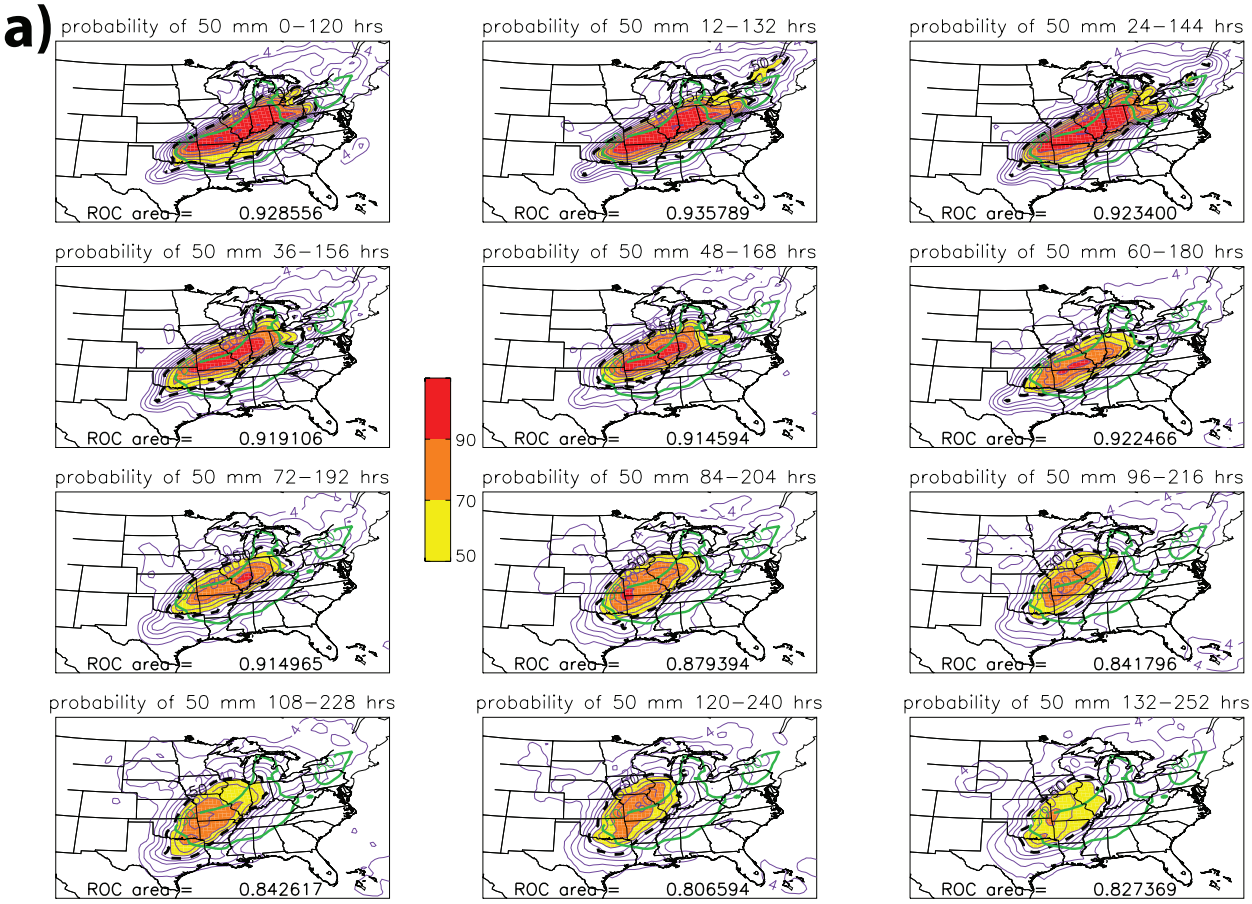
a)
probability of 50 mm 0–120 hrs
ROC area = 0.928556
probability of 50 mm 12–132 hrs
ROC area = 0.935789
probability of 50 mm 24–144 hrs
ROC area = 0.923400
probability of 50 mm 36–156 hrs
ROC area = 0.919106
probability of 50 mm 48–168 hrs
ROC area = 0.914594
probability of 50 mm 60–180 hrs
ROC area = 0.922466
probability of 50 mm 72–192 hrs
ROC area = 0.914965
probability of 50 mm 84–204 hrs
ROC area = 0.879394
probability of 50 mm 96–216 hrs
ROC area = 0.841796
probability of 50 mm 108–228 hrs
ROC area = 0.842617
probability of 50 mm 120–240 hrs
ROC area = 0.806594
probability of 50 mm 132–252 hrs
ROC area = 0.827369
90
70
50

b)

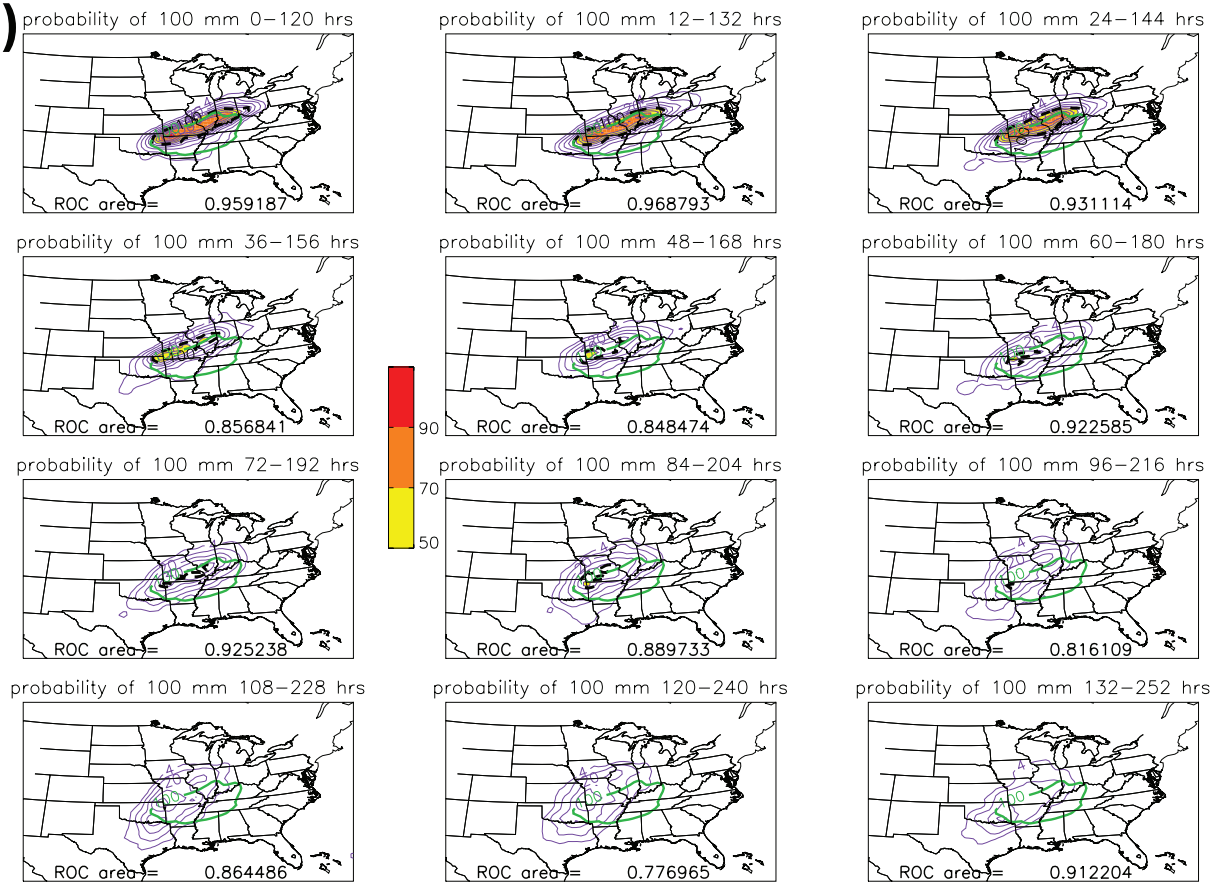
probability of 100 mm 0–120 hrs
ROC area = 0.959187
probability of 100 mm 12–132 hrs
ROC area = 0.968793
probability of 100 mm 24–144 hrs
ROC area = 0.931114
probability of 100 mm 36–156 hrs
ROC area = 0.856841
probability of 100 mm 48–168 hrs
ROC area = 0.848474
probability of 100 mm 60–180 hrs
ROC area = 0.922585
probability of 100 mm 72–192 hrs
ROC area = 0.925238
probability of 100 mm 84–204 hrs
ROC area = 0.889733
probability of 100 mm 96–216 hrs
ROC area = 0.816109
probability of 100 mm 108–228 hrs
ROC area = 0.864486
probability of 100 mm 120–240 hrs
ROC area = 0.776965
probability of 100 mm 132–252 hrs
ROC area = 0.912204
90
70
50

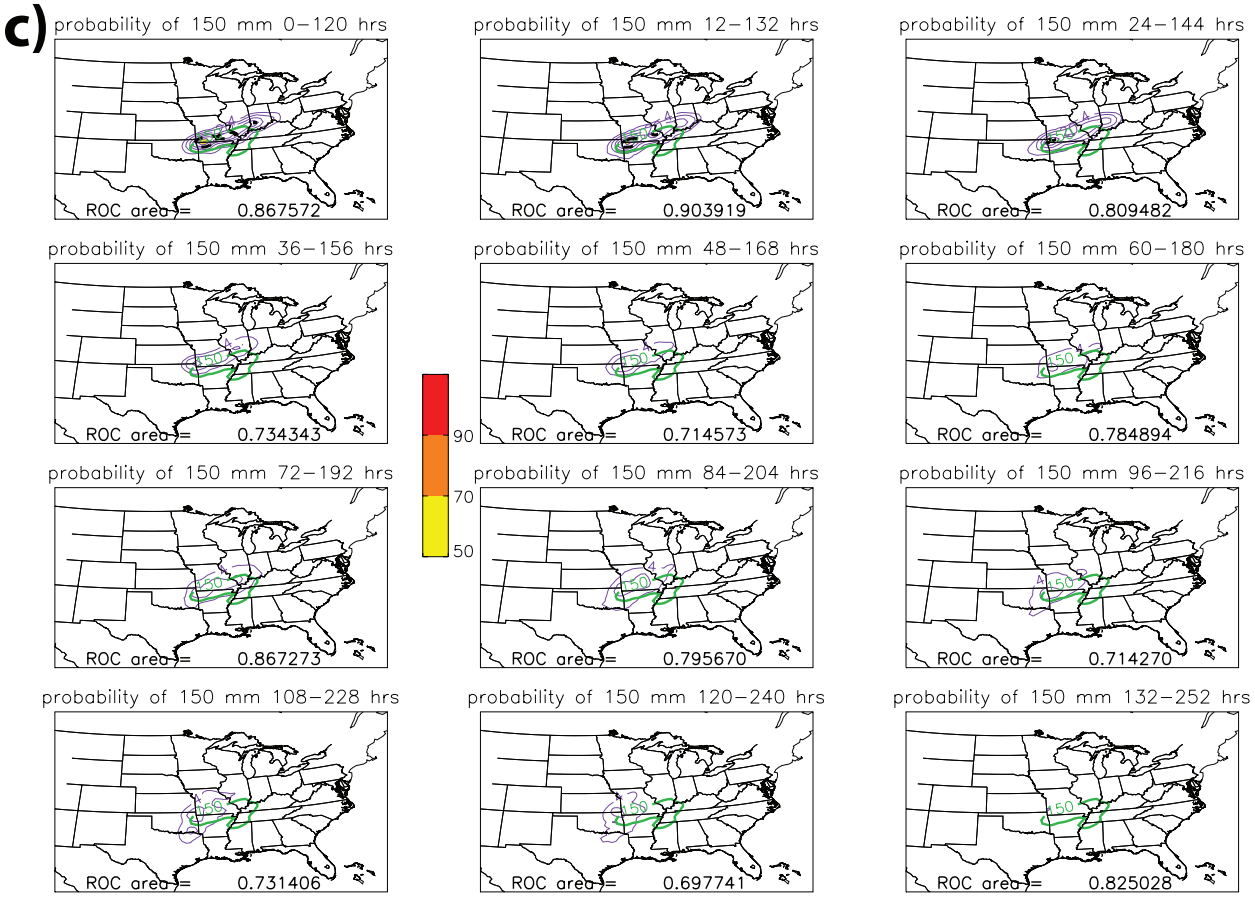

Figure 7.8: As in Fig. 7.5, except for in the 252-hr period between 1200 UTC 23 April and 1200 UTC 28 April 2011.

7.6 Discussion

In this chapter, the forecast skill of both the 29 April-4 May 2010 and 23-28 April 2011 widespread precipitation events was compared. From calculating the ensemble ETS at different lead times and thresholds, it appears the heavy precipitation from the 29 April-4 May 2010 event was better forecasted, specifically at the longer lead times. (Table 7.1). The ROC area was also a useful tool to assess the forecast skill for the two widespread rain events. At a threshold of 50 and 100 mm, the ROC area for both the widespread rain events was about the same, however, at a threshold of 150 mm, the ROC area was much better for the 29 April-4 May 2010 event. This indicates that heavier precipitation amounts for the 23-28 April 2011 widespread rain event were

not well forecasted. (Table 7.2). Looking at the 500-hPa height spaghetti plots at 0000 UTC 3 May 2010 and 1200 UTC 3 May 2010, there was very little agreement between ensemble members (Figs. 7.1a and 7.2a). The standard deviation in 500-hPa height at 0000 UTC 3 May 2010 and 1200 UTC 3 May 2010 indicated the most spread was related to the strength of the ridge along the western coast of the United States and the strength of the upper-level trough digging into the central United States (Figs. 7.1b and 7.2b). The spaghetti plots of 500-hPa heights for 0000 UTC 27 April 2011 and 1200 UTC 27 April 2011 show much more agreement among the ensemble members (Fig. 7.3a and 7.4a). As for the standard deviation plots of 500-hPa height at 0000 UTC 27 April 2011 and 1200 UTC 27 April 2011, the most uncertainty lies at the base of the 500-hPa trough digging into the south central United States and the placement of the occluded low in the Upper-Midwest (Figs. 7.3b and 7.4b). Overall, the upper-level synoptic pattern was predicted with more agreement among ensemble members for the 23-28 April 2011 widespread precipitation event. Taking a look at 500-hPa forecast error, it is very apparent the 29 April-4 May 2010 widespread rain event had far more forecast error than the 23-28 April 2011 event and therefore was forecasted with more uncertainty (Figs. 7.5 and 7.6). Finally, looking at the raw ensemble probabilities, it appears the location of the 23-28 April 2011 event was better anticipated than the 29 April-4 May 2010 event, but proved to have more difficulty forecasting the location of higher rainfall thresholds, 100 and 150 mm (Figs. 7.7. and 7.8). This finding is consistent with the results from calculating the ensemble ETS above (Table 7.1).

CHAPTER 8

CONCLUSIONS AND FUTURE WORK

8.1 Conclusions

This study made use of the ECMWF, NCEP, and UKMET EPS in order to assess their forecast skill of 22 widespread, precipitation events from 2007 to 2011. Overall, the ECMWF had a more skillful forecast for almost every event, which doesn't come as a surprise because the ECMWF has maintained a higher horizontal resolution than both the NCEP and the UKMET (Table 3.1). This will allow forecasters to put more confidence into the ECMWF ensemble prediction system for widespread rain events of similar spatial scale. The one widespread precipitation event that proved to be a challenge for each of the three models was the MCV over the southern plains of the United States from 25-30 June 2007 (Fig. 4.2a). The 29 April-4 May 2010 and 23-28 April 2011 events were then examined in greater detail in order to pinpoint the processes that were favorable or detrimental to the system's development.

The 29 April-4 May 2010 case study used ECMWF ensemble forecasts to explore the processes responsible for the development and maintenance of a multiday precipitation event that occurred in early May 2010, due to two successive quasi-stationary mesoscale convective systems (Moore et al. 2012). This precipitation event proved to have uncertainty in medium range predictions, relative to other events of similar spatial and temporal scales, with low skill and large spread in ensemble forecasts. The accuracy of each forecast is dependent on each of the atmospheric variables the member used in order to make its forecast. For this particular case, one would think that a strong low pressure system and deep upper-level trough would bring about heavier precipitation and severe weather. However, the reverse was true for the 29 April-4

May 2010 widespread, precipitation event. The strong low pressure system caused much stronger winds out of the south, pushing the moisture up into the Great Lakes. The members forecasting for the weak low pressure system and shallow trough proved to be accurate. The weak low pressure system caused much weaker southerly flow, pulling moisture from the Gulf of Mexico as far north as Tennessee, where it rained out. These relatively small differences in the height field ultimately resulted in vastly different forecasts of precipitation over Tennessee and surrounding areas. This strong sensitivity to small-scale differences in the initial conditions highlights the importance of using ensembles for predicting the development of precipitation systems over both land and ocean, especially for an event such as the 29 April-4 May 2010 precipitation event, which received national attention for having produced extensive flooding, multiple tornadoes, hail and wind reports across the area.

The 23-28 April 2011 case study also used ECMWF ensemble forecasts to explore the processes responsible for the development and maintenance of a multiday precipitation event. In relation to other heavy rain events of similar spatial and temporal scales, medium-range forecasts of this event had high skill and small spread in ensemble forecasts. In this case, the largest difference in the ensemble members' forecasts was the strength of the upper-level trough and associated occluded low, as well as the speed at which this system moved off to the east. These relatively small differences in the height field ultimately resulted in different forecasts of precipitation over the Mississippi Valley. This sensitivity to small-scale differences in the initial conditions highlights the importance of using ensembles for predicting the development of precipitation systems over both land and ocean. This is especially true for a weather event such as the 23-28 April 2011 episode, which received national attention for having killed over 300 people, and spawned the fourth deadliest tornado outbreak in United States history.

Undoubtedly, anticipating and communicating this event to the public by the broader weather community reduced the loss of life, however, more improvements to the accuracy of these forecasts can be made (Grumm 2011a). If one can better understand the key factors that were favorable for, or detrimental to, the development of widespread, multiple day rainfall, such as the 29 April-4 May 2010 and 23-28 April 2011 events, a better forecast could be made for future events of similar spatial scale.

Comparison between the 29 April-4 May 2010 and 23-28 April 2011 widespread precipitation events provided information regarding which of the two case studies was better predicted in relation to both location and amount of precipitation. Heavy rainfall totals, exceeding the 100 and 150 mm threshold, were better anticipated for the 29 April-4 May 2010 event. This may be a result of the pronounced "atmospheric river" playing a large role in the moisture transport for this event. Location of the precipitation, however, was better predicted for the 23-28 April 2011 widespread rain event. There was very little uncertainty in the synoptic setup of the upper atmosphere for this particular event, likely contributing to the correct placement of the precipitation event.

8.2 Suggestions for future work

One avenue for future work would be to investigate why the wet ensemble members overpredicted the amount of time-integrated moisture flux yet underpredicted the total amount of precipitation for the 23-28 April 2011 widespread, multiday precipitation event. The representation of mesoscale processes in global models at coarse resolution may play an important role in the underprediction of precipitation.

Combining additional ensemble forecasts from different systems into a grand ensemble (the so-called superensemble) is another avenue for future work made possible by the availability

of TIGGE data. Numerous studies have found a multimodel superensemble increases forecast skill in a variety of ways: typhoon tracks and intensity, daily precipitation, rain rates, etc. (Krishnamurti et al. 2001, 2003, Kumar et al. 2003, 2007, Mishra and Krishnamurti 2007). Krishnamurti et al. (2001) suggests that the superensemble generally exhibits a much higher skill compared to the ensemble mean and the participating member models for many forecast variables, including daily precipitation. The use of a grand ensemble could potentially increase the hit rate for prediction of high-impact weather without increasing the false-alarm rate (Bougeault et al. 2010).

REFERENCES

Accadia, C., S. Mariani, M. Casaioli, A. Lavagnini, and A. Speranza, 2003: Sensitivity of precipitation forecast skill scores to bilinear interpolation and a simple nearest-neighbor average method on high-resolution verification grids. *Wea. Forecasting,* **18,** 918-932.

Bartels, D. L., and R. A. Maddox, 1991: Midlevel cyclonic vortices generated by mesoscale convective systems. *Mon. Wea. Rev.,* **119,** 104–118.

Bayler, G. M., R. M. Aune, and W. H. Raymond, 2000: NWP cloud initialization using GOES sounder data and improved modeling of nonprecipitating clouds. *Mon. Wea. Rev.,* **128,** 3911-3920.

Bell, G. D., and J. E. Janowiak, 1995: Atmospheric circulation associated with the Midwest floods of 1993. *Bull. Amer. Meteor. Soc.,* **76,** 681-695.

Benton, G. S., and M. A. Estoque, 1954: Water-vapor transfer over the North American continent. *J. Meteor.*, **11,** 462-477.

Bluestein, H. B., and M. H. Jain, 1985: Formation of mesoscale lines of precipitation: Severe squall lines in Oklahoma during the spring. J. Atmos. Sci., **42,** 1711-1732.

Bodner, M. J., N. W. Junker, R. H. Grumm, and R. S. Schumacher, 2011: Comparison of atmospheric circulation patterns during the 2008 and 1993 historic Midwest floods. *Nat. Wea. Digest,* **35,** 103-119.

Bond, N. A., and G. A. Vecchi, 2003: The influence of the Madden-Julian oscillation on precipitation in Oregon and Washington. *Wea. Forecasting,* **18,** 600-613.

Bosart, L. F., and F. Sanders, 1981: The Johnstown flood of July 1977: A long-lived convective system. *J. Atmos. Sci.,* **38,** 1616-1642.

Böttger, Horst, François Lalaurette, and Dominique Marbouty, cited 2011: ECMWF forecasting

system in support of severe weather prediction in the medium range. [Available online at http://www.wmo.int/pages/prog/www/DPS/TC-DPFS-2002/Papers-Posters/Topic4-Boettger.pdf.]

Bougeault, P., and Coauthors, 2010: The THORPEX Interactive Grand Global Ensemble. *Bull. Amer. Meteor. Soc.*, **91,** 1059–1072.

Bowler, N. E., A. Arribas, S. E. Beare, K. R. Mylne, and G. J. Shutts, 2009: The local ETKF and SKEB: Upgrades to the MOGREPS short-range ensemble prediction system. *Quart. J. Roy. Meteor. Soc.*, **135,** 767-776.

Boyd, B. M., S. Roberts, 2010: What if the 1 – 4 May 2010 historic Nashville, Tennessee flood occurred east Tennessee?. [Available online at http://74.125.155.132/scholar?q=cache:Z7lPjS2HSJUJ:scholar.google.com/+nashville+tennessee+flood+april+29+2010+to+may+4+2010&hl=en&as_sdt=0,44.]

Bright, D. R., and P. A. Nutter, 2004: On the challenges of identifying the "best" ensemble member in operational forecasting. Preprints, *16th Conf. on Numerical Weather Prediction,* Seattle, WA, Amer. Meteor. Soc., J11.3.

Brooks, H. E., and C. A. Doswell, 1993: New technology and numerical weather prediction wasted opportunity? *Weather*, **48,** 173-177.

_____, M. S. Tracton, D. J. Stensrud, G. J. DiMego, and Z. Toth, 1995: Short-range ensemble forecasting (SREF): Report from a workshop. *Bull. Amer. Meteor. Soc.*, **76,** 1617-1624.

Buizza, R., and T. N. Palmer, 1995: The singular-vector structure of the atmospheric general circulation. *J. Atmos. Sci.*, **52,** 1434-1456.

_____, A. Hollingsworth, F. Lalaurette, and A. Ghelli, 1999: Probabilistic predictions of precipitation using the ECMWF ensemble prediction system. *Wea. Forecasting*, **14,** 168-

189.

_____, J.-R. Bidlot, N. Wedi, M. Fuentes, M. Hamrud, G. Holt, and F. Vitart 2007: The new ECMWF VAREPS (Variable Resolution Ensemble Prediction System). *Quart. J. Roy. Meteor. Soc.*, **133,** 681–695.

Carbin, G. and J. Guyer, 2012: Tornadoes 2011: An unprecedented year. *Weatherwise*, **65,** 12-19.

Centre for Australian Weather and Climate Research, 2010: Forecast verification: Issues, methods and FAQ. [Available online at http://www.cawcr.gov.au/projects/verification/.]

Chappell, C. F., 1986: Quasi-stationary convective events. *Mesoscale Meteorology and Forecasting*, P. S. Ray, Ed., Amer. Meteor. Soc., 289-309.

Chen, M., W. Shi, P. Xie, V. B. S. Silva, V. E. Kousky, R. W. Higgins, and J. E. Janowiak, 2008: Assessing objective techniques for guage-based analyses of global daily precipitation. *J. Geophys. Res.*, **113,** D04110, doi:10.1029/2007JD009132.

Chien, F.-C., Y.-H. Kuo, and M.-J. Yang, 2002: Precipitation forecast of MM5 in the Taiwan area during the 1998 Mei-yu season. *Wea. Forecasting*, **17,** 739-754.

Corfidi, S. F., N. W. Junker, and F. H. Glass, 1990: The Louisiana/Mississippi flash flood and severe weather outbreak of 15-16 November 1987. Preprints. *16th Conf. on Severe Local Storms*, Kananaskis Park, AB, Canada, Amer. Meteor. Soc., 627-633.

_____, 1996: Predicting the movement of mesoscale convective complexes. *Wea. Forecasting*, **11,** 41-46.

_____, 2003: Cold pools and MCS propagation: Forecasting the motion of downwind-developing MCSs. *Wea. Forecasting*, **18,** 997-1017.

Craig, G. C., C. Keil, and D. Leuenberger, 2011: Constraints on the impact of radar rainfall data

assimilation on forecasts of cumulus convection. *Quart. J. Roy. Meteor. Soc.,* **138,** 340-352.

Dettinger, M. D., 2004: Fifty-two years of "pineapple-express" storms across the west coast of North America. PIER project Rep. CEC-500-2005-004, U. S. Geological Survey, Scripps Institution of Oceanography for the California Energy Commission, PIER Energy-Related Environmental Research, 15 pp. [Available online at http://65.74.139.74/2005publications/CEC-500-2005-004/CEC-500-2005-004.PDF.]

_____, F. M. Ralph, T. Das, P. J. Neiman, and D. Cayan, 2011: Atmospheric rivers, floods and the water resources of California. *Water,* **3,** 455-478.

Dirmeyer, P. A., and J. L. Kinter III, 2009: The "Maya Express": Floods in the U.S. Midwest. *Eos, Trans. Amer. Geophys. Union*, **90,** 101-102.

_____, and _____, 2010: Floods over the U.S. Midwest: A regional water cycle perspective. *J. Hydrometeor.,* **11,** 1172-1181.

Djurić, D., and M. S. Damiani, 1980: On the formation of the low-level jet over Texas. *Mon. Wea. Rev.,* **108,** 1854-1865.

Doswell, C. A., A. R. Moller, and R. W. Przybylinski, 1990: A unified set of conceptual models for variations on the supercell theme. Preprints, *16th Conf. Severe Local Storms,* Kananaskis Park, AB, Canada, Amer. Meteor. Soc., 40-45.

_____, 1994: Flash flood-producing convective storms: Current understanding and research. *Proc. U.S.-Spain Workshop on Natural Hazards,* Barcelona, Spain, National Science Foundation, 97-107.

_____, H. E. Brooks, and R. A. Maddox, 1996: Flash flood forecasting: An ingredients-based methodology. *Wea. Forecasting*, **11,** 560-581.

_____, G. W. Carbin, and H. E. Brooks, 2012: The tornadoes of spring 2011 in the USA: An historical perspective. *Weather,* **67,** 88-94.

Du, J., S. L. Mullen, and F. Sanders, 1997: Short-range ensemble forecasting of quantitative precipitation. *Mon. Wea. Rev.,* **125,** 2427-2459.

Ebert, E. E., 2001: Ability of a poor man's ensemble to predict the probability and distribution of precipitation. *Mon. Wea. Rev.,* **129,** 2461-2480.

_____, U. Damrath, W. Wergen, and M. E. Baldwin, 2003: The WGNE assessment of short-term quantitative precipitation forecasts. *Bull. Amer. Meteor. Soc.,* **84,** 481-492.

Eckel, F. A., and M. K. Walters, 1998: Calibrated probabilistic quantitative precipitation forecasts based on the MRF ensemble. *Wea. Forecasting,* **13,** 1132-1147.

ECMWF, cited 2010: Horizontal resolution increase. [Available online at http://www.ecmwf.int/products/changes/horizontal_resolution_2009/.]

_____, cited 2012: Different perturbation techniques. [Available online at http://www.ecmwf.int/products/forecasts/guide/Different_perturbation_techniques.html.]

Epstein, E. S., 1969: Stochastic dynamic prediction. *Tellus,* **21,** 739-759.

Fleming, R. J., 1971a: On stochastic dynamic prediction. I. The energetics of uncertainty and the question of closure. *Mon. Wea. Rev.,* **99,** 851-872.

_____, 1971b: On stochastic dynamic prediction. II. Predictability and utility. *Mon. Wea. Rev.,* **99,** 927-938.

Fritsch, J. M., R. J. Kane, and C. R. Chelius, 1986: The contribution of mesoscale convective weather systems to the warm-season precipitation in the United States. *J. Appl. Meteor.,* **25,** 1333-1345.

_____, and R. E. Carbone, 2004: Improving quantitative precipitation forecasts in the warm

season: A USWRP research and development strategy. *Bull. Amer. Meteor. Soc.,* **85,** 955-965.

Froude, L. S. R., L. Bengtsson, and K. I. Hodges, 2007: The prediction of extratropical storm tracks by the ECMWF and NCEP ensemble prediction systems. *Mon. Wea. Rev.*, **135,** 2545-2567.

Galarneau, T. J. Jr., T. M. Hamill, R. M. Dole, and J. Perlwitz, 2012: A multiscale analysis of the extreme weather events over western Russia and northern Pakistan during July 2010. *Mon. Wea. Rev.,* **140,** 1639-1664.

Gallus, W. A., and M. Segal, 2001: Impact of improved initialization of mesoscale features on convective system rainfall in 10-km Eta simulations. *Wea. Forecasting,* **16,** 680-696.

_____, M. E. Baldwin, and K. L. Elmore, 2007: Evaluation of probabilistic precipitation forecasts determined from Eta and AVN Forecasted Amounts. *Wea. Forecasting,* **22,** 207-215.

Glass, F. H., D. L. Ferry, J. T. Moore, and S. M. Nolan, 1995: Characteristics of heavy convective rainfall events across the Mid-Mississippi Valley during the warm season: Meteorological conditions and a conceptual model. Preprints, *14th Conf. on Weather Analysis and Forecasting,* Dallas, TX, Amer. Meteor. Soc., 34-41.

_____, J. P. Gagan, and J. T. Moore, 2001: The extre me east-central Missouri flash flood of 6-7 May 2000. Preprints, *Symp. On Precipitation Extremes: Prediction, Impacts, and Responses,* Albuquerque, NM, Amer. Meteor. Soc., 174-179.

Gleeson, T. A., 1970: Statistical-dynamical predictions. *J. Appl. Meteor.,* **9,** 333-344.

Goebbert, K. H., A. D. Schenkman, C. M. Shafer, and N. A. Snook, 2008: An overview of the summer 2007 excessive rain event in the Southern Plains. Preprints, *22nd Conf. on*

Hydrology, New Orleans, LA, Amer. Meteor. Soc., P1.2. [Available online at http://ams.confex.com/ams/pdfpapers/135330.pdf.]

Graham, R. A., and R. H. Grumm, 2010: Utilizing normalized anomalies to assess synoptic-scale weather events in the western United States. *Wea. Forecasting,* **25,** 428-445.

Grumm, R. H., and M. Bodner, 2008: Uncertainty with a potential winter storm: The east coast storm of 14 January 2008. [Available online at http://nws.met.psu.edu/severe/2008/14Jan2008.pdf.]

_____, 2011a: The value of standardized anomalies in understanding the historic tornadic event of 27–28 April 2011. [Available online at http://nws.met.psu.edu/severe/2011/27Apr2011.pdf.]

_____, 2011b: Anticipating record events using patterns and pattern forecast: Mid-Mississippi Valley floods of April 2011. [Available online at http://nws.met.psu.edu/sref/severe/2011/26Apr2011.pdf.]

Hakim, G. J., and R. D. Torn, 2008: Ensemble synoptic analysis. *Meteor. Monographs*, **33**, 147-161.

Halverson, J. B., and T. D. Rabenhorst, 2010: Mega-snow in the Megalopolis: The Mid-Atlantic's blockbuster winter of 2009-2010. *Weatherwise,* **63,** 16-23.

Hamill, T. M., and S. J. Colucci, 1997: Verification of Eta-RSM short-range ensemble forecasts. *Mon. Wea. Rev.,* **125,** 1312-1327.

_____, 1999: Hypothesis tests for evaluating numerical precipitation forecasts. *Wea. Forecasting,* **14,** 155-167.

_____, C. Snyder, S. L. Mullen, Z. Toth, and D. P. Baumhefner, 2000: Ensemble forecasting in the short to medium range: Report from a workshop. *Bull. Amer. Meteor. Soc.*, **81,** 2653-

2664.

_____, and J. Juras, 2006: Measuring forecast skill: Is it real skill or is it the varying climatology? *Quart. J. Roy. Meteor. Soc.,* **132,** 2905-2923.

Hart, R. E., and R. H. Grumm, 2001: Using normalized climatological anomalies to rank synoptic-scale events objectively. *Mon. Wea. Rev.,* **129,** 2426-2442.

Hawblitzel, D. P., F. Zhang, Z. Meng, and C. A, 2007: Probabilistic evaluation of the dynamics and predictability of the mesoscale convective vortex of 10 – 13 June 2003. *Mon. Wea. Rev.*, **135,** 1544-1563.

Higgins, R. W., Y. Yao, E. S. Yarosh, J. E. Janowiak, and K. C. Mo, 1997: Influence of the Great Plains low-level jet on summertime precipitation and moisture transport over the central United States. *J. Climate,* **10,** 481-507.

_____, V. Kousky, and P. Xie , 2011: Extreme precipitation events in the south-central United States during May and June 2010: Historical perspective, role of ENSO, and trends. *J. Hydrometeor.*, **12,** 1056-1070.

Houze, R. A., Jr., K. L. Ramussen, S. Medina, S. R. Brodzik, and U. Romatschke, 2011: Anomalous atmospheric events leading to the summer 2010 floods in Pakistan. *Bull. Amer. Meteor. Soc.,* **92,** 291-298.

Junker, N. W., and R. S. Schneider, 1997: Two case studies of quasi-stationary convection during the 1993 Great Midwest Flood. *Natl. Wea. Dig.*, **21,** 5-17.

_____, R. S. Schneider, and S. L. Fauver, 1999: A study of heavy rainfall events during the Great Midwest Flood of 1993. *Wea. Forecasting*, **14,** 701-712.

_____, R. H. Grumm, R. Hart, L. F. Bosart, K. M. Bell, and F. J. Pereira, 2008: Use of standardized anomaly fields to anticipate extreme rainfall in the mountains of northern

California. *Wea. Forecasting,* **23,** 336-356.

_____, M., M. J. Brennan, F. Pereira, M. J. Bodner, and R. H. Grumm, 2009: Assessing the potential for rare precipitation events with standardized anomalies and ensemble guidance at the hydrometeorological prediction center. *Bull. Amer. Meteor. Soc.,* **90,** 445-453.

Juying, X., and R. A. Scofield, 1989: Satellite-derived rainfall estimates and propagation characteristics associated with the mesoscale convective systems (MCSs). NOAA Tech. Memo. NESDIS 25, 49 pp.

Kahana, R., B. Ziv, Y. Enzel, and U. Dayan, 2002: Synoptic climatology of major floods in the Negev Desert, Israel. *Int. J. Climatol.,* **22,** 867-882.

Krishnamurti, T. N., S. Surendran, D. W. Shin, R. J. Correa-Torres, T. S. V. V. Kumar, E. Williford, C. Kummerow, R. F. Adler, J. Simpson, R. Kakar, W. S Olson, and F. J. Turk, 2001: Real-time multianalysis-multimodel superensemble forecasts of precipitation using TRMM and SSM/I products. *Mon. Wea. Rev.,* **129,** 2861-2883.

_____, K. Rajendran, T. S. V. V. Kumar, S. Lord, Z. Toth, X. Zou, S. Cocke, J. E. Ahlquist, and I. M. Navon, 2003: Improved skill for the anomaly correlation of geopotential heights at 500 hPa. *Mon. Wea. Rev.,* **131,** 1082-1102.

Kumar, T. S. V. V., T. N. Krishnamurti, M. Fiorino, and M. Nagata, 2003: Numerical prediction of typhoon tracks and intensity using a multimodel superensemble. *Mon. Wea. Rev.,* **131,** 574-583.

_____, J. Sanjay, B. K. Basu, A. K. Mitra, D. V. Bhaskar Rao, O. P. Sharma, P. K. Pal, and T. N. Krishnamurti, 2007: Experimental superensemble forecasts of tropical cyclones over the Bay of Bengal. *Nat. Hazards,* **41,** 471-485.

Larget, B., 2005: Regression. [Available online at http://www.stat.wisc.edu/courses/st371-

larget/regression-handout.pdf.]

Lau, W. K. M., and K.-M. Kim, 2012: The 2010 Pakistan flood and Russian heat wave: Teleconnection of hydrometeorological extremes. *J. Hydrmeteor.,* **13,** 392-403.

Leith, C. E., 1974: Theoretical skill of Monte Carlo forecasts. *Mon. Wea. Rev.,* **102,** 409-418.

Lorenz, E. N., 1963: Deterministic nonperiodic flow. *J. Atmos. Sci.,* **20,** 130-141.

Lyon, B., 2003: Enhanced seasonal rainfall in northern Venezuela and the extreme events of December 1999. *J. Climate,* **16,** 2302-2306.

Maddox, R. A., C. F. Chappell, and L. R. Hoxit, 1979: Synoptic and meso-α scale aspects of flash flood events. *Bull. Amer. Meteor. Soc.,* **60,** 115-123.

_____, and G. K. Grice, 1986: The Austin, Texas, flash flood: An examination from two perspectives – forecasting and research. *Wea. Forecasting,* **1,** 66-76.

Majumdar, S. J., and P. M. Finocchio, 2010: On the ability of global ensemble prediction systems to predict tropical cyclone track probabilities. *Wea. Forecasting,* **25,** 659-680.

Mishra, A. K., and T. N. Krishnamurti, 2006: Current status of multimodel superensemble and operational NWP forecast of the Indian summer monsoon. *J. Earth Syst. Sci.,* **116,** 369-384.

Mo, K. C., J Nogues-Paegle, and J. Paegle, 1995: Physical mechanisms of the 1993 summer floods. *J. Atmos. Sci.,* **52,** 879-895.

Moller, A. R., and C. A. Doswell, 1988: A proposed advanced storm spotters' training program. Preprints, *15th Conf Severe Local Storms.* Baltimore, MD, Amer. Meteor. Soc., 173-177.

_____, C. A. Doswell, and R. Przybylinski, 1990: High precipitation supercells: A conceptual model and documentation. Preprints, *16th Conf. Severe Local Storms,* Kananaskis, AB, Canada, Amer. Meteor. Soc., 52-57.

Molteni, F., R. Buizza, T. N. Palmer, and T. Petroliagis, 1996: The ECMWF ensemble prediction system: Methodology and validation. *Quart. J. Roy. Meteor. Soc.*, **122,** 73-119.

Moore, B. J., P. J. Neiman, F. M. Ralph, and F. E. Barthold, 2012: Physical processes associated with heavy flooding rainfall in Nashville, Tennessee, and vicinity during 1-2 May, 2010: The role of an atmospheric river and Mesoscale convective systems. *Mon. Wea. Rev.,* **140,** 358-378.

Moore, J. T., F. H. Glass, C. E. Graves, S. M. Rochette, and M. J. Singer, 2003: The environment of warm-season elevated thunderstorms associated with heavy rainfall over the central United States. *Wea. Forecasting,* **18,** 861-878.

Mullen, S. L., and D. P. Baumhefner, 1991: Monte Carlo simulations of explosive cyclogenesis using a low-resolution, global spectral model. Preprints, *9th Conf. on Numerical Weather Prediction,* Denver, CO Amer. Meteor. Soc., 750-751.

_____, and _____, 1994: Monte Carlo simulations of explosive cyclogenesis. *Mon. Wea. Rev.,* **122,** 1548-1567.

_____, and R. Buizza, 2001: Quantitative precipitation forecasts over the United States by the ECMWF Ensemble Prediction System. *Mon. Wea. Rev.,* **129,** 638-663.

Mureau, R., F. Molteni, and T. N. Palmer, 1993: Ensemble prediction using dynamically conditioned perturbations. *Quart. J. Roy. Meteor. Soc.*, **119,** 299-323.

National Oceanic and Atmospheric Administration's National Weather Service, 2010a: Middle TN weekend rainfall totals. [Available online at http://www.srh.noaa.gov/news/display_cmsstory.php?wfo=ohx&storyid=51806&source=2.]

_____, 2010b: Record or near-record river flood levels across middle Tennessee. [Available

online at http://www.srh.noaa.gov/news/display_cmsstory.php?wfo=ohx&storyid=51780&source=2.]

_____, 2010c: Update: rainiest day in Nashville's history. [Available online at http://www.srh.noaa.gov/news/display_cmsstory.php?wfo=ohx&storyid=51772&source=2.]

_____, cited 2011a: National Weather Service Glossary. [Available online at http://www.nws.noaa.gov/glossary/.]

_____, 2011b: Remembering the May 2010 Tennessee flood. [Available online at http://www.srh.noaa.gov/news/display_cmsstory.php?wfo=ohx&storyid=67318&source=2.]

_____, 2011c: Record floods of Greater Nashville: Including flooding in middle Tennessee and western Kentucky, May 1-4, 2010. National Oceanic and Atmospheric Administration Service Assessment. [Available online at http://www.weather.gov/os/assessments/pdfs/Tenn_Flooding.pdf.]

_____, 2011d: April Severe Weather Events Set New Tornado records for Alabama. [Available online at http://www.srh.noaa.gov/bmx/?n=climo_2011torstats.]

_____, 2011e: Historic tornado outbreak April 27, 2011. [Available online at http://www.srh.noaa.gov/bmx/?n=event_04272011.]

_____, 2012: The historic tornadoes of April 2011. National Oceanic and Atmospheric Administration Service Assessment. [Available online at http://www.nws.noaa.gov/om/assessments/pdfs/historic_tornadoes.pdf.]

Neiman, P. J., F. M. Ralph, G. A. Wick, J. Lundquist, and M. D. Dettinger, 2008a:

Meteorological characteristics and overland precipitation impacts of atmospheric rivers affecting the West Coast of North America based on eight years of SSM/I satellite observations. *J. Hydrometeor*., **9,** 22-47.

_____, _____, _____, Y.-H. Kuo, T.-K. Wee, Z. Ma, G. H. Taylor, and M. D. Dettinger, 2008b: Diagnosis of an intense atmospheric river impacting the Pacific Northwest: Storm summary and offshore vertical structure observed with COSMIC satellite retrievals. *Mon. Wea. Rev.,* **136,** 4398-4420.

_____, L. J. Schick, F. M. Ralph, M. Hughes, and G. A. Wick, 2011: Flooding in western Washington: The connection to atmospheric rivers. *J. Hydrometeor.,* **12,** 1337-1358.

Newell, R. E., N. E. Newell, Y. Zhu, and C. Scott, 1992: Tropospheric rivers? - A pilot study. *Geophys. Res. Lett.,* **19,** 2401-2404.

Palmer, T. N., 2000: Predicting uncertainty in forecasts of weather and climate. *Rep. Prog. Phys.,* **63,** 71-116.

Pappenberger, F., J. Bartholmes, J. Thielen, H. L. Cloke, R. Buizza, and A. de Roo, 2008: New dimensions in early flood warning cross the globe using grand-ensemble weather predictions. *Geophys. Res. Lett.*, **35,** 1-7, L10404, doi:10.1029/2008GL033837.

Park, Y. Y., R. Buizza, and M. Leutbecher, 2008: TIGGE: Preliminary results on comparing and combining ensembles. *Quart. J. Roy. Meteor. Soc.,* **134,** 2029-2050.

Parker, M. D., and R. H. Johnson, 2000: Organizational modes of midlatitudes mesoscale convective systems. *Mon. Wea. Rev.,* **128,** 3413-3436.

Petroliagis, T., R. Buizza, A. Lanzinger, and T. N. Palmer, 1997: Potential use of the ECMWF Ensemble Prediction System in cases of extreme weather events. *Meteor. Appl.,* **4,** 69-84.

Ralph, F. M., P. J. Neiman, and G. A. Wick, 2004: Satellite and CALJET aircraft observations of

atmospheric rivers over the eastern North Pacific Ocean during the winter of 1997/98. *Mon. Wea. Rev.,* **132,** 1721-1745.

_____, _____, and R. Rotunno, 2005: Dropsonde observations in low-level jets over the northeastern Pacific Ocean from CALJET-1998 and PACJET-2001: Mean vertical-profile and atmospheric-river characteristics. *Mon. Wea. Rev.,* **133,** 889-910.

_____, _____, G. A. Wick, S. I. Gutman, M. D. Dettinger, D. R. Cayan, and A. B. White, 2006: Flooding on California's Russian River: Role of atmospheric rivers. *Geophys. Res. Lett.,* **33,** L13801, doi:10.1029/2006GL026689.

_____, _____, G. N. Kiladis, K. Weickmann, and D. W. Reynolds, 2011: A multiscale observational case study of a Pacific atmospheric river exhibiting tropical-extratropical connections and a mesoscale frontal wave. *Mon. Wea. Rev.,* **139,** 1169-1189.

_____, and M. D. Dettinger, 2011: Storms, floods, and the science of atmospheric rivers. *Eos, Trans. Amer. Geophys*. Union, **92,** 265-266.

Rochette, S. M., and J. T. Moore, 1996: Initiation of an elevated mesoscale convective system associated with heavy rainfall. *Wea. Forecasting,* **11,** 443-457.

Rogash, J. A., and R. D. Smith, 2000: Multiscale overview of a violent tornado outbreak with attendant flash flooding. *Wea. Forecasting,* **15,** 416-431.

_____, and J. Racy, 2002: Some meteorological characteristics of significant tornado events occurring in proximity to flash flooding. *Wea. Forecasting,* **17,** 155-159.

Rogers, E., D. G. Deaven, and G. J. DiMego:1995: The regional analysis system for the operational "early" eta model: Original 80-km configuration and recent changes. *Wea. Forecasting,* **10,** 810-825.

Romatschke, U., and R. A. Houze Jr., 2011: Characteristics of precipitating convective systems

in the South Asian monsoon. *J. Hydrometeor.*, **12,** 3-26.

_____, and _____, 2011: Characteristics of precipitating convective systems in the premonsoon season of South Asia. *J. Hydrometeor.,* **12,** 157-180.

Roulston, M. S., and L. A. Smith, 2003: Combining dynamical and statistical ensembles. *Tellus*, **55A,** 16-30.

Schaefer, J. T., 1990: The critical success index as an indicator of warning skill. *Wea. Forecasting*, **5,** 570-575.

Schumacher, R. S., and R. H. Johnson, 2005: Organization and environmental properties of extreme-rain-producing mesoscale convective systems. *Mon. Wea. Rev.,* **133,** 961-976.

_____, and _____, 2006: Characteristics of U.S. extreme rain events during 1999-2003. *Wea. Forecasting,* **21,** 69-85.

_____, and _____, 2009: Quasi-stationary, extreme-rain-producing convective systems associated with midlevel cyclonic circulations. *Wea. Forecasting,* **24,** 555-574.

_____, and C. A. Davis, 2010: Ensemble-based forecast uncertainty analysis of diverse heavy rainfall events. *Wea. Forecasting,* **25,** 1103-1122.

_____, 2011: Ensemble-based analysis of factors leading to the development of a multiday warm-season heavy rain event. *Mon. Wea. Rev.,* **139,** 3016-3035.

Schwartz, B. E., C. F. Chappell, W. E. Togstad, and X.-P. Zhong, 1990: The Minneapolis flash flood: Meteorological analysis and operational response. *Wea. Forecasting,* **5,** 3-21.

Shi, J., and R. A. Scofield, 1987: Satellite observed mesoscale convective system (MCS) propagation characteristics and a 3-12 hour heavy precipitation forecast index. NOAA Tech. Memo. NESDIS 20, 43 pp.

Sippel, J. A., and F. Zhang, 2008: A probabilistic analysis of the dynamics and predictability of

tropical cyclogenesis. *J. Atmos. Sci.,* **65,** 3440-3459.

_____, and _____, 2010: Factors affecting the predictability of Hurricane Humberto (2007). *J. Atmos. Sci.,* **67,** 1759-1778.

Smith, B. L., S. E. Yuter, P. J. Neiman, and D. E. Kingsmill, 2010: Water vapor fluxes and orographic precipitation over northern California associated with a landfalling atmospheric river. *Mon. Wea. Rev.,* **138,** 74-100.

Smith, J. A., M. L. Baeck, Y. Zhang, and C. A. Doswell III, 2001: Extreme rainfall and flooding from supercell thunderstorms. *J. Hydrometeor.,* **2,** 469-489.

Stensrud, D. J., J.-W. Bao, and T. T. Warner, 2000: Using initial condition and model physics perturbations in short-range ensemble simulations of mesoscale convective systems. *Mon. Wea. Rev.,* **128,** 2077-2107.

Stohl, A., C. Forster, and H. Sodemann, 2008: Remote sources of water vapor forming precipitation on the Norwegian west coast at 60°N – A tale of hurricanes and an atmospheric river. *J. Geophys. Res.,* **113,** D05102, doi:10.1029/2007JD009006.

Torn, R. D., 2010: Diagnosis of the downstream ridging associated with extratropical transition using short-term ensemble forecasts. *J. Atmos. Sci.,* **67,** 817-833.

Toth, Z., and E. Kalnay, 1993: Ensemble forecasting at NMC: The generation of perturbations. *Bull. Amer. Meteor. Soc.,* **74,** 2317-2330.

Tracton, M. S., and E. Kalnay, 1993: Operational ensemble prediction at the National Meteorological Center: Practical aspects. *Wea. Forecasting,* **8,** 379-398.

Trenberth, K. E., and C. J. Guillemot, 1996: Physical processes involved in the 1988 drought and 1993 floods in North America. *J. Climate,* **9,** 1288-1298.

Uccellini, L. W., 1980: On the role of upper tropospheric jet streaks and leeside cyclogenesis in

the development of low-level jets in the Great Plains. *Mon. Wea. Rev.,* **108,** 1689-1696.

US Army Corps of Engineers: Morganza Floodway. [Available online at http://www.mvn.usace.army.mil/bcarre/morganza.asp#.]

Venugopal, V., S. Basu, and E. Foufoula-Georgiou, 2005: A new metric for comparing precipitation patterns with an application to ensemble forecasts. *J. Geophys. Res.,* **110,** D08111, doi: 10.1029/2004JD005395.

Wang, C., S.-K. Lee, and D. B. Enfield, 2007: Impact of the Atlantic warm pool on the summer climate of the Western Hemisphere. *J. Climate,* **20,** 5021-5040.

_____, _____, and _____, 2008: Climate response to anomalously large and small Atlantic warm pools during the summer. *J. Climate,* **21,** 2437-2450.

Wei, M., Z. Toth, R. Wobus, and Y. Zhu, 2008: Initial perturbations based on the ensemble transform (ET) technique in the NCEP global operational forecast system. *Tellus,* **60A,** 62-79.

Whitaker, J. S., and A. F. Loughe, 1998: The relationship between ensemble spread and ensemble mean skill. *Mon. Wea. Rev.,* **126,** 3292-3302.

Whiteman, C. D., X. Bian, and S. Zhong, 1997: Low-level jet climatology from enhanced rawinsonde observations at a situ in the southern Great Plains. *J. Appl. Meteor.,* **36,** 1363-1376.

Wilks, D. S., 2005: Statistical Methods in the Atmospheric Sciences. 2nd ed. Academic Press, 648 pp.

Xu, M., D. J. Stensrud, J.-W. Bao, and T. T. Warner, 2001: Applications of the adjoint technique to short-range ensemble forecasting of mesoscale convective systems. *Mon. Wea. Rev.,* **129,** 1395-1418.

Zhu, Y., and R. E. Newell, 1998: A proposed algorithm for moisture fluxes from atmospheric rivers. *Mon. Wea. Rev.*, **126,** 725-735.